PAULO JOSÉ PEREIRA LIMA TEIXEIRA

Construção de um atlas transcriptômico para o estudo da doença vassoura de bruxa do cacaueiro

Campinas
2013

UNIVERSIDADE ESTADUAL DE CAMPINAS

INSTITUTO DE BIOLOGIA

PAULO JOSÉ PEREIRA LIMA TEIXEIRA

Construção de um atlas transcriptômico para o estudo da doença vassoura de bruxa do cacaueiro

Tese apresentada ao Instituto de Biologia da Unicamp para obtenção do Título de Doutor em Genética e Biologia Molecular, na área de Genética de Microorganismos.

Orientador: Prof. Dr. Gonçalo Amarante Guimarães Pereira

Coorientador: Dr. Jorge Maurício Costa Mondego

Campinas
2013

FICHA CATALOGRÁFICA ELABORADA POR
MARA JANAINA DE OLIVEIRA – CRB8/6972
BIBLIOTECA DO INSTITUTO DE BIOLOGIA - UNICAMP

T235c

Teixeira, Paulo José Pereira Lima, 1986-
Construção de um atlas transcriptômico para o estudo da doença vassoura de bruxa do cacaueiro / Paulo José Pereira Lima Teixeira. – Campinas, SP: [s.n.], 2013.

Orientador: Gonçalo Amarante Guimarães Pereira.
Coorientador: Jorge Maurício Costa Mondego.
Tese (doutorado) – Universidade Estadual de Campinas, Instituto de Biologia.

1. Cacau. 2. *Moniliophthora perniciosa*. 3. Vassoura-de-bruxa. 4. RNA-seq. 5. Transcriptoma. I. Pereira, Gonçalo Amarante Guimarães, 1964-. II. Mondego, Jorge Mauricio Costa. III. Universidade Estadual de Campinas. Instituto de Biologia. IV. Título.

Informações para Biblioteca Digital

Título em Inglês: A comprehensive transcriptome atlas for the study of the witches` broom disease of cacao
Palavras-chave em Inglês:
Cacao
Moniliophthora perniciosa
Witches' broom disease
RNA-seq
Transcriptome
Área de concentração: Genética de Microrganismos
Titulação: Doutor em Genética e Biologia Molecular
Banca examinadora:
Gonçalo Amarantes Guimarães Pereira [Orientador]
Antônio Vargas de Oliveira Figueira
Celso Eduardo Benedetti
Fabio Papes
Maria Sueli Soares Felipe
Data da defesa: 26-02-2013
Programa de Pós Graduação: Genética e Biologia Molecular

Campinas, 26 de fevereiro de 2013.

BANCA EXAMINADORA

Prof. Dr. Gonçalo Amarante Guimarães Pereira (Orientador)

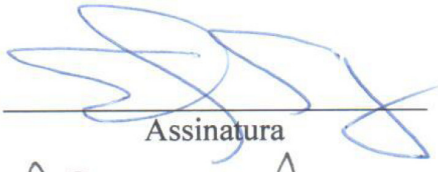

Assinatura

Prof. Dr. Antônio Vargas de Oliveira Figueira

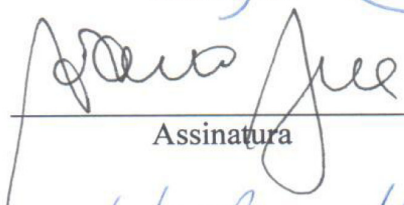

Assinatura

Prof. Dr. Celso Eduardo Benedetti

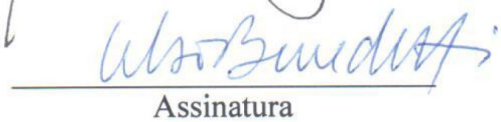

Assinatura

Prof. Dr. Fabio Papes

Assinatura

Profa. Dra. Maria Sueli Soares Felipe

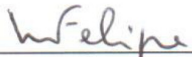

Assinatura

Prof. Dr. Marcelo Menossi Teixeira

Assinatura

Prof. Dr. Paulo Arruda

Assinatura

Profa. Dra. Suely Lopez Gomes

Assinatura

Dedico esta tese ao meu pai, quem despertou meu gosto pela ciência; e à minha mãe, por alimentar os meus sonhos.

AGRADECIMENTOS

Agradeço aos meus pais e meus irmãos pelo carinho, incentivo e suporte em todos os momentos de minha vida. Vocês são os maiores responsáveis por todas as minhas conquistas.

Agradeço à minha grande família. Eu precisaria de uma página inteira para mencionar todos meus avós, tios e primos! Obrigado por torcerem por mim.

Agradeço à querida Daniela Thomazella por todo carinho e companheirismo ao longo dos últimos anos. Sua influência e apoio foram essenciais para eu superar cada dificuldade encontrada. Agradeço também à doutora Daniela Thomazella pela produtiva colaboração, ensinamentos e discussões científicas.

Agradeço à Tata, vó Veva, tio Pedrinho, Mônica (Miss), Fábio e Elvira pelo carinho e amizade. Obrigado por serem uma segunda família para mim.

Agradeço aos meus grandes amigos Ricardo Tiozão, Fábio Rauber, Luige Peru, Felipe Caçapa, Felipe Beça, Mike, Vivi, Zelão, Danilo, Murilo e Jamanta. Vocês fizeram tudo ser muito mais fácil.

Agradeço a todos os alunos de iniciação científica com quem tive a honra de trabalhar: Taís Herig, Victor Negri, Paula Prado, Gabriel Fiorin, Renato Oliveira e Natália Costa. Devo muito do que aprendi em meu doutorado a vocês.

Agradeço aos colegas do LGE e à enorme equipe responsável pela administração do laboratório.

Agradeço aos amigos bioinformatas Osvaldo e Gustavão, que foram fundamentais na realização deste trabalho.

Agradeço ao Dr. Jorge Mondego pela amizade e por me acompanhar desde o início da minha formação científica.

Agradeço ao Dr. Piotr Mieczkowski e aos amigos da Universidade da Carolina do Norte por me receberem de braços abertos e darem todo suporte necessário para a realização deste trabalho.

Agradeço ao meu orientador e amigo Gonçalo Pereira pela confiança e conselhos durante minha formação. Tenho muito orgulho de ter sido formado em seu laboratório.

Agradeço à Fundação de Amparo à Pesquisa do Estado de São Paulo (FAPESP) por financiar este trabalho (processos 2009/51018-1 e 2009/50119-9).

"O sucesso é um por cento de inspiração e noventa e nove por cento de transpiração"

Thomas Edison

ÍNDICE

RESUMO

O cacaueiro se destaca como uma das principais culturas perenes na agricultura, sendo economicamente relevante por fornecer a matéria prima para a fabricação do chocolate, um produto que movimenta bilhões de dólares no mercado mundial a cada ano. Apesar de sua importância, o cacaueiro é drasticamente atacado por diversas doenças que diminuem sua produtividade e reduzem a qualidade das amêndoas do cacau. Dentre estas, a vassoura de bruxa, causada pelo basidiomiceto *Moniliophthora perniciosa*, é um importante fator limitante da produção cacaueira nas Américas. Utilizando tecnologias de sequenciamento de DNA de nova geração, realizamos uma abrangente análise transcriptômica da vassoura de bruxa neste trabalho. Um banco de dados denominado Atlas Transcriptômico da Vassoura de Bruxa foi construído, o qual compreende aproximadamente 60 bibliotecas de RNA-seq representativas dos mais variados estágios de desenvolvimento, condições de crescimento e respostas a estresse do fungo *M. perniciosa* sob condições *in vitro* e *in planta*. O primeiro capítulo desta tese apresenta uma análise global do Atlas Transcriptômico da vassoura de bruxa. Este conjunto de dados tem suportado uma série de estudos específicos relacionados a variados aspectos da doença, os quais são apresentados e detalhados nos demais capítulos da tese. Notavelmente, uma análise detalhada da interação biotrófica entre o cacaueiro e o fungo *M. perniciosa* (Capítulo II) revelou a ocorrência de intensa reprogramação transcricional e importantes alterações fisiológicas em plantas infectadas, incluindo a ativação de respostas de defesa ineficientes e a ocorrência de privação de carbono. Curiosamente, um processo de senescência prematura se estabelece no tecido infectado e parece ser um evento central no desenvolvimento da doença, possivelmente disparando o início da fase necrotrófica desta interação planta-patógeno. Ainda, nossos dados também permitiram a identificação de potenciais efetores de virulência em *M. perniciosa,* como também a caracterização do *status* metabólico do fungo durante a infecção do cacaueiro. Um modelo detalhado que sumariza os aspectos moleculares da vassoura de bruxa foi elaborado. De maneira geral, o Atlas Transcriptômico da Vassoura de Bruxa representa um importante avanço no estudo desta doença e tem servido como ponto de partida para uma série de estudos adicionais. A utilização destes dados na identificação e caracterização de potenciais fatores de patogenicidade de *M. perniciosa* (Capítulos III, IV e VI) e de mecanismos de defesa do cacaueiro (Capítulo V) também é apresentada nesta tese.

ABSTRACT

Cacao stands out as one of the major perennial crops in the world, being economically relevant as the source of chocolate, a multi-billion dollar product appreciated worldwide. Despite its importance, cacao is seriously affected by several diseases that reduce crop yield and decrease the quality of cocoa beans. Among them, the witches` broom disease (WBD), caused by the basidiomycete *Moniliophthora perniciosa*, is a major constraint for cacao production in the Americas. Using next generation sequencing technologies, a comprehensive transcriptomic analysis of WBD was performed. We developed a database named "WBD Transcriptome Atlas", which comprises approximately 60 RNA-seq libraries that represent a wide range of developmental stages, growth conditions and stress responses of the fungus, either under *in vitro* or *in planta* conditions. The first chapter of this thesis presents a global analysis of the WBD Transcriptome Atlas. This data set has supported a number of specific analyses related to several aspects of WBD, which are presented and detailed in the other chapters of the thesis. Strikingly, a detailed analysis of the biotrophic interaction between *M. perniciosa and* cacao (Chapter I) revealed the occurrence of intense transcriptional reprogramming and remarkable physiological alterations in infected plants, including the activation of ineffective defense responses and the occurrence of carbon deprivation. Curiously, a premature senescence process is established in infected tissues and appears to be a central event in WBD, possibly triggering the onset of the necrotrophic stage of this plant-pathogen interaction. Additionally, our data also allowed the identification of potential virulence effectors in *M. perniciosa*, as well as the characterization of the metabolic status of the fungus during cacao infection. A detailed model summarizing the molecular aspects of WBD is presented. Overall, the WBD Transcriptome Atlas represents an important advance in the study of this disease and constitutes a starting point for a number of additional studies. The use of these data in the identification and characterization of potential pathogenicity factors of *M. perniciosa* (Chapters III, IV and VI) and defense mechanisms of cacao (Chapter V) will also be presented in this thesis.

REVISÃO BIBLIOGRÁFICA

O cacaueiro

O cacaueiro (*Theobroma cacao*) pertence à família Malvaceae *sensu lato* (Alverson *et al.*, 1999) e tem como centro de origem a região da Bacia Amazônica (Motamayor *et al.*, 2008; Thomas *et al.*, 2012). Na natureza, esta planta tem o aspecto semelhante a uma grande touceira, devido ao desenvolvimento de muitas brotações que partem das raízes (Figura 1A). No entanto, em plantios comerciais as plantas são conduzidas pela poda e assim adquirem um aspecto de árvore (Figura 1B). As flores do cacaueiro (Figura 1C) são bastante pequenas, amarelo-avermelhadas e inodoras, e nascem unidas aos ramos e tronco da planta. Seu fruto (Figura 1D) contém de 30 a 50 sementes cobertas por uma polpa doce e mucilaginosa largamente utilizada na produção de bebidas finas, geleias, sorvetes e sucos. Entretanto, a principal importância do cacau está na utilização de suas sementes (Figura 1E) como matéria prima para a produção de chocolate (Bartley, 2005). A indústria do chocolate movimenta bilhões de dólares no mercado mundial todos os anos, o que faz do cacaueiro uma das culturas perenes de maior importância na agricultura.

A domesticação do cacaueiro é bastante antiga e data do período anterior ao descobrimento das Américas, sendo atribuída às civilizações Olmeca, Maia e Asteca (Hurst *et al.*, 2002; Henderson *et al.*, 2007; Powis *et al.*, 2011). Estas civilizações utilizavam o cacau para a confecção de uma bebida especial (denominada xocolātl), preparada para uso em cerimônias solenes religiosas ou para a realeza. As amêndoas do cacau eram consideradas tão valiosas que foram utilizadas até mesmo como moeda. Além disso, o cacau também possuía valor divino para estas civilizações, o que influenciou o botânico Carlos Lineu a classificá-lo como *Theobroma cacao* (do grego, *Theo* = deuses; *broma* = alimento, ou seja, alimento dos deuses) (Paradis, 1979). Após a chegada dos espanhóis na América, o cacau foi levado à Europa, onde foi então utilizado para o preparo do chocolate. Para possibilitar a manutenção do novo hábito, diversos países europeus passaram a cultivar o cacaueiro em suas colônias ao redor do mundo, contribuindo para a disseminação da cultura para além da América (Coe & Coe, 1996).

Figura 1. Características gerais do cacaueiro. (A) Cacaueiro selvagem apresentando aspecto de touceira. (B) Árvore de cacau cultivada com frutos. (C) Flor do cacaueiro, que se desenvolve no tronco da árvore. (D) Detalhe de um fruto de cacau maduro. (E) Amêndoas de cacau, principal produto de valor econômico do cacaueiro. Imagem adaptada de Thomazella *et al*. (2012b).

O cacaueiro está adaptado a climas quentes e úmidos, sendo cultivado principalmente nas Américas Central e do Sul, África e Ásia. Atualmente, a África destaca-se como o principal continente produtor, respondendo por mais de 70% de todo cacau produzido no mundo. Por outro lado, os Estados Unidos e a Europa processam cerca de 50% da produção mundial, resultando em um intenso fluxo comercial entre os países produtores e os consumidores (Figura 2).

No Brasil, o cultivo do cacaueiro ocorre nos estados do Pará, Rondônia, Espírito Santo e principalmente no sul da Bahia, região cuja produção corresponde a 75% do total nacional. Uma importante característica do cacaueiro é a necessidade de sombra para o seu desenvolvimento, o que faz com que seu o cultivo seja realizado às sombras de árvores nativas. Este sistema de cultura, denominado “cabruca”, tem importante papel na preservação de trechos de Mata Atlântica nas áreas de produção (Lobão *et al.*, 2007). Atualmente, o Brasil produz cerca de 220 mil

toneladas de amêndoas de cacau por ano, ocupando a sexta posição no *ranking* de produção, atrás de Costa do Marfim, Indonésia, Gana, Nigéria e Camarões. No entanto, até 1994 o Brasil ocupava a segunda posição neste *ranking*, chegando a produzir 400 mil toneladas por ano (ICCO, 2012). Esta redução na produção teve considerável impacto econômico para o Brasil, que não foi capaz de suprir a demanda da indústria chocolateira nacional e passou da condição de exportador para importador de cacau. O principal motivo desta queda produtiva foi a introdução na Bahia da doença conhecida como vassoura de bruxa, causada pelo fungo *Moniliophthora perniciosa*.

Figura 2. Produção mundial e exportação de amêndoas de cacau em 2005/2006. Apesar de o cacau ser produzido por países em desenvolvimento nas regiões tropicais do globo, a maior parte deste produto é utilizada em países desenvolvidos da Europa e nos Estados Unidos. A indústria do chocolate depende ainda de uma série de indústrias acessórias, o que movimenta bilhões de dólares todos os anos no mercado do chocolate. Imagem adaptada de Organização Internacional do Cacau (ICCO - http://www.icco.org).

Moniliophthora perniciosa e a vassoura de bruxa

O fungo basidiomiceto *Moniliophthora perniciosa* (Stahel) Aime & Phillips-Mora pertence à família Marasmiaceae da ordem Agaricales (Aime & Phillips-Mora, 2005). Este fungo é originário da Amazônia e apresenta grande variabilidade genética e uma complexa biologia (Purdy & Schmidt, 1996; Meinhardt *et al.*, 2008). Atualmente, três biótipos distintos são reconhecidos de acordo com a especificidade de hospedeiros: O biótipo S, patógeno de plantas da família Solanaceae, como a pimenteira e o tomateiro; o biótipo L, patógeno de lianas; e o biótipo C, patógeno de *Theobroma spp*. Este último é o agente etiológico da vassoura de bruxa no cacaueiro, que representa um dos principais fatores limitantes para a produção de cacau nas Américas (Purdy & Schmidt, 1996; Evans, 2007; Meinhardt *et al.*, 2008). O primeiro relato desta doença no estado da Bahia ocorreu em 1989 e, a partir desse ano, a produção brasileira foi drasticamente reduzida (Pereira *et al.*, 1996). Considerando o grande potencial destrutivo da vassoura de bruxa, uma possível disseminação desta doença nos países africanos poderia gerar uma grave crise no mercado mundial de cacau e seus derivados.

Moniliophthora perniciosa possui ciclo de vida hemibiotrófico, apresentando duas fases de desenvolvimento bem diferenciadas: uma biotrófica, em que infecta tecidos vivos do hospedeiro, e uma necrotrófica, em que coloniza os tecidos mortos da planta (Figura 3). A infecção se inicia quando basidiósporos do fungo germinam sobre tecidos meristemáticos em atividade do cacaueiro (Frias *et al.*, 1991). Ao penetrar na planta, o patógeno inicia sua fase biotrófica, apresentando hifas mononucleadas sem grampos de conexão[*] (Silva & Matsuoka, 1999). Nesta fase, o fungo é encontrado em baixa densidade no tecido infectado e cresce apenas no espaço intercelular (Calle *et al.*, 1982; Orchard *et al.*, 1994; Penman *et al.*, 2000). Os principais sintomas detectados no cacaueiro são hipertrofia, hiperplasia e perda de dominância apical, resultando na formação de ramos anormais denominados “vassouras verdes”.

[*] Estrutura utilizada para a transferência de núcleos entre células vizinhas em basidiomicetos.

Após um período de 8 a 12 semanas, as vassouras verdes iniciam um processo de necrose e morrem, sendo, então, denominadas “vassouras secas”. O nome dado à doença se deve à semelhança morfológica entre os ramos mortos e vassouras. A morte do tecido infectado é acompanhada da transição para a fase necrotrófica do fungo (Evans, 1980; Meinhardt *et al.*, 2008), porém, ainda não se sabe exatamente se esta mudança de fase é causa ou consequência da morte do ramo infectado. Ao contrário da fase biotrófica, a fase necrotrófica do patógeno apresenta micélio binucleado com grampos de conexão e cresce intensamente, podendo ser encontrada no interior das células do hospedeiro (Evans, 1980; Silva & Matsuoka, 1999). Após períodos intermitentes de chuva e seca, o fungo necrotrófico inicia a produção de basidiomas (Wheeler, 1985; Almeida *et al.*, 1997). Em seguida, ocorre liberação de basidiósporos que, levados por água ou vento, podem infectar outras plantas, reiniciando o ciclo de vida do patógeno.

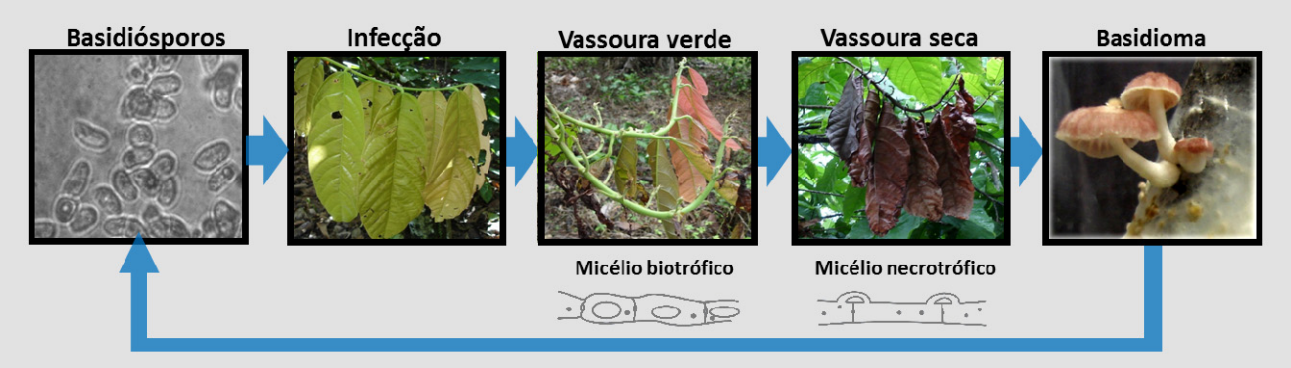

Figura 3. Representação do ciclo de vida do fungo *M. perniciosa*. Basidiósporos germinam sobre tecido meristemático do cacaueiro resultando na formação da vassoura verde, a qual é colonizada pelo micélio biotrófico. A morte do tecido infectado é acompanhada pela mudança para a fase necrotrófica do fungo. Este tecido morto é denominado vassoura seca. Neste estágio da doença são produzidos os basidiomas, que liberam os basidiósporos, reiniciando o ciclo de vida do patógeno.

Além da infecção de ramos em crescimento, que caracteriza os sintomas típicos da doença, *M. perniciosa* também pode atacar outras estruturas do cacaueiro, incluindo frutos jovens e flores (Evans, 1980). A infecção em frutos leva a um processo de amadurecimento alterado, deformação e posterior necrose (Baker, 1957). Em flores ocorre normalmente o desenvolvimento de pequenos frutos partenocárpicos (Pereira, 2000). Nos diferentes tecidos, os sintomas

observados durante a fase biotrófica sugerem fortemente a ocorrência de um desequilíbrio hormonal nesta etapa da doença. Normalmente, apesar de causar a morte do tecido infectado, a vassoura de bruxa não é letal para o cacaueiro. Porém, árvores infectadas parecem sofrer grandes alterações fisiológicas que influenciam diretamente na quantidade e qualidade dos frutos produzidos, o item de valor econômico do cacaueiro.

Muitos métodos para controle da doença vêm sendo utilizados, porém sem muito sucesso. Dentre as tentativas realizadas destacam-se a poda fitossanitária (Lima *et al.*, 1991), o uso de fungicidas (Bastos, 1989), o controle biológico (Bastos & Dias, 1992) e o desenvolvimento de variedades de cacau resistentes (Pires & Luz, 1995). No entanto, um plano viável e efetivo para o controle da vassoura de bruxa ainda não foi implantado nas regiões afetadas.

O Projeto Genoma Vassoura de Bruxa

Com o objetivo de gerar informações a respeito da biologia do fungo *M. perniciosa* e da doença vassoura de bruxa do cacaueiro, no ano 2000 foi iniciado o Projeto Genoma Vassoura de Bruxa[*]. Sob coordenação do Prof. Dr. Gonçalo Amarante Guimarães Pereira, o projeto inicialmente envolveu o LGE (Laboratório de Genômica e Expressão da Unicamp), a UESC (Universidade Estadual Santa Cruz), a UFBA (Universidade Federal da Bahia), a CEPLAC (Comissão Executiva do Plano da Lavoura Cacaueira), o CENARGEN-EMBRAPA e a UEFS (Universidade Estadual de Feira de Santana). Desde seu início, o projeto tem suportado uma série de estudos acerca de processos envolvidos no estabelecimento desta interação planta-patógeno. O estado da arte das pesquisas relacionadas à doença vassoura de bruxa do cacaueiro é sumarizado na Figura 4.

Através da metodologia de *Whole Genome Shotgun* e sequenciamento Sanger (Sanger *et al.*, 1977), o projeto determinou 75 Mpb em sequências de DNA de *M. perniciosa*, representando um *draft* inicial do genoma deste patógeno. As primeiras análises do genoma nuclear de *M. perniciosa,* bem como de seu genoma mitocondrial*,* foram publicadas em 2008 (Mondego *et al.*,

[*] www.lge.ibi.unicamp.br/vassoura

2008; Formighieri *et al.*, 2008). Posteriormente, através de uma colaboração estabelecida entre o Laboratório de Genômica e Expressão da Unicamp (LGE) e o Departamento de Agricultura dos Estados Unidos (USDA), novas sequências do genoma de *M. perniciosa* foram obtidas por meio do método de pirosequenciamento utilizando o sequenciador *454 Genome Sequencer FLX* (Roche). Em 2010, uma parceria firmada com o Centro de Ciências Genômicas da Universidade da Carolina do Norte (CCGS) permitiu a obtenção de ainda mais sequências do genoma deste patógeno, o que resultou em uma montagem de alta qualidade deste genoma.

Logo nos primeiros anos do projeto genoma, uma análise cariotípica do fungo *M. perniciosa* foi iniciada utilizando-se linhagens do patógeno coletadas em diversas localizações do Brasil e da América do Sul. Notavelmente, apenas dois genótipos distintos foram identificados na região cacaueira da Bahia, ao passo que uma enorme variabilidade genética foi verificada entre as linhagens coletadas na Amazônia (Rincones *et al.*, 2003; Rincones *et al.*, 2006). Este resultado suporta a ideia de que a vassoura de bruxa se disseminou na Bahia a partir de poucos focos de infecção, possivelmente envolvendo ação humana (Pereira *et al.*, 1996; Andebrhan *et al.*, 1999). As análises cariotípicas permitiram ainda estimar o tamanho do genoma do fungo *M. perniciosa*, calculado na época em aproximadamente 30 Mpb. Entretanto, com base nos sequenciamentos mais recentes, o tamanho do genoma deste patógeno é agora estimado em 47 Mpb (dados não publicados).

Em 2005, nosso grupo publicou uma análise bioquímica bastante abrangente da interação entre o cacaueiro e o patógeno *M. perniciosa* (Scarpari *et al.*, 2005). Nenhum trabalho até aquele momento havia investigado a vassoura de bruxa de forma tão detalhada e as informações obtidas serviram de base para uma série de novas hipóteses. O estudo apontou características fisiológicas de tecidos infectados, descrevendo alterações nos conteúdos de açúcares, aminoácidos, metabólitos secundários, pigmentos, etileno e ácido graxo. Em particular, verificou-se a existência de elevadas quantidades de glicerol em vassouras verdes, indicando um importante papel deste

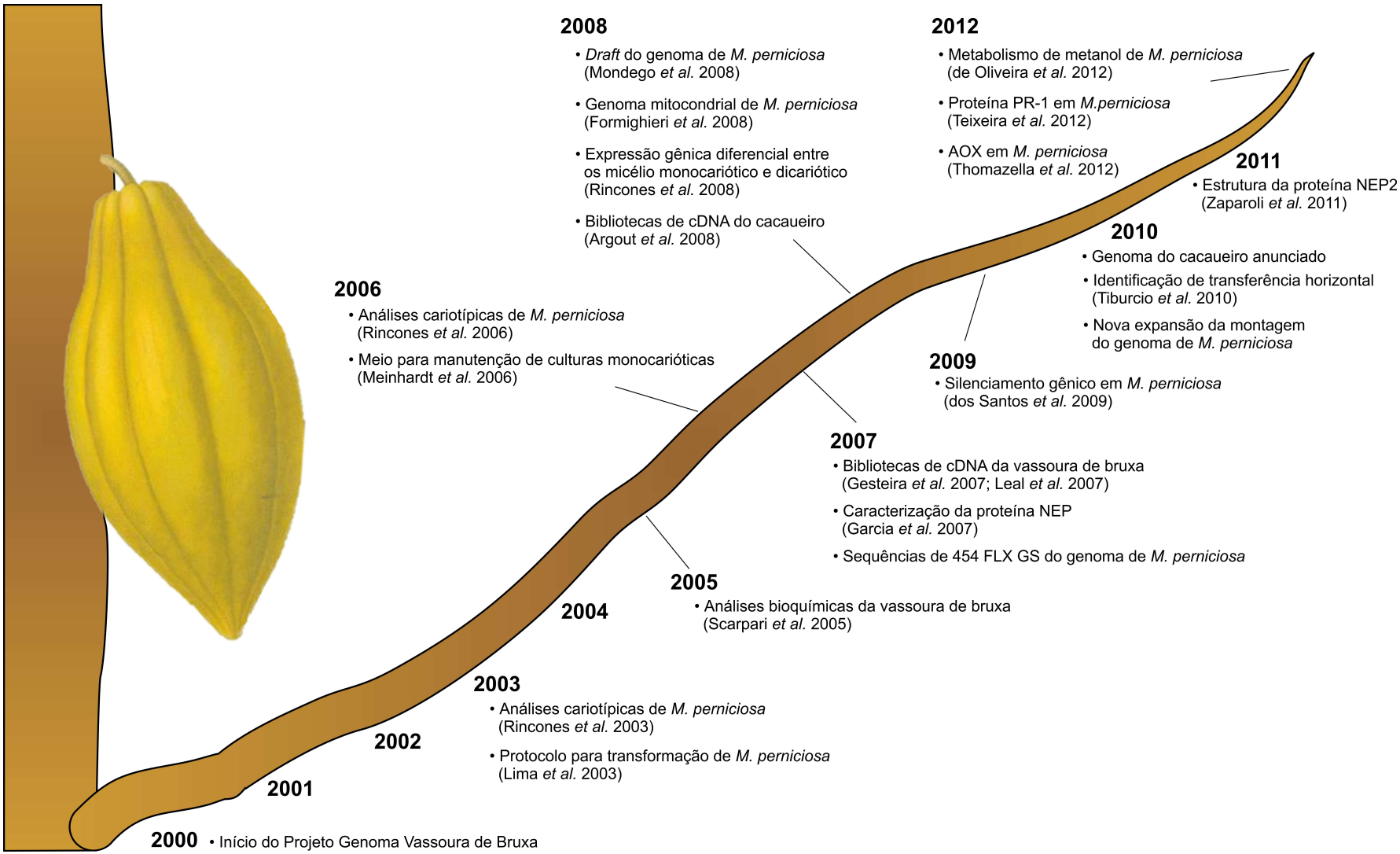

Figura 4. Histórico do estudo da doença vassoura de bruxa a partir do início do projeto genoma. Trabalhos descrevendo os mais importantes resultados e outros acontecimentos relevantes são apresentados.

composto no desenvolvimento da doença. Destaca-se, ainda, que estes experimentos foram realizados no estado da Bahia, uma vez que o cacaueiro requer altas umidades e temperaturas para seu desenvolvimento, condições que ainda não estavam disponíveis em nosso laboratório. De maneira similar, o estudo do fungo em laboratório era bastante limitado pela complexidade de seu ciclo de vida. Nesta época, os experimentos eram realizados exclusivamente com o micélio dicariótico (necrotrófico) do patógeno, o qual não é infectivo (mas é facilmente cultivado). Por outro lado, o micélio monocariótico (biotrófico) é instável e rapidamente sofre dicariotização em condições padrão de cultivo, indicando que estímulos específicos são necessários para manutenção da biotrofia em *M. perniciosa*. Em vista disso, diversos meios de cultura foram avaliados buscando-se mimetizar as condições encontradas pelo fungo durante a infecção do cacaueiro. Com base nos resultados de Scarpari *et al.* (2005), um meio de cultura contendo glicerol como única fonte de carbono foi desenvolvido e mostrou-se capaz de manter o crescimento do micélio monocariótico de *M. perniciosa* (Meinhardt *et al.*, 2006).

Apesar de se tratar de uma condição artificial, o micélio monocariótico cultivado *ex planta* representou um novo modelo para estudos relacionados à patogenicidade de *M. perniciosa.* Bibliotecas de cDNA e *microarrays* foram utilizados para verificar a expressão diferencial de genes entre os micélios monocariótico e dicariótico em condições axênicas (Rincones *et al.*, 2008). Os resultados obtidos indicaram que o micélio monocariótico de *M. perniciosa* apresenta alta atividade metabólica, porém o metabolismo não parece ser direcionado para crescimento celular, mas sim para a síntese de metabólitos secundários e proteínas possivelmente envolvidas na sobrevivência e interação com o cacaueiro. Por outro lado, uma maior expressão de genes envolvidos com o metabolismo energético e crescimento foi verificada no micélio dicariótico. Este trabalho também reportou a identificação de um gene codificante de uma enzima similar a metanol oxidases (MOX), a qual poderia mediar a oxidação do metanol liberado como produto da degradação de pectina vegetal. De fato, a expressão do gene *MOX* é aumentada tanto na presença de pectina como também de metanol. Ainda, *M. perniciosa* é capaz de se desenvolver em meios de cultura

contendo metanol como única fonte de carbono, sugerindo que a degradação deste álcool pode ser importante para o desenvolvimento do patógeno (de Oliveira *et al.*, 2012 - Ver Anexo II).

O draft do genoma e as bibliotecas de cDNA do fungo também revelaram outros genes potencialmente relevantes para o estabelecimento da vassoura de bruxa. Dentre estes, genes codificantes de proteínas PR-1 (Teixeira *et al.*, 2012 - Ver Capítulo IV) e de uma oxidase alternativa (Thomazella *et al.*, 2012a - Ver Capítulo VI) foram descritos como importantes para o desenvolvimento biotrófico do patógeno. Além disso, um gene codificante de uma proteína NEP (*Necrosis and ethylene-inducing protein*) também foi identificado logo após a realização dos primeiros sequenciamentos do genoma do fungo. Proteínas NEP já haviam sido caracterizadas em outros fitopatógenos como sendo capazes de induzir necrose em diferentes plantas (Bailey, 1995; Qutob *et al.*, 2002) e, por este motivo, este gene passou a ser estudado em *M. perniciosa*. De fato, Garcia *et al.* (2007) demonstraram que a NEP de *M. perniciosa* é capaz de causar morte do tecido do cacaueiro. Mais recentemente, nosso grupo resolveu a estrutura tridimensional desta proteína, apontando aminoácidos importantes para sua atividade (Zaparoli *et al.*, 2011 - Ver Anexo I). Com base na versão *draft* do genoma, Tiburcio *et al.* (2010) investigaram a ocorrência de eventos de transferência horizontal em *M. perniciosa*. De modo interessante, o gene *NEP* foi identificado como um dos genes candidatos a terem sido obtidos de outras espécies, sendo possivelmente transferido por oomicetos do gênero *Phytophthora*.

As primeiras análises moleculares da resposta do cacaueiro ao fungo *M. perniciosa* foram publicadas em 2007. Gesteira *et al*. (2007) construíram bibliotecas de cDNA para identificar genes expressos durante a vassoura de bruxa. Este trabalho utilizou um *pool* de amostras coletadas em diferentes momentos da interação (de 1 até 90 dias após a infecção). Por outro lado, Leal *et al.* (2007) realizaram a construção de bibliotecas subtrativas de cDNA dos estágios iniciais da doença (fase assintomática – de 1 a 10 dias após a infecção). Ambos os trabalhos focaram na comparação de plantas suscetíveis e resistentes à vassoura de bruxa, apontando possíveis genes

do cacaueiro envolvidos nas respostas de defesa contra *M. perniciosa*. Genes do patógeno, entretanto, não foram analisados nestes estudos.

Apesar destes e outros trabalhos envolvendo a construção de bibliotecas de cDNA (Jones *et al.*, 2002; Verica *et al.*, 2004; Gesteira *et al.*, 2007; Leal *et al.*, 2007), poucos genes do cacaueiro tinham sua sequência conhecida até o fim de 2008. Em um esforço para se expandir o conhecimento molecular sobre esta planta, Argout *et al.* (2008) apresentaram uma extensiva análise de ESTs (*expressed sequence tags*) baseada no sequenciamento de 56 bibliotecas distintas de cDNA. Este trabalho levou à obtenção de 48.594 unigenes[*] e permitiu uma avaliação mais detalhada dos genes transcritos pelo cacaueiro. Em setembro de 2010, dois consórcios independentes anunciaram a conclusão do sequenciamento do genoma do cacaueiro. Sob coordenação do centro de pesquisa francês CIRAD, o consórcio ICGS (*International Cocoa Genome Sequencing Consortium,* http://cocoagendb.cirad.fr) publicou o genoma da variedade Criollo (Argout *et al.*, 2011), a qual é principalmente utilizada na fabricação do chamado chocolate fino. Por outro lado, um segundo consórcio liderado pela chocolateira Mars (*Cacao Genome Database*, www.cacaogenomedb.org), optou pelo sequenciamento da variedade Forastero, a qual corresponde a 80% de todo cacau cultivado no mundo. Os resultados desta segunda iniciativa também foram disponibilizados ao público, porém, a análise do genoma completo desta variedade não foi publicada até o momento. A disponibilidade da sequência genômica do cacaueiro abre possibilidades sem precedentes para a realização de estudos quanto à biologia molecular da vassoura de bruxa.

Atualmente, a principal limitação do projeto se diz respeito à manipulação genética do fungo *M. perniciosa*. Muitos esforços foram empregados nos últimos anos, resultando apenas em avanços modestos. Protocolos de transformação foram desenvolvidos e permitem a inserção de fragmentos de DNA em posições aleatórias no genoma do fungo (Lima *et al.*, 2003; Lopes *et al.*, 2008). No entanto, a deleção de genes específicos através de recombinação homóloga não foi

[*] Sequências únicas que representam genes.

realizada até o momento. Em 2009, um estudo reportou o silenciamento transitório de dois genes de *M. perniciosa* utilizando-se dsRNA (Caribé dos Santos *et al.*, 2009). Apesar de este trabalho descrever alterações fenotípicas nas linhagens obtidas, o método desenvolvido é restrito ao micélio dicariótico do patógeno. O desenvolvimento de ferramentas que permitam a realização de análises funcionais de genes de *M. perniciosa* é um passo fundamental para o entendimento de sua interação com a planta durante a vassoura de bruxa.

A evolução das tecnologias de sequenciamento de DNA

Em 1977, Frederick Sanger publicou um importante método para determinação da sequência de nucleotídeos em uma molécula de DNA (Sanger *et al.*, 1977), sendo então laureado com o prêmio Nobel de Química em 1980. O método de Sanger foi automatizado e originou a primeira geração de sequenciadores de DNA, os quais foram oficialmente lançados no mercado em meados da década de 80. Apesar de serem continuamente aperfeiçoadas ao longo do tempo, as plataformas de primeira geração permaneceram como a única opção para o sequenciamento de DNA durante cerca de 20 anos. Foi utilizando estes equipamentos que alguns dos genomas mais importantes para a ciência foram sequenciados, incluindo o de *Saccharomyces cerevisiae* (Goffeau *et al.*, 1996), *Escherichia coli* (Blattner *et al.*, 1997), *Drosophila melanogaster* (Adams *et al.*, 2000), *Arabidopsis thaliana* (Kaul *et al.*, 2000) e o próprio genoma humano (Lander *et al.*, 2001; Venter *et al.*, 2001). Destaca-se ainda o fato de o Brasil ter sido responsável pelo sequenciamento do primeiro genoma de um organismo fitopatogênico, a bactéria *Xylella fastidiosa* (Simpson *et al.*, 2000), em uma iniciativa que marcou o nascimento da genômica em nosso país. Cada um destes projetos, entretanto, demandou uma enorme quantidade de recursos e levou anos para a sua finalização, refletindo a grande complexidade metodológica e os altos custos de operação inerentes aos sequenciadores de primeira geração.

Nos últimos anos, o desenvolvimento das chamadas tecnologias de sequenciamento de nova geração (*next generation sequencing*) iniciou uma nova era no campo da genômica e

transcriptômica (Metzker, 2010). Projetos genomas, que antes eram realizados apenas por grandes centros ou consórcio de múltiplos laboratórios, passaram a ser realizados por laboratórios individuais de forma simples e com custos extremamente reduzidos. Iniciativas antes inimagináveis foram lançadas com base no uso de tais tecnologias. O projeto *1000 Genomes*, por exemplo, propõe a identificação da maior parte da variabilidade genética da espécie humana através do sequenciamento de 2500 indivíduos de variadas etnias (Durbin *et al.*, 2010; Abecasis *et al.*, 2012). De maneira similar, o projeto *1001 Genomes* visa identificar a variação genética existente na planta modelo *Arabidopsis thaliana*. Ainda, o projeto TCGA (*The Cancer Genome Atlas*) tem o objetivo de catalogar mutações genéticas associadas ao desenvolvimento de câncer através do sequenciamento de genomas e transcriptomas dos mais variados tipos de tecidos cancerígenos em diversos pacientes (http://cancergenome.nih.gov/). Destaca-se ainda o projeto *Genome 10K*, que propõe o sequenciamento do genoma de dez mil espécies diferentes de vertebrados, ou seja, aproximadamente uma espécie por gênero conhecido (Genome 10K Community of Scientists, 2009) e o projeto *i5K*, que sequenciará o genoma de 5000 espécies de insetos nos próximos cinco anos. No Brasil, destaca-se o Projeto 80+, o qual é coordenado pela pesquisadora Mayana Zatz (USP) e tem como meta a análise do genoma de aproximadamente mil pessoas saudáveis com mais de 80 anos. Tais exemplos, dentre muitos outros, mostram a extraordinária evolução da genômica nos últimos anos.

O primeiro dos sequenciadores de nova geração (*Genome Sequencer FLX* - 454 *Life Sciences*/Roche) foi lançado em 2005. Utilizando-se esta tecnologia, o genoma do conhecido cientista James Watson foi sequenciado em apenas dois meses a um custo 100 vezes menor do que o realizado com métodos de primeira geração baseados em eletroforese capilar (Wheeler *et al.*, 2008). Outras duas empresas logo entraram no mercado: *Life Technologies* (anteriormente *Applied Biosystems*) e Illumina (anteriormente Solexa). Apesar dos sequenciadores destas empresas produzirem sequências consideravelmente mais curtas (35 pb em comparação às sequências de aproximadamente 200 pb gerados pelo 454 GS FLX na época), estas plataformas

se destacaram pela grande quantidade de sequências produzidas, resultando em baixíssimos custos por base sequenciada. Atualmente, a Illumina domina a maior parte do mercado de sequenciadores de nova geração. Seu equipamento mais potente, denominado HiSeq 2500, é capaz de gerar 6 bilhões de sequências de até 100 pb a cada 11 dias, correspondendo a 600 Gb em sequências (aproximadamente 200 coberturas do genoma humano). Em uma verdadeira corrida estabelecida entre as empresas, novas atualizações e modelos de sequenciadores têm sido frequentemente anunciados, aumentando cada vez mais a quantidade e qualidade das sequências produzidas. Seguindo este ritmo, espera-se que as atuais tecnologias estejam ultrapassadas dentro de poucos anos; entretanto, os avanços científicos alcançados pelo uso de tais tecnologias permanecem como base para futuras descobertas.

Recentemente, as chamadas tecnologias de sequenciamento de terceira geração foram anunciadas e aplicam o conceito de *real time sequencing*, no qual a atividade de uma DNA polimerase é monitorada em tempo real durante a síntese de uma fita de DNA (Eid *et al.*, 2009). O único sequenciador de terceira geração disponível até o momento é o PacBio RS da empresa Pacific Biosciences. Apesar de ainda apresentar altíssima taxa de erro (15%), este equipamento é capaz de produzir sequências com tamanho médio de 5 mil nucleotídeos, o que pode vir a revolucionar a forma com a qual genomas são montados. Apesar das atraentes perspectivas quanto à evolução da genômica devido às novas tecnologias de sequenciamento, importantes limitações têm sido apontadas principalmente no que se diz respeito à capacidade computacional necessária para o processamento das sequências bem como à existência de cientistas qualificados para a realização de análises e interpretações dos dados produzidos.

O sequenciamento de transcriptomas utilizando novas tecnologias de sequenciamento

O sequenciamento Sanger foi largamente utilizado para análises transcriptômicas nos chamados “projetos ESTs”. Uma vez que o transcriptoma corresponde apenas à região codante do genoma, o sequenciamento de cDNA permite a identificação direta dos genes de um organismo a

custos menores e sem a complexidade da montagem e análise de um genoma completo. O primeiro grande projeto envolvendo o sequenciamento de bibliotecas de cDNA foi publicado em 1991 pelo grupo do pesquisador americano Craig Venter, o qual reportou o sequenciamento de regiões codantes do cérebro humano (Adams *et al.*, 1991). A partir de então, tal estratégia passou a ser adotada na análise dos mais variados modelos biológicos, sendo de especial importância para o estudo de organismos com genoma complexo. Como exemplo, o projeto brasileiro SUCEST foi de grande relevância para a determinação da sequência de milhares de genes da cana de açúcar, uma planta de notável interesse econômico cujo genoma não foi sequenciado até o momento (Vettore *et al.*, 2003).

Ainda que os dados obtidos por sequenciamento de primeira geração possam ser utilizados na determinação de níveis de expressão gênica (Carulli *et al.*, 1998), a acurácia deste tipo de análise é bastante comprometida pela relativa baixa quantidade de sequências normalmente produzidas nestes projetos. Métodos alternativos baseados em sequenciamento Sanger foram desenvolvidos para superar esta limitação, incluindo a construção de bibliotecas subtrativas de cDNA (Diatchenko *et al.*, 1996) ou a técnica conhecida por SAGE (S*erial Analysis of Gene Expression*) (Velculescu *et al.*, 1995). Mesmo assim, os *microarrays* foram a tecnologia de escolha para estudos de expressão gênica em larga escala durante muitos anos (Marioni *et al.*, 2008). Desenvolvida em meados da década de 90 (Schena *et al.*, 1995), esta tecnologia levou a importantes avanços em diversas áreas de estudo da biologia e medicina. Dentre as milhares de aplicações, pode-se citar a avaliação da expressão gênica diferencial em doenças, como o câncer (DeRisi *et al.*, 1996), o efeito de fármacos na expressão gênica (Petricoin III *et al.*, 2002) ou a expressão gênica em microrganismos cultivados em condições específicas (Stanley *et al.*, 2003). Apesar da grande revolução em análises transcriptômicas, a tecnologia dos *microarrays* apresenta uma série de características metodológicas que a tornam consideravelmente complexa e laboriosa (Shendure, 2008), tais como o uso de um *chip* com um número finito de sondas de sequências

necessariamente conhecidas e a realização de uma série de normalizações necessárias para evitar erros sistemáticos da técnica.

Em junho de 2008, Nagalakshmi *et al.* (2008) utilizaram pela primeira vez o termo “RNA-seq” ao descrever uma detalhada caracterização do transcriptoma de *Saccharomyces cerevisiae* com base em tecnologias de sequenciamento de nova geração. Este trabalho mapeou regiões de exons e introns com alta resolução, além de apresentar *start codons* alternativos e identificar regiões transcritas anteriormente desconhecidas no genoma desse organismo. No mês seguinte, Mortazavi *et al.* (2008) descreveram o uso do RNA-seq na quantificação dos níveis de expressão gênica em diferentes tecidos de camundongo, descrevendo um método de normalização que passou a ser amplamente adotado em análises de RNA-seq (RPKM - *reads per kilobase of exon model per million mapped reads*). A facilidade no preparo das amostras, juntamente com o grande volume de informações obtidas e o baixo custo do processo fizeram do RNA-seq uma abordagem extremamente vantajosa e inovadora.

Diferentemente dos métodos baseados em plataformas de primeira geração, o RNA-seq resulta em milhões de sequências por amostra, o que permite que a expressão gênica seja eficientemente quantificada. Ainda, diversos trabalhos comparativos demonstraram maior precisão dos dados obtidos por RNA-seq em relação aos *microarrays* ('t Hoen *et al.*, 2008; Marioni *et al.*, 2008; Shendure, 2008). Como vantagem, o RNA-seq destaca-se por apresentar maior sensibilidade a transcritos pouco abundantes e capacidade de detecção de pequenas variações de expressão (Marioni *et al.*, 2008). Além disso, o RNA-seq permite simultaneamente a análise detalhada da estrutura do transcriptoma e a quantificação dos níveis de expressão gênica com alta precisão, vantagem que não é oferecida por nenhuma outra técnica disponível atualmente. Por outro lado, a inexistência de um método de análise padrão e amplamente aceito na comunidade científica configura-se como a principal desvantagem desta metodologia. Mesmo assim, as novas tecnologias de sequenciamento já são consideradas sucessoras dos *microarrays* na análise global de expressão gênica.

As principais etapas em uma análise de expressão gênica por RNA-seq são apresentadas na Figura 5. O mRNA de uma amostra biológica de interesse é inicialmente isolado e então utilizado no preparo de bibliotecas para sequenciamento. Após o sequenciamento, as sequências obtidas (ou *reads*) são alinhadas contra uma referência, que pode ser o genoma ou o transcriptoma do organismo analisado. Caso nenhuma referência esteja disponível, os próprios *reads* de RNA-seq podem ser utilizados na obtenção de uma sequência de referência (montagem *de novo* do transcriptoma). Entretanto, devido ao pequeno tamanho destas sequências, é comum que montagens que utilizem apenas *reads* de RNA-seq apresentem-se relativamente fragmentadas. Apesar disso, esta estratégia permite que a técnica de RNA-seq seja utilizada em análises de expressão gênica de organismos que possuem poucos ou nenhum dado molecular disponível. Os arquivos obtidos após o alinhamento podem ser utilizados para a visualização do transcriptoma, uma abordagem interessante para a anotação manual de regiões codantes de um gene, por exemplo. Após o alinhamento na referência, a quantidade de sequências obtidas para cada gene é computada e, então, normalizada para permitir a comparação entre diferentes amostras ou genes. Existem diversos métodos e *softwares* disponíveis para a normalização dos dados e identificação de genes diferencialmente expressos, variando principalmente quanto ao modelo estatístico adotado. Entretanto, a lógica da análise permanece a mesma e se baseia no fato de que a quantidade de sequências obtidas para um determinado transcrito é diretamente proporcional à sua abundância na amostra original. Ou seja, quanto mais expresso for um gene, mais sequências deverão ser obtidas. Como resultado da análise, obtém-se uma lista dos genes em estudo com os respectivos valores de expressão e significância estatística quando diferentes amostras são comparadas. A interpretação destes dados e a correlação com fenômenos biológicos constituem a etapa final do processo. No entanto, considerando-se a importância e complexidade desta etapa, não é exagero considera-la como o verdadeiro início do trabalho.

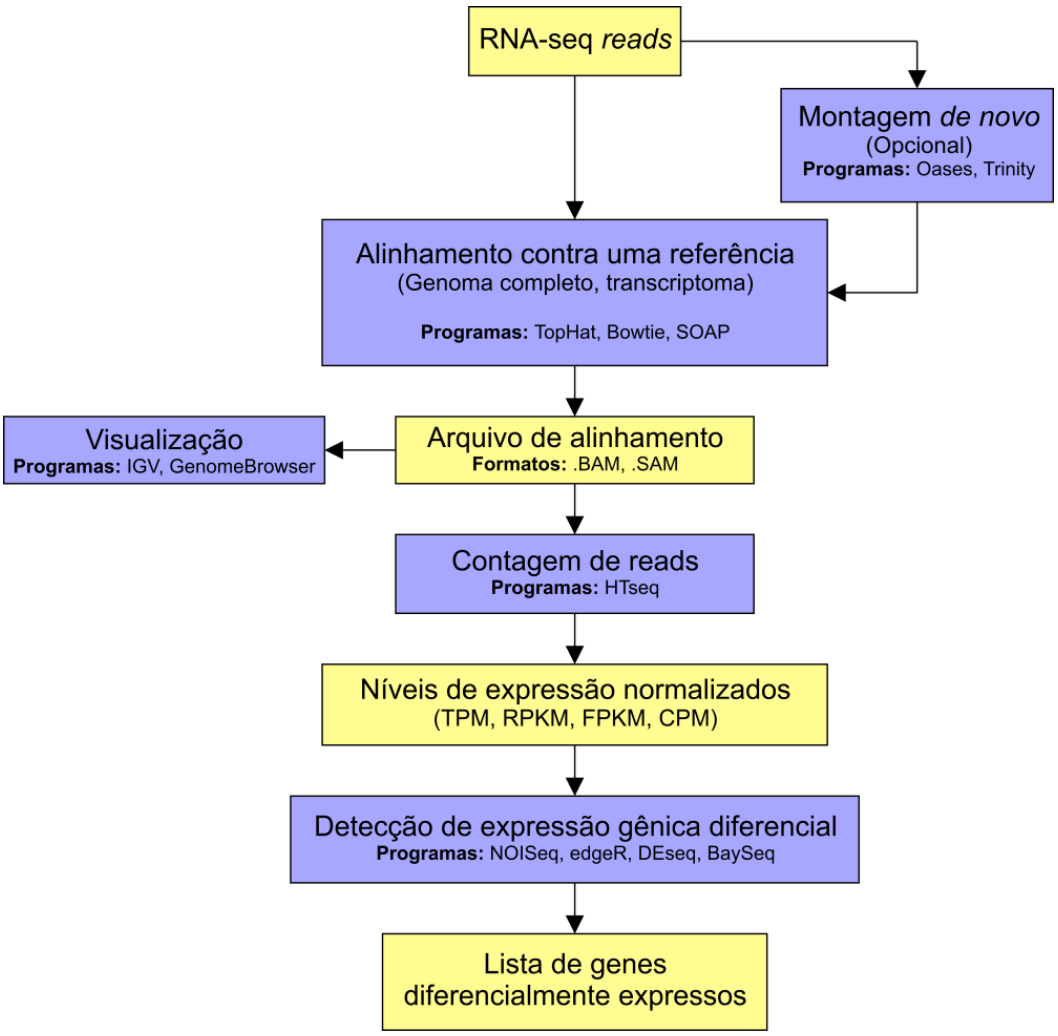

Figura 5. Principais etapas em análises de expressão gênica utilizando-se RNA-seq. Arquivos são marcados em amarelos e procedimentos são apresentados em azul.

OBJETIVO

Considerando-se o limitado conhecimento sobre os mecanismos moleculares que governam o desenvolvimento da vassoura de bruxa, a presente tese teve como objetivo central a "Construção de um modelo que explique a base molecular da interação entre o cacaueiro e o fungo *M. perniciosa"*.

Utilizamos as tecnologias de sequenciamento de nova geração (RNA-seq) para realizar uma análise transcriptômica abrangente desta doença e estabelecer bases para estudos mais específicos. Os dados de expressão gênica forneceram uma primeira linha de evidências sobre aspectos relevantes da doença, que foram então aprofundados em trabalhos adicionais. Os resultados apresentados nesta tese estão organizados em seis capítulos, conforme ilustrado na Figura 6.

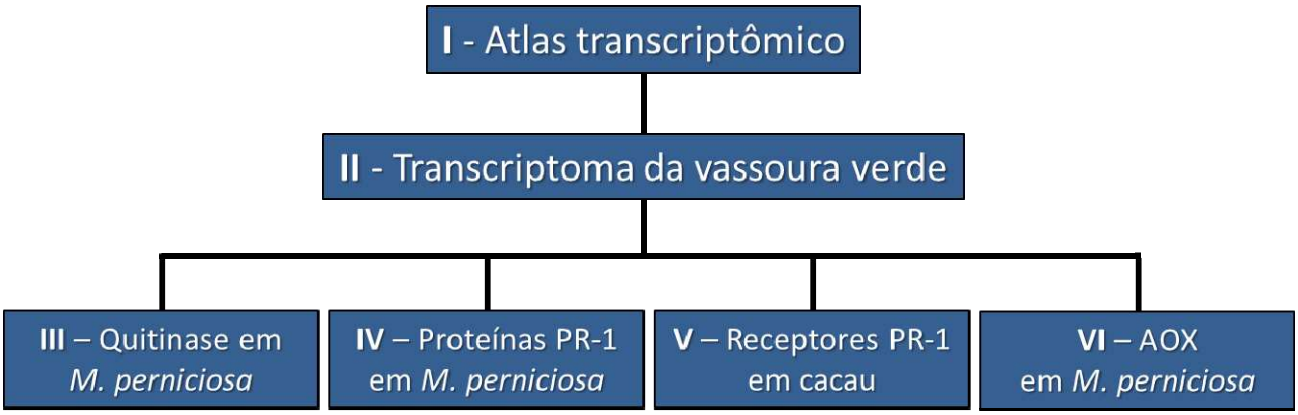

Figura 6. Organização geral desta tese. O primeiro capítulo apresenta uma visão geral do Atlas Transcriptômico da Vassoura de Bruxa. Dentre as condições que compõem esta base de dados, realizamos uma análise detalhada do estágio de vassoura verde da doença, a qual é apresentada no segundo capítulo. A análise do transcriptoma da vassoura verde revelou genes relevantes para o estabelecimento da doença que foram, então, alvos de estudos mais aprofundados apresentados nos demais capítulos desta tese.

REFERÊNCIAS BIBLIOGRÁFICAS

't Hoen PA, Ariyurek Y, Thygesen HH, Vreugdenhil E, Vossen RH, de Menezes RX, Boer JM, van Ommen GJ, den Dunnen JT (2008) Deep sequencing-based expression analysis shows major advances in robustness, resolution and inter-lab portability over five microarray platforms. Nucleic Acids Res **36**: e141

Abecasis GR, Auton A, Brooks LD, DePristo MA, Durbin RM, Handsaker RE, Kang HM, Marth GT, McVean GA (2012) An integrated map of genetic variation from 1,092 human genomes. Nature **491**: 56-65

Adams MD, Celniker SE, Holt RA, Evans CA, Gocayne JD, Amanatides PG, Scherer SE, Li PW, Hoskins RA, Galle RF, *et al.* (2000) The genome sequence of *Drosophila melanogaster*. Science **287**: 2185-2195

Adams MD, Kelley JM, Gocayne JD, Dubnick M, Polymeropoulos MH, Xiao H, Merril CR, Wu A, Olde B, Moreno RF, *et al.* (1991) Complementary DNA sequencing: expressed sequence tags and human genome project. Science **252**: 1651-1656

Aime MC, Phillips-Mora W (2005) The causal agents of witches' broom and frosty pod rot of cacao (chocolate, *Theobroma cacao*) form a new lineage of Marasmiaceae. Mycologia **97**: 1012-1022

Almeida O, Chiacchio F, Rocha H (1997) Sobrevivência de *Crinipellis perniciosa* (Stahel) Singer em vassouras secas de cacaueiros (*Theobroma cacao* L.) do estado da Bahia. Agrotrópica **9**: 23-28

Alverson WS, Whitlock BA, Nyffeler R, Bayer C, Baum DA (1999) Phylogeny of the core Malvales: evidence from ndhF sequence data. Am J Bot **86**: 1474

Andebrhan T, Figueira A, Yamada MM, Cascardo J, Furtek DB (1999) Molecular fingerprinting suggests two primary outbreaks of witches' broom disease (*Crinipellis perniciosa*) of *Theobroma cacao* in Bahia, Brazil. European Journal of Plant Pathology **105**: 167-175

Argout X, Fouet O, Wincker P, Gramacho K, Legavre T, Sabau X, Risterucci AM, Da SC, Cascardo J, Allegre M, *et al.* (2008) Towards the understanding of the cocoa transcriptome: Production and analysis of an exhaustive dataset of ESTs of *Theobroma cacao* L. generated from various tissues and under various conditions. BMC Genomics **9**: 512

Argout X, Salse J, Aury JM, Guiltinan MJ, Droc G, Gouzy J, Allegre M, Chaparro C, Legavre T, Maximova SN, *et al.* (2011) The genome of *Theobroma cacao*. Nat Genet **43**: 101-108

Bailey BA (1995) Purification of A Protein from Culture Filtrates of *Fusarium oxysporum* That Induces Ethylene and Necrosis in Leaves of *Erythroxylum coca*. Phytopathology **85**: 1250-1255

Baker R (1957) Witches´ broom disease of cocoa (*Marasmius perniciosa* Stahel). Phytopathological paper. Commonwealth Mycological Institute, Kew,

Bartley BGD (2005) The Genetic Diversity of Cacao and its Utilization. CAB International, Wallingford,

Bastos C (1989) Avaliação de Fungicidas Sistêmicos no Controle da Vassoura-de-Bruxa do Cacaueiro. Agrotrópica **1**: 128-132

Bastos C, Dias J (1992) Redução na Produção de Basidiocarpos de *Crinipellis perniciosa* por *Trichoderma viride*. Summa Phytopathologica **18**: 235-238

Blattner FR, Plunkett G, III, Bloch CA, Perna NT, Burland V, Riley M, Collado-Vides J, Glasner JD, Rode CK, Mayhew GF, *et al.* (1997) The complete genome sequence of *Escherichia coli* K-12. Science **277**: 1453-1462

Calle H, Cook AA, Fernando SY (1982) Histology of witches' broom caused in cacao by *Crinipellis perniciosa*. Phytopathology **72**: 1479-1481

Caribé dos Santos AC, Sena JA, Santos SC, Dias CV, Pirovani CP, Pungartnik C, Valle RR, Cascardo JC, Vincentz M (2009) dsRNA-induced gene silencing in *Moniliophthora perniciosa*, the causal agent of witches' broom disease of cacao. Fungal Genet Biol **46**: 825-836

Carulli JP, Artinger M, Swain PM, Root CD, Chee L, Tulig C, Guerin J, Osborne M, Stein G, Lian J, *et al.* (1998) High throughput analysis of differential gene expression. J Cell Biochem Suppl **30-31**: 286-296

Coe SD, Coe MD (1996) The true history of chocolate. Thames & Hudson, New York,

de Oliveira BV, Teixeira GS, Reis O, Barau JG, Teixeira PJ, do Rio MC, Domingues RR, Meinhardt LW, Paes Leme AF, Rincones J, *et al.* (2012) A potential role for an extracellular methanol oxidase secreted by *Moniliophthora perniciosa* in Witches' broom disease in cacao. Fungal Genet Biol **49**: 922-932

DeRisi J, Penland L, Brown PO, Bittner ML, Meltzer PS, Ray M, Chen Y, Su YA, Trent JM (1996) Use of a cDNA microarray to analyse gene expression patterns in human cancer. Nat Genet **14**: 457-460

Diatchenko L, Lau YF, Campbell AP, Chenchik A, Moqadam F, Huang B, Lukyanov S, Lukyanov K, Gurskaya N, Sverdlov ED, *et al.* (1996) Suppression subtractive hybridization: a method for generating differentially regulated or tissue-specific cDNA probes and libraries. Proc Natl Acad Sci U S A **93**: 6025-6030

Durbin RM, Abecasis GR, Altshuler DL, Auton A, Brooks LD, Durbin RM, Gibbs RA, Hurles ME, McVean GA (2010) A map of human genome variation from population-scale sequencing. Nature **467**: 1061-1073

Eid J, Fehr A, Gray J, Luong K, Lyle J, Otto G, Peluso P, Rank D, Baybayan P, Bettman B, *et al.* (2009) Real-time DNA sequencing from single polymerase molecules. Science **323**: 133-138

Evans HC (1980) Pleomorphism in *Crinipellis perniciosa*, causal agent of witches' broom disease of cocoa. Transactions of the British Mycological Society **74**: 515-523

Evans HC (2007) Cacao diseases-the trilogy revisited. Phytopathology **97**: 1640-1643

Formighieri EF, Tiburcio RA, Armas ED, Medrano FJ, Shimo H, Carels N, Goes-Neto A, Cotomacci C, Carazzolle MF, Sardinha-Pinto N, *et al.* (2008) The mitochondrial genome of the phytopathogenic basidiomycete *Moniliophthora perniciosa* is 109 kb in size and contains a stable integrated plasmid. Mycol Res **112**: 1136-1152

Frias G, Purdy L, Schmidt R (1991) Infection biology of *Crinipellis perniciosa* on vegetative flushes of cacao. Plant Disease **75**: 552-556

Garcia O, Macedo JA, Tiburcio R, Zaparoli G, Rincones J, Bittencourt LM, Ceita GO, Micheli F, Gesteira A, Mariano AC, *et al.* (2007) Characterization of necrosis and ethylene-inducing proteins (NEP) in the basidiomycete *Moniliophthora perniciosa*, the causal agent of witches' broom in *Theobroma cacao*. Mycol Res **111**: 443-455

Genome 10K Community of Scientists (2009) Genome 10K: a proposal to obtain whole-genome sequence for 10,000 vertebrate species. J Hered **100**: 659-674

Gesteira AS, Micheli F, Carels N, Da Silva AC, Gramacho KP, Schuster I, Macedo JN, Pereira GA, Cascardo JC (2007) Comparative analysis of expressed genes from cacao meristems infected by *Moniliophthora perniciosa*. Ann Bot **100**: 129-140

Goffeau A, Barrell BG, Bussey H, Davis RW, Dujon B, Feldmann H, Galibert F, Hoheisel JD, Jacq C, Johnston M, *et al.* (1996) Life with 6000 genes. Science **274**: 546, 563-546, 567

Henderson JS, Joyce RA, Hall GR, Hurst WJ, McGovern PE (2007) Chemical and archaeological evidence for the earliest cacao beverages. Proc Natl Acad Sci U S A **104**: 18937-18940

Hurst WJ, Tarka SM, Jr., Powis TG, Valdez F, Jr., Hester TR (2002) Cacao usage by the earliest Maya civilization. Nature **418**: 289-290

ICCO (2012) ICCO Quarterly Bulletin of Cocoa Statistics, Vol. XXXIV, No.4, Cocoa year 2007/08. http://www.icco org/statistics/production aspx.

Jones PG, Allaway D, Gilmour DM, Harris C, Rankin D, Retzel ER, Jones CA (2002) Gene discovery and microarray analysis of cacao (*Theobroma cacao* L.) varieties. Planta **216**: 255-264

Kaul S, Koo HL, Jenkins J, Rizzo M, Rooney T, Tallon LJ, Feldblyum T, Nierman W, Benito MI, Lin XY, *et al.* (2000) Analysis of the genome sequence of the flowering plant *Arabidopsis thaliana*. Nature **408**: 796-815

Lander ES, Int Human Genome Sequencing Consortium, Linton LM, Birren B, Nusbaum C, Zody MC, Baldwin J, Devon K, Dewar K, Doyle M, *et al.* (2001) Initial sequencing and analysis of the human genome. Nature **409**: 860-921

Leal GA, Albuquerque PS, Figueira A (2007) Genes differentially expressed in *Theobroma cacao* associated with resistance to witches' broom disease caused by *Crinipellis perniciosa*. Mol Plant Pathol **8**: 279-292

Lima E, Barros E, Araújo J, Thiébaut J (1991) Frequência da Poda Fitossanitária no Controle da Vassoura-de-bruxa do Cacaueiro. Agrotrópica **3**: 75-80

Lima JO, dos Santos JK, Pereira JF, de Resende ML, de Araujo EF, de Queiroz MV (2003) Development of a transformation system for *Crinipellis perniciosa*, the causal agent of witches' broom in cocoa plants. Curr Genet **42**: 236-240

Lobão D, Setenta W, Lobão E, Curvelo K, Valle R (2007) Cacau cabruca: sistema agrossilvicultural tropical. In R Valle, ed, Ciência, Tecnologia e Manejo do Cacaueiro. Gráfica e Editora Vital LTDA, Ilhéus, pp 290-323

Lopes FJ, de Queiroz MV, Lima JO, Silva VAO, de Araujo EF (2008) Restriction enzyme improves the efficiency of genetic transformations in *Moniliophthora perniciosa*, the causal agent of witches' broom disease in *Theobroma cacao*. Brazilian Archives of Biology and Technology **51**: 27-34

Marioni JC, Mason CE, Mane SM, Stephens M, Gilad Y (2008) RNA-seq: an assessment of technical reproducibility and comparison with gene expression arrays. Genome Res **18**: 1509-1517

Meinhardt LW, Bellato CM, Rincones J, Azevedo RA, Cascardo JC, Pereira GA (2006) In vitro production of biotrophic-like cultures of *Crinipellis perniciosa*, the causal agent of witches' broom disease of *Theobroma cacao*. Curr Microbiol **52**: 191-196

Meinhardt LW, Rincones J, Bailey BA, Aime MC, Griffith GW, Zhang D, Pereira GA (2008) *Moniliophthora perniciosa*, the causal agent of witches' broom disease of cacao: what's new from this old foe? Mol Plant Pathol **9**: 577-588

Metzker ML (2010) Sequencing technologies - the next generation. Nat Rev Genet **11**: 31-46

Mondego JM, Carazzolle MF, Costa GG, Formighieri EF, Parizzi LP, Rincones J, Cotomacci C, Carraro DM, Cunha AF, Carrer H, *et al.* (2008) A genome survey of *Moniliophthora perniciosa* gives new insights into Witches' Broom Disease of cacao. BMC Genomics **9**: 548

Mortazavi A, Williams BA, McCue K, Schaeffer L, Wold B (2008) Mapping and quantifying mammalian transcriptomes by RNA-Seq. Nat Methods **5**: 621-628

Motamayor JC, Lachenaud P, da Silva E Mota JW, Loor R, Kuhn DN, Brown JS, Schnell RJ (2008) Geographic and genetic population differentiation of the Amazonian chocolate tree (*Theobroma cacao* L). PLoS One **3**: e3311

Nagalakshmi U, Wang Z, Waern K, Shou C, Raha D, Gerstein M, Snyder M (2008) The transcriptional landscape of the yeast genome defined by RNA sequencing. Science **320**: 1344-1349

Orchard J, Collin H, Hardwick K, Isaac S (1994) Changes in morphology and measurement of cytokin levels during the development of witches' broom on cocoa. Plant Pathol **43**: 65-72

Paradis L (1979) Le cacao précolombien: monnaies d'échange et breuvage des dieux. J Agric Trad Bot Appl **26**: 3-4

Penman D, Britton G, Hardwick K, Collin H, Isaac S (2000) Chitin as a measure of biomass of *Crinipellis perniciosa*, causal agent of witches' broom disease of *Theobroma cacao*. Mycol Res **104**: 671-675

Pereira JL, deAlmeida LCC, Santos SM (1996) Witches' broom disease of cocoa in Bahia: Attempts at eradication and containment. Crop Protection **15**: 743-752

Pereira J (2000) Management of Witches´ Broom disease of cocoa: a contemporary retrospective. Cocoa Produces´s Alliance, Lagos, Nigeria,

Petricoin III EF, Hackett JL, Lesko LJ, Puri RK, Gutman SI, Chumakov K, Woodcock J, Feigal DW, Jr., Zoon KC, Sistare FD (2002) Medical applications of microarray technologies: a regulatory science perspective. Nat Genet **32 Suppl**: 474-479

Pires J, Luz E (1995) Resistência à Vassoura-de-Bruxa na espécie *Theobroma cacao*. Fitopatologia Brasileira **20**: 303

Powis TG, Cyphers A, Gaikwad NW, Grivetti L, Cheong K (2011) Cacao use and the San Lorenzo Olmec. Proc Natl Acad Sci U S A **108**: 8595-8600

Purdy LH, Schmidt RA (1996) Status of cacao witches' broom: biology, epidemiology, and management. Annu Rev Phytopathol **34**: 573-594

Qutob D, Kamoun S, Gijzen M (2002) Expression of a *Phytophthora sojae* necrosis-inducing protein occurs during transition from biotrophy to necrotrophy. Plant J **32**: 361-373

Rincones J, Mazotti GD, Griffith GW, Pomela A, Figueira A, Leal GA, Jr., Queiroz MV, Pereira JF, Azevedo RA, Pereira GA, *et al.* (2006) Genetic variability and chromosome-length polymorphisms of the witches' broom pathogen *Crinipellis perniciosa* from various plant hosts in South America. Mycol Res **110**: 821-832

Rincones J, Meinhardt LW, Vidal BC, Pereira GA (2003) Electrophoretic karyotype analysis of *Crinipellis perniciosa*, the causal agent of witches' broom disease of *Theobroma cacao*. Mycol Res **107**: 452-458

Rincones J, Scarpari LM, Carazzolle MF, Mondego JM, Formighieri EF, Barau JG, Costa GG, Carraro DM, Brentani HP, Vilas-Boas LA, *et al.* (2008) Differential gene expression between the biotrophic-like and saprotrophic mycelia of the witches' broom pathogen *Moniliophthora perniciosa*. Mol Plant Microbe Interact **21**: 891-908

Sanger F, Nicklen S, Coulson AR (1977) DNA sequencing with chain-terminating inhibitors. Biotechnology **24**: 104-108

Scarpari LM, Meinhardt LW, Mazzafera P, Pomella AW, Schiavinato MA, Cascardo JC, Pereira GA (2005) Biochemical changes during the development of witches' broom: the most important disease of cocoa in Brazil caused by *Crinipellis perniciosa*. J Exp Bot **56**: 865-877

Schena M, Shalon D, Davis RW, Brown PO (1995) Quantitative monitoring of gene expression patterns with a complementary DNA microarray. Science **270**: 467-470

Shendure J (2008) The beginning of the end for microarrays? Nat Methods **5**: 585-587

Silva SDVM, Matsuoka K (1999) Histologia da Interação *Crinipellis perniciosa* em Cacaueiros Suscetível e Resistente à Vassoura de Bruxa. Fitopatologia Brasileira **24**: 54-59

Simpson AJ, Reinach FC, Arruda P, Abreu FA, Acencio M, Alvarenga R, Alves LM, Araya JE, Baia GS, Baptista CS, *et al.* (2000) The genome sequence of the plant pathogen *Xylella fastidiosa*. Nature **406**: 151-159

Stanley NR, Britton RA, Grossman AD, Lazazzera BA (2003) Identification of catabolite repression as a physiological regulator of biofilm formation by *Bacillus subtilis* by use of DNA microarrays. J Bacteriol **185**: 1951-1957

Teixeira PJ, Thomazella DP, Vidal RO, do Prado PF, Reis O, Baroni RM, Franco SF, Mieczkowski P, Pereira GA, Mondego JM (2012) The fungal pathogen *Moniliophthora perniciosa* has genes similar to plant PR-1 that are highly expressed during its interaction with cacao. PLoS One **7**: e45929

Thomas E, van ZM, Loo J, Hodgkin T, Galluzzi G, van EJ (2012) Present spatial diversity patterns of *Theobroma cacao* L. in the neotropics reflect genetic differentiation in pleistocene refugia followed by human-influenced dispersal. PLoS One **7**: e47676

Thomazella DP, Teixeira PJ, Oliveira HC, Saviani EE, Rincones J, Toni IM, Reis O, Garcia O, Meinhardt LW, Salgado I, *et al.* (2012a) The hemibiotrophic cacao pathogen *Moniliophthora perniciosa* depends on a mitochondrial alternative oxidase for biotrophic development. New Phytol **194**: 1025-1034

Thomazella DP, Teixeira PJ, Pereira GA (2012b) Biotecnologia na Cultura do Cacaueiro. In GMA Cançado, LN Londe, eds, Biotecnologia Aplicada à Agropecuária, Ed 1. Grafica e Editora Sul Minas, Poços de Caldas, pp 145-170

Tiburcio RA, Costa GG, Carazzolle MF, Mondego JM, Schuster SC, Carlson JE, Guiltinan MJ, Bailey BA, Mieczkowski P, Meinhardt LW, *et al.* (2010) Genes acquired by horizontal transfer are potentially involved in the evolution of phytopathogenicity in *Moniliophthora perniciosa* and *Moniliophthora roreri*, two of the major pathogens of cacao. J Mol Evol **70**: 85-97

Velculescu VE, Zhang L, Vogelstein B, Kinzler KW (1995) Serial analysis of gene expression. Science **270**: 484-487

Venter JC, Adams MD, Myers EW, Li PW, Mural RJ, Sutton GG, Smith HO, Yandell M, Evans CA, Holt RA, *et al.* (2001) The sequence of the human genome. Science **291**: 1304-1351

Verica JA, Maximova SN, Strem MD, Carlson JE, Bailey BA, Guiltinan MJ (2004) Isolation of ESTs from cacao (*Theobroma cacao* L.) leaves treated with inducers of the defense response. Plant Cell Rep **23**: 404-413

Vettore AL, da Silva FR, Kemper EL, Souza GM, da Silva AM, Ferro MI, Henrique-Silva F, Giglioti EA, Lemos MV, Coutinho LL, *et al.* (2003) Analysis and functional annotation of an expressed sequence tag collection for tropical crop sugarcane. Genome Res **13**: 2725-2735

Wheeler B (1985) The growth of *Crinipellis perniciosa* in living and dead cocoa tissue. Symp Ser Br Mycol Soc **10**: 103-116

Wheeler DA, Srinivasan M, Egholm M, Shen Y, Chen L, McGuire A, He W, Chen YJ, Makhijani V, Roth GT, *et al.* (2008) The complete genome of an individual by massively parallel DNA sequencing. Nature **452**: 872-876

Zaparoli G, Barsottini MR, de Oliveira JF, Dyszy F, Teixeira PJ, Barau JG, Garcia O, Costa-Filho AJ, Ambrosio AL, Pereira GA, *et al.* (2011) The crystal structure of necrosis- and ethylene-inducing protein 2 from the causal agent of cacao's Witches' Broom disease reveals key elements for its activity. Biochemistry **50**: 9901-9910

Capítulo I

A comprehensive transcriptome atlas for the study of the witches' broom disease of cacao

Paulo José P.L. Teixeira, Osvaldo Reis, Daniela P.T. Thomazella, Gustavo G.L. Costa, Piotr Mieczkowski, Gonçalo A.G. Pereira

APRESENTAÇÃO

O primeiro capítulo desta tese apresenta a construção e as análises globais do Atlas Transcriptômico da Vassoura de Bruxa. Iniciada em 2009, esta iniciativa foi favorecida por dois fatores principais: (I) O grande amadurecimento do Projeto Genoma Vassoura de Bruxa nos últimos anos, principalmente no que se diz respeito à obtenção de todo ciclo de vida do patógeno como também da doença em ambiente controlado de laboratório. (II) O fácil acesso às tecnologias de sequenciamento de nova geração, garantido através de uma colaboração estabelecida com a Universidade da Carolina do Norte (EUA). O Atlas Transcriptômico é baseado em uma série de experimentos que tiveram como objetivo amostrar condições relevantes do desenvolvimento do fungo *Moniliophthora perniciosa* e também da progressão da doença. Por se tratar de uma ferramenta de caráter exploratório, optou-se inicialmente por sequenciar os transcriptomas de um grande número de diferentes amostras ao invés de realizar repetições de uma quantidade limitada de amostras. Posteriormente, sequenciamentos adicionais foram realizados de forma a permitir análises detalhadas de condições de interesse (por exemplo, vassoura verde – apresentada no Capítulo II desta tese). O Atlas Transcriptômico da Vassoura de Bruxa tem suportado uma série de trabalhos em nosso laboratório, permitindo a investigação de aspectos antes inexplorados assim como a formulação de novas hipóteses quanto ao desenvolvimento da doença vassoura de bruxa do cacaueiro.

INTRODUÇÃO

O basidiomiceto *Moniliophthora perniciosa* é o agente etiológico da doença vassoura de bruxa no cacaueiro (*Theobroma cacao*), um dos principais fatores limitantes da produção de cacau nas Américas. Em 1989, relatou-se pela primeira vez a ocorrência da doença no sul da Bahia, principal região produtora brasileira (Pereira *et al.*, 1996). Desde então, a produção cacaueira do Brasil foi drasticamente reduzida e o país, que era um dos principais produtores de amêndoas de cacau do mundo até então, transformou-se em poucos anos em um importador do produto (Purdy & Schmidt, 1996; Meinhardt *et al.*, 2008). *M. perniciosa* pode infectar qualquer tecido meristemático em desenvolvimento do seu hospedeiro, incluindo ramos, frutos e flores (Meinhardt *et al.*, 2008). O ciclo de vida deste fungo é classificado como hemibiotrófico, havendo dois estágios miceliares distintos que se desenvolvem em paralelo aos sintomas observados na planta (Evans, 1980). Inicialmente, o fungo assume um estágio biotrófico e infecta tecidos vivos do cacaueiro. Nesta fase da doença, são observadas drásticas alterações morfológicas no tecido infectado, particularmente a hipertrofia e perda de dominância apical em ramos, o que dá origem a estruturas denominadas “vassouras verdes”. Ainda, a infecção de frutos resulta em amadurecimento anormal e deformações no tecido da planta, enquanto que a infecção de flores leva ao desenvolvimento de pequenos frutos partenocárpicos com aspecto de morangos (Meinhardt *et al.*, 2008). Com a progressão da doença, ocorre morte do tecido vegetal e o fungo assume seu segundo estágio, classificado como necrotrófico. Neste estágio da doença, o patógeno produz os basidiomas que então liberam esporos capazes de infectar novas plantas (Wheeler, 1985).

Análises de expressão gênica em larga escala estabeleceram-se como uma poderosa ferramenta de pesquisa em biologia (Brady *et al.*, 2006). O estudo dos principais organismos modelo envolveu a construção de extensivas bases de dados reunindo um grande número de experimentos em genômica funcional. Por exemplo, a iniciativa AtGenExpress constitui um importante esforço para desvendar o transcriptoma da planta *Arabidopsis thaliana* (Kilian *et al.*, 2007). De maneira similar, o projeto *The Riken mouse genome encyclopedia* forneceu bases para

a identificação e anotação de milhares de genes expressos em camundongo (Hayashizaki, 2003). Tais projetos foram baseados nas tecnologias tradicionais de *microarrays* e/ou sequenciamento Sanger de bibliotecas de cDNA.

Análises de expressão gênica em larga escala foram anteriormente realizadas para o estudo da vassoura de bruxa do cacaueiro (Rincones *et al.*, 2008; Pires *et al.*, 2009; Leal *et al.*, 2010). Estes trabalhos pioneiros investigaram as diferenças entre os micélios biotrófico e necrotrófico de *M. perniciosa* em condições *in vitro* de desenvolvimento (Rincones *et al.*, 2008), a formação de estruturas reprodutivas neste fungo (Pires *et al.*, 2009) e o efeito da deprivação de nitrogênio na expressão gênica global do patógeno (Leal *et al.*, 2010). Além disso, análises de expressão gênica também revelaram algumas das respostas do cacaueiro à infecção (Gesteira *et al.*, 2007; Leal *et al.*, 2007; da Hora Junior *et al.*, 2012). Entretanto, a complexidade metodológica e os altos custos das estratégias empregadas representam importantes limitações nestes estudos. Por exemplo, dos 17.008 genes de *M. perniciosa*, apenas 2.528 foram analisados no trabalho de Rincones *et al*., (2008). Similarmente, uma análise recente baseada em *macroarrays* avaliou apenas 2.855 dos cerca de 30.000 genes do cacaueiro (da Hora Junior *et al.*, 2012).

Os recentes avanços nas tecnologias de sequenciamento de DNA têm permitido a realização de análises de expressão gênica de forma eficiente a custos bastante reduzidos (Metzker, 2010). Ainda, a técnica RNA-seq oferece como vantagens a menor complexidade metodológica e uma maior sensibilidade em relação a tecnologias anteriores (Marioni *et al.*, 2008). Com o objetivo de ampliar nosso conhecimento a respeito da vassoura de bruxa do cacaueiro e estabelecer uma base para o estudo dessa doença, iniciamos a construção de um extensivo banco de dados denominado Atlas Transcriptômico da Vassoura de Bruxa. Utilizando RNA-seq, cerca de 60 bibliotecas representativas das mais variadas condições de desenvolvimento de *M. perniciosa* *in vitro* e *in planta* foram sequenciadas. Esta iniciativa constitui um importante avanço no entendimento desta doença e abre novas possibilidades para a realização de estudos funcionais tanto com *M. perniciosa* como também com o cacaueiro.

MATERIAIS E MÉTODOS

Isolados de *Moniliophthora perniciosa* e variedades de *Theobroma cacao*

Os experimentos foram realizados com os isolados FA553 e BP10 de *M. perniciosa*, os quais foram coletados no município de Ilhéus (BA) e apresentam patogenicidade a cacaueiros suscetíveis. O isolado APS1, representativo do biótipo S de *M. perniciosa* e originário do estado de Minas Gerais, também foi utilizado. A variedade de *Theobroma cacao* utilizada foi a "Comum", a qual é suscetível à vassoura de bruxa. As plântulas foram mantidas em casa de vegetação a temperatura média de 26°C, umidade acima de 80% e fotoperíodo de 12h.

Obtenção de basidiomas e basidiósporos de *Moniliophthora perniciosa*

Basidiomas foram obtidos utilizando-se a metodologia proposta por (Griffith & Hedger, 1993) com modificações. Este método consiste na utilização de um substrato à base de galhos e folhas triturados de cacaueiro (77% p/v), aveia (20% p/v), $CaSO_4$ (3% p/v) e água suficiente para formar uma mistura pastosa. O fungo em estágio necrotrófico foi inoculado neste substrato e mantido em estufa a 25°C. Após a completa colonização pelo fungo (aproximadamente um mês), o substrato foi pendurado dentro de uma caixa de acrílico e regado diariamente para manutenção da umidade acima de 80%. Os basidiomas produzidos tiveram os esporos coletados em uma solução previamente descrita por Frias *et al.,* (1995) (glicerol 16%; MES 0,01 M; Tween 20 0,01%; pH 6,1). O glicerol presente nesta solução impede a germinação dos basidiósporos durante a coleta e também age como um crioprotetor, permitindo o congelamento dos basidiósporos para armazenamento.

Cultivo *in vitro* dos micélios biotrófico e necrotrófico de *M. perniciosa*

A fase necrotrófica de *M. perniciosa* foi mantida em meio de cultura sólido MYEA (5 g/L de extrato de levedura, 17 g/L de extrato malte e 20 g/L de ágar), em estufa à 28°C. O cultivo deste micélio em meio líquido foi realizado inoculando-se pequenos cubos da cultura em 50 mL do novo

meio. Para obtenção da fase biotrófica, aproximadamente 3,8 x 10^5 basidiósporos foram inoculados em 50 mL de meio de cultura líquido específico para manutenção da fase biotrófica (5 g/L de extrato de levedura Difco™; 50 mL/L de glicerol; 2,5 g/L de K_2HPO_4; e 1 mL/L elementos traços diluídos em 100 mL de água: 500 mg de $FeSO_4 \bullet 7H_2O$; 156 mg de $MnSO_4$; 167 mg de $ZnCl_2$; 200 mg de $CoCl_2$; Meinhardt *et al.*, 2006). As culturas foram mantidas a 28°C e agitação constante de 120 rpm.

Infecção de plântulas

As infecções de plântulas foram realizadas segundo o procedimento descrito por Frias *et al.* (1995). As plântulas a serem inoculadas foram inicialmente submetidas a uma câmara úmida, sendo cobertas por sacos plásticos previamente umedecidos para induzir a abertura dos estômatos. Este tratamento foi realizado 24 horas antes da inoculação dos basidiósporos. Posteriormente, gotas de aproximadamente 30 µL de suspensão de esporos (concentração aproximada de 10^5 esporos/mL) foram aplicadas sobre o meristema apical em atividade das plântulas. A câmara úmida foi, então, mantida por mais 48 horas.

Coleta de material para sequenciamento de transcriptomas

Uma colaboração estabelecida com a *High Throughtput Sequencing Facility* da Universidade da Carolina do Norte (EUA) nos garantiu acesso às mais modernas tecnologias de sequenciamento de DNA. Para a construção do Atlas Transcriptômico da Vassoura de Bruxa, diferentes amostras foram coletadas de forma a representar condições relevantes para o estudo da doença. As seções seguintes descrevem os experimentos realizados para a obtenção de tais amostras.

<u>*Micélios biotrófico, saprotrófico e em transição de fase*</u> – O fungo *M. perniciosa* foi cultivado a partir de basidiósporos em meio de cultura para manutenção da fase biotrófica (Meinhardt *et al.*, 2006).

Coletas do micélio foram então realizadas em três momentos de interesse (Figura 1): após sete dias de crescimento, representando o micélio monocariótico (biotrófico); após quatorze dias de crescimento, representando a transição de fase; e após vinte e oito dias de crescimento, representando micélio dicariótico (necrotrófico). Antes de cada coleta, o micélio foi observado em microscópio para a confirmação do estágio de desenvolvimento do fungo. Adicionalmente, micélio necrotrófico previamente crescido em meio MYEA foi cultivado nas mesmas condições e coletado nos mesmos pontos do micélio em desenvolvimento acima descrito.

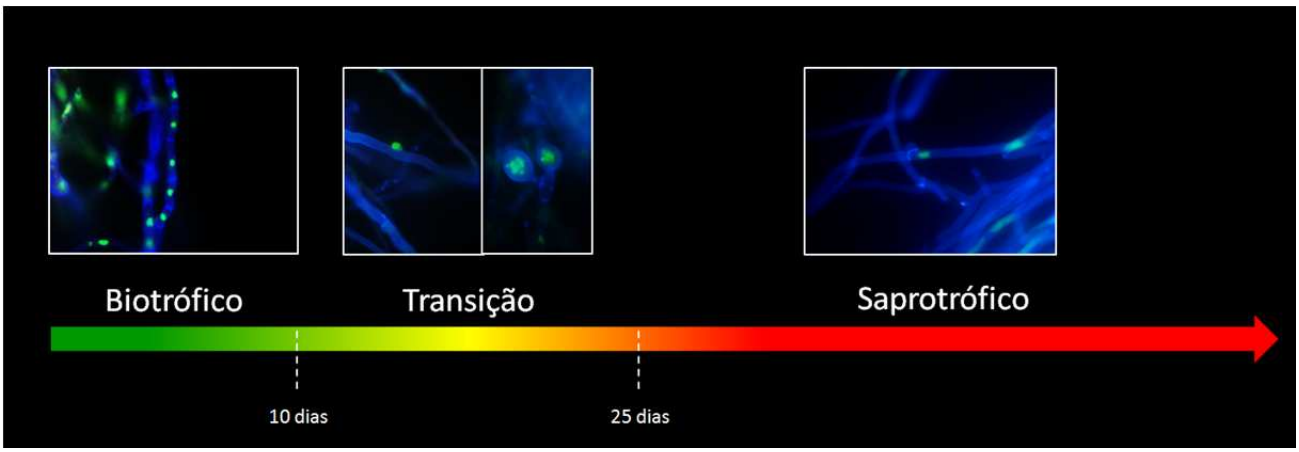

Figura 1. Padrão do desenvolvimento *in vitro* de *M. perniciosa* a partir da germinação dos esporos. Durante aproximadamente 10 dias de cultivo é possível identificar na cultura apenas hifas biotróficas (monocarióticas), que apresentam crescimento pouco intenso, um núcleo por célula e não possuem grampos de conexão. A amostra representante deste estágio foi coletada após 7 dias de cultivo. A partir do décimo dia, sinais de transição para a fase saprotrófica tornam-se gradativamente evidentes, iniciando-se a formação de grampos de conexão.Além disso, verifica-se a existência de células inchadas e multinucleadas. O material neste estágio foi coletado após 14 dias de cultivo. Após cerca de 25 dias, o fungo é encontrado sobretudo em seu estágio necrotrófico, apresentando grande massa miceliar e células binucleadas com grampos de conexão. A amostra representante deste estágio foi coletada após 28 dias de cultivo.

Interação em vassouras – Este experimento foi realizado visando à análise de expressão de genes do fungo e do cacaueiro durante a progressão da vassoura de bruxa. Além disso, o experimento permite a comparação entre os padrões de expressão gênica do fungo cultivado *in planta* e *in vitro*. Plântulas de cacau foram inoculadas com basidiósporos de *M. perniciosa* e amostras foram coletadas em quatro diferentes estágios da doença (Figura 2): vassoura verde (30 dias após infecção); início da necrose do tecido infectado (47 dias após infecção); necrose avançada (66 dias

após infecção) e vassoura seca (111 dias depois da infecção). Plântulas sadias com a mesma idade das infectadas também foram coletadas em cada um dos quatro pontos para serem utilizadas como controle.

Figura 2. Plântulas infectadas utilizadas no sequenciamento de transcriptomas da interação entre *M. perniciosa* e o cacaueiro. (A) Estágio de vassoura verde. Notar crescimento exagerado e maior calibre da vassoura em relação ao caule da plântula. (B) Momento da doença em que se inicia a necrose do tecido infectado (seta). A necrose se inicia a partir da extremidade das folhas. (C) Estágio de necrose bastante avançada, havendo grande comprometimento do tecido infectado. (D) Estágio de vassoura seca, em que o tecido infectado do cacaueiro já se encontra morto.

Interação em frutos – Este experimento permite a análise dos genes do fungo e do hospedeiro em um segundo tipo de tecido infectado. Frutos em diversos momentos da doença (Figura 3) foram coletados em campo na fazenda Porto Novo no município de Ilhéus (BA). Três estágios da doença foram analisados: fase inicial (fruto com amadurecimento alterado), fruto parcialmente necrosado (com necrose externa avançada) e fruto podre. Além disso, coletou-se um fruto sadio para ser utilizado como controle do experimento. As sementes e as cascas de cada um dos frutos foram coletadas independentemente.

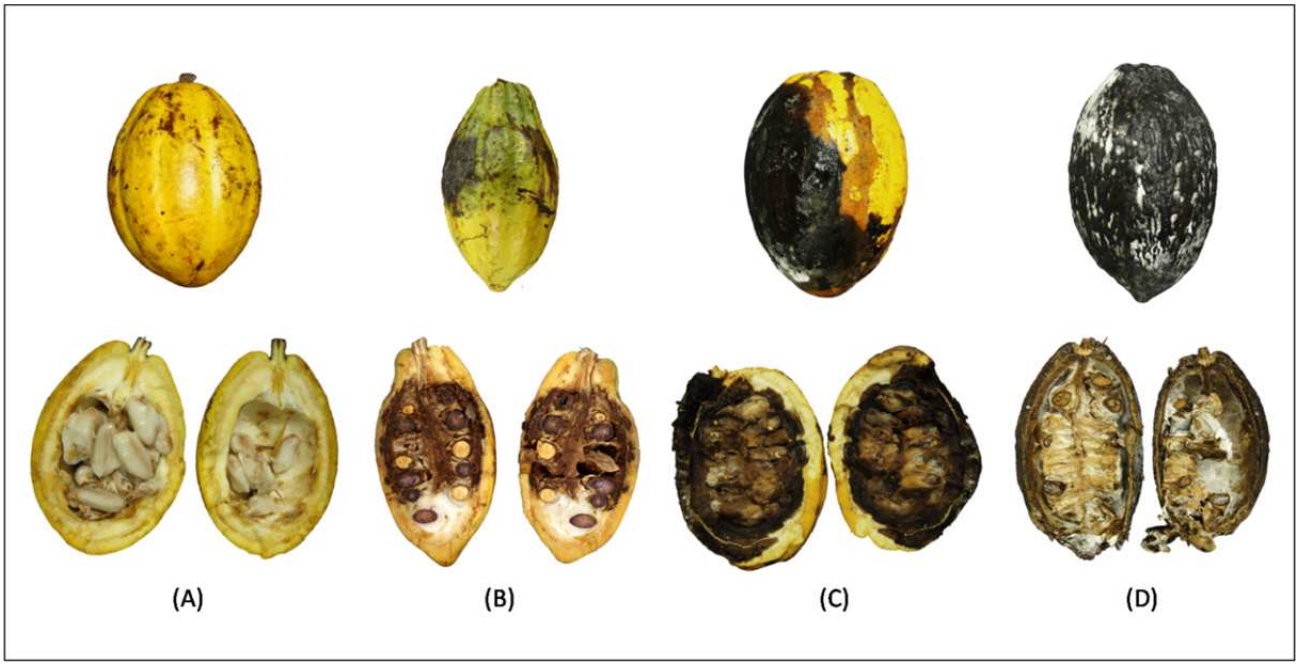

Figura 3. Frutos utilizados no sequenciamento de transcriptoma da interação cacau-*M.perniciosa*. (A) Fruto controle não infectado. (B) Fruto apresentando sintomas iniciais da vassoura de bruxa. Observa-se amadurecimento desigual em diferentes regiões do fruto e alteração bastante evidente no interior do fruto. (C) Fruto apresentando estágio avançado de necrose (D) Fruto podre, cuja proliferação do fungo é bastante intensa.

Basidiósporos em germinação – Este experimento teve como objetivo a análise do transcriptoma de *M. perniciosa* durante a germinação dos basidiósporos, processo de fundamental relevância para o estabelecimento da infecção. Para isso, uma alíquota de 2mL de suspensão de esporos com concentração aproximada de 10^7 esporos/mL foi dividida em duas parcelas. Essas parcelas foram gentilmente centrifugadas a 1000x*g* durante 5 minutos para precipitação dos esporos e

remoção da solução de coleta. Uma das parcelas foi ressuspendida em 1mL de solução de coleta, a qual impede a germinação dos basidiósporos, constituindo o controle do experimento. A outra parcela foi ressuspendida no mesmo volume de água estéril para permitir a germinação dos basidiósporos. Ambas alíquotas foram depositadas em pequenos béqueres e incubadas sob agitação de 120 rpm a 28°C durante 4 horas. Após a incubação, as suspensões foram observadas em microscópio para a confirmação da germinação dos basidiósporos (Figura 4).

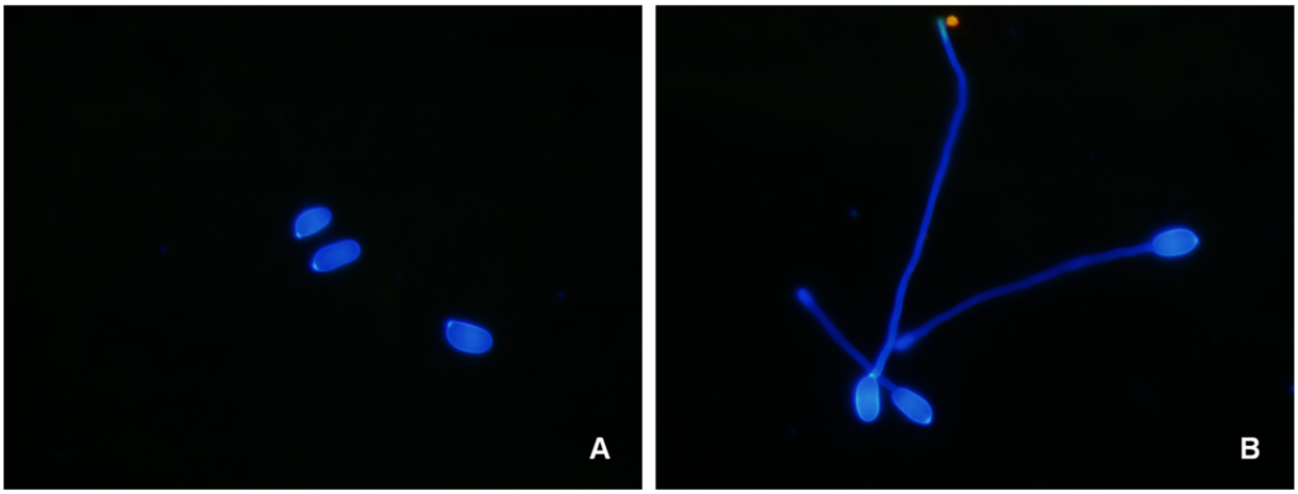

Figura 4. Basidiósporos de *M. perniciosa* coletados para sequenciamento de transcriptomas. (A) Amostra controle representando basidiósporos não germinados. (B) Amostra contendo basidiósporos germinados *in vitro*. Os basidiósporos foram corados com Calcofluor *White* e visualizados em microscópio de epifluorescência utilizando-se luz UV para excitação. Aumento de 200X.

<u>*Cultivo do fungo na presença de diferentes fontes de carbono*</u> – O micélio necrotrófico de *M. perniciosa* foi cultivado por sete dias no meio descrito por Meinhardt *et al.,* (2006) (contendo 1% de glicerol como fonte de carbono), a 28°C e agitação de 150 rpm. Após este período, o micélio foi filtrado, lavado com água estéril e transferido para um novo meio de cultura com igual composição, porém variando-se a fonte de carbono (1% de glicerol, 1% de glicose, 1% de metanol, 1% de ácido poligalacturônico, 1% de pectina ou 1% de extrato de cacau). O fungo foi mantido nos novos meios de cultura por um período de 24h.

Cultivo do fungo na presença de fungicidas – O micélio necrotrófico de *M. perniciosa* foi cultivado por sete dias em meio MYEA a 28°C e agitação de 150 rpm. Após este período, adicionou-se ao meio 30 mg/L de azoxistrobina (inibidor da cadeia respiratória principal de fungos), 0,75 g/L de SHAM (ácido salicilhidroxâmico - inibidor da enzima oxidase alternativa) ou a combinação de ambas as drogas. O fungo foi mantido na presença das drogas por um período de quatro horas. Como controles, o micélio foi tratado com metanol (solvente da azoxistrobina), etanol (solvente do SHAM) ou a combinação de metanol e etanol (solventes de ambas as drogas).

Outras amostras coletadas – O Atlas Transcriptômico da Vassoura de Bruxa inclui ainda estruturas reprodutivas do fungo (primórdios de basidomas e basidiomas maduros) e micélio necrotrófico jovem e senescente de *M. perniciosa* (Formighieri *et al.*, 2008). Além disso, micélio necrotrófico do isolado APS1 (biótipo S) também foi amostrado em condições padrão de cultivo (meio MYEA, temperatura de 28°C e agitação de 150 rpm).

Extrações de RNA

Para extração de RNA, todas as amostras, exceto os basidiósporos, foram maceradas em nitrogênio líquido com auxílio de um cadinho e pistilo. A parede celular dos basidiósporos foi rompida agitando vigorosamente a amostra na presença de 100 mg de *glass beads* (0,4 a 0,6 µm. Sigma-Aldrich, EUA) em 400 µL de tampão de extração (10 mM de Tris-HCl pH 7,5; 10 mM de EDTA e 0,5% de SDS). O RNA total de micélio e basidiósporos de *M. perniciosa* foi isolado através do método do fenol ácido quente (Sambrook *et al.*, 1989). O RNA de sementes de cacau foi extraído de acordo com os procedimentos descritos por Laloi *et al.* (2002). Para extração do RNA de cascas de cacau e meristemas foi utilizado um protocolo ainda não publicado padronizado em nosso laboratório. Basicamente, 100 mg de tecido macerado foram homogeneizados em 1,4 mL de tampão de extração contendo 100 mM de Tris-HCl, pH 8.0; 30 mM de EDTA; 300 mM de LiCl; 2M de NaCl; 2% de CTAB; 2% de PVP e 10% de β-mercaptoetanol. O RNA foi extraído duas

vezes com 500 µL de clorofórmio e precipitado com 3M de cloreto de lítio a 4°C durante 16h. O *pellet* de RNA obtido após centrifugação foi lavado com etanol 70% e ressuspendido em 20 µL de H_2O DEPC. Após a extração, a integridade dos RNAs de todas as amostras foi verificada em gel de agarose-formaldeído e a quantificação foi realizada no espectrofotômetro ND-1000 (NanoDrop, EUA).

Construção de bibliotecas para sequenciamento em larga escala

Os sequenciamentos em larga escala para obtenção de transcriptomas (RNA-seq) foram realizados na *High Throughtput Sequencing Facility*, sob orientação do Dr. Piotr Mieczkowski, pesquisador do Centro de Ciências Genômicas da Universidade da Carolina do Norte (*Carolina Center for Genome Sciences*). As bibliotecas foram preparadas segundo instruções fornecidas pela Illumina. Basicamente, o RNA mensageiro (mRNA) foi purificado a partir de 1 a 10µg de RNA total utilizando-se *Sera-Mag Magnetic Oligo(dT) Beads* (Thermo Scientific, EUA), e então fragmentado na presença de cátions divalentes sob elevadas temperaturas. Após isso, o mRNA clivado foi copiado na primeira fita de cDNA utilizando-se *random hexamer primers* e a enzima transcriptase reversa *SuperScript II* (Invitrogen, EUA). A segunda fita de cDNA foi sintetizada utilizando as enzimas *DNA polimerase I* e *RNAse H*. Em seguida, as enzimas *T4 DNA polimerase* e *Klenow DNA polimerase* foram utilizadas para obtenção de extremidades abruptas do cDNA. Uma adenina foi então adicionada à extremidade 3' das moléculas de cDNA utilizando-se a enzima *Klenow exo-.* Em seguida, realizou-se a ligação de adaptadores (que possuem uma timina *overhang*) para amplificação e sequenciamento do cDNA. Os adaptadores não ligados foram separados através de eletroforese e purificação de fragmentos de 200 a 300 pares de base, correspondentes ao cDNA ligado aos adaptadores. Finalmente, as bibliotecas foram enriquecidas através de 15 ciclos de PCR utilizando-se *primers* complementares às sequencias dos adaptadores. A concentração e a qualidade das bibliotecas foram aferidas utilizando-se o fluorômetro *Qubit* (Invitrogen, EUA) e o sistema de eletroforese capilar *Experion* (Bio-Rad, EUA).

Os sequenciamentos foram realizados utilizando-se os equipamentos *Genome Analyzer IIx* ou *HiSeq2000* (Illumina, EUA). Sequências *single-ends* e *paired-ends* com tamanhos entre 37 e 50 pb foram produzidas (ver Tabela 1 para detalhes).

Mapeamento de *reads* e análise de expressão gênica

Após o sequenciamento das bibliotecas, os *reads* obtidos foram submetidos a análises bioinformáticas. O programa Bowtie (Langmead *et al.*, 2009) foi utilizado para alinhar os *reads* contra uma referência constituída de 17.008 modelos gênicos de *M. perniciosa* e 34.997 modelos gênicos do cacau (versão 0.9, disponíveis publicamente em http://www.cacaogenomedb.org). O alinhamento foi realizado permitindo-se até um *mismatch* e excluindo-se *reads* mapeados em mais de uma posição na referência. A quantidade de *reads* mapeada em cada gene foi dividida pelo tamanho do gene (em kilobases). A seguir, este valor foi normalizado pelo total de *reads* mapeados da biblioteca (em milhões de *reads*). Desta forma, o valor de expressão de cada gene foi dado em RPKM (*reads per kilobase exon model per million mapped reads*), de forma que o nível de expressão de genes dentro de uma mesma biblioteca e em bibliotecas diferentes sejam comparáveis (Mortazavi *et al.*, 2008).

RESULTADOS E DISCUSSÃO

Uma visão geral do Atlas Transcriptômico da Vassoura de Bruxa

O Atlas Transcriptômico da Vassoura de Bruxa é composto por 61 bibliotecas de RNA-seq que representam aproximadamente 45 condições de grande relevância para o estudo desta doença do cacaueiro. Foram obtidos os transcriptomas dos principais estágios de desenvolvimento do patógeno *M. perniciosa*, incluindo basidiósporos, micélio biotrófico, micélio em transição de fase, micélio necrotrófico, primórdios de basidiomas e basidiomas maduros. Também foram sequenciadas amostras do fungo cultivado em diferentes fontes de carbono ou tratado com inibidores das cadeias respiratórias mitocondriais. Transcriptomas de frutos e ramos infectados em variados estágios da doença também foram sequenciados, permitindo ainda a análise dos genes do cacaueiro durante a vassoura de bruxa. As características gerais dos dados obtidos são apresentadas na Tabela 1. De forma simplificada, as bibliotecas podem ser divididas em três classes: (I) amostras de *M. perniciosa* se desenvolvendo *in vitro*, (II) amostras de plantas não infectadas, (III) interação entre os dois organismos (plantas infectadas). Independente da classe a que pertence, cada biblioteca foi mapeada contra uma referência contendo 17.008 genes de *M. perniciosa* e 34.997 genes de *T. cacao*, o que permitiu a determinação da proporção de transcritos originários de cada organismo. Sequências que mapearam em mais de uma posição na referência foram desconsideradas. Como esperado, bibliotecas de *M. perniciosa* em condições *in vitro* (classe I) apresentam baixa proporção de *reads* mapeando com genes do cacau. Similarmente, bibliotecas de plantas sadias (classe II) apresentam uma fração bastante pequena de *reads* com similaridade a genes do fungo. A ocorrência de alinhamentos inespecíficos pode ser atribuída ao pequeno tamanho das sequências produzidas. Ainda, sequências não mapeadas com *gene models* de nenhum dos organismos são em geral oriundas de RNA ribossomal ou de uma parcela de genes não preditos nestes genomas.

Tabela 1. Informações gerais das bibliotecas de RNA-seq que constituem o Altas Transcriptômico da Vassoura de Bruxa.

Bibliotecas	Característica dos *reads* *	Código	Número de *reads*	*Reads* alinhados com *M. perniciosa*	*Reads* alinhados com *T. cacao*	*Reads* não alinhados	*Reads* com alinhamento múltiplo
Primórdio de basidiomas	36pb SE	PRD1	29.033.649	20.889.128 (71,95%)	57.469 (0,20%)	7.889.542 (27,17%)	197.510 (0,68%)
Basidioma	36pb SE	BDA4	30.384.732	22.043.093 (72,55%)	32.369 (0,11%)	8.132.797 (26,77%)	176.473 (0,58%)
Esporos não germinados	36pb SE	NGS1	30.251.513	17.457.084 (57,71%)	62.275 (0,21%)	12.586.881 (41,61%)	145.273 (0,48%)
Esporos germinando	36pb SE	GE1	27.753.555	17.306.432 (62,36%)	97.469 (0,35%)	9.870.428 (35,56%)	479.226 (1,73%)
Micélio biotrófico (7 dias)	36pb SE	BIO7	28.631.853	19.045.946 (66,52%)	24.262 (0,08%)	9.332.929 (32,60%)	228.716 (0,80%)
Micélio necrotrófico (7 dias)	36pb SE	SAP7	31.235.935	21.451.378 (68,68%)	33.086 (0,11%)	9.505.120 (30,43%)	246.351 (0,79%)
Micélio biotrófico (14 dias – transição de fase)	37pb SE	PTA1	31.267.280	21.228.907 (67,89%)	30.947 (0,10%)	9.790.362 (31,31%)	217.064 (0,69%)
Micélio necrotrófico (14 dias)	36pb SE	NEC14	25.707.455	16.401.069 (63,80%)	46.932 (0,18%)	9.041.946 (35,17%)	217.508 (0,85%)
Micélio biotrófico (28 dias – transição de fase completa)	35pb SE	SB1	24.030.203	14.498.660 (60,34%)	48.891 (0,20%)	9.338.461 (38,86%)	144.191 (0,60%)
Micélio necrotrófico (28 dias)	35pb SE	NS28	22.731.804	13.832.791 (60,85%)	56.011 (0,25%)	8.683.371 (38,20%)	159.631 (0,70%)
Micélio necrotrófico jovem (isolado BP10)	36pb SE	BN1	28.377.071	19.969.255 (71,30%)	130.383 (0,47%)	7.699.959 (27,49%)	207.617 (0,74%)
Micélio necrotrófico jovem (isolado FA553)	36pb SE	FN3	19.324.580	13.511.491 (69,92%)	12.221 (0,06%)	5.620.394 (29,08%)	180.474 (0,93%)
Micélio necrotrófico senescente (isolado BP10)	36pb SE	BV3	29.261.911	17.263.836 (59,00%)	124.675 (0,43%)	11.671.430 (39,89%)	201.970 (0,69%)
Micélio necrotrófico senescente (isolado FA553)	36pb SE	FV2	20.069.353	13.965.623 (69,59%)	16.999 (0,08%)	5.833.817 (29,07%)	252.914 (1,26%)
M. perniciosa tratado com SHAM	35pb SE	DPT1	27.402.510	19.308.794 (70,46%)	11.696 (0,04%)	7.661.358 (27,96%)	420.662 (1,54%)
M. perniciosa tratado com azoxistrobina	35pb SE	DPT2	24.559.919	18.244.204 (74,28%)	9.747 (0,04%)	6.038.587 (24,59%)	267.381 (1,09%)
M. perniciosa tratado com SHAM + azoxistrobina	35pb SE	DPT3	25.839.171	19.050.685 (73,73%)	7.544 (0,03%)	6.552.000 (25,36%)	228.942 (0,89%)

(Continua)

(Continuação)

Bibliotecas	Característica dos *reads* *	Código	Número de *reads*	*Reads* alinhados com *M. perniciosa*	*Reads* alinhados com *T. cacao*	*Reads* não alinhados	*Reads* com alinhamento múltiplo
M. perniciosa tratado com etanol (controle SHAM)	35pb SE	DPT4	28.144.082	20.632.032 (73,31%)	20.315 (0,07%)	7.255.476 (25,78%)	236.259 (0,84%)
M. perniciosa tratado com metanol (controle azoxistrobina)	35pb SE	DPT5	25.714.105	18.008.772 (70,03%)	45.990 (0,18%)	7.488.256 (29,12%)	171.087 (0,67%)
M. perniciosa tratado com etanol + metanol (controle SHAM + azoxistrobina)	35pb SE	DPT6	27.061.209	19.752.482 (72,99%)	15.836 (0,06%)	7.071.245 (26,13%)	221.646 (0,82%)
M. perniciosa induzido com glicerol	35pb SE	OLP1	27.044.195	19.566.074 (72,35%)	52.147 (0,19%)	7.172.835 (26,52%)	253.139 (0,94%)
M. perniciosa induzido com pectina	35pb SE	PECP1	31.776.484	23.299.766 (73,32%)	23.770 (0,07%)	8.210.155 (25,84%)	242.793 (0,76%)
M. perniciosa induzido com ácido poligalacturônico	36pb SE	POP1	28.165.627	21.384.681 (75,92%)	28.755 (0,10%)	6.541.075 (23,22%)	211.116 (0,75%)
M. perniciosa induzido com glicose	35pb SE	GliP1	24.732.386	17.682.780 (71,50%)	47.195 (0,19%)	6.791.259 (27,46%)	211.152 (0,85%)
M. perniciosa induzido com metanol	35pb SE	METP1	25.290.296	18.852.591 (74,54%)	35.054 (0,14%)	6.144.153 (24,29%)	258.498 (1,02%)
M. perniciosa induzido com extrato de cacau	50pb PE	CAP1	55.556.098	32.358.702 (58,25%)	50 (0,00%)	23.109.373 (41,60%)	87.973 (0,16%)
Micélio necrotrófico *in vitro* (Biótipo S)	36pb SE	APS1	23.270.869	15.005.302 (64,48%)	25.113 (0,11%)	8.020.106 (34,46%)	220.348 (0,95%)
Micélio necrotrófico *in vitro* (Biótipo S)	36pb SE	APS2	21.756.303	14.737.140 (67,74%)	16.693 (0,08%)	6.782.538 (31,18%)	219.932 (1,01%)
Micélio necrotrófico *in vitro* (Biótipo S)	36pb SE	APS4	20.775.150	14.098.804 (67,86%)	14.600 (0,07%)	6.446.710 (31,03%)	215.036 (1,04%)
Fruto sadio (casca)	37pb SE	HS2	27.677.832	5.017.823 (18,13%)	15.820.914 (57,16%)	6.438.191 (23,26%)	400.904 (1,45%)
Fruto sadio (sementes)	35pb SE	HPB2	22.285.402	1.460 (0,01%)	18.559.342 (83,28%)	3.307.284 (14,84%)	417.316 (1,87%)
Fruto em início da infecção (casca)	36pb SE	GS3	28.219.072	11.697.285 (41,45%)	8.996.616 (31,88%)	7.098.503 (25,15%)	426.668 (1,51%)
Fruto em início da infecção (sementes)	37pb SE	GPB1	26.588.983	7.665.964 (28,83%)	11.921.476 (44,84%)	6.587.615 (24,78%)	413.928 (1,56%)
Fruto necrosando (casca da região viva)	36pb SE	DG2	28.435.732	8.452.317 (29,72%)	13.015.189 (45,77%)	6.517.977 (22,92%)	450.249 (1,58%)

(Continua)

(Continuação)

Bibliotecas	Característica dos *reads* *	Código	Número de *reads*	*Reads* alinhados com *M. perniciosa*	*Reads* alinhados com *T. cacao*	*Reads* não alinhados	*Reads* com alinhamento múltiplo
Fruto necrosando (casca da região morta)	36pb SE	DR2	26.387.255	5.114.399 (19,38%)	409.706 (1,55%)	20.785.788 (78,77%)	77.362 (0,29%)
Fruto necrosando (sementes)	36pb SE	DPB1	24.623.147	5.323.965 (21,62%)	13.082.945 (53,13%)	5.822.164 (23,65%)	394.073 (1,60%)
Fruto podre (casca)	35pb SE	BS5	16.184.686	8.828.807 (54,55%)	46.416 (0,29%)	7.194.054 (44,45%)	115.409 (0,71%)
Fruto podre (sementes)	36pb SE	BPB1	28.007.214	19.969.255 (71,30%)	130.383 (0,47%)	7.699.959 (27,49%)	207.617 (0,74%)
Vassoura verde	36pb SE	GB1	13.143.266	63.460 (0,48%)	10.721.871 (81,58%)	2.103.718 (16,01%)	254.217 (1,93%)
Cacau sadio (controle vassoura verde)	35pb SE	HA1	28.205.254	18 (0,00%)	22.730.507 (80,59%)	4.878.816 (17,30%)	595.913 (2,11%)
Vassoura início da necrose	35pb SE	NA4	30.140.571	254.929 (0,85%)	24.651.039 (81,79%)	4.604.255 (15,28%)	630.348 (2,09%)
Cacau sadio (controle início da necrose)	35pb SE	HB3	28.411.022	38 (0,00%)	22.985.707 (80,90%)	4.650.190 (16,37%)	775.087 (2,73%)
Vassoura necrose avançada	35pb SE	NB1	26.499.917	544.250 (2,05%)	9.463.480 (35,71%)	16.141.073 (60,91%)	351.114 (1,32%)
Cacau sadio (controle vassoura avançada)	36pb SE	HC1	28.726.748	69 (0,00%)	24.198.706 (84,24%)	4.005.587 (13,94%)	522.386 (1,82%)
Vassoura seca	35pb SE	DB1	23.646.179	432.408 (1,83%)	105.084 (0,44%)	23.098.221 (97,68%)	10.466 (0,04%)
Cacau sadio (controle vassoura seca)	36pb SE	HD2	23.400.070	17 (0,00%)	20.250.789 (86,54%)	2.716.578 (11,61%)	432.686 (1,85%)
Basidioma (directional)	36pb SE	DIBDA4	32.104.741	13.970.948 (43,52%)	15.973 (0,05%)	18.023.132 (56,14%)	94.688 (0,29%)
Micélio monocariótico (directional)	36pb SE	DIBIO1	19.097.253	13.056.877 (68,37%)	5.200 (0,03%)	5.893.876 (30,86%)	141.300 (0,74%)
Micélio dicariótico (directional)	36pb SE	DISAP1	9.290.622	5.415.453 (58,29%)	6.233 (0,07%)	3.808.816 (41,00%)	60.120 (0,65%)
Vassoura verde (directional)	36pb SE	DIGB2	32.968.672	60.455 (0,18%)	21.003.030 (63,71%)	11.418.912 (34,64%)	486.275 (1,47%)
Cacau sadio (controle vassoura verde – directional)	36pb SE	DIHCA1	31.258.985	167 (0,00%)	22.468.826 (71,88%)	8.316.458 (26,61%)	473.534 (1,51%)

(Continua)

(Continuação)

Bibliotecas	Característica dos *reads* *	Código	Número de *reads*	*Reads* alinhados com *M. perniciosa*	*Reads* alinhados com *T. cacao*	*Reads* não alinhados	*Reads* com alinhamento múltiplo
Vassoura verde	50pb PE	NZ3	77,308,238	265.238 (0,34%)	56.884.442 (73,58%)	19.436.411 (25,14%)	722.147 (0,93%)
Vassoura verde	48pb PE	VV4C	103,196,353	158.021 (0,15%)	82.127.996 (79,58%)	19.768.446 (19,16%)	1.141.890 (1,11%)
Vassoura verde	48pb PE	VV3F	90,591,723	186.831 (0,21%)	71.473.561 (78,90%)	17.947.875 (19,81%)	983.456 (1,09%)
Vassoura verde	48pb PE	VV1D	83,953,292	196.086 (0,23%)	67.870.238 (80,84%)	15.023.953 (17,90%)	863.015 (1,03%)
Vassoura verde	48pb PE	VV0E	207,441,756	904.727 (0,44%)	167.016.562 (80,51%)	37.216.370 (17,94%)	2.304.097 (1,11%)
Cacau sadio (controle vassoura verde)	48pb PE	HA2	96,856,054	12 (0,00%)	73.928.395 (76,33%)	21.642.608 (22,35%)	1.285.039 (1,33%)
Cacau sadio (controle vassoura verde)	48pb PE	CS4B	80,950,589	91 (0,00%)	65.521.727 (80,94%)	14.698.132 (18,16%)	730.639 (0,90%)
Cacau sadio (controle vassoura verde)	48pb PE	CS3D	86,454,964	208 (0,00%)	68.962.874 (79,77%)	16.462.275 (19,04%)	1.029.607 (1,19%)
Cacau sadio (controle vassoura verde)	48pb PE	CS2E	82,560,659	633 (0,00%)	68.560.121 (83,04%)	12.864.461 (15,58%)	1.135.444 (1,38%)
Cacau sadio (controle vassoura verde)	48pb PE	CS0D	89,659,731	27 (0,00%)	73.930.327 (82,46%)	14.077.162 (15,70%)	1.652.215 (1,84%)

Cada linha da tabela representa uma biblioteca diferente.

* SE: Bibliotecas *single-end*. PE: Bibliotecas *paired-end.*

A análise de ramos infectados (vassouras – classe III) revelou que a quantidade total de transcritos do fungo é maior nos estágios avançados da doença (Figura 5), o que está de acordo com a maior taxa de crescimento do micélio necrotrófico (Penman *et al.*, 2000). Apesar de pequena, a proporção de transcritos do fungo detectada em plantas infectadas foi consideravelmente maior do que a proporção de alinhamentos inespecíficos observados em plantas sadias (Tabela 1). Surpreendentemente, a biblioteca construída a partir de vassoura seca apresentou uma elevada quantidade de *reads* que não mapearam com o hospedeiro ou com o patógeno. A diminuição de transcritos do cacaueiro era esperada nesse estágio da doença, uma vez que a planta apresenta avançado estado de necrose. Por outro lado, esperava-se encontrar a prevalência de transcritos de *M. perniciosa*. A inspeção dos *reads* não mapeados revelou a existência de ascomicetos saprofíticos na amostra, os quais provavelmente se desenvolveram como oportunistas no tecido morto da planta.

Figura 5. Proporção de transcritos de *M. perniciosa* em plantas infectadas durante a progressão da vassoura de bruxa.

A existência de outros fungos é facilmente observada em vassouras secas no campo, o que está de acordo com nossos resultados obtidos em casa de vegetação. Desta forma, é possível que o fungo *M. perniciosa* esteja sujeito a intensa competição com outros microrganismos durante seu desenvolvimento na vassoura seca. Suportando esta ideia, Rincones *et al.*, (2008) reportaram elevada expressão de um gene codificante da proteína antifúngica KP4 (Clausen *et al.*, 2000) no micélio necrotrófico de *M. perniciosa*, o que também foi validado por nossos dados de RNA-seq. Experimentos controlados utilizando réplicas biológicas adicionais e, preferencialmente, incluindo vassouras secas coletadas em campo, são necessários para se confirmar esta hipótese.

A interação entre o cacaueiro e o fungo *M. perniciosa* também foi avaliada em cascas e sementes de frutos. Em contraste com a infecção em ramos, uma proporção relativamente alta de transcritos do fungo foi identificada nos frutos (tipicamente de 30 a 60%). Assim como em vassoura seca, sequências de microrganismos oportunistas foram identificadas nas cascas de um fruto podre. Por outro lado, transcritos de outros fungos não foram identificados nas sementes deste mesmo fruto, sugerindo que *M. perniciosa* não enfrente competição com oportunistas no interior de frutos. Desta forma, é possível que a infecção deste tecido ofereça vantagens importantes para o desenvolvimento de *M. perniciosa*, tais como ausência de competidores e elevada disponibilidade nutricional. Uma característica típica de *M. perniciosa* são os sintomas iniciados a partir do interior dos frutos, o que fortalece a ideia de que este é um ambiente vantajoso para o desenvolvimento do fungo.

O Atlas Transcriptômico como ferramenta para anotação gênica

Uma utilidade primária dos dados de RNA-seq obtidos se dá quanto à predição e/ou confirmação de regiões codantes do genoma. O alinhamento dos *reads* contra uma referência de DNA genômico evidencia regiões transcritas, permitindo a definição de fronteiras entre exons e introns, por exemplo. É possível definir ainda as regiões de início e fim da transcrição de um gene, e identificar variações de *splicing*. A Figura 6 mostra um exemplo de mapeamento de *reads* contra

um gene do fungo *M. perniciosa*. Observa-se que a cobertura de *reads* é intensa nos exons e baixa nos introns. Esta ferramenta é extremamente útil na análise de estrutura gênica, permitindo a identificação das regiões que fazem parte de transcritos maduros, uma informação de grande importância na realização de um projeto genoma.

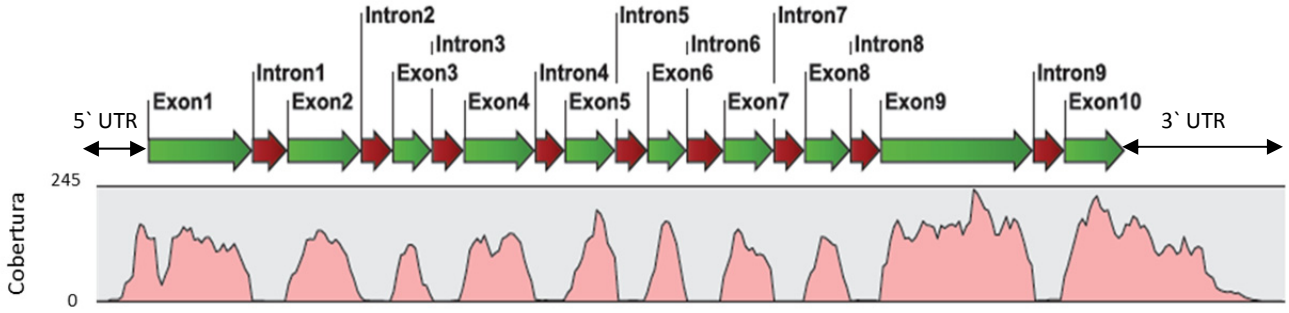

Figura 6. Alinhamento de *reads* de RNA-seq em um fragmento de DNA genômico do fungo *M. perniciosa*. A região apresentada corresponde ao gene codificante da proteína oxidase alternativa. Observam-se regiões correspondentes aos exons e introns, evidenciados pela diferença de cobertura de *reads* nessas regiões.

Ainda, nosso conjunto de dados inclui bibliotecas denominadas “direcionais” (Tabela 1). Diferentemente das bibliotecas de RNA-seq convencionais, estas bibliotecas não envolvem a síntese de cDNA dupla fita, sendo construídas apenas com as moléculas originais de mRNA da célula. Como consequência, o sentido de cada transcrito é preservado, permitindo a identificação da direção da transcrição de cada gene expresso. A Figura 7 exemplifica um alinhamento utilizando bibliotecas direcionais.

Análises de expressão gênica: Quando cada gene é necessário?

A grande variedade de bibliotecas de RNA-seq permite que cada gene de *M. perniciosa* tenha seu perfil de expressão inspecionado de forma abrangente. O genoma deste fungo codifica aproximadamente 17 mil genes, dos quais uma pequena parcela pode ter funções biológicas atribuídas com base em similaridade com proteínas de outros organismos. Isto se torna ainda mais relevante considerando-se que basidiomicetos formam um grupo de fungos pouco estudados, de forma que muitas proteínas são descritas apenas como “hipotéticas”. Ainda, proteínas envolvidas

com a virulência de fitopatógenos costumam sofrer rápida evolução, não apresentando similaridade significativa com proteínas de outros organismos (Dou & Zhou, 2012).

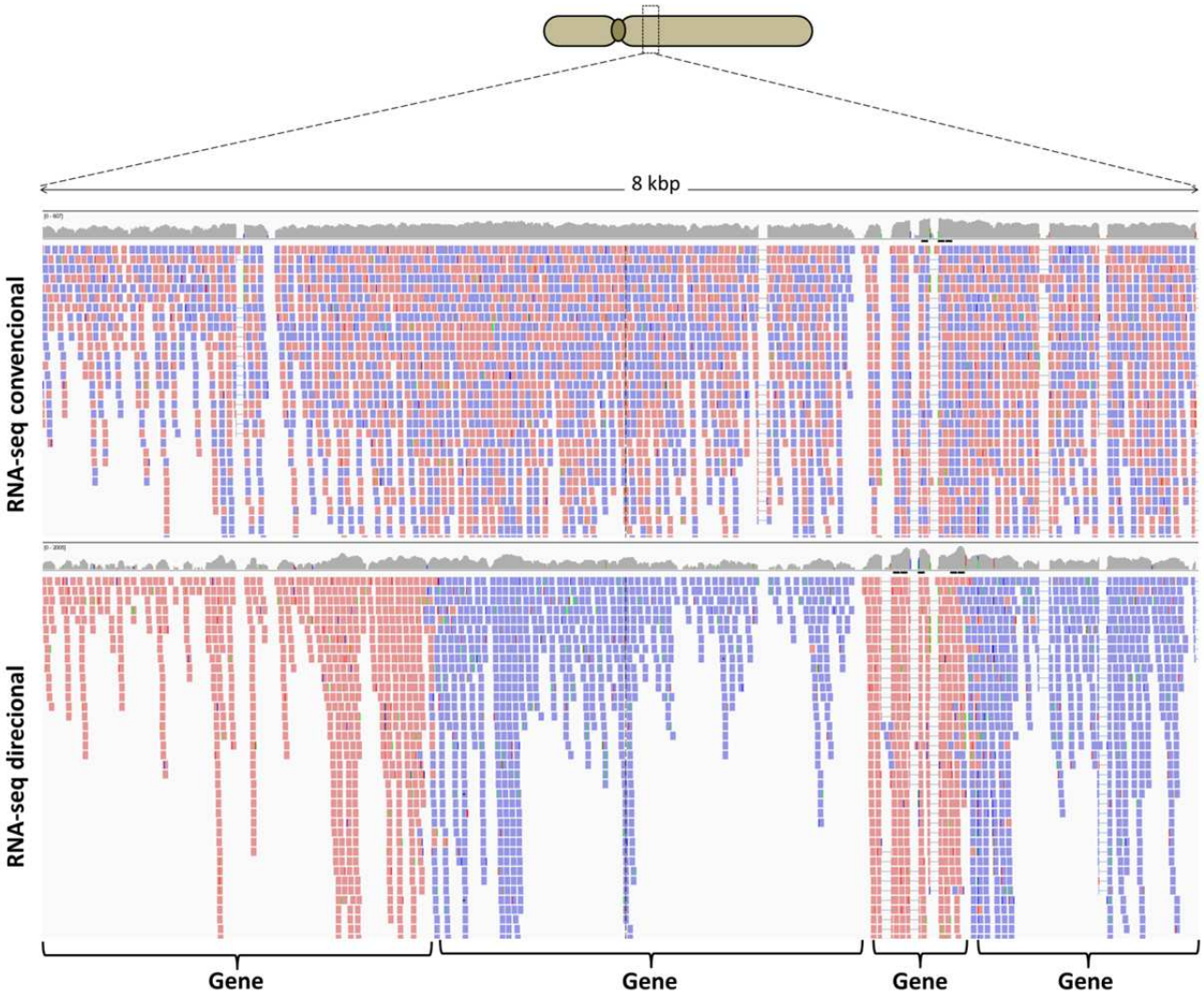

Figura 7. Visualização de alinhamentos de *reads* de RNA-seq em uma região de aproximadamente 8 kbp do genoma de *M. perniciosa*. O painel superior mostra o alinhamento de sequências obtidas por RNA-seq convencional, enquanto que o painel inferior mostra o alinhamento de uma biblioteca de RNA-seq direcional. Verifica-se que a definição dos limites entre os genes é bem demarcada utilizando-se *reads* de RNA-convencional. *Reads* marcados em cores diferentes mapearam em fitas distintas do DNA genômico.

Neste contexto, o Atlas Transcriptômico da Vassoura de Bruxa é uma ferramenta de grande utilidade para a elaboração de hipóteses e investigação de mecanismos envolvidos na interação entre o patógeno *M. perniciosa* e o cacaueiro. Como exemplo, a Figura 8 mostra a

expressão de um gene de *M. perniciosa* codificante para uma invertase extracelular. Invertases são enzimas que catalisam a quebra da sacarose em glicose e frutose. A sacarose, por sua vez, é a forma pela qual o carbono assimilado durante a fotossíntese é transportado em plantas. Notavelmente, este gene apresenta elevada expressão durante a germinação dos esporos, um estágio altamente comprometido com o estabelecimento da infeção. Com base neste dado, é possível especular que *M. perniciosa* utilize sacarose encontrada na planta para sustentar seu desenvolvimento inicial e colonização do hospedeiro. A germinação dos esporos relaciona-se diretamente com a virulência do fungo e será mais bem investigada em trabalhos futuros do grupo.

Similarmente, a Figura 9 apresenta a expressão de um gene aparentemente específico de *M. perniciosa* (*no hit* em buscas por sequências similares em bases de dados). A sua expressão exclusiva durante a interação biotrófica com o cacaueiro pode ser um forte indício de um papel na patogenicidade deste fungo. Apesar disso, o perfil de expressão gênica constitui apenas uma primeira linha de evidências quanto à função da proteína codificada. Neste contexto, candidatos a fatores de patogenicidade (efetores) têm sido selecionados para estudos funcionais específicos, como por exemplo, a resolução da estrutura tridimensional da proteína codificada.

Também é interessante ilustrar o perfil de expressão do gene NEP2 (*necrosis- and ethylene-inducing protein*). Este gene codifica uma proteína com capacidade de causar necrose no cacaueiro, sendo apontado como central na virulência de *M. perniciosa* (Garcia *et al.*, 2007). Em concordância com seu papel biológico, nossos dados de RNA-seq mostram que o gene *NEP2* é distintivamente expresso nos estágios da doença em que pronunciada necrose é observada no cacaueiro, ou seja, na transição entre o estágio biotrófico para o necrotrófico da vassoura de bruxa (Figura 10). Surpreendentemente, o gene NEP também é altamente expresso quando *M. perniciosa* é cultivado *in vitro* na presença de ácido salicil hidroxâmico (SHAM). Esta molécula é um inibidor da enzima mitocondrial oxidase alternativa (AOX), cujo funcionamento parece ser importante para a manutenção do desenvolvimento biotrófico de *M. perniciosa* (Thomazella *et al.*, 2012 – Ver capítulo VI).

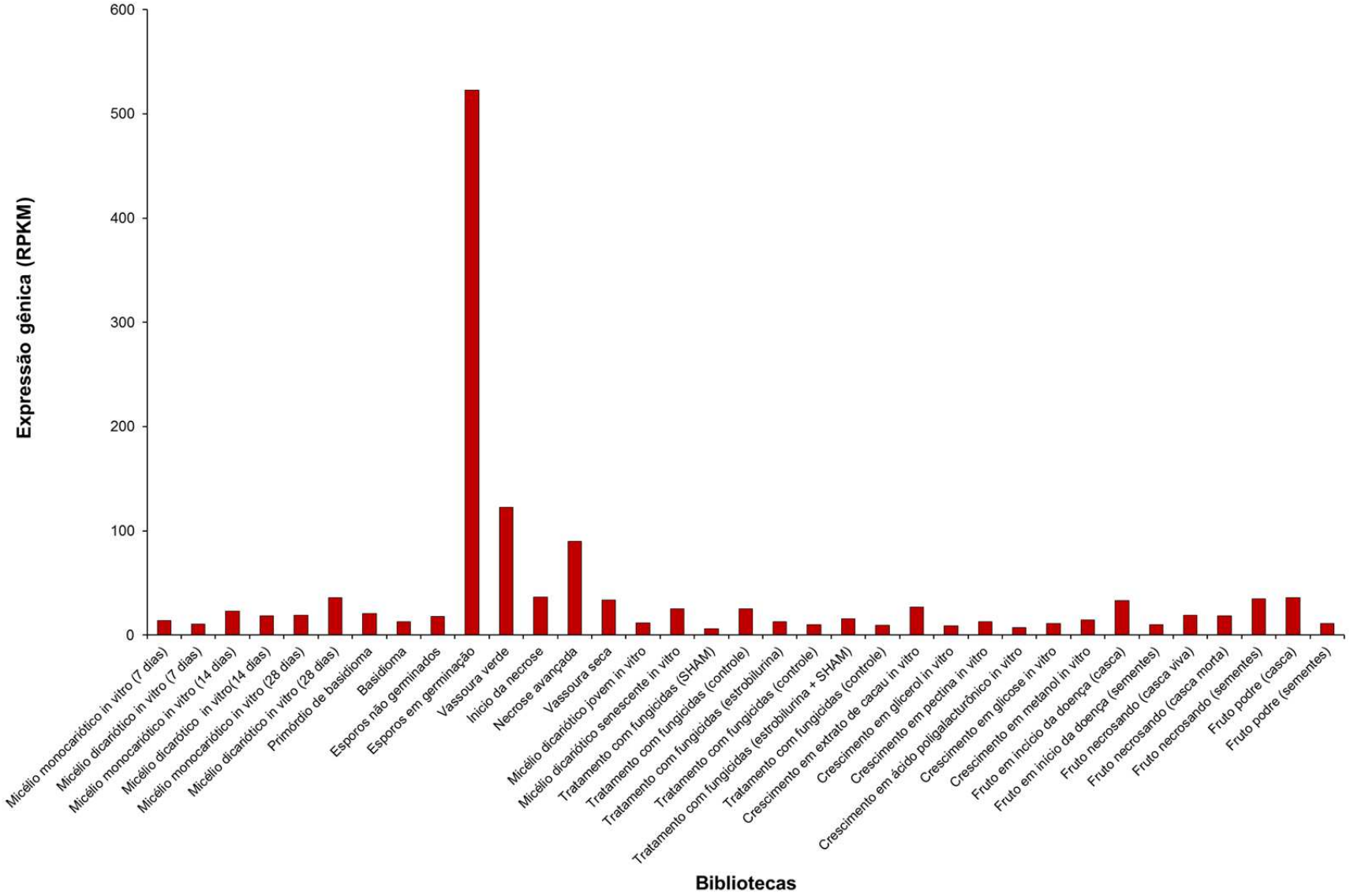

Figura 8. Perfil de expressão de um gene que codifica uma invertase extracelular em *M. perniciosa*.

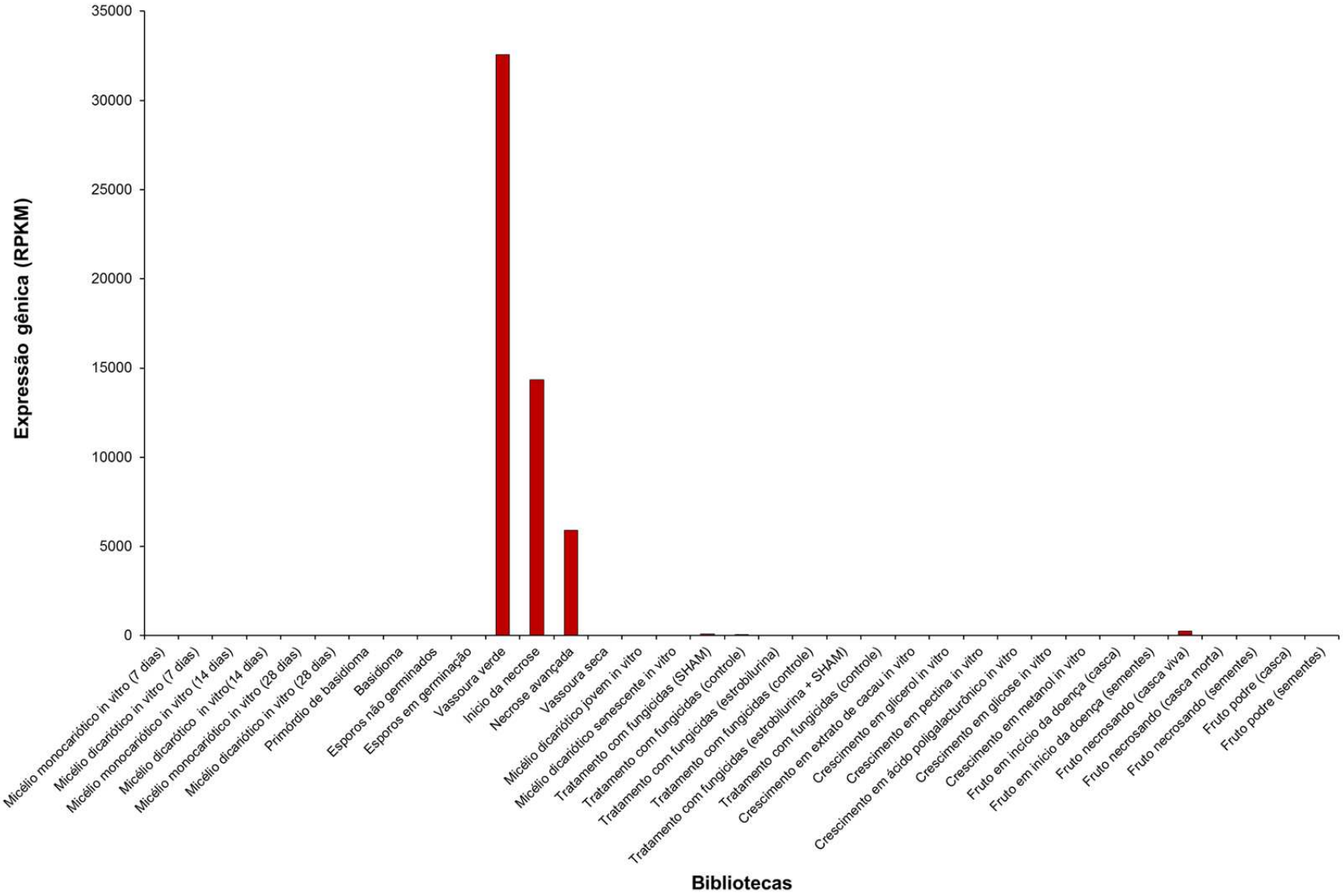

Figura 9. Perfil de expressão de um gene que codifica um candidato a efetor em *M. perniciosa*. Verifica-se que o gene é majoritariamente expresso durante interação biotrófica com o cacaueiro.

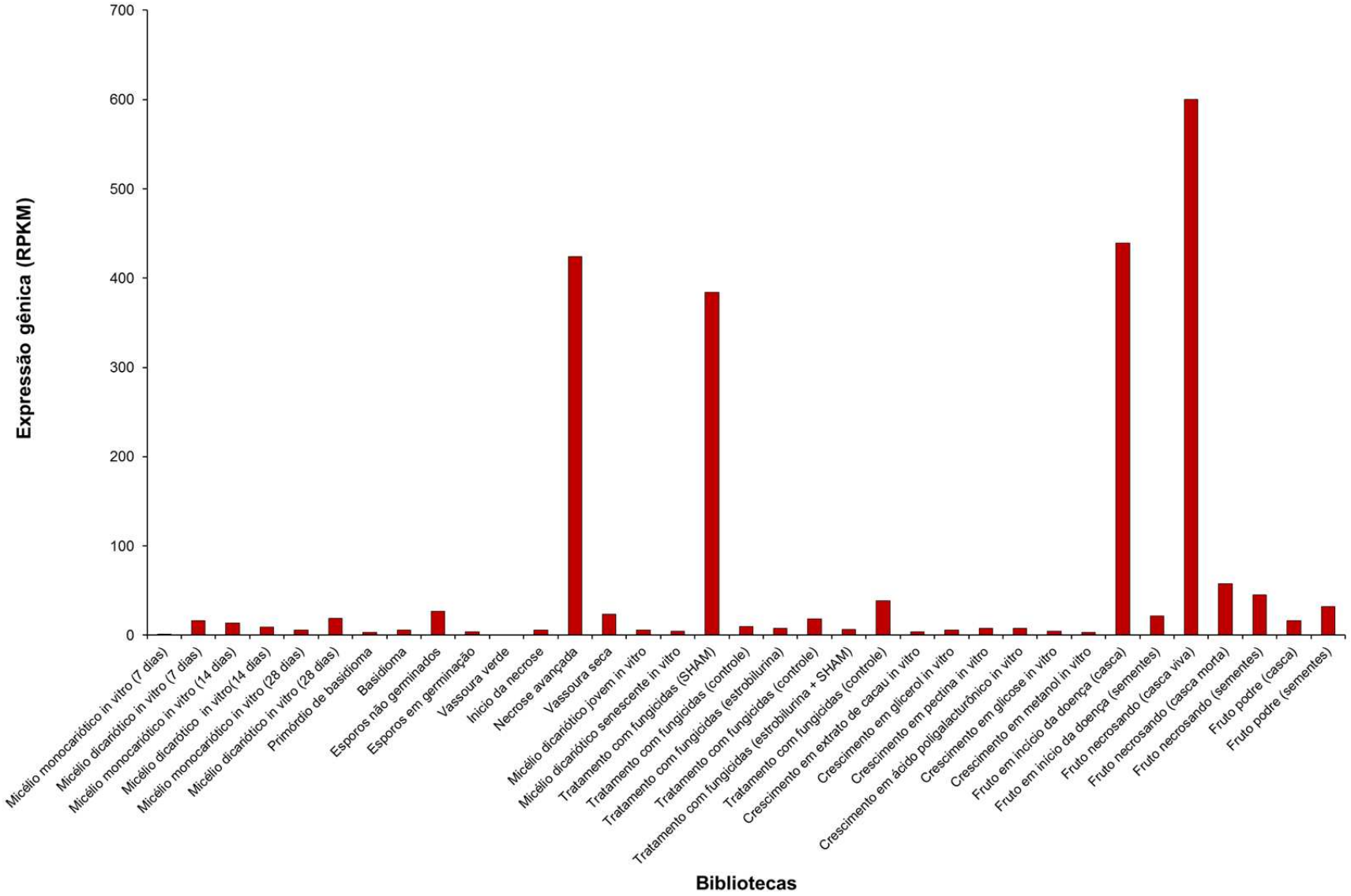

Figura 10. Perfil de expressão do gene *NEP2* de *M. perniciosa*, o qual codifica uma proteína capaz de necrosar os tecidos do cacaueiro.

Desta forma, a indução do gene *NEP2* em uma condição em que o funcionamento da enzima AOX é bloqueado pode indicar um *crosstalk* direto entre o metabolismo energético do fungo e a transição para a sua fase necrotrófica. Os exemplos mencionados mostram de forma simplificada como um abrangente Atlas Transcriptômico pode ser utilizado no estudo de organismos ainda pouco compreendidos. Análises mais detalhadas têm o potencial de revelar processos relevantes para um determinado fenômeno biológico. Por exemplo, a busca por outros genes com perfil de expressão similar ao do gene *NEP2* pode indicar novos candidatos envolvidos na morte do cacaueiro. Ainda, a análise de genes corregulados pode revelar regiões promotoras responsáveis pela regulação da expressão gênica em condições de interesse para o estudo da vassoura de bruxa.

Análise global do Atlas Transcriptômico da Vassoura de Bruxa

A análise global das bibliotecas de RNA-seq revelou interessantes características da biologia do patógeno *M. perniciosa*. A relação entre diferentes transcriptomas do fungo é apresentada na Figura 11. Nesta análise, três grandes grupos podem ser observados: (I) transcriptomas do fungo durante seu desenvolvimento *in vitro* (vermelho), (II) transcriptomas do fungo durante a infecção de frutos (amarelo), (III) transcriptomas do fungo durante a infecção de ramos (verde). Desta forma, é possível afirmar que a programação genética do patógeno é claramente diferente em cada uma destas situações. Apesar de trabalhos anteriores terem se baseado no desenvolvimento *in vitro* de *M. perniciosa* para a identificação e mecanismos de patogenicidade (Rincones *et al*., 2008; Leal *et al*., 2010), nossos resultados indicam que o estudo do patógeno diretamente durante sua interação com o cacaueiro deve indicar aspectos ainda inexplorados e de grande relevância para o entendimento da doença (ver Capítulo II para uma análise detalhada).

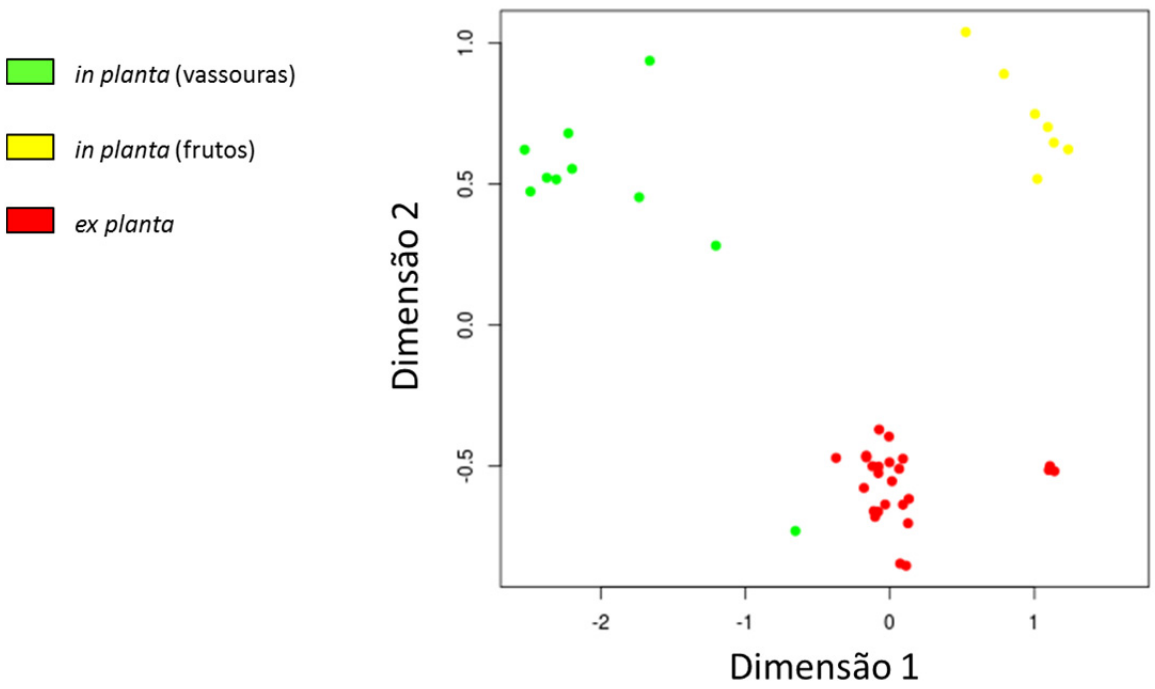

Figura 11. Relação entre diferentes transcriptomas do fungo *M. perniciosa*. A técnica de redução de variáveis *multidimensional scaling* (MDS - Robinson *et al.*, 2010) foi aplicada para que os dados pudessem ser plotados em duas dimensões. Observam-se três grupos distintos: transcriptomas do fungo *in vitro*, transcriptomas do fungo durante a infecção de frutos e transcriptomas do fungo durante a infecção de ramos. O ponto verde junto às amostras *in vitro* representa o estágio de vassoura seca da doença, na qual o fungo coloniza o tecido morto da planta.

A clara diferença entre os transcriptomas de *M. perniciosa* durante as infecções de frutos e ramos pode refletir a utilização de estratégias específicas para a colonização de diferentes tecidos do cacaueiro. Recentemente, Skibbe *et al.*, (2010) demonstraram que o fungo *Ustilago maydis* utiliza genes de virulência completamente diferentes ao infectar estruturas diferentes do milho. Similarmente, o patógeno *Magnaporthe oryzae* é capaz de infectar folhas e raízes do arroz, adotando estratégias específicas para cada tecido (Marcel *et al.*, 2010). Enquanto a infecção de folhas resulta em rápida necrose do tecido da planta, o fungo apresenta um comportamento similar ao de um endofítico durante a infecção de raízes, permanecendo em contato com as células vivas do hospedeiro durante um longo tempo (Marcel *et al.*, 2010).

Esta observação abre novas possibilidades para o estudo da virulência de *M. perniciosa*, cuja colonização em frutos foi pouco explorada até o momento. Nossos dados indicam que *M. perniciosa* expressa um conjunto de genes codificantes de enzimas responsáveis pela geração de peróxido de hidrogênio durante a infecção de frutos. Além disso, muitos genes envolvidos no metabolismo de ferro também foram identificados (dados não mostrados), o que sugere fortemente a ocorrência da chamada reação de Fenton (Baldrian & Valaskova, 2008). Este processo, já descrito para fungos saprofíticos como o basidiomiceto *Postia placenta* (Martinez *et al.*, 2009), baseia-se na reação do peróxido de hidrogênio com o ferro resultando na produção de radical hidroxila. Este radical, por sua vez, é altamente reativo e atua na degradação da parede celular vegetal. Considerando-se a rigidez da casca do cacau, uma estratégia mais agressiva parece ser necessária para a degradação da parede celular do fruto. Análises comparativas entre os transcriptomas de frutos e ramos estão sendo iniciadas em nosso laboratório e têm o potencial de indicar mais claramente as diferenças entre as estratégias de infecção dos diferentes órgãos do cacaueiro.

Curiosamente, a espécie *M. roreri* não é capaz de infectar ramos do cacaueiro, sendo considerado um patógeno mais especializado (Evans, 2007). Desta forma, é possível que a estratégia de infecção de ramos por *M. perniciosa* se diferencie consideravelmente dos mecanismos de patogenicidade de *M. roreri*. Neste sentido, estudos comparativos têm o potencial de indicar aspectos comuns e diferentes nas estratégias de infecção destas espécies proximamente relacionadas. É interessante ressaltar ainda que variedades tolerantes à vassoura de bruxa costumam apresentar menor incidência de ramos infectados, porém, observa-se que a tolerância muitas vezes não se manifesta em almofadas florais ou frutos. Assim, nossos dados fornecem uma possível explicação para esta observação e podem direcionar estratégias visando à obtenção de variedades de cacau plenamente resistentes à vassoura de bruxa.

Disponibilização dos dados do Atlas Transcriptômico da Vassoura de Bruxa

Um *website* está em fase final de desenvolvimento para facilitar o acesso às informações produzidas neste trabalho. Ferramentas de busca serão implantadas de forma que os pesquisadores possam acessar os valores de expressão de genes específicos em bibliotecas de RNA-seq de interesse. As informações estarão inicialmente disponíveis apenas aos pesquisadores do Laboratório de Genômica e Expressão da Unicamp e a grupos colaboradores. No entanto, os dados poderão ser publicamente acessados após a publicação de artigos científicos. De modo geral, o Atlas Transcriptômico da Vassoura de Bruxa representa um importante avanço no estudo desta doença do cacaueiro e tem servido como ponto de partida para uma série de estudos adicionais, alguns dos quais serão melhor explorados nos próximos capítulos desta tese.

REFERÊNCIAS

Baldrian P, Valaskova V (2008) Degradation of cellulose by basidiomycetous fungi. FEMS Microbiol Rev **32**: 501-521

Brady SM, Long TA, Benfey PN (2006) Unraveling the dynamic transcriptome. Plant Cell **18**: 2101-2111

Clausen M, Krauter R, Schachermayr G, Potrykus I, Sautter C (2000) Antifungal activity of a virally encoded gene in transgenic wheat. Nat Biotechnol **18**: 446-449

da Hora Junior BT, Poloni JF, Lopes MA, Dias CV, Gramacho KP, Schuster I, Sabau X, Cascardo JC, Mauro SM, Gesteira AS, *et al.* (2012) Transcriptomics and systems biology analysis in identification of specific pathways involved in cacao resistance and susceptibility to witches' broom disease. Mol Biosyst **8**: 1507-1519

Dou D, Zhou JM (2012) Phytopathogen effectors subverting host immunity: different foes, similar battleground. Cell Host Microbe **12**: 484-495

Evans HC (1980) Pleomorphism in *Crinipellis perniciosa*, causal agent of witches' broom disease of cocoa. Transactions of the British Mycological Society **74**: 515-523

Evans HC (2007) Cacao diseases-the trilogy revisited. Phytopathology **97**: 1640-1643

Formighieri EF, Tiburcio RA, Armas ED, Medrano FJ, Shimo H, Carels N, Goes-Neto A, Cotomacci C, Carazzolle MF, Sardinha-Pinto N, *et al.* (2008) The mitochondrial genome of the phytopathogenic basidiomycete *Moniliophthora perniciosa* is 109 kb in size and contains a stable integrated plasmid. Mycol Res **112**: 1136-1152

Frias G, Purdy LH, Schmidt RA (1995) An inoculation method for evaluating resistence of cacao to *Crinipellis perniciosa*. Plant Disease **79**: 787-791

Garcia O, Macedo JA, Tiburcio R, Zaparoli G, Rincones J, Bittencourt LM, Ceita GO, Micheli F, Gesteira A, Mariano AC, *et al.* (2007) Characterization of necrosis and ethylene-inducing proteins (NEP) in the basidiomycete *Moniliophthora perniciosa*, the causal agent of witches' broom in *Theobroma cacao*. Mycol Res **111**: 443-455

Gesteira AS, Micheli F, Carels N, Da Silva AC, Gramacho KP, Schuster I, Macedo JN, Pereira GA, Cascardo JC (2007) Comparative analysis of expressed genes from cacao meristems infected by *Moniliophthora perniciosa*. Ann Bot **100**: 129-140

Griffith G, Hedger J (1993) A novel method for producing basidiocarps of the cocoa pathogen *Crinipellis perniciosa* using a bran-vermiculite medium. Neth J P Path **99**: 227-230

Hayashizaki Y (2003) The Riken mouse genome encyclopedia project. C R Biol **326**: 923-929

Kilian J, Whitehead D, Horak J, Wanke D, Weinl S, Batistic O, D'Angelo C, Bornberg-Bauer E, Kudla J, Harter K (2007) The AtGenExpress global stress expression data set: protocols, evaluation and model data analysis of UV-B light, drought and cold stress responses. Plant J **50**: 347-363

Laloi M, McCarthy J, Morandi O, Gysler C, Bucheli P (2002) Molecular and biochemical characterisation of two aspartic proteinases TcAP1 and TcAP2 from Theobroma cacao seeds. Planta **215**: 754-762

Langmead B, Trapnell C, Pop M, Salzberg SL (2009) Ultrafast and memory-efficient alignment of short DNA sequences to the human genome. Genome Biol **10**: R25

Leal GA, Albuquerque PS, Figueira A (2007) Genes differentially expressed in *Theobroma cacao* associated with resistance to witches' broom disease caused by *Crinipellis perniciosa*. Mol Plant Pathol **8**: 279-292

Leal GA, Gomes LH, Albuquerque PS, Tavares FC, Figueira A (2010) Searching for *Moniliophthora perniciosa* pathogenicity genes. Fungal Biol **114**: 842-854

Marcel S, Sawers R, Oakeley E, Angliker H, Paszkowski U (2010) Tissue-adapted invasion strategies of the rice blast fungus *Magnaporthe oryzae*. Plant Cell **22**: 3177-3187

Marioni JC, Mason CE, Mane SM, Stephens M, Gilad Y (2008) RNA-seq: an assessment of technical reproducibility and comparison with gene expression arrays. Genome Res **18**: 1509-1517

Martinez D, Challacombe J, Morgenstern I, Hibbett D, Schmoll M, Kubicek CP, Ferreira P, Ruiz-Duenas FJ, Martinez AT, Kersten P, *et al.* (2009) Genome, transcriptome, and secretome analysis of wood decay fungus *Postia placenta* supports unique mechanisms of lignocellulose conversion. Proc Natl Acad Sci U S A **106**: 1954-1959

Meinhardt LW, Bellato CM, Rincones J, Azevedo RA, Cascardo JC, Pereira GA (2006) In vitro production of biotrophic-like cultures of *Crinipellis perniciosa*, the causal agent of witches' broom disease of *Theobroma cacao*. Curr Microbiol **52**: 191-196

Meinhardt LW, Rincones J, Bailey BA, Aime MC, Griffith GW, Zhang D, Pereira GA (2008) *Moniliophthora perniciosa*, the causal agent of witches' broom disease of cacao: what's new from this old foe? Mol Plant Pathol **9**: 577-588

Metzker ML (2010) Sequencing technologies - the next generation. Nat Rev Genet **11**: 31-46

Mortazavi A, Williams BA, McCue K, Schaeffer L, Wold B (2008) Mapping and quantifying mammalian transcriptomes by RNA-Seq. Nat Methods **5**: 621-628

Penman D, Britton G, Hardwick K, Collin H, Isaac S (2000) Chitin as a measure of biomass of *Crinipellis perniciosa*, causal agent of witches' broom disease of *Theobroma cacao*. Mycol Res **104**: 671-675

Pereira JL, deAlmeida LCC, Santos SM (1996) Witches' broom disease of cocoa in Bahia: Attempts at eradication and containment. Crop Protection **15**: 743-752

Pires AB, Gramacho KP, Silva DC, Goes-Neto A, Silva MM, Muniz-Sobrinho JS, Porto RF, Villela-Dias C, Brendel M, Cascardo JC, *et al.* (2009) Early development of *Moniliophthora perniciosa* basidiomata and developmentally regulated genes. BMC Microbiol **9**: 158

Purdy LH, Schmidt RA (1996) Status of cacao witches' broom: biology, epidemiology, and management. Annu Rev Phytopathol **34**: 573-594

Rincones J, Scarpari LM, Carazzolle MF, Mondego JM, Formighieri EF, Barau JG, Costa GG, Carraro DM, Brentani HP, Vilas-Boas LA, *et al.* (2008) Differential gene expression between the biotrophic-like and saprotrophic mycelia of the witches' broom pathogen *Moniliophthora perniciosa*. Mol Plant Microbe Interact **21**: 891-908

Robinson MD, McCarthy DJ, Smyth GK (2010) edgeR: a Bioconductor package for differential expression analysis of digital gene expression data. Bioinformatics **26**: 139-140

Sambrook J, Fritsch E, Maniatis T (1989) Molecular cloning: a laboratory manual. Cold Spring Harbour Lab Press, EUA,

Skibbe DS, Doehlemann G, Fernandes J, Walbot V (2010) Maize tumors caused by *Ustilago maydis* require organ-specific genes in host and pathogen. Science **328**: 89-92

Thomazella DP, Teixeira PJ, Oliveira HC, Saviani EE, Rincones J, Toni IM, Reis O, Garcia O, Meinhardt LW, Salgado I, *et al.* (2012) The hemibiotrophic cacao pathogen *Moniliophthora perniciosa* depends on a mitochondrial alternative oxidase for biotrophic development. New Phytol **194**: 1025-1034

Wheeler B (1985) The growth of *Crinipellis perniciosa* in living and dead cocoa tissue. Symp Ser Br Mycol Soc **10**: 103-116

Capítulo II

High-resolution transcript profiling of the atypical biotrophic interaction between *Theobroma cacao* and the fungal pathogen *Moniliophthora perniciosa*

Paulo José P.L. Teixeira*, Daniela P.T. Thomazella*, Osvaldo Reis, Paula F.V. do Prado, Maria C.S. do Rio, Gustavo G.L. Costa, Ramon O. Vidal, Jorge M.C. Mondego, Piotr Mieczkowski, Gonçalo A.G. Pereira

* Autores com igual contribuição

Trabalho submetido para publicação na revista *The Plant Cell*.

APRESENTAÇÃO

Este capítulo apresenta uma análise transcriptômica detalhada da interação biotrófica entre o fungo *Moniliophthora perniciosa* e o cacaueiro. Em contraste com a maioria dos patógenos hemibiotróficos, que apresentam uma fase biotrófica rápida e assintomática, o desenvolvimento biotrófico de *M. perniciosa* pode durar de dois a três meses e é responsável pelos principais sintomas da doença na planta. Esta particularidade torna a vassoura de bruxa um interessante modelo de estudo para a compreensão de interações planta-patógeno. Ainda que o Atlas Transcriptômico da Vassoura de Bruxa seja constituído por dezenas de bibliotecas específicas, decidimos dedicar grande parte de nossos esforços para dissecar este estágio peculiar da doença. O trabalho envolveu o sequenciamento de dez bibliotecas de RNA-seq e a realização de análises bioquímicas e histológicas que, em conjunto, revelaram importantes aspectos da vassoura de bruxa. Surpreendentemente, verificamos que plantas infectadas sofrem um processo de senescência em decorrência de privação nutricional. Esta senescência parece ser um evento central no desenvolvimento da doença, podendo induzir a mudança para o estágio necrotrófico de *M. perniciosa*. Um modelo que sumariza a base molecular e fisiológica da interação biotrófica entre *M. perniciosa* e o cacaueiro foi elaborado. Além de investigar as respostas da planta ao patógeno, este é o primeiro trabalho a apresentar o perfil transcricional do fungo *M. perniciosa* durante seu desenvolvimento *in planta.*

Nota: Este trabalho possui uma grande quantidade de material suplementar que não pode ser apresentado na versão impressa desta tese. Por isso, disponibilizamos este material *online* em:

www.lge.ibi.unicamp.br/tese/paulo
Login: Banca _examinadora
Senha: material_suplementar

High-resolution transcript profiling of the atypical biotrophic interaction between *Theobroma cacao* and the fungal pathogen *Moniliophthora perniciosa*

Paulo José Pereira Lima Teixeira[a,1], Daniela Paula de Toledo Thomazella[a,1], Osvaldo Reis[a], Paula Favoretti Vital do Prado[a], Maria Carolina Scatolin do Rio[a,2], Gustavo Gilson Lacerda Costa[a], Ramon Oliveira Vidal[a,3], Jorge Maurício Costa Mondego[b], Piotr Mieczkowski[c], Gonçalo Amarante Guimarães Pereira[a,4]

[a] Laboratório de Genômica e Expressão, Departamento de Genética, Evolução e Bioagentes, Instituto de Biologia, Universidade Estadual de Campinas (UNICAMP), Campinas, SP, Brazil.
[b] Centro de Pesquisa e Desenvolvimento em Recursos Genéticos Vegetais, Instituto Agronômico de Campinas, Campinas, SP, Brazil.
[c] Department of Genetics, School of Medicine, University of North Carolina at Chapel Hill, Chapel Hill, NC, United States of America.

[1] Contributed equally to this study.
[2] Current address: Laboratório Nacional de Biociências, Centro Nacional de Pesquisa em Energia e Materiais, Campinas, SP, Brazil.
[3] Current address: CHU Sainte-Justine Research Center, Université de Montréal, Montréal, QC, Canada.
[4] To whom correspondence should be addressed. E-mail: goncalo@unicamp.br; phone: +55-19-35216237.

Calculated number of pages: 16.4

Running title: RNA-seq survey of witches' broom disease

The author responsible for distribution of materials integral to the findings presented in this article in accordance with the policy described in the Instructions for Authors (www.plantcell.org) is: Gonçalo A.G. Pereira (goncalo@unicamp.br).

SYNOPSIS

This work dissects the intriguing biotrophic interaction between *Theobroma cacao* and the fungus *Moniliophthora perniciosa* in the devastating witches' broom disease. Infection by *M. perniciosa* leads to massive genetic reprogramming in cacao tissues, which culminates in the onset of a premature senescence process. A detailed molecular model of this peculiar plant-pathogen interaction is presented.

ABSTRACT

Witches` broom disease (WBD), caused by the hemibiotrophic fungus *Moniliophthora perniciosa*, is one of the most devastating diseases of *Theobroma cacao*, the chocolate tree. In contrast to other hemibiotrophic interactions, the WBD biotrophic stage lasts for months and is responsible for the most distinctive symptoms of the disease, which comprise drastic morphological changes in the infected shoots. Here, we used the dual RNA-seq approach to simultaneously assess the transcriptomes of cacao and *M. perniciosa* during their peculiar biotrophic interaction. Infection with *M. perniciosa* triggers massive metabolic reprogramming in the diseased tissues. Although apparently vigorous, the infected shoots are energetically expensive structures characterized by the induction of ineffective defense responses and by a clear carbon deprivation signature. Remarkably, the infection culminates in the establishment of a senescence process in the host, which signals the end of the WBD biotrophic stage. Thus, *M. perniciosa* biotrophic mycelia develop as long-term parasites that orchestrate changes in plant metabolism to increase the availability of soluble nutrients before plant death. Collectively, our results provide unprecedented findings on an intriguing tropical disease and advance our understanding of the development of biotrophic plant-pathogen interactions.

INTRODUCTION

Crop diseases caused by fungi represent a major constraint to agricultural productivity, leading to drastic economic losses each year (Fisher et al., 2012). In general, the outcome of a disease process depends on the molecular interplay between the pathogen and its host and involves substantial transcriptional changes in both organisms. In response to microbial invasion, plants activate an array of defense mechanisms (e.g., reinforcement of cell walls, production of reactive oxygen species, accumulation of antimicrobial compounds). By contrast, pathogens have devised different strategies to evade plant immunity as well as to feed on and reproduce in the host tissues (Dodds and Rathjen, 2010). Dissecting the molecular mechanisms governing plant-pathogen interactions is an important step towards developing novel and effective strategies to control diseases and improve food security.

Tropical areas have a suitable climate for the cultivation of a large number of crops. However, they are also highly prone to the development of a variety of pathogenic microorganisms. Despite the importance of tropical plants in maintaining the growing human population, plant diseases of tropical regions have traditionally received little attention. The basidiomycete *Moniliophthora perniciosa* causes witches' broom disease (WBD) in *Theobroma cacao*, the chocolate tree (Aime and Phillips-Mora, 2005). This highly destructive disease has negatively affected cacao productivity in many American countries and is a threat to global cocoa production (Purdy and Schmidt, 1996; Meinhardt et al., 2008). WBD is a challenging disease to study, as it results from the interaction between two non-model organisms that exhibit complex life cycles. Furthermore, genetic tools that would be suitable for analyzing these organisms are limited. On the other hand, the economic importance of WBD and the limited knowledge on tropical plant-pathogen interactions make the study of this disease of great relevance.

The *M. perniciosa* lifestyle is classified as hemibiotrophic (Evans, 1980). However, it has some distinctive characteristics that set WBD aside from other well-studied pathosystems. In general, hemibiotrophic pathogens (e.g., *Magnaporthe oryzae* and *Colletotrichum spp.*) display an

initial transient and asymptomatic biotrophic stage that is rapidly followed by a destructive necrotrophic phase, wherein the most prominent disease symptoms develop (Perfect and Green, 2001; Munch et al., 2008). Conversely, the *M. perniciosa* biotrophic stage is extremely prolonged, lasting even longer than typical biotrophic interactions (e.g., those exhibited by powdery mildews, rusts and smut diseases). During this stage, *M. perniciosa* slowly grows between living cacao cells and is found at very low density within the infected tissues. Even so, biotrophic colonization induces drastic physiological and morphological alterations in the plant (Purdy and Schmidt, 1996; Meinhardt et al., 2008). After 2 to 3 months of biotrophic development, the infected tissues become necrotic as WBD enters the necrotrophic stage of development (Evans, 1980).

Although *M. perniciosa* can also infect flowers and young fruits, the infection of shoots is responsible for the typical symptoms of the disease, namely the formation of abnormal structures called “green brooms” (Griffith et al., 2003). Infected shoots become swollen, with irregular growth and loss of apical dominance, suggesting the occurrence of hormonal imbalances during disease development. Moreover, important biochemical alterations were verified to occur in cacao plants during WBD (Scarpari et al., 2005). Changes in soluble sugar, amino acid, secondary metabolite, ethylene and glycerol content were observed in cacao shoots upon infection, indicating that a remarkable degree of genetic reprogramming took place in the infected tissue (Scarpari et al., 2005). Notably, the green broom stage is considered a commitment point in WBD progression, and cacao plants are not able to stall fungal development once these structures have formed.

Despite considerable advances in our understanding of WBD over the past few years (Scarpari et al., 2005; Mondego et al., 2008; Rincones et al., 2008), our knowledge of the intriguing biotrophic interaction established between *M. perniciosa* and cacao is still very limited. Previous studies investigated cacao responses to *M. perniciosa* infection at the transcriptional level (Gesteira et al., 2007; Leal et al., 2007; da Hora Junior et al., 2012). However, they mainly involved comparisons between resistant and susceptible genotypes, with the aim of identifying resistance mechanisms. Consequently, little emphasis has been placed on the molecular events underlying

the complexity of compatible interactions in WBD. Moreover, the number of genes analyzed in these studies was restricted by the use of Sanger-based cDNA sequencing and/or nucleic acid hybridization techniques. Such methodologies were also applied for large-scale gene expression analyses in *M. perniciosa,* providing initial insight into the pathogen's biology (Rincones et al., 2008; Pires et al., 2009; Leal et al., 2010). Nevertheless, these studies have addressed the transcriptional regulation of *M. perniciosa* exclusively under artificial conditions, and the genetic program governing the fungal interaction with cacao remains unexplored.

Advances in next-generation sequencing technologies have opened new avenues to realizing high-throughput analyses with the potential of uncovering key aspects of host-microbe interactions (Studholme et al., 2011). The RNA-seq approach allows the simultaneous inspection of transcriptomes from both the pathogen and its host with a high level of accuracy and depth, providing the big picture of an infective process (Westermann et al., 2012). With the purpose of dissecting the *M. perniciosa*-cacao interaction and establishing a foundation for the study of this disease, a comprehensive transcriptomic analysis of WBD has recently been initiated with the construction of the WBD Transcriptome Atlas (Teixeira et al. unpublished data). Using RNA-seq, we analyzed a wide range of developmental stages, growth conditions and stress responses of the fungus, both under *in vitro* and *in planta* conditions.

This work provides a detailed transcriptomic analysis of the biotrophic interaction between *M. perniciosa* and cacao, which corresponds to the green broom stage of WBD. We identified important alterations in the transcriptome of infected cacao plants that suggest the induction of a premature senescence process triggered by depletion of nutrients in the infected tissues. The RNA-seq data was significantly corroborated by complementary histological and biochemical assays. Moreover, the pathogen's transcriptome was analyzed in unprecedented depth, allowing the characterization of the fungal nutritional and infective strategies during WBD and the identification of putative virulence effectors. Overall, these data provide novel insights into the complex hemibiotrophic interaction between *M. perniciosa* and cacao, and represent a major advance in our

understanding of a tropical plant disease.

RESULTS

Symptoms of infected plants

Cacao seedlings inoculated with basidiospores of the pathogen *M. perniciosa* were inspected for the development of the typical symptoms of WBD. The first visible symptom, a slight swelling of the plant apical meristem, was detected approximately 20 days post infection. Within 30 days of inoculation, the typical symptoms of the green broom stage of WBD were clearly observed (Figure 1A): diseased leaves were chlorotic (Figure 1B) and stems exhibited hypertrophic and exacerbated growth and loss of apical dominance, as evidenced by the proliferation of lateral buds (Figure 1C). Moreover, in this stage of WBD, the fungus was restricted to the narrow space between cacao cells (Figure 1D). A healthy plant is shown in Figure 1E for comparison. Interestingly, histological analyses also revealed a clear reduction in the starch content of green brooms in comparison to healthy non-infected plants (Figure 1F and Figure 1G).

Sequencing the green broom transcriptome

Five biological replicates of each condition (healthy seedlings and seedlings at 30 days after infection) were collected for transcriptome sequencing using RNA-seq. A preliminary RNA-seq run of an infected plant using the Illumina Genome Analyzer IIx sequencer revealed that less than 1% of all reads correspond to *M. perniciosa* transcripts. For this reason, we opted to use the Illumina Hiseq 2000 sequencer, which has a much higher sequence throughput, thus improving the detection of rare (i.e., fungal) transcripts. Considering that there were five biological replicates of each condition, we produced a total of 562 million and 436 million paired reads for infected and healthy (control) plants, respectively (Table 1). All reads were aligned against 34,997 gene models of cacao, which are available at www.cacaogenomedb.org. For each RNA-seq library, approximately 80% of the reads mapped to the cacao reference. Also, reads were mapped against

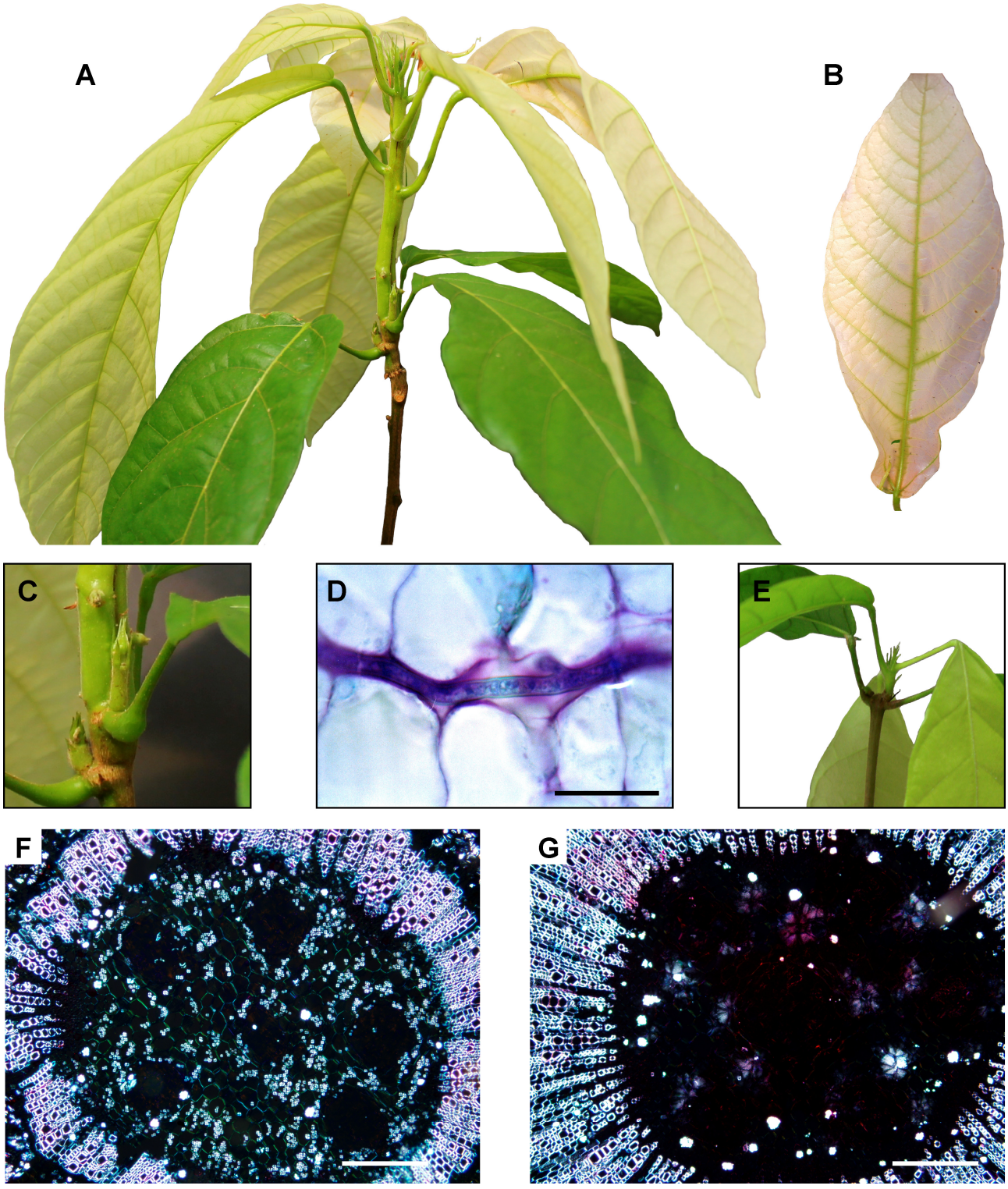

Figure 1. The green broom stage of witches` broom disease. (A) Apical portion of representative infected plant illustrating the major morphological changes caused by *Moniliophthora perniciosa* infection. (B) Leaf chlorosis observed in green brooms. (C) Detail of the loss of apical dominance observed in infected plants. (D) Histological analysis showing fungal growth, which is restricted to the cacao intercellular space. Bar = 25 µm. (E) Healthy cacao plant. (F) Cortical region of healthy plants visualized under polarized light showing numerous starch grains. Bar = 200 µm. (G) Infected plants are depleted in starch grains. Bar = 200 µm.

17,008 gene models of *M. perniciosa* for the analysis of the fungal transcriptome. Whereas an insignificant fraction of reads (0.0002%) from control libraries mapped to *M. perniciosa* genes, approximately 0.3% of the reads derived from infected seedlings mapped to the fungal reference (Table 1). The small proportion of *M. perniciosa* reads in green brooms is consistent with the low density of fungal cells in the green broom stage of WBD (Penman et al., 2000).

Table 1. Sequencing metrics of the ten RNA-seq libraries.

Source	Library	Total paired-reads	Mapping to *T. cacao*	Mapping to *M. perniciosa*
Infected plants				
	I1	77,308,238	56,400,430 (72.95%)	264,332 (0.34%)
	I2	207,441,756	165,626,752 (79.84%)	900,907 (0.43%)
	I3	83,953,292	67,319,071 (80.19%)	195,224 (0.23%)
	I4	90,591,723	70,903,224 (78.27%)	185,943 (0.21%)
	I5	103,196,353	81,436,515 (78.91%)	157,297 (0.15%)
	Total	562,491,362	441,685,992 (78.52%)	1,703,703 (0.30%)
Healthy plants				
	H1	89,659,731	73,116,542 (81.54%)	26 (0.00%)
	H2	82,560,659	67,931,619 (82.28%)	632 (0.00%)
	H3	86,454,964	68,434,420 (79.16%)	204 (0.00%)
	H4	80,950,589	65,107,761 (80.43%)	91 (0.00%)
	H5	96,856,054	73,239,227 (75.62%)	14 (0.00%)
	Total	436,481,997	347,829,569 (79.69%)	967 (0.00%)

Genes differentially expressed between infected and healthy plants were defined using the edgeR software package (Robinson et al., 2010). Of the 34,997 cacao genes, 17,713 were expressed in the conditions analyzed. Among them, 1,269 were up-regulated in green brooms and 698 were down-regulated, totaling 1,967 differentially expressed genes (see Supplemental Data Set 1 online). In addition, qPCR assays were performed to validate gene expression values obtained by RNA-seq. To this purpose, the expression of 28 cacao genes was analyzed in two plants that were also sequenced by RNA-seq. A strong correlation (R^2>0.92) was observed between the results obtained using the two techniques (Figure 2A), demonstrating the reliability of the data produced. Finally, we performed hierarchical clustering and principal component analysis (PCA) to assess the biological variability among all samples. The results indicated that most of the

variation in gene expression is a consequence of the infection process. Two distinct groups were formed in the hierarchical clustering: one group comprised of infected plants and the other comprised of healthy plants (Figure 2B). Similarly, PCA showed that the transcriptomes of infected and healthy plants are clearly different from each other (Figure 2C).

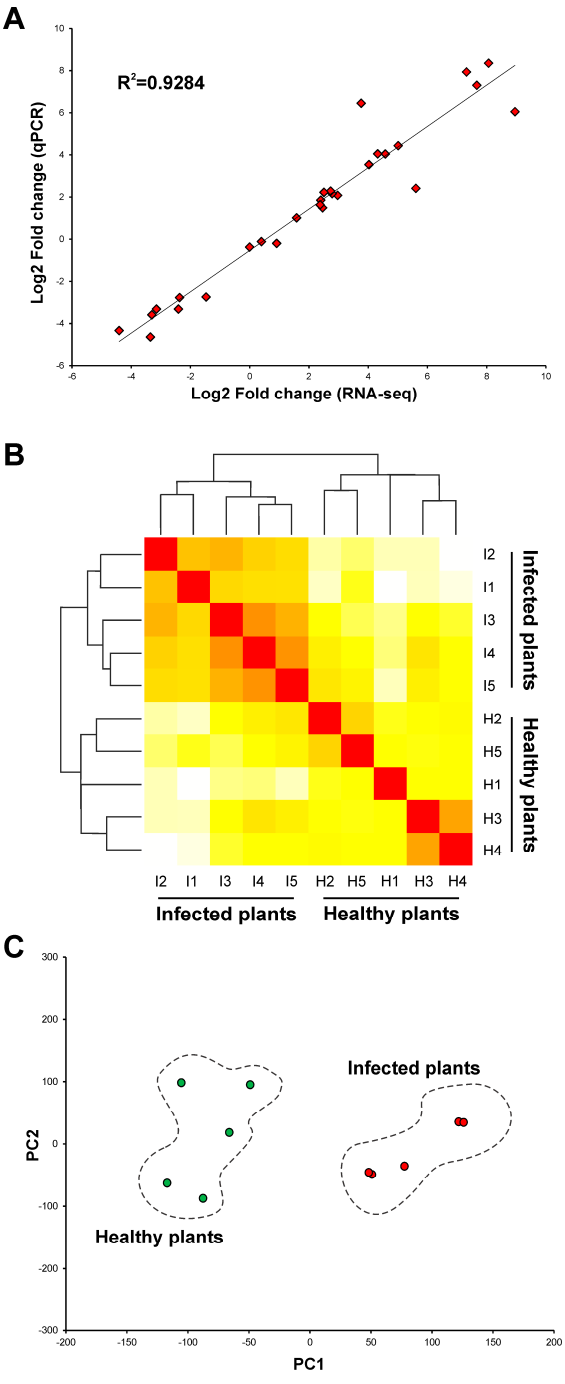

Figure 2. Global evaluation of the RNA-seq experiment. (A) Comparison between gene expression values obtained by qPCR and RNA-seq. Fold changes were calculated for 28 cacao genes and a high correlation (R2>0.92) was observed between the two techniques. (B) Hierarchical clustering of the ten samples used in this study showing two distinct clades: one comprised of infected plants and the other comprised of healthy plants. Individual plants were identified according to the nomenclature presented in Table 1. (C) Principal component analysis displaying the intrinsic biological variation among samples. The result confirms the clear distinction between the transcriptomes of infected and healthy plants.

Metabolic pathways and protein domain enrichment analyses: an overview of the transcriptional responses of infected plants

Global analyses of diseased cacao plants were performed to provide an overview of the physiological alterations caused by *M. perniciosa* infection. Individual gene responses in metabolic pathways were visualized using the MapMan tool (Figure 3A). A remarkable repression of genes related to photosynthesis, tetrapyrrole (chlorophyll chromophore) biosynthesis, starch biosynthesis, desaturation of fatty acids and nitrogen assimilation was verified. By contrast, an induction of genes involved in secondary metabolism, cell wall modification and lipid degradation was observed. A complete list of MapMan pathways differentially represented in green brooms is provided in Supplemental Data Set 2 online. In addition, enrichment analysis of InterPro terms showed specific domains and families differentially represented in green brooms (Figure 3B; see Supplemental Data Set 3 online). Protein domains/families related to defense, hormonal metabolism, signaling pathways, stress responses and cell wall modification were over-represented. Conversely, under-represented terms included proteins associated with photosynthesis, chlorophyll biosynthesis, chloroplastic RNA polymerase and desaturation of fatty acids. In general, these results indicated important changes that occur in the green broom stage of WBD, which will be explored in the following sections.

Transcriptional alterations in infected plants

Infected cacao tissues undergo carbon starvation during WBD

Remarkable changes in the primary metabolism of cacao plants are observed in the green broom stage of WBD. Thirty-day-old leaves developed from apical meristems were expected to be photosynthetically active. However, as a consequence of the disease, genes related to the photosynthetic apparatus were down-regulated (Figure 4A; see Supplemental Data Set 4 online). Concomitantly, severe chlorosis (Figure 1B) and lower rates of CO_2 assimilation (Figure 4B) were observed in leaves developed from infected tissues in comparison to healthy plants. By contrast,

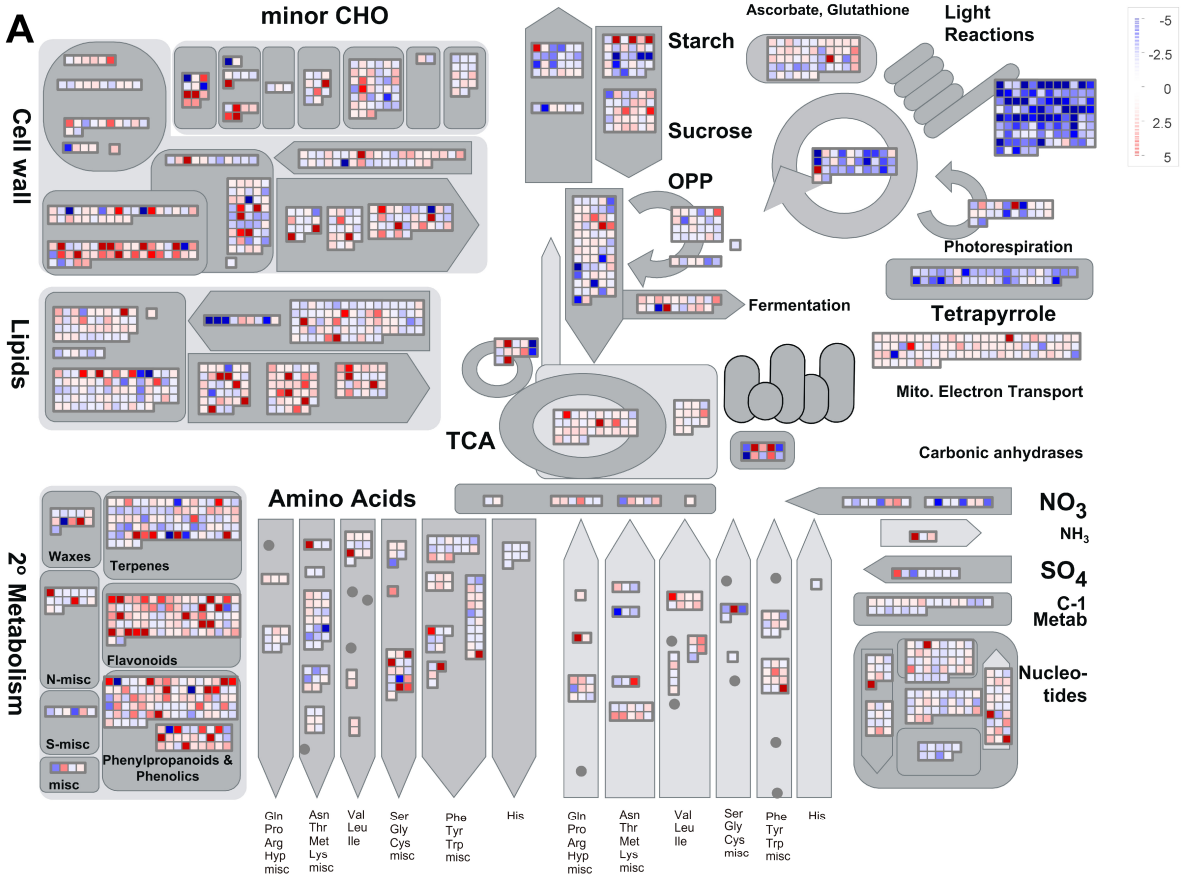

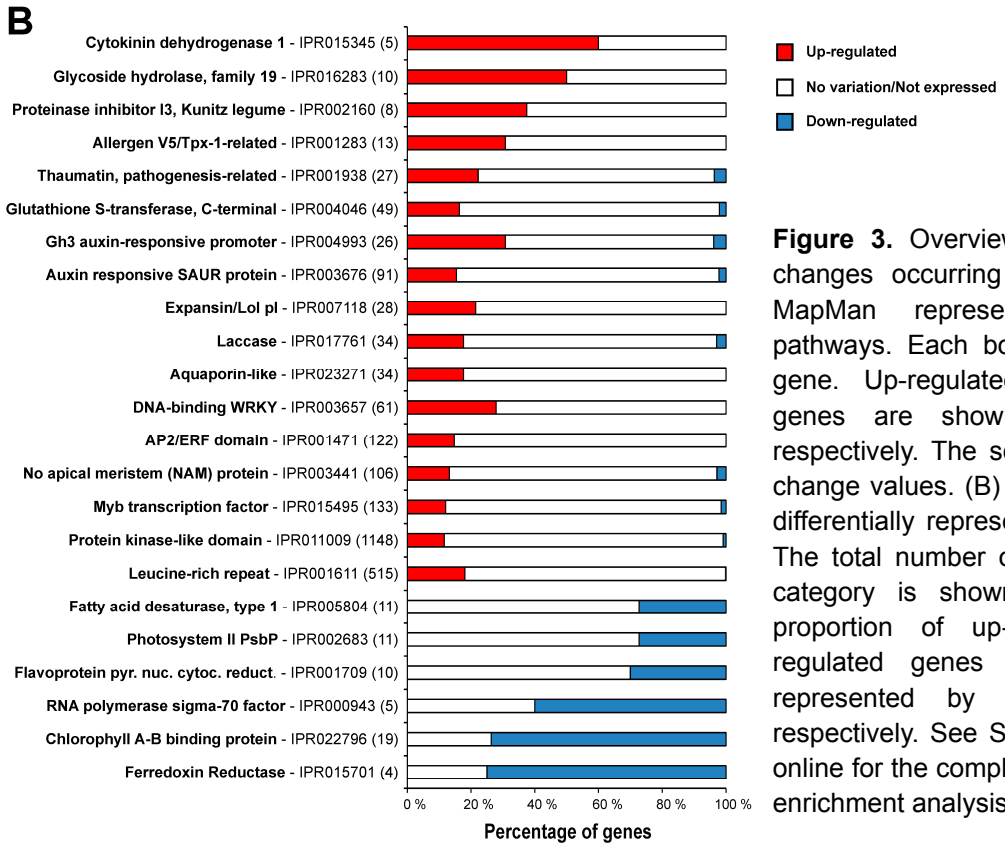

Figure 3. Overview of the transcriptional changes occurring in green brooms. (A) MapMan representation of metabolic pathways. Each box depicts an individual gene. Up-regulated and down-regulated genes are shown in red and blue, respectively. The scale bar represents fold change values. (B) Selected InterPro terms differentially represented in infected plants. The total number of cacao genes in each category is shown in parenthesis. The proportion of up-regulated and down-regulated genes within a category is represented by red and blue bars, respectively. See Supplemental Data Set 3 online for the complete result of the InterPro enrichment analysis.

up-regulation of genes related to the breakdown of sucrose (cell wall invertase) and transport of hexoses (hexose transporters) was verified, indicating that the disease interferes with the normal development of cacao meristematic tissues, resulting in the maintenance of their primary sink capacity.

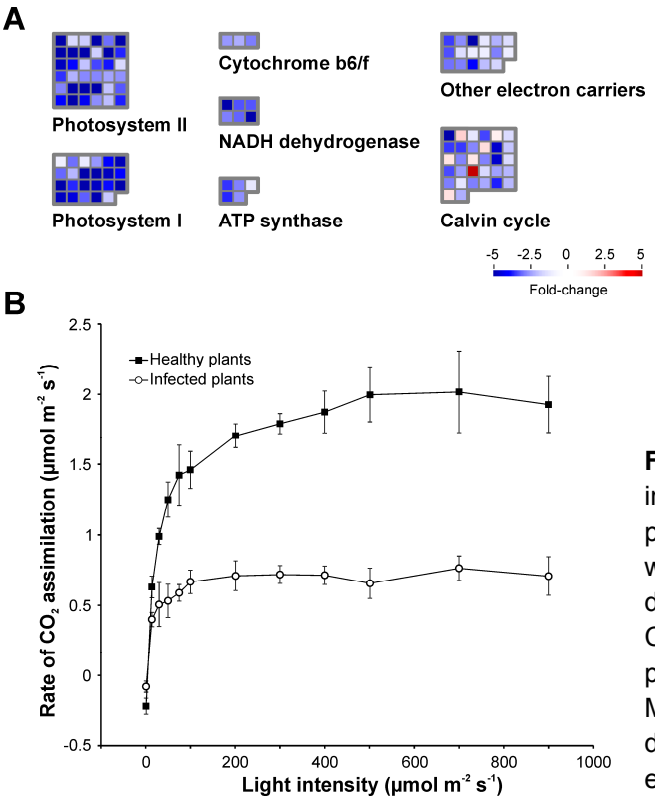

Figure 4. Photosynthetic metabolism is impaired in infected cacao plants. (A) Genes involved in photosynthesis are down-regulated in green brooms when compared to healthy plants. Gene classes were defined according to the MapMan ontology. (B) Consistent with the RNA-seq results, infected plants presented lower rates of CO_2 assimilation. Measurements were performed in triplicate under different light intensities. Error bars represent standard errors.

In parallel, genes associated with the degradation of carbohydrate and lipid storage molecules (starch and triacylglycerol, respectively) were also up-regulated, including genes encoding amylases and lipases (see Supplemental Data Set 4 online). Indeed, reduced amounts of starch granules were clearly observed in infected tissues (Figure 1F and Figure 1G), suggesting that, upon infection, the plant mobilizes these storage molecules as complementary sources of energy. In addition, genes related to the fatty acid β-oxidation pathway (see Supplemental Data Set 4 online), a process by which fatty acids are broken down to produce energy, were over-expressed. The final product of fatty acid β-oxidation is acetyl-CoA, which can directly enter the glyoxylate

cycle. In the glyoxylate cycle, lipids are converted into carbohydrates through the enzymes isocitrate lyase and malate synthase, both of which have elevated levels of transcription in the green broom stage of WBD. The remaining glycerol, derived from lipid degradation, might also be used as energy source. The transcription of a gene encoding a FAD-dependent glycerol-3-phosphate dehydrogenase was increased, suggesting that the phosphorylated form of glycerol (glycerol-3-phosphate) may be directly respired in the mitochondrial electron transport chain. Overall, the general disarrangement in plant metabolism caused by the *M. perniciosa* infection appears to culminate in the deprivation of carbon skeletons, compelling the plant to obtain energy from alternative sources.

Host nitrogen metabolism is directed towards the production of carbon skeletons

In addition to carbohydrates and lipids, plant amino acids also seem to be energetically consumed in green brooms. Genes involved in the catabolism of several amino acids were up-regulated (see Supplemental Data Set 4 online), which may result in the release of ammonium and intermediate compounds to the TCA cycle or to other metabolic processes. In contrast, nitrogen assimilation (from nitrate/ammonium to glutamine), which is a high energy consuming process, is impaired in green brooms. Diseased plants showed decreased expression of *nitrate/nitrite reductases* and *glutamine synthetase* genes, which encode critical enzymes for primary nitrogen assimilation. Remarkably, despite the overall degradation of amino acids, asparagine biosynthesis was transcriptionally induced (see Supplemental Data Set 4 online). Along with genes that are directly involved in nitrogen biosynthesis/catabolism, several transporters that mediate the uptake of extracellular amino acids and peptides were up-regulated (see Supplemental Data Set 3 online). Additionally, a cacao gene that is orthologous to the tonoplast intrinsic gene subfamily of *Arabidopsis thaliana* (TIP2;1) was over-expressed in green brooms. TIP2;1 was shown to mediate the extracytosolic transport of ammonium across the tonoplast and may participate in vacuolar compartmentalization of this toxic compound (Loqué et al., 2005).

Insight into the hormonal metabolism of green brooms

The symptoms observed in infected cacao tissues suggest the occurrence of significant and essentially unexplored hormonal imbalances during WBD. To identify signatures of hormonal responses in infected cacao plants, we used the Hormonometer software, which compares the variation in gene expression of a query experiment with indexed datasets of hormone treatments (Volodarsky et al., 2009). Since this software requires *Arabidopsis* genes as input, we used 8,870 putative orthologs of cacao genes that were expressed in our experiment. To evaluate the Hormonometer performance using this gene set, we analyzed public gene expression data of *Arabidopsis* mutants with known alterations in hormone levels (i.e., *eto1*, *arr21*, *nahG* and *nph4 arf19*). As shown in Figure 5, the Hormonometer profile of each *Arabidopsis* mutant is highly representative of the global hormonal alterations that occur in these plants, thus validating the use of this set of genes.

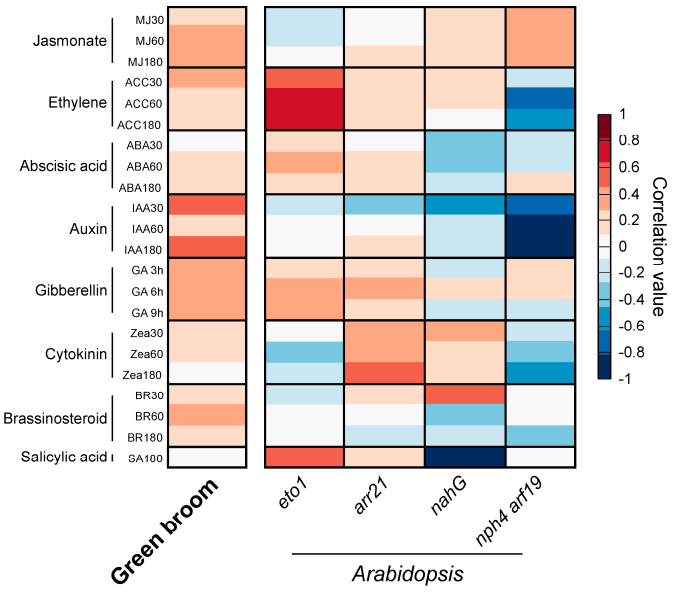

Figure 5. Identification of hormonal signatures based on transcriptomic data. The analysis was conducted using the Hormonometer software, which compares gene expression data of a query experiment with datasets of hormone responses. Transcriptomes of *Arabidopsis* mutants with known alterations in hormonal responses were used as controls (*arr21* - increased cytokinin response; *eto1* - increased ethylene response; *nahG* - reduced salycilic acid levels; *nph arf19/IAA* - reduced auxin signaling). A positive correlation between the query transcriptome and a hormone treatment is denoted in red, whereas a negative correlation is represented by blue.

Auxins. The Hormonometer profile of green brooms showed a strong correlation with auxin responses (Figure 5). Primary auxin-responsive genes fall into three major classes: *GH3*, *Aux/IAA* (auxin/indole-3-acetic acid protein) and *SAUR* (small auxin-up RNA). In accordance with the Hormonometer result, InterPro terms representing proteins encoded by these three classes of genes were significantly enriched in infected plants (Figure 3B; see Supplemental Data Set 3 online). Furthermore, members of the PIN and PILS (PIN-LIKES) class of auxin transporters were differentially expressed (see Supplemental Data Set 5 online), suggesting the existence of altered levels of auxin in green brooms. Genes involved in auxin biosynthesis were not differentially expressed.

Gibberellins. The Hormonometer analysis also indicated a high correlation between green brooms and gibberellin treatments (Figure 5). Several genes involved in the gibberellin response were up-regulated in green brooms, including α-amylases, invertases, GAST-like (Gibberellic acid stimulated transcript-like), pectinesterases, XTHs (xyloglucan endotransglycosylase/hydroxylases) and expansins. Many of these gibberellin-responsive genes mediate cell elongation/expansion and their increased expression is in agreement with the morphological alterations observed in infected cacao shoots (Figure 1). Genes encoding enzymes involved in gibberellin perception (GID1-like), biosynthesis (GA3ox) and inactivation (GA2ox) were also identified among the up-regulated genes (see Supplemental Data Set 5 online).

Cytokinins. Although some components of the cytokinin signaling circuitry were up-regulated in infected plants (see Supplemental Data Set 5 online), a clear signature of cytokinin responses was not evident in the green broom stage of WBD (Figure 5). In accordance, a gene involved in cytokinin biosynthesis (*IPT* - isopentenyltransferase) was repressed in infected plants. Also, other genes related to the cytokinin response and biosynthesis were not differentially expressed. Instead, many genes related to cytokinin degradation (cytokinin oxidases) or inactivation (cytokinin glucosyltransferases) showed increased transcript levels (see Supplemental Data Set 5 online), indicating that cytokinins are being degraded/inactivated in this stage of WBD.

Salicylic Acid, Jasmonic Acid and Ethylene. The Hormonometer analysis showed no correlation between green brooms and salicylic acid (SA) responses. By contrast, higher correlation values were verified for both jasmonic acid (JA) and ethylene (ET) (Figure 5). In particular, transcripts related to ET biosynthesis were increased in green brooms (see Supplemental Data Set 5 online). Moreover, a large number of genes encoding ERF (Ethylene response factor) transcription factors were notably over-expressed in infected plants, supporting the participation of ET in WBD.

M. perniciosa *triggers plant defense responses during the biotrophic interaction with cacao*

A remarkable characteristic of the green broom transcriptome is the prevalence of transcripts related to defense responses (Figure 6). Several genes encoding putative immune receptors were differentially expressed in infected plants (see Supplemental Data Set 6 online). Remarkably, of the 1,269 up-regulated genes in green brooms, at least 143 genes (11%) belong to the receptor-like kinase (RLK) or receptor-like protein (RLP) classes. These proteins are transmembrane receptors that perceive extracellular molecules, including microbe-associated molecular patterns (MAMPS) (Monaghan and Zipfel, 2012). InterPro terms related to kinases as well as to different extracellular domains commonly found in these proteins (e.g., LRR, lectin, malectin and WAK) were significantly enriched in infected plants (Figure 2B; see Supplemental Data Set 3 online). In addition to RLKs and RLPs, the expression of cacao receptors belonging to the NB-LRR family was also induced by *M. perniciosa* infection (see Supplemental Data Set 6 online). These genes encode intracellular proteins that directly or indirectly recognize pathogen effectors, leading to strong resistance responses (Jones and Dangl, 2006).

Along with immune receptors, a large number of genes encoding antimicrobial proteins was up-regulated in green brooms (Figure 6). Many of these genes belong to the Pathogenesis-related superfamily (PR), which comprises a heterogeneous group of 17 families that are part of the plant-inducible defense mechanisms against pathogens. Transcripts of genes encoding members of the

PR-1 (unknown activity), PR-2 (β-1-3-glucanase), PR-3, PR-4, PR-8, PR-11 (chitinase), PR-5 (thaumatin), PR-6 (protease inhibitor) and PR-10 (ribonuclease) families accumulated during WBD. Other up-regulated defense genes include WRKY transcription factors, polygalacturonase inhibitors, peroxidases and NADPH oxidases, which are responsible for the production of superoxide ions (see Supplemental Data Set 6 online). Therefore, cacao defense responses seem to be active in the green broom stage of WBD.

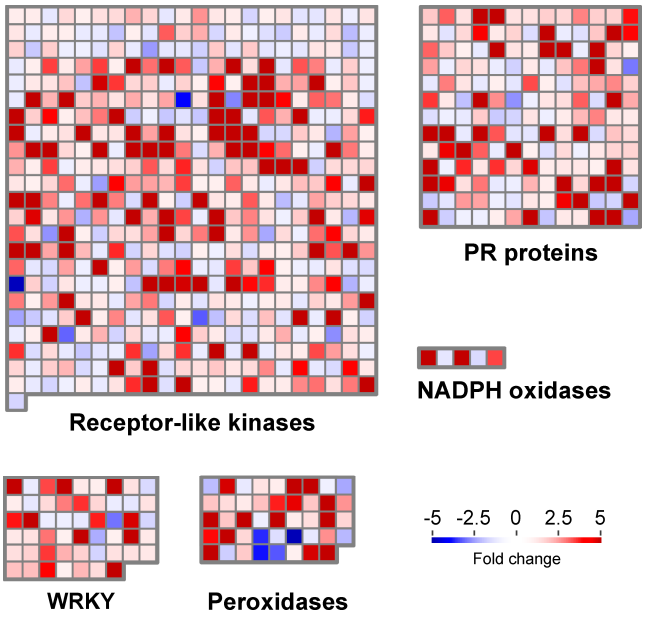

Figure 6. Cacao defense mechanisms are activated during the green broom stage of witches' broom disease. Selected classes of genes with known functions in plant defense responses are shown. The classification was performed according to the MapMan ontology. Each square represents an individual gene within a category. Up-regulated and down-regulated genes in infected plants are shown in red and blue, respectively. The scale bar represents fold change values.

Genes associated with secondary metabolism and cell wall modification are up-regulated in green brooms

Despite the evident impairment in the primary metabolism of green brooms, infected cacao tissues seem to allocate carbon skeletons and energy to the production of secondary metabolites (see Supplemental Data Set 7 online). Such metabolites are well-known stress indicators and are implicated in defense responses against microbes and animals. Several genes related to the

synthesis of flavonols, anthocyaninins, terpenoids and alkaloids were strongly up-regulated in green brooms (see Supplemental Data Set 7 online). Moreover, genes involved in lignin synthesis were also induced, indicating that lignin is deposited in infected tissues, possibly as an attempt to limit pathogen colonization. Indeed, histological analyses revealed the existence of cell wall reinforcement in infected tissues (Figure 7), supporting the idea that the plant perceives the pathogen and activates defense mechanisms during infection. Remarkably, a large number of genes encoding cell wall-modifying enzymes were up-regulated in green brooms, including expansins, endoglucanases, xyloglucan endotransglycosylases/hydrolases and glycosyl transferases. Transcripts of genes associated with the biosynthesis of cellulose and hemicellulose also accumulated in infected tissues.

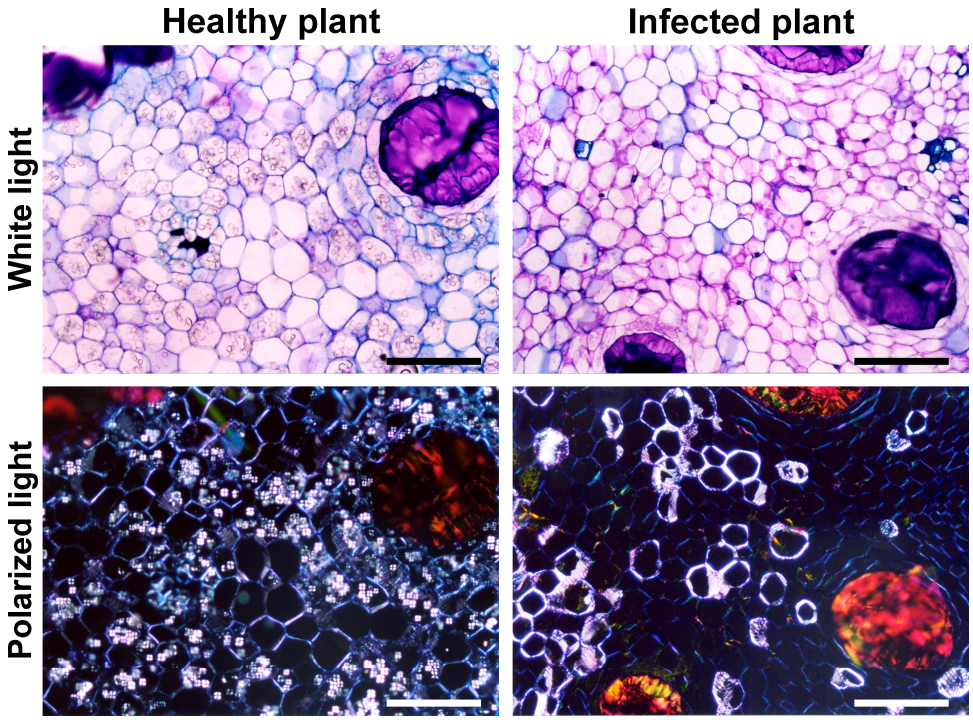

Figure 7. Histological analysis showing plant cell wall reinforcement in green brooms. In addition to the reduction in starch content, infected plants show reinforcement of cell walls, which is in line with the idea that the cacao host perceives the pathogen and mounts defense responses during the green broom stage of witches' broom disease. Samples were stained with toluidine blue and visualized under white and polarized lights. Bars = 200 µm.

Identification of fungal transcripts

As mentioned above, only a small proportion (0.3%) of the transcripts detected in infected plants were of fungal origin. The sequencing of the five infected plants resulted in a total of 562 million paired reads, of which 1.7 million mapped to *M. perniciosa* genes (Table 1). Using a threshold of 1 RPKM (reads per kilobase per million mapped reads) to consider a gene as being expressed, we detected around 13,000 *M. perniciosa* genes in our experiment, corresponding to 76% of the predicted fungal gene models. To evaluate the effect of sequencing depth on our ability to detect *M. perniciosa* transcripts, we generated different subsets of our RNA-seq data using randomly selected reads. We verified that only genes with the highest expression values are detected at low sequencing depths. However, the number of expressed genes starts to stabilize with approximately 0.5 million mapped paired reads, and few additional genes are detected by increasing the sequencing depth (see Supplemental Figure 1 online). This result indicates that most of the *M. perniciosa* genes that are expressed in green brooms were sampled in our experiment. Supplemental Data Set 8 online presents the expression levels of each of the 17,008 *M. perniciosa* genes.

The green broom transcriptome unravels candidate pathogenicity factors in M. perniciosa

The current version of the *M. perniciosa* genome encodes 193 candidate secreted effector proteins (CSEP), which were defined as secreted proteins that lack clearly characterized homologs in other sequenced organisms (see Supplemental Data Set 9 online). Remarkably, several of the most highly expressed fungal genes in green brooms encode CSEPs (Table 2), supporting an important role for these proteins during infection. In total, 35 CSEP-encoding genes with RPKM > 50 were identified in infected plants. In general, these genes encode small cysteine-rich proteins, with a mean size of 179 aa and a Cys content of 4.3%, both of which are typical of virulence effectors (Stergiopoulos and de Wit, 2009). Furthermore, inspection of the WBD Transcriptome Atlas revealed that most of these 35 *CSEP* genes are preferentially or even exclusively expressed

during the fungal biotrophic interaction with cacao (see Supplemental Figure 2 online), thus providing additional evidence that they encode potential effectors. Analysis of the CSEP protein sequences did not reveal the presence of any reported motif that presumably mediates the entrance of microbial effectors into plant cells (e.g., RXLR, RSIDELD, CHXC and Y/F/WXC motifs) (Kale et al., 2010; Godfrey et al., 2010; Zuccaro et al., 2011; Kemen et al., 2011).

Table 2. Most highly expressed *M. perniciosa* genes during the green broom stage of WBD.

			Gene expression values (RPKM)[a]					
GeneID	**Gene annotation**	**Length (aa)**	**I1**	**I2**	**I3**	**I4**	**I5**	**Mean**
MP13831	No hits (CSEP)	185	47106	73411	92642	81894	99895	78990
MP14755	No hits (CSEP)	246	81666	50657	67109	81134	63814	68876
MP14757	No hits (CSEP)	270	22364	19546	25939	27095	36987	26386
MP15869	No hits	243	36079	10330	17487	24296	19698	21578
MP13352	MpPR-1g	252	9121	16141	17621	20775	20990	16930
MP15868	Hypothetical protein	143	17204	5903	10031	12341	12508	11597
MP16558	No hits (CSEP)	269	12680	9664	9827	10544	12103	10964
MP09913	No hits (CSEP)	84	2166	13141	13579	9870	11194	9990
MP14724	No hits	203	8858	7721	11358	8550	11281	9554
MP13834	No hits (CSEP)	183	5449	6958	11154	10006	12669	9247
MP13136	No hits	97	2741	10858	10471	8982	9493	8509
MP09729	Alcohol dehydrogenase	347	5849	13822	8228	6722	6577	8240
MP09537	Glycoside hydrolase 18	438	8276	6000	6013	7077	6662	6805
MP15315	MpCP12	155	3881	5014	6892	4963	5948	5339
MP15025	Endoglucanase v-like	157	2618	5578	5479	5764	4372	4762
MP15342	Endo-polygalacturonase	385	3198	1998	5065	5894	5545	4340
MP16511	MpCP11	186	4228	4687	3871	3288	4170	4049
MP04874	Elongation factor ef1-α	460	4877	4243	4033	3799	3172	4025
MP12125	MpPR-1h	245	6069	2605	3137	4132	4178	4024
MP15312	MpCP4	192	3966	3115	4043	4003	4172	3860

[a] Reads per kilobase per million mapped reads

In addition to *CSEPs*, fungal genes that are highly expressed in green brooms include members of the Cerato-platanin and PR-1 (plant pathogenesis-related 1) families, both of which appear to play a role in *M. perniciosa* virulence (Table 2) (Teixeira et al., 2012). Moreover, genes encoding fasciclin-like proteins are induced in *M. perniciosa* and possibly mediate the adhesion between cacao and fungal cells. We also identified genes encoding proteins with CFEM domains, which are commonly associated with fungal pathogenesis (Kulkarni et al., 2003). Interestingly, chitin

deacetylase genes were also highly expressed by *M. perniciosa* during its biotrophic interaction with cacao. Chitin deacetylases catalyze the modification of chitin to chitosan and may constitute a protective mechanism of the fungal cell wall against hydrolytic enzymes produced by the plant (El Gueddari et al., 2002). A selection of *M. perniciosa* genes potentially involved in pathogenesis is provided in Supplemental Data Set 10 online.

Genes involved in pectin breakdown are highly expressed during the biotrophic development of M. perniciosa

The analysis of the green broom transcriptome revealed a strikingly high level of expression of genes encoding pectinolytic enzymes in *M. perniciosa*. During its biotrophic stage, the pathogen seems to produce a complete set of enzymes necessary for the breakdown of pectin, including pectin methylesterases, polygalacturonases and pectate lyases (see Supplemental Data Set 10 online). Moreover, transcripts of genes involved in the metabolism of sub-products of pectin degradation were also identified (methanol oxidase, formaldehyde dehydrogenase and formate dehydrogenase). In addition to pectin, *M. perniciosa* also seems to be able to degrade cellulose and hemicellulose during the green broom stage of WBD. Genes encoding putative cellulases, xylanases, arabinofuranosidases, manosidases and acetylesterases were identified among the highly expressed fungal genes (see Supplemental Data Set 10 online). Even so, the fungus may use only a small part of its large arsenal of plant cell wall degrading enzymes. The *M. perniciosa* genome encodes at least 301 secreted carbohydrate-active enzymes (CAZymes), which potentially cleave all major polysaccharides of the plant cell wall. However, only 56 CAZymes showed RPKM > 50 during *M. perniciosa* growth in green brooms. Thus, this result may be indicative of limited plant cell wall degradation during the biotrophic stage of WBD.

M. perniciosa *has a great potential for cellular detoxification and stress tolerance*

By inspecting the green broom transcriptome, we found that *M. perniciosa* expresses an

arsenal of genes encoding enzymes involved in detoxification and stress tolerance. Reactive oxygen species (ROS), such as superoxide anions ($O_2^{\bullet -}$), hydroxyl radicals (•OH) and hydrogen peroxide (H_2O_2), are produced by plants to halt pathogen invasion (Apel and Hirt, 2004). *M. perniciosa* genes encoding the anti-oxidative enzymes superoxide dismutase (SOD), catalase and peroxiredoxin were highly expressed in green brooms (See Supplemental Data Set 10 online), indicating that the fungus can deal with ROS toxicity during infection.

Additionally, many fungal genes encoding cytochrome P450 enzymes were identified (See Supplemental Data Set 10 online). These proteins oxidize a vast array of metabolic intermediates and environmental compounds and are important for adaptation to hostile ecological niches (Moktali et al., 2012). We also identified genes encoding transporters of the major facilitator superfamily (MFS) and of the ATP-binding cassette superfamily (ABC), whose members have been associated with fungal pathogenesis, acting through the extrusion of host defense molecules and through the secretion of fungal virulence factors (Coleman and Mylonakis, 2009). Overall, our results indicate that *M. perniciosa* is subjected to highly stressful conditions during cacao infection and that a distinctive ability to counteract such conditions might be a central aspect in its virulence.

Evidence on the nutritional strategy of the M. perniciosa *biotrophic mycelium*

Colonizing the plant apoplast and being devoid of specialized feeding structures (i.e., haustoria), the *M. perniciosa* biotrophic mycelium might have the ability to take up soluble compounds that are transported through the apoplast. To understand *M. perniciosa* nutrition during the green broom stage, we sought to identify genes related to nutrient uptake, especially from nitrogen and carbon derivatives. Fungal proteinases along with an oligopeptide transporter were highly expressed during infection (See Supplemental Data Set 10 online), indicating that this fungus has the apparatus to degrade plant proteins secreted in the apoplast and capture the resulting peptides. Interestingly, an asparaginase, which catalyzes the release of ammonia from asparagines, was also highly expressed by *M. perniciosa* during its biotrophic interaction with

cacao. Furthermore, a large number of transcripts related to many sugar transporters were identified in green brooms (See Supplemental Data Set 10 online). It is likely that saccharides derived from the degradation of complex sugars of the plant cell wall, such as pectin, cellulose and hemicellulose, and also sugars translocated to green brooms (i.e., sucrose) can be absorbed by *M. perniciosa* through those transporters and used as energy sources.

DISCUSSION

Plants and microorganisms constantly confront each other in a battle for growth and survival, and the outcome of such encounters directly interferes with human agricultural production. Dynamic and tightly regulated alterations in gene expression occur in both interacting organisms. In this regard, large-scale gene expression analyses of plant-pathogen interactions are of great relevance in unveiling the molecular basis of a specific disease (Wise et al., 2007). Recently, the term “dual RNA-seq” was created to refer to the use of RNA-seq in transcriptomic analyses in which gene expression changes in both the pathogen and the host are analyzed simultaneously (Westermann et al., 2012). Whereas some studies have preferentially focused on either the pathogen or the host at one time (Xu et al., 2011; Weßling et al., 2012; Kunjeti et al., 2012; Martinelli et al., 2012; Petre et al., 2012), only a few studies have involved the comprehensive analysis of both organisms (Tierney et al., 2012; Kawahara et al., 2012). Here, we present an in-depth transcriptomic analysis of the *Moniliophthora perniciosa*-cacao interaction, which vastly expands our current knowledge of witches` broom disease and also contributes to our general understanding of plant-pathogen interactions. Based on these results, we present a model that describes the major molecular and physiological aspects of WBD (Figure 8).

The most prominent symptoms of WBD include intense growth of infected stems, with hypertrophy and hyperplasia of tissues and loss of apical dominance (Figure 1). These characteristics have long been ascribed to the occurrence of hormonal imbalances during the disease (Evans, 1980). However, the precise contribution of each hormone to the development of

green brooms was hitherto unclear. In this study, we verified that the transcription of genes related to plant hormone signaling is noticeably altered in response to *M. perniciosa* infection (Figure 5). Gene expression data point to the existence of gibberellins in green brooms, which is supported by the considerable stem elongation of infected plants (Figure 1). Additionally, auxin-responsive genes were up-regulated, but no genes related to auxin biosynthesis were differentially expressed. Although the importance of auxin during WBD remains to be confirmed, the production of this hormone by *M. perniciosa* had already been described (Kilaru et al., 2007). Therefore, it is possible that the up-regulation of auxin-responsive genes verified in infected cacao plants may be due to the production of this hormone by *M. perniciosa*. Various pathogens are known to produce auxin (Akiyoshi et al., 1983; Glickmann et al., 1998; Maor et al., 2004; Vandeputte et al., 2005; Reineke et al., 2008), which has been reported to attenuate the defense responses mediated by salicylic acid (SA), thus favoring biotrophic development (Navarro et al., 2006; Wang et al., 2007). Unlike auxins, cytokinins and SA act synergistically in defense responses (Argueso et al., 2012; Naseem and Dandekar, 2012). Remarkably, genes related to the degradation and inactivation of cytokinins are up-regulated in green brooms, which is in agreement with an attenuated SA-mediated response.

The prevalence of genes related to biotic stress is an important finding in our analysis, and points to the production of antimicrobial proteins, secondary metabolites and the reinforcement of cell walls by infected plants. Thus, it is likely that a significant part of plant energy is directed to sustain defense responses, which is a cost-intensive process (Bolton, 2009). In contrast to many biotrophs (Wäspi et al., 2001; Panstruga, 2003; Caldo et al., 2006; Doehlemann et al., 2008), the *M. perniciosa* biotrophic mycelium does not strongly suppress host defenses during colonization. Similarly, *Colletotrichum graminicola*, another hemibiotrophic pathogen, was recently reported not to employ the suppression of plant defenses as a virulence strategy (Vargas et al., 2012). Remarkably, whereas cacao plants perceive and respond to *M. perniciosa* during its biotrophic colonization, the fungus also tries to counteract plant defenses through the expression of genes

related to the detoxification of host toxins (e.g., efflux pumps and cytochrome P450) and protection against oxidative stress (e.g., SOD, catalase and peroxiredoxin). Accordingly, Thomazella *et al.* (2012) reported the activation of an alternative respiratory pathway mediated by the enzyme alternative oxidase as a protective mechanism of *M. perniciosa* against the oxidative stress generated during the biotrophic stage of WBD.

Given that the establishment of a compatible interaction between *M. perniciosa* and cacao does occur, we can assume that defense responses were ineffective in preventing the establishment of the *M. perniciosa* biotrophic mycelium. According to the definition proposed by Jones and Dangl (2006), the defense response verified in green brooms can be classified as a basal defense response, i.e., one that is activated by virulent pathogens on susceptible hosts. This weaker form of defense is usually a consequence of the activity of effector proteins deployed by the pathogen with the aim of neutralizing the host immune system, and thus favoring pathogenesis. Although no effector protein has been characterized in *M. perniciosa* so far, our RNA-seq analysis identified some candidate effectors that are highly and exclusively expressed in green brooms (see Supplemental Figure 2 online), and these effectors represent interesting targets for future studies. Our transcriptomic data (Figure 5, see Supplemental Data Set 5 online) also showed that ET synthesis and responses are induced in green brooms. In agreement, increased concentrations of this hormone have already been detected in infected cacao plants (Scarpari et al., 2005). As ET defense responses are usually effective against necrotrophs (Glazebrook, 2005), it is possible that the successful establishment of WBD is favored by the development of inappropriate plant defenses against *M. perniciosa*.

Apart from the energetic cost of an ineffective defense mechanism, cacao plants expend energy to sustain the exaggerated growth of infected tissues during the prolonged biotrophic phase of WBD. In this regard, we verified that remarkable transcriptional alterations related to plant carbohydrate metabolism take place in the infected cacao plants. Genes encoding a cell wall

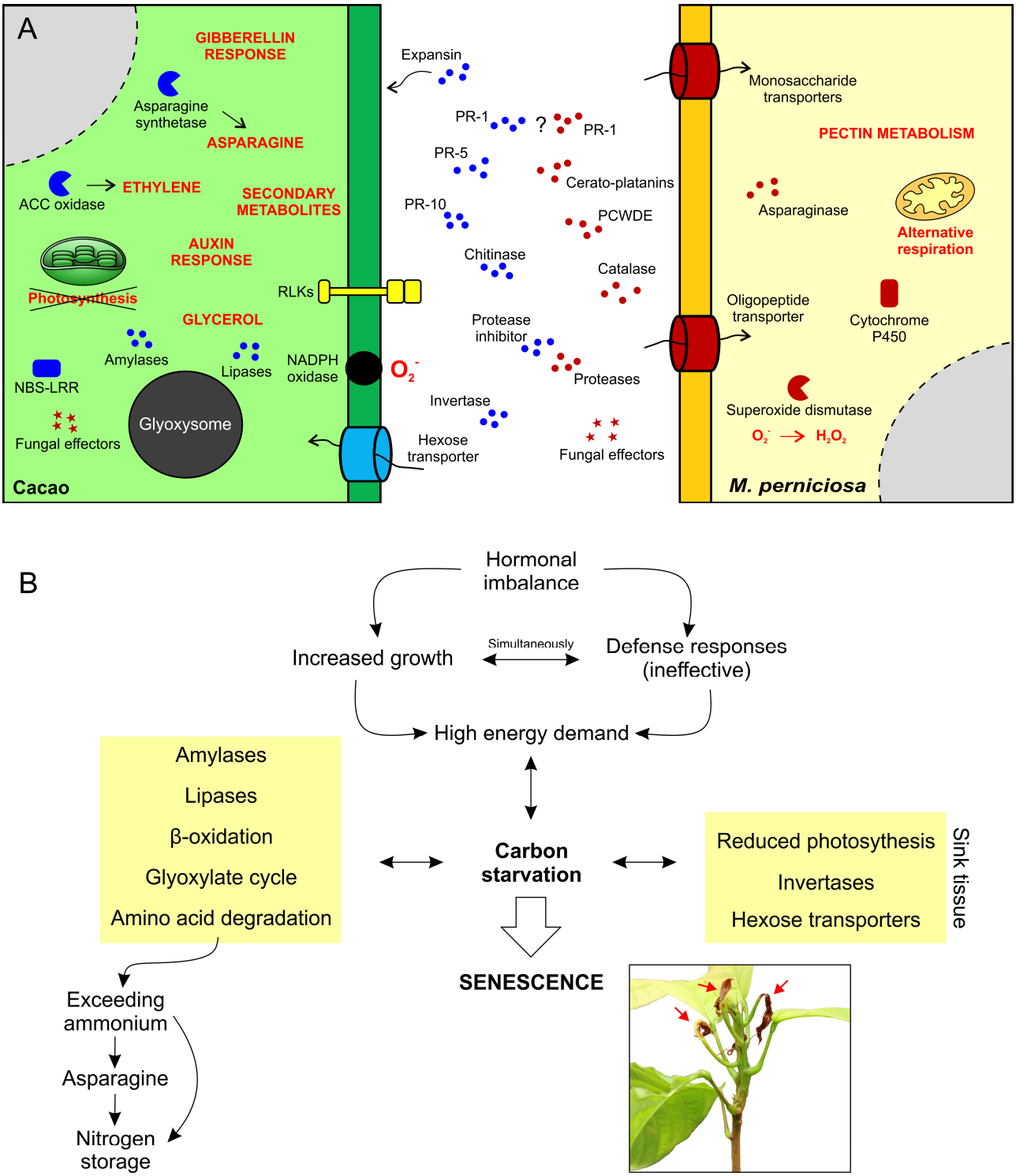

Figure 8. A representative model of the biotrophic interaction between cacao and *Moniliophthora perniciosa*. (A) Representation of proteins and metabolic processes with important roles in witches' broom disease. Plant and fungal molecules are depicted in blue and red, respectively. (B) A summary of the identified physiological alterations in green brooms that culminate in the establishment of a senescence process triggered by nutrient starvation. The plant in the inset shows the first signs of necrosis (red arrows), which are similar to those of regular plant senescence.

invertase – which breaks sucrose into fructose and glucose – and hexose transporters are up-regulated. In addition, a clear reduction in the transcription of genes relating to photosynthesis was verified upon infection (Figure 4). These characteristics are typical of developing sink tissues, which reallocate nutrients from other plant organs to sustain their growth and development (Berger et al., 2007). Since *M. perniciosa* can only infect meristematic tissues, which are generally sinks, it is likely that the fungus reprograms the regular development of cacao meristems to prevent the transition from sink to source tissues. Other pathogens also induce the formation of local sinks to increase nutrient availability in the infected parts (Chou et al., 2000; Fotopoulos et al., 2003; Bonfig et al., 2006; Deeken et al., 2006; Horst et al., 2008; Chandran et al., 2010). In agreement with this notion, distinctive characteristics of these interactions include reduced photosynthesis and the simultaneous up-regulation of plant genes encoding invertases and hexose transporters. Although WBD severely impacts the development of the infected parts and significantly reduces the number of fruits per tree, the disease is not lethal to the whole cacao tree. It is possible that the decrease in tree productivity is, at least in part, a consequence of nutrient allocation to the infected parts.

In comparison to healthy tissues, green brooms have decreased starch contents (Figure 1), and, accordingly, amylase-coding genes are over-expressed, thus indicating that this storage carbohydrate may be used as an energy source. Moreover, the higher number of transcripts related to lipases, β-oxidation and glyoxylate cycle enzymes indicates that lipids are also metabolized as a source of energy by the infected tissue. A sub-product of lipid catabolism is glycerol, which has been previously identified in higher concentrations in infected cacao plants (Scarpari et al., 2005). The glyoxylate cycle is associated with two major developmental processes in plants, i.e., seed germination and senescence. During germination, lipid reserves are used to fuel the growth and development of the growing embryo (Graham, 2008). In addition, glyoxysomal activity is involved in the nutrient recycling of senescent tissues (Buchanan-Wollaston, 1997). Therefore, the expression of genes encoding enzymes of the glyoxylate cycle in green brooms is in line with the significant metabolic reprogramming that takes place during WBD.

Along with carbohydrates and lipids, the carbon skeleton of amino acids seems to be used to sustain green broom development and metabolism. However, the use of amino acids increases ammonium levels in cells, which can be toxic to the plant. To handle ammonium toxicity, green brooms seem to employ two different strategies: (i) the expression of a gene encoding a TIP (Tonoplast Intrinsic Protein – TIP2;1) transporter, which mediates ammonia storage in vacuoles (Loqué et al., 2005); and (ii) the expression of an asparagine synthetase (ASN), which is homologous to the *Asn*1 from *A. thaliana* and mediates the incorporation of nitrogen into aspartate to produce asparagine (Lam et al., 1994). This amino acid is an optimal nitrogen transport and reserve molecule due to its high nitrogen/carbon ratio and stability. Therefore, its production is typically associated with situations of low carbon availability (Lam et al., 1994). Supporting our findings, increased amounts of asparagine were previously reported in green brooms (Scarpari et al., 2005). Interestingly, *Asn*1 is also called *Din*6 (*Dark Inducible* gene 6), and its expression is induced in senescing tissues and after treatment with exogenous photosynthesis inhibitors (Fujiki et al., 2001).

Altogether, these results indicate that infected tissues appear to have a paucity of carbon skeletons, and thus use alternative sources (i.e., starch, lipids and amino acids) to obtain energy. However, considering that green brooms appear to develop as nutrient sinks, the carbon deprivation signature in infected tissues is unexpected. In fact, with the progression of WBD, a callus-like structure is formed on the basal region of the infected growing shoot (see Supplemental Figure 3 online). This structure was shown to disrupt the communication between healthy and infected parts, intercepting the translocation of nutrients to the diseased shoot (Barau et al., manuscript in preparation). Consequently, infected tissues are isolated from the plant, being forced to use their own stores and structures to obtain energy. As a result, carbon deprivation might occur, culminating in the onset of a senescence process triggered by nutrient starvation. Therefore, senescence, which is a developmentally regulated and highly controlled process that leads to the

death of the plant tissue, appears to be responsible for the initial death of infected parts during WBD development.

Indeed, a typical characteristic of WBD is the death of infected tissues beginning on the edges of leaves (Figure 8), which is similar to the pattern of foliar senescence (Gan and Amasino, 1997). Also, Ceita *et al.* (2007) showed that programmed cell death precedes the necrotrophic stage in WBD. Therefore, it is quite possible that the onset of necrosis in WBD is a physiological process of cacao caused by the metabolic disarrangement of WBD rather than a direct action of the pathogen. Consistent with this idea, *M. perniciosa NEP* genes (Necrosis and Ethylene-inducing Protein), which are involved in the necrosis of cacao tissues, are not expressed when the first signs of death are observed in infected plants (Zaparoli et al., 2011). However, as necrosis progresses, the fungus expresses this gene, thus actively participating in the death of the plant. A pioneer report by Evans (1980) suggested two possible causes for the death of infected tissues: (i) accelerated host senescence or (ii) the action of fungal toxins. In this regard, our results provide evidence that both processes might occur consecutively in the disease.

In this scenario, the biotrophic mycelium of *M. perniciosa* appears to take advantage of the soluble nutrients that are being produced by the infected tissues. In contrast to many biotrophic/hemibiotrophic pathogens, the biotrophic mycelium of *M. perniciosa* does not employ any feeding structure (e.g., haustoria or invasive hyphae), and it exclusively inhabits the intercellular space of cacao meristematic tissues (Calle et al., 1982). Thus, the fungus might depend on soluble nutrients derived from the apoplast. In agreement, fungal genes encoding oligopeptide and monosaccharide transporters, proteases and an asparaginase are up-regulated. In addition, the middle lamellae, wherein *M. perniciosa* develops, is very rich in pectin (Albersheim et al., 1960). Remarkably, genes associated with pectinolytic metabolism are highly expressed in green brooms (see Supplemental Data Set 10 online). Also, a byproduct of pectin degradation is methanol, and a recent report showed that *M. perniciosa* is able to utilize methanol as a sole carbon source (de

Oliveira et al., 2012). In this regard, our results suggest that this compound is a possible carbon source for the fungus during its biotrophic development.

In conclusion, we identified several physiological alterations occurring in cacao plants in response to *M. perniciosa* infection and also pointed to potential virulence strategies employed by the fungus during the green broom stage of WBD. In particular, this work represents an important step towards understanding the factors responsible for triggering the death of the infected tissues in WBD, which have been considered to be uncertain to date. Our data sets and the disease model presented here provide a firm basis for further studies on the physiological and molecular processes identified in this interaction. For instance, it will be important to evaluate precisely how senescence signals the end of the biotrophic stage of WBD. Overall, the peculiarities identified in this biotrophic interaction make WBD a very interesting and innovative model in the field of plant pathology.

METHODS

Biological material

Theobroma cacao cv. “Comum” (Forastero genotype) and the *Moniliophthora perniciosa* isolate BP10 were used in this study. Cacao seedlings were grown for approximately three months in a greenhouse under controlled conditions of temperature (26°C) and humidity (>80%), and a photoperiod of 12 h. Active apical meristems were inoculated with 30 µL of a basidiospore suspension (10^5 spores mL^{-1}), following the procedures described by Frias et al. (1995). After 30 days, infected tissues representing the mature green broom stage were excised and used for RNA isolation. As controls, the corresponding tissues of mock inoculated seedlings were collected at the same timepoint. Five biological replicates were used for each condition.

RNA isolation and RNA-seq library preparation

RNA isolation was performed as described by Azevedo et al. (2003) with minor modifications. For each sample, 5 µg total RNA was used to prepare the mRNA-seq library according to the TrueSeq RNA Sample Prep Kit protocol (Illumina). Library quality control and quantification were performed with an Experion DNA 1K Chip (Bio-Rad) and a Qubit fluorometer (Invitrogen), respectively. For each library, approximately 75 million 48 bp paired end sequences were generated using an Illumina HiSeq 2000 sequencer.

Read mapping and gene expression analysis

After removing low quality sequences containing uncalled bases (Ns), we used the software Bowtie (Langmead et al., 2009) to align the RNA-seq reads against 34,997 and 17,008 gene models of *T. cacao* and *M. perniciosa*, respectively. Cacao gene models were downloaded from the Cacao Genome Database (version 0.9 - www.cacaogenomedb.org) and *M. perniciosa* gene models were obtained from the Witches` Broom Genome Project (www.lge.ibi.unicamp.br/vassoura). Bowtie alignment parameters were set to allow a maximum of two mismatches and to exclude

reads mapping in more than one position on the reference. Moreover, only reads for which both pairs were successfully aligned were considered. Gene expression values for *M. perniciosa* were defined according to the RPKM method (reads per kilobase per million mapped reads; Mortazavi et al., 2008). Differential expression analyses were performed for cacao genes with the edgeR package (Robinson *et al.*, 2010) using the Benjamini-Hochberg method for correction of multiple comparisons. Genes with a false discovery rate (FDR) of below 0.01 were considered differentially expressed between conditions. To assess the variability among samples, we carried out hierarchical clustering and principal component analysis (PCA) using cacao genes. Hierarchical clustering was performed based on Euclidean distances. PCA was conducted using the prcomp command with default parameters in the R software.

Functional classification based on the MapMan ontology and InterPro terms

The MapMan software (Thimm et al., 2004) was used to visualize cacao gene expression data in the context of metabolic pathways. MapMan uses a plant-specific ontology that classifies genes into well-defined hierarchical categories, denominated BINs. Cacao genes were assigned to BINs using the Mercator automated annotation pipeline (http://mapman.gabipd.org/web/guest/mercator). Differentially represented MapMan pathways were defined by a two-tailed Wilcoxon rank sum test corrected by the Benjamin-Hochberg method (FDR≤0.05). Additionally, enriched InterPro terms were identified using the BiNGO plugin for Cytoscape (Maere et al., 2005). To this purpose, a customized annotation file was created according to the software instructions to allow the use of InterPro terms in enrichment analyses. A hypergeometric test combined with a Benjamin and Hochberg FDR correction with a cutoff of 0.05 was applied.

Hormonometer analysis

Hormonometer software (Volodarsky et al., 2009) was used to evaluate transcriptional similarities between green brooms and hormone responses. Since this software only accepts

Arabidopsis gene IDs as input, we defined the putative *Arabidopsis* orthologs of cacao genes by bi-directional Blast analyses. The 8870 resulting genes that were expressed in our experiment were then used to investigate the hormonal profile of green brooms. To validate the analysis using this set of genes, we used public gene expression data of *Arabidopsis* mutants with known hormonal alterations: *arr21* (increased cytokinin response; GEO: GSE5699), *eto1* (increased ethylene response; GEO: GSE20897), nahG (reduced salycilic acid levels; GEO: GSE5727) and *nph arf19*/IAA (reduced auxin signaling; GEO: GSE627).

Comparing RNA-seq and qPCR results

qPCR assays were performed to contrast RNA-seq results with an independent technique. To this end, the expression of 28 cacao genes was analyzed in plants that were also sequenced by RNA-seq (Infected plant #2 and Healthy plant #1 – Table 1). All qPCRs were conducted on a StepOne Plus Real Time PCR System (Applied Biosystems) using SYBR Green I for the detection of PCR products. Each reaction was performed in a final volume of 16 µl, containing 8 µl SYBR Green PCR Master Mix (Applied Biosystems), 250 nM each primer and 50 ng cDNA template. No-template reactions were included as negative controls for each set of primers used. The thermal cycling conditions were 94^{o}C for 10 min, followed by 40 cycles of 94^{o}C for 15 s, 55^{o}C for 30 s and 60^{o}C for 1 min, with fluorescence detection at the end of each cycle. The amplification of a single product per reaction was confirmed by melting curve analysis. All reactions were carried out in technical triplicates. Relative fold differences in mRNA abundance were defined by the mathematical model described by Livak and Schmittgen (2001). Data were normalized using four reference genes that showed little variation in the RNA-seq analysis (α-tubulin, actin, 60S ribosomal L35 and 60S ribosomal L11). Primers used in the experiment are listed in Supplemental Table 1 online.

Determination of photosynthetic rates

Photosynthetic rates were determined using the LI-6400 portable gas exchange system (LI-COR). Measurements in infected and healthy cacao plants were performed in biological triplicates on the most recent fully expanded stem leaf. The CO_2 assimilation rate was measured at 25°C under light intensity ranging from 0 to 900 µmol photons m^{-2} s^{-1}. The CO_2 concentration of the air entering the chamber was maintained at 350 µmol mol^{-1}. Plants analyzed in this experiment were similar to those used for transcriptome sequencing.

Histological analyses

Green brooms and the corresponding tissues of healthy plants were fixed in Karnovisky solution (50 mL 1% glutaraldehyde; 20 mL 4% paraformaldehyde; 30 mL 0.2 M phosphate buffer pH 7.2; Karnovsky, 1965). Samples were left in the fixative solution for 48 h, washed and stored in 70% ethanol. After dehydration using a graded ethanol series (30, 50, 70, 90 and 100%), tissues were embedded in plastic resin (Historesin® Leica; Gerrits and Smid, 1983) and transverse sections (12 - 16 µm thick) were cut with a steel knife. Sections were then incubated in a toluidine blue solution (0.01%, dissolved in citrate buffer; O' Brien et al., 1964). Samples were observed under white and polarized lights using an Olympus BX51 microscope coupled to an Olympus DP72 camera. All analyses were repeated at least three times with consistent results.

Supplemental Data

The following materials are available in the online version of this article.

Supplemental Figure 1. Number of *M. perniciosa* genes detected at different sequencing depths.

Supplemental Figure 2. Expression profiles of *M. perniciosa* CSEP genes.

Supplemental Figure 3. Callus-like structure formed on the basal region of infected shoots.

Supplemental Table 1. Primer sequences used for qPCR analyses.

Supplemental Data Set 1. Expression analysis of cacao genes based on the edgeR software.

Supplemental Data Set 2. MapMan BINs enriched in green brooms.

Supplemental Data Set 3. InterPro terms enriched in green brooms.

Supplemental Data Set 4. Differentially expressed cacao genes related to photosynthetic, carbon and nitrogen metabolism.

Supplemental Data Set 5. Differentially expressed cacao genes related to hormonal metabolism.

Supplemental Data Set 6. Differentially expressed cacao genes related to defense responses.

Supplemental Data Set 7. Differentially expressed cacao genes related to secondary metabolism and cell wall modification.

Supplemental Data Set 8. Expression values defined for *M. perniciosa* genes during cacao infection.

Supplemental Data Set 9. List of *M. perniciosa* CSEP-encoding genes.

Supplemental Data Set 10. Selected *M. perniciosa* genes thought to be involved in cacao infection.

ACKNOWLEDGMENTS

We thank Dr. Halley Caixeta de Oliveira for valuable suggestions and critical reading of the manuscript, Dr. Marc Lohse for his assistance with MapMan annotation and Ricardo Silverio Machado for helping with the measurements of photosynthesis. We thank the University of North Carolina High Throughput Sequencing Facility team for intense support with RNA-seq. This work was supported by Fundação de Amparo à Pesquisa do Estado de São Paulo (FAPESP, 2009/51018-1, 2009/50119-9, 2006/59843-3, 2008/54527 and 2012/09136-0).

AUTHOR CONTRIBUTIONS

P.J.P.L.T. designed the research. P.J.P.L.T., P.F.V.P. and M.C.S.R. performed experimental procedures. O.R., G.G.L.C. and R.O.V. performed bioinformatics analyses. P.M. contributed reagents/materials/analysis tools. P.J.P.L.T. and D.P.T.T. interpreted the data. J.M.C.M. participated in the analysis of fungal genes. P.J.P.L.T. and D.P.T.T. wrote the article. G.A.G.P. supervised the project.

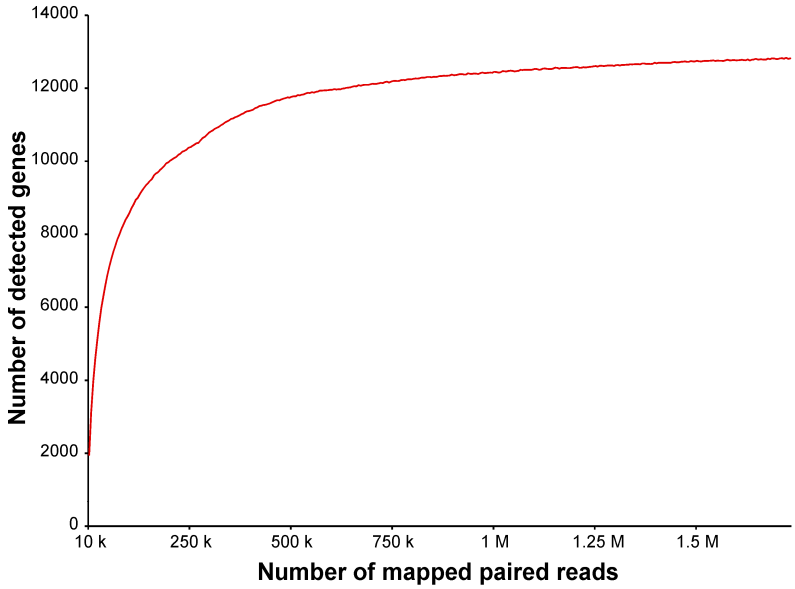

Supplemental Figure 1. Number of *Moniliophthora perniciosa* genes detected at different sequencing depths. The number of reads mapping to *M. perniciosa* in our experiment (1.7 million) is sufficient to identify the majority of expressed fungal genes. A gene was considered expressed if it had an expression value of at least 1 RPKM (reads per kilobase per million mapped reads).

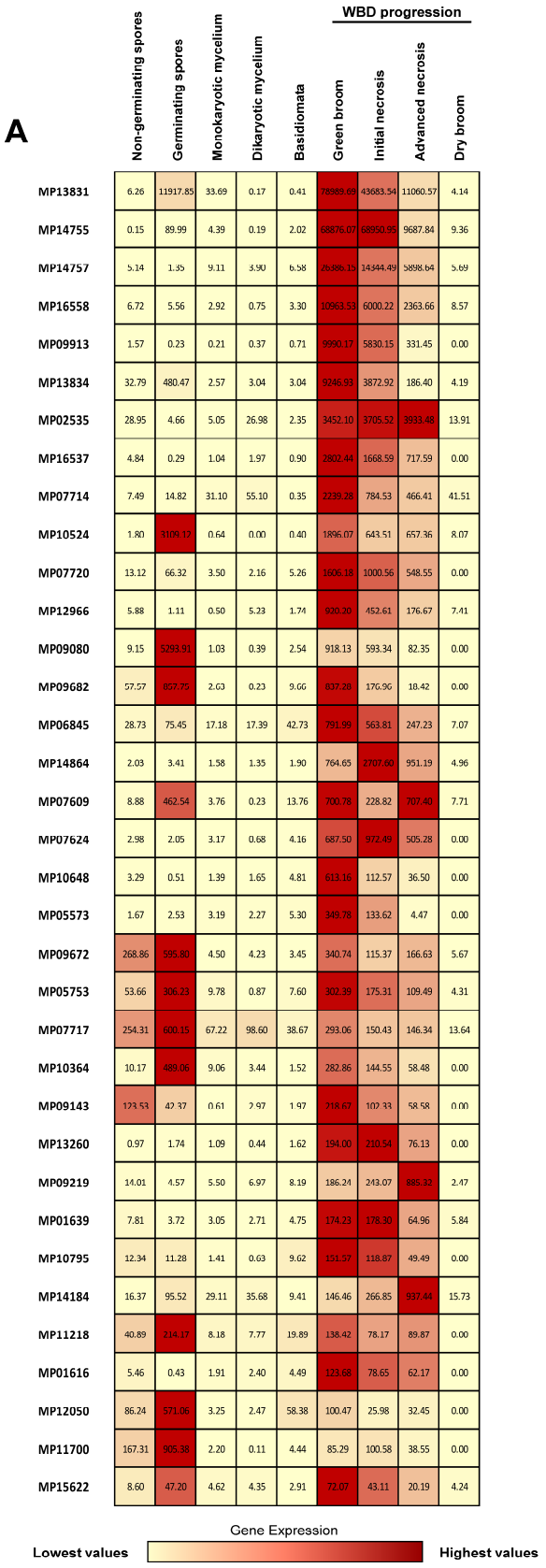

Supplemental Figure 2. Expression profiles of *Moniliophthora perniciosa* CSEP genes. The expression patterns of 35 CSEPs were assessed in different RNA-seq libraries that are part of the “Witches’ Broom Disease Transcriptome Atlas”. Although most of these genes are preferentially expressed in the biotrophic stage of witches’ broom disease, some of them are also highly expressed during spore germination, which represents a committed step towards plant colonization. (A) Heatmap showing the relative transcript abundance in different conditions. (B) Graphical representation of the gene expression values.

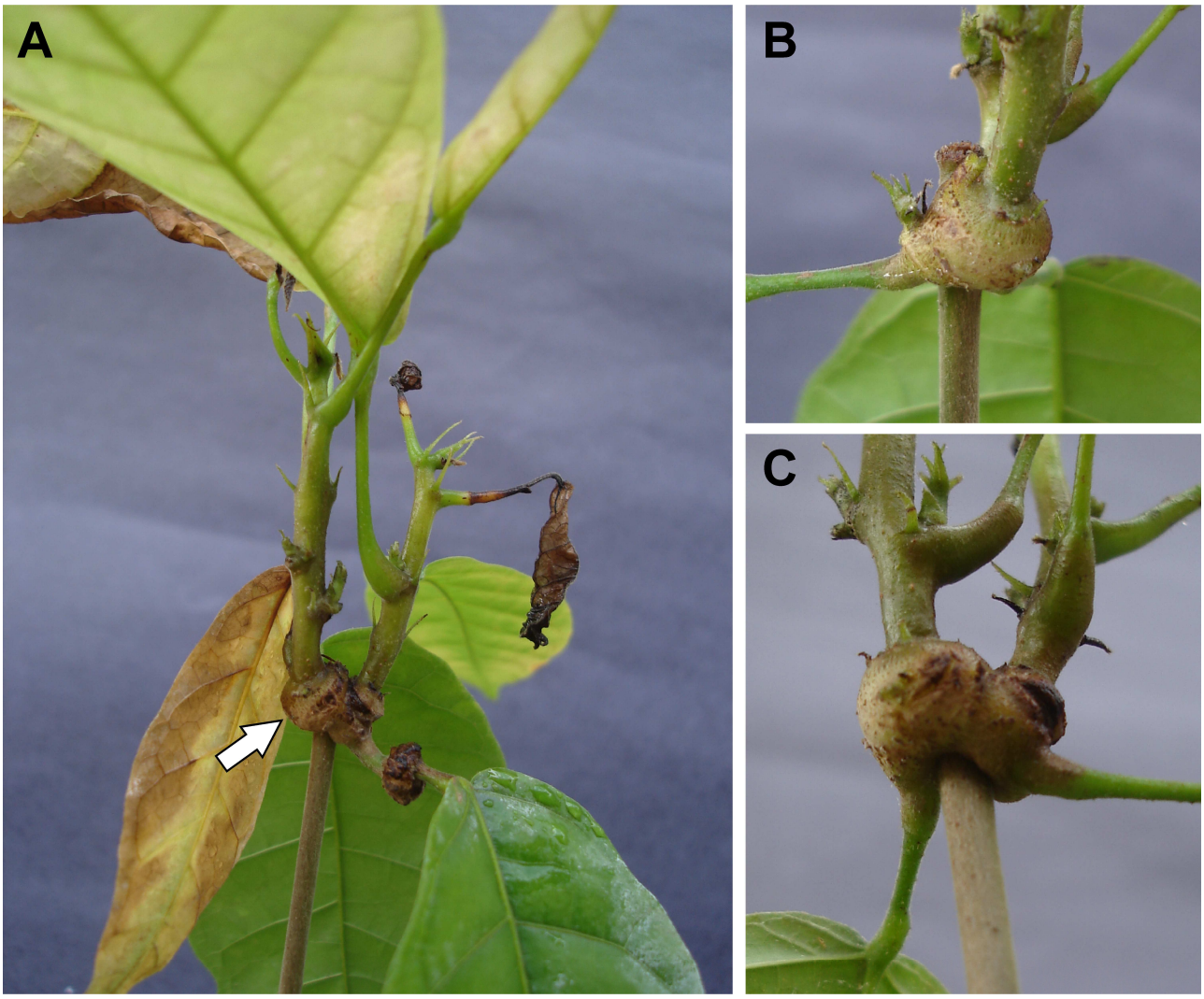

Supplemental Figure 3. Callus-like structure formed on the basal region of infected shoots. (A) These structures (arrow) are formed during witches' broom disease progression and block the communication between healthy and infected parts of the plant. Note that the pattern of necrosis in infected shoots is similar to that of regular senescence. (B) and (C) Details of the callus-like structures.

REFERENCES

Aime, M.C. and Phillips-Mora, W. (2005). The causal agents of witches' broom and frosty pod rot of cacao (chocolate, *Theobroma cacao*) form a new lineage of Marasmiaceae. Mycologia. **97:** 1012-1022.

Akiyoshi, D.E., Morris, R.O., Hinz, R., Mischke, B.S., Kosuge, T., Garfinkel, D.J., Gordon, M.P., and Nester, E.W. (1983). Cytokinin/auxin balance in crown gall tumors is regulated by specific loci in the T-DNA. Proc.Natl.Acad.Sci.U.S.A **80:** 407-411.

Albersheim, P., MUHLETHALER, K., and FREY-WYSSLING, A. (1960). Stained pectin as seen in the electron microscope. J.Biophys.Biochem.Cytol. **8:** 501-506.

Apel, K. and Hirt, H. (2004). Reactive oxygen species: metabolism, oxidative stress, and signal transduction. Annu.Rev.Plant Biol. **55:** 373-399.

Argueso, C.T., Ferreira, F.J., Epple, P., To, J.P., Hutchison, C.E., Schaller, G.E., Dangl, J.L., and Kieber, J.J. (2012). Two-component elements mediate interactions between cytokinin and salicylic acid in plant immunity. PLoS.Genet. **8:** e1002448.

Azevedo, H., Lino-Neto, T., and Tavares, R.M. (2003). An improved method for high-quality RNA isolation from needles of adult maritime pine trees. Plant Molecular Biology Reporter **21:** 333-338.

Berger, S., Sinha, A.K., and Roitsch, T. (2007). Plant physiology meets phytopathology: plant primary metabolism and plant-pathogen interactions. J.Exp.Bot. **58:** 4019-4026.

Bolton, M.D. (2009). Primary metabolism and plant defense--fuel for the fire. Mol.Plant Microbe Interact. **22:** 487-497.

Bonfig, K.B., Schreiber, U., Gabler, A., Roitsch, T., and Berger, S. (2006). Infection with virulent and avirulent *P. syringae* strains differentially affects photosynthesis and sink metabolism in *Arabidopsis* leaves. Planta **225:** 1-12.

Buchanan-Wollaston, V. (1997). The molecular biology of leaf senescence. Journal of Experimental Botany **48:** 181-199.

Caldo, R.A., Nettleton, D., Peng, J., and Wise, R.P. (2006). Stage-specific suppression of basal defense discriminates barley plants containing fast- and delayed-acting Mla powdery mildew resistance alleles. Mol.Plant Microbe Interact. **19:** 939-947.

Calle, H., Cook, A.A., and Fernando, S.Y. (1982). Histology of witches' broom caused in cacao by *Crinipellis perniciosa*. Phytopathology **72:** 1479-1481.

Ceita, G.D., Macedo, J.N.A., Santos, T.B., Alemanno, L., Gesteira, A.D., Micheli, F., Mariano, A.C., Gramacho, K.P., Silva, D.D., Meinhardt, L., Mazzafera, P., Pereira, G.A.G., and Cascardo, J.C.D. (2007). Involvement of calcium oxalate degradation during programmed cell death in *Theobroma cacao* tissues triggered by the hemibiotrophic fungus *Moniliophthora pemiciosa*. Plant Science **173:** 106-117.

Chandran, D., Inada, N., Hather, G., Kleindt, C.K., and Wildermuth, M.C. (2010). Laser microdissection of *Arabidopsis* cells at the powdery mildew infection site reveals site-specific processes and regulators. Proc.Natl.Acad.Sci.U.S.A **107:** 460-465.

Chou, H.M., Bundock, N., Rolfe, S.A., and Scholes, J.D. (2000). Infection of *Arabidopsis thaliana* leaves with *Albugo candida* (white blister rust) causes a reprogramming of host metabolism. Mol.Plant Pathol. **1:** 99-113.

Coleman, J.J. and Mylonakis, E. (2009). Efflux in fungi: la pièce de résistance. PLoS.Pathog. **5:** e1000486.

da Hora Junior, B.T., Poloni, J.F., Lopes, M.A., Dias, C.V., Gramacho, K.P., Schuster, I., Sabau, X., Cascardo, J.C., Mauro, S.M., Gesteira, A.S., Bonatto, D., and Micheli, F. (2012). Transcriptomics and systems biology analysis in identification of specific pathways involved in cacao resistance and susceptibility to witches' broom disease. Mol.Biosyst. **8:** 1507-1519.

de Oliveira, B.V., Teixeira, G.S., Reis, O., Barau, J.G., Teixeira, P.J., do Rio, M.C., Domingues, R.R., Meinhardt, L.W., Paes Leme, A.F., Rincones, J., and Pereira, G.A. (2012). A potential role for an extracellular methanol oxidase secreted by *Moniliophthora perniciosa* in Witches' broom disease in cacao. Fungal.Genet.Biol. **49:** 922-932.

Deeken, R., Engelmann, J.C., Efetova, M., Czirjak, T., Muller, T., Kaiser, W.M., Tietz, O., Krischke, M., Mueller, M.J., Palme, K., Dandekar, T., and Hedrich, R. (2006). An integrated view of gene expression and solute profiles of *Arabidopsis* tumors: a genome-wide approach. Plant Cell **18:** 3617-3634.

Dodds, P.N. and Rathjen, J.P. (2010). Plant immunity: towards an integrated view of plant-pathogen interactions. Nat.Rev.Genet. **11:** 539-548.

Doehlemann, G., Wahl, R., Horst, R.J., Voll, L.M., Usadel, B., Poree, F., Stitt, M., Pons-Kuhnemann, J., Sonnewald, U., Kahmann, R., and Kamper, J. (2008). Reprogramming a maize plant: transcriptional and metabolic changes induced by the fungal biotroph *Ustilago maydis*. Plant J. **56:** 181-195.

El Gueddari, N.E., Rauchhaus, U., Moerschbacher, B.M., and Deising, H.B. (2002). Developmentally regulated conversion of surface-exposed chitin to chitosan in cell walls of plant pathogenic fungi. New Phytologist **156:** 103-112.

Evans, H.C. (1980). Pleomorphism in *Crinipellis perniciosa*, causal agent of Witches' broom disease of cocoa. Trans.Br.Mycol.Soc. **74:** 515-526.

Fisher, M.C., Henk, D.A., Briggs, C.J., Brownstein, J.S., Madoff, L.C., McCraw, S.L., and Gurr, S.J. (2012). Emerging fungal threats to animal, plant and ecosystem health. Nature **484:** 186-194.

Fotopoulos, V., Gilbert, M.J., Pittman, J.K., Marvier, A.C., Buchanan, A.J., Sauer, N., Hall, J.L., and Williams, L.E. (2003). The monosaccharide transporter gene, AtSTP4, and the cell-wall invertase, Atßfruct1, are induced in *Arabidopsis* during infection with the fungal biotroph *Erysiphe cichoracearum*. Plant Physiol **132:** 821-829.

Frias, G., L.H.Purdy, and R.A.Schmidt (1995). An inoculation method for evaluating resistence of cacao to *Crinipellis perniciosa*. Plant Disease **79:** 787-791.

Fujiki, Y., Yoshikawa, Y., Sato, T., Inada, N., Ito, M., Nishida, I., and Watanabe, A. (2001). Dark-inducible genes from *Arabidopsis thaliana* are associated with leaf senescence and repressed by sugars. Physiol Plant **111:** 345-352.

Gan, S. and Amasino, R.M. (1997). Making Sense of Senescence (Molecular Genetic Regulation and Manipulation of Leaf Senescence). Plant Physiol **113:** 313-319.

Gerrits, P.O. and Smid, L. (1983). A new, less toxic polymerization system for the embedding of soft tissues in glycol methacrylate and subsequent preparing of serial sections. J.Microsc. **132:** 81-85.

Gesteira, A.S., Micheli, F., Carels, N., Da Silva, A.C., Gramacho, K.P., Schuster, I., Macedo, J.N., Pereira, G.A., and Cascardo, J.C. (2007). Comparative analysis of expressed genes from cacao meristems infected by *Moniliophthora perniciosa*. Ann.Bot. **100:** 129-140.

Glazebrook, J. (2005). Contrasting mechanisms of defense against biotrophic and necrotrophic pathogens. Annu.Rev.Phytopathol. **43:** 205-227.

Glickmann, E., Gardan, L., Jacquet, S., Hussain, S., Elasri, M., Petit, A., and Dessaux, Y. (1998). Auxin production is a common feature of most pathovars of *Pseudomonas syringae*. Mol.Plant Microbe Interact. **11:** 156-162.

Godfrey, D., Bohlenius, H., Pedersen, C., Zhang, Z., Emmersen, J., and Thordal-Christensen, H. (2010). Powdery mildew fungal effector candidates share N-terminal Y/F/WxC-motif. BMC.Genomics **11:** 317.

Graham, I.A. (2008). Seed storage oil mobilization. Annu.Rev.Plant Biol. **59:** 115-142.

Griffith, G.W., Nicholson, J., Nenninger, A., Birch, R.N., and Hedger, J.N. (2003). Witches' brooms and frosty pods: two major pathogens of cacao. New Zealand Journal of Botany **41:** 423-435.

Horst, R.J., Engelsdorf, T., Sonnewald, U., and Voll, L.M. (2008). Infection of maize leaves with *Ustilago maydis* prevents establishment of C4 photosynthesis. J.Plant Physiol **165:** 19-28.

Jones, J.D. and Dangl, J.L. (2006). The plant immune system. Nature **444:** 323-329.

Kale, S.D., Gu, B., Capelluto, D.G., Dou, D., Feldman, E., Rumore, A., Arredondo, F.D., Hanlon, R., Fudal, I., Rouxel, T., Lawrence, C.B., Shan, W., and Tyler, B.M. (2010). External lipid PI3P mediates entry of eukaryotic pathogen effectors into plant and animal host cells. Cell **142:** 284-295.

Karnovsky, M.J. (1965). A formaldehyde-glutaraldehyde fixative of high osmolality for use in electron microscopy. J.Cell.Biol. **27:** 137-139.

Kawahara, Y., Oono, Y., Kanamori, H., Matsumoto, T., Itoh, T., and Minami, E. (2012).

Simultaneous RNA-seq analysis of a mixed transcriptome of rice and blast fungus interaction. PLoS.One. **7:** e49423.

Kemen, E., Gardiner, A., Schultz-Larsen, T., Kemen, A.C., Balmuth, A.L., Robert-Seilaniantz, A., Bailey, K., Holub, E., Studholme, D.J., Maclean, D., and Jones, J.D. (2011). Gene gain and loss during evolution of obligate parasitism in the white rust pathogen of *Arabidopsis thaliana*. PLoS.Biol. **9:** e1001094.

Kilaru, A., Bailey, B.A., and Hasenstein, K.H. (2007). *Moniliophthora perniciosa* produces hormones and alters endogenous auxin and salicylic acid in infected cocoa leaves. FEMS Microbiol.Lett. **274:** 238-244.

Kulkarni, R.D., Kelkar, H.S., and Dean, R.A. (2003). An eight-cysteine-containing CFEM domain unique to a group of fungal membrane proteins. Trends Biochem.Sci. **28:** 118-121.

Kunjeti, S.G., Evans, T.A., Marsh, A.G., Gregory, N.F., Kunjeti, S., Meyers, B.C., Kalavacharla, V.S., and Donofrio, N.M. (2012). RNA-Seq reveals infection-related global gene changes in *Phytophthora phaseoli*, the causal agent of lima bean downy mildew. Mol.Plant Pathol. **13:** 454-466.

Lam, H.M., Peng, S.S., and Coruzzi, G.M. (1994). Metabolic regulation of the gene encoding glutamine-dependent asparagine synthetase in *Arabidopsis thaliana*. Plant Physiol **106:** 1347-1357.

Langmead, B., Trapnell, C., Pop, M., and Salzberg, S.L. (2009). Ultrafast and memory-efficient alignment of short DNA sequences to the human genome. Genome Biol. **10:** R25.

Leal, G.A., Albuquerque, P.S., and Figueira, A. (2007). Genes differentially expressed in *Theobroma cacao* associated with resistance to witches' broom disease caused by *Crinipellis perniciosa*. Mol.Plant Pathol. **8:** 279-292.

Leal, G.A., Gomes, L.H., Albuquerque, P.S., Tavares, F.C., and Figueira, A. (2010). Searching for *Moniliophthora perniciosa* pathogenicity genes. Fungal.Biol. **114:** 842-854.

Livak, K.J. and Schmittgen, T.D. (2001). Analysis of relative gene expression data using real-time quantitative PCR and the 2(-Delta Delta C(T)) Method. Methods **25:** 402-408.

Loqué, D., Ludewig, U., Yuan, L., and von, W.N. (2005). Tonoplast intrinsic proteins AtTIP2;1 and AtTIP2;3 facilitate NH_3 transport into the vacuole. Plant Physiol **137:** 671-680.

Maere, S., Heymans, K., and Kuiper, M. (2005). BiNGO: a Cytoscape plugin to assess overrepresentation of gene ontology categories in biological networks. Bioinformatics **21:** 3448-3449.

Maor, R., Haskin, S., Levi-Kedmi, H., and Sharon, A. (2004). *In planta* production of indole-3-acetic acid by *Colletotrichum gloeosporioides* f. sp. aeschynomene. Appl.Environ.Microbiol. **70:** 1852-1854.

Martinelli, F., Uratsu, S.L., Albrecht, U., Reagan, R.L., Phu, M.L., Britton, M., Buffalo, V., Fass, J., Leicht, E., Zhao, W., Lin, D., D'Souza, R., Davis, C.E., Bowman, K.D., and Dandekar,

A.M. (2012). Transcriptome profiling of citrus fruit response to huanglongbing disease. PLoS.One. **7:** e38039.

Meinhardt, L.W., Rincones, J., Bailey, B.A., Aime, M.C., Griffith, G.W., Zhang, D., and Pereira, G.A. (2008). *Moniliophthora perniciosa*, the causal agent of witches' broom disease of cacao: what's new from this old foe? Mol.Plant Pathol. **9:** 577-588.

Moktali, V., Park, J., Fedorova-Abrams, N.D., Park, B., Choi, J., Lee, Y.H., and Kang, S. (2012). Systematic and searchable classification of cytochrome P450 proteins encoded by fungal and oomycete genomes. BMC.Genomics **13:** 525.

Monaghan, J. and Zipfel, C. (2012). Plant pattern recognition receptor complexes at the plasma membrane. Curr.Opin.Plant Biol. **15:** 349-357.

Mondego, J.M., Carazzolle, M.F., Costa, G.G., Formighieri, E.F., Parizzi, L.P., Rincones, J., Cotomacci, C., Carraro, D.M., Cunha, A.F., Carrer, H., Vidal, R.O., Estrela, R.C., Garcia, O., Thomazella, D.P., de Oliveira, B.V., Pires, A.B., Rio, M.C., Araujo, M.R., de Moraes, M.H., Castro, L.A., Gramacho, K.P., Goncalves, M.S., Neto, J.P., Neto, A.G., Barbosa, L.V., Guiltinan, M.J., Bailey, B.A., Meinhardt, L.W., Cascardo, J.C., and Pereira, G.A. (2008). A genome survey of *Moniliophthora perniciosa* gives new insights into Witches' Broom Disease of cacao. BMC.Genomics **9:** 548.

Mortazavi, A., Williams, B.A., McCue, K., Schaeffer, L., and Wold, B. (2008). Mapping and quantifying mammalian transcriptomes by RNA-Seq. Nat.Methods **5:** 621-628.

Munch, S., Lingner, U., Floss, D.S., Ludwig, N., Sauer, N., and Deising, H.B. (2008). The hemibiotrophic lifestyle of *Colletotrichum* species. J.Plant Physiol **165:** 41-51.

Naseem, M. and Dandekar, T. (2012). The role of auxin-cytokinin antagonism in plant-pathogen interactions. PLoS.Pathog. **8:** e1003026.

Navarro, L., Dunoyer, P., Jay, F., Arnold, B., Dharmasiri, N., Estelle, M., Voinnet, O., and Jones, J.D. (2006). A plant miRNA contributes to antibacterial resistance by repressing auxin signaling. Science **312:** 436-439.

O' Brien, T.P., Feder, N., and Mccully, M.E. (1964). Polychromatic Staining of Plant Cell Walls by Toluidine Blue O. Protoplasma **59:** 368-&.

Panstruga, R. (2003). Establishing compatibility between plants and obligate biotrophic pathogens. Curr.Opin.Plant Biol. **6:** 320-326.

Penman, D., Britton, G., Hardwick, K., Collin, H.A., and Isaac, S. (2000). Chitin as a measure of biomass of *Crinipellis perniciosa*, causal agent of witches' broom disease of *Theobroma cacao*. Mycological Research **104:** 671-675.

Perfect, S.E. and Green, J.R. (2001). Infection structures of biotrophic and hemibiotrophic fungal plant pathogens. Mol.Plant Pathol. **2:** 101-108.

Petre, B., Morin, E., Tisserant, E., Hacquard, S., Da, S.C., Poulain, J., Delaruelle, C., Martin,

F., Rouhier, N., Kohler, A., and Duplessis, S. (2012). RNA-Seq of early-infected poplar leaves by the rust pathogen *Melampsora larici-populina* uncovers PtSultr3;5, a fungal-induced host sulfate transporter. PLoS.One. **7:** e44408.

Pires, A.B., Gramacho, K.P., Silva, D.C., Goes-Neto, A., Silva, M.M., Muniz-Sobrinho, J.S., Porto, R.F., Villela-Dias, C., Brendel, M., Cascardo, J.C., and Pereira, G.A. (2009). Early development of *Moniliophthora perniciosa* basidiomata and developmentally regulated genes. BMC.Microbiol. **9:** 158.

Purdy, L.H. and Schmidt, R.A. (1996). Status of cacao witches' broom: biology, epidemiology, and management. Annu Rev Phytopathol **34:** 573-594.

Reineke, G., Heinze, B., Schirawski, J., Buettner, H., Kahmann, R., and Basse, C.W. (2008). Indole-3-acetic acid (IAA) biosynthesis in the smut fungus *Ustilago maydis* and its relevance for increased IAA levels in infected tissue and host tumour formation. Mol.Plant Pathol. **9:** 339-355.

Rincones, J., Scarpari, L.M., Carazzolle, M.F., Mondego, J.M., Formighieri, E.F., Barau, J.G., Costa, G.G., Carraro, D.M., Brentani, H.P., Vilas-Boas, L.A., de Oliveira, B.V., Sabha, M., Dias, R., Cascardo, J.M., Azevedo, R.A., Meinhardt, L.W., and Pereira, G.A. (2008). Differential gene expression between the biotrophic-like and saprotrophic mycelia of the witches' broom pathogen *Moniliophthora perniciosa*. Mol.Plant Microbe Interact. **21:** 891-908.

Robinson, M.D., McCarthy, D.J., and Smyth, G.K. (2010). edgeR: a Bioconductor package for differential expression analysis of digital gene expression data. Bioinformatics **26:** 139-140.

Scarpari, L.M., Meinhardt, L.W., Mazzafera, P., Pomella, A.W., Schiavinato, M.A., Cascardo, J.C., and Pereira, G.A. (2005). Biochemical changes during the development of witches' broom: the most important disease of cocoa in Brazil caused by *Crinipellis perniciosa*. J.Exp.Bot. **56:** 865-877.

Stergiopoulos, I. and de Wit, P.J. (2009). Fungal effector proteins. Annu.Rev.Phytopathol. **47:** 233-263.

Studholme, D.J., Glover, R.H., and Boonham, N. (2011). Application of high-throughput DNA sequencing in phytopathology. Annu.Rev.Phytopathol. **49:** 87-105.

Teixeira, P.J., Thomazella, D.P., Vidal, R.O., do Prado, P.F., Reis, O., Baroni, R.M., Franco, S.F., Mieczkowski, P., Pereira, G.A., and Mondego, J.M. (2012). The fungal pathogen *Moniliophthora perniciosa* has genes similar to plant PR-1 that are highly expressed during its interaction with cacao. PLoS.One. **7:** e45929.

Thimm, O., Blasing, O., Gibon, Y., Nagel, A., Meyer, S., Kruger, P., Selbig, J., Muller, L.A., Rhee, S.Y., and Stitt, M. (2004). MAPMAN: a user-driven tool to display genomics data sets onto diagrams of metabolic pathways and other biological processes. Plant J **37:** 914-939.

Thomazella, D.P., Teixeira, P.J., Oliveira, H.C., Saviani, E.E., Rincones, J., Toni, I.M., Reis, O., Garcia, O., Meinhardt, L.W., Salgado, I., and Pereira, G.A. (2012). The hemibiotrophic cacao pathogen *Moniliophthora perniciosa* depends on a mitochondrial alternative oxidase for biotrophic development. New Phytol. **194:** 1025-1034.

Tierney, L., Linde, J., Muller, S., Brunke, S., Molina, J.C., Hube, B., Schock, U., Guthke, R., and Kuchler, K. (2012). An Interspecies Regulatory Network Inferred from Simultaneous RNA-seq of *Candida albicans* Invading Innate Immune Cells. Front Microbiol. **3:** 85.

Vandeputte, O., Oden, S., Mol, A., Vereecke, D., Goethals, K., El, J.M., and Prinsen, E. (2005). Biosynthesis of auxin by the gram-positive phytopathogen *Rhodococcus fascians* is controlled by compounds specific to infected plant tissues. Appl.Environ.Microbiol. **71:** 1169-1177.

Vargas, W.A., Martin, J.M., Rech, G.E., Rivera, L.P., Benito, E.P., Diaz-Minguez, J.M., Thon, M.R., and Sukno, S.A. (2012). Plant defense mechanisms are activated during biotrophic and necrotrophic development of *Colletotricum graminicola* in maize. Plant Physiol **158:** 1342-1358.

Volodarsky, D., Leviatan, N., Otcheretianski, A., and Fluhr, R. (2009). HORMONOMETER: a tool for discerning transcript signatures of hormone action in the *Arabidopsis* transcriptome. Plant Physiol **150:** 1796-1805.

Wang, D., Pajerowska-Mukhtar, K., Culler, A.H., and Dong, X. (2007). Salicylic acid inhibits pathogen growth in plants through repression of the auxin signaling pathway. Curr.Biol. **17:** 1784-1790.

Wäspi, U., Schweizer, P., and Dudler, R. (2001). Syringolin reprograms wheat to undergo hypersensitive cell death in a compatible interaction with powdery mildew. Plant Cell **13:** 153-161.

Weßling, R., Schmidt, S.M., Micali, C.O., Knaust, F., Reinhardt, R., Neumann, U., Ver Loren van, T.E., and Panstruga, R. (2012). Transcriptome analysis of enriched *Golovinomyces orontii* haustoria by deep 454 pyrosequencing. Fungal.Genet.Biol. **49:** 470-482.

Westermann, A.J., Gorski, S.A., and Vogel, J. (2012). Dual RNA-seq of pathogen and host. Nat.Rev.Microbiol. **10:** 618-630.

Wise, R.P., Moscou, M.J., Bogdanove, A.J., and Whitham, S.A. (2007). Transcript profiling in host-pathogen interactions. Annu.Rev.Phytopathol. **45:** 329-369.

Xu, L., Zhu, L., Tu, L., Liu, L., Yuan, D., Jin, L., Long, L., and Zhang, X. (2011). Lignin metabolism has a central role in the resistance of cotton to the wilt fungus *Verticillium dahliae* as revealed by RNA-Seq-dependent transcriptional analysis and histochemistry. J.Exp.Bot. **62:** 5607-5621.

Zaparoli, G., Barsottini, M.R., de Oliveira, J.F., Dyszy, F., Teixeira, P.J., Barau, J.G., Garcia, O., Costa-Filho, A.J., Ambrosio, A.L., Pereira, G.A., and Dias, S.M. (2011). The crystal structure of necrosis- and ethylene-inducing protein 2 from the causal agent of cacao's Witches' Broom disease reveals key elements for its activity. Biochemistry **50:** 9901-9910.

Zuccaro, A., Lahrmann, U., Guldener, U., Langen, G., Pfiffi, S., Biedenkopf, D., Wong, P., Samans, B., Grimm, C., Basiewicz, M., Murat, C., Martin, F., and Kogel, K.H. (2011). Endophytic life strategies decoded by genome and transcriptome analyses of the mutualistic root symbiont *Piriformospora indica*. PLoS.Pathog. **7:** e1002290.

Capítulo III

The fungal pathogen *Moniliophthora perniciosa* uses an inactivated chitinase to counteract cacao defenses

Paulo José P.L. Teixeira*, Gabriel L. Fiorin*, Mario R.O. Barsottini, Piotr Mieczkowski, Andre L.B. Ambrosio, Gonçalo A.G. Pereira

* Autores com igual contribuição

Manuscrito em preparação

APRESENTAÇÃO

Este capítulo apresenta a caracterização de uma quitinase do fungo *Moniliophthora perniciosa* com possível papel na neutralização das defesas do cacaueiro. O gene codificante desta proteína, denominado *MpChi*, foi identificado durante a inspeção de bibliotecas de RNA-seq de vassouras verdes e destacou-se por estar entre os genes mais expressos pelo fungo no estágio infectivo da doença. Em fungos, quitinases possuem função principalmente no desenvolvimento (remodelamento da parede celular) e nutrição (parasitismo de insetos ou outros fungos). No entanto, uma participação direta na infecção de plantas nunca foi reportada. Neste sentido, a elevada expressão deste gene durante a colonização do cacaueiro por *M. perniciosa* foi um achado bastante inesperado, que nos levou a inspecionar o sítio ativo da enzima codificada por este gene. Curiosamente, verificou-se que esta proteína possui uma substituição de um importante aminoácido do seu sítio catalítico (glutamato 167 substituído por uma glutamina). Esta mutação já foi artificialmente realizada em quitinases de vários outros organismos, sempre resultando na completa extinção da atividade quitinolítica da enzima. Diante de seu padrão de expressão e possível ausência de atividade quitinolítica, formulou-se a hipótese de que a proteína MpChi seria um mecanismo de proteção de *M. perniciosa* contra quitinases produzidas pela planta. Esta proteção poderia ser alcançada pela ligação da proteína à parede celular do fungo, bloqueando o acesso das enzimas hidrolíticas da planta. Este trabalho está sendo realizado em conjunto com o aluno de iniciação científica Gabriel Lorencini Fiorin (processo FAPESP 2011/23315-1) e encontra-se em sua etapa final.

INTRODUÇÃO

Plantas estão continuamente expostas a uma ampla variedade de microrganismos e desenvolveram diversos mecanismos de defesa para combater potenciais patógenos (Jones & Dangl, 2006). A primeira linha de defesa ativa do sistema imune de plantas baseia-se no reconhecimento de moléculas elicitoras por receptores de membrana denominados PRRs (*pattern recognition receptors*). Estas moléculas, conhecidas como MAMPs (*microbe-associated molecular patterns*), costumam ser evolutivamente estáveis e indispensáveis para os microrganismos, constituindo alvos ideais para o reconhecimento pela planta (Boller & Felix, 2009). Conhecidos exemplos de MAMPs incluem flagelina e lipopolissacarídeos de bactérias e quitina de fungos. A ativação dos PRRs induz a produção de espécies reativas de oxigênio, fluxos de ions, intensa reprogramação transcricional e síntese de novas proteínas que limitam o desenvolvimento do microrganismo invasor (Jones & Dangl, 2006). No entanto, microrganismos patogênicos desenvolveram interessantes mecanismos para impedir a ativação ou mitigar as defesas de seus hospedeiros (Jones & Dangl, 2006; Stergiopoulos & De Wit, 2009).

A secreção de proteínas efetoras por patógenos é uma estratégia fundamental para o estabelecimento da infecção (Dou & Zhou, 2012). Além de manipular a fisiologia dos hospedeiros, efetores podem interferir no sistema imune das plantas interagindo diretamente com uma proteína de defesa ou inibindo vias de sinalização específicas (Stergiopoulos & De Wit, 2009; Dou & Zhou, 2012). Ainda, efetores podem evitar o reconhecimento do patógeno pelo hospedeiro. Por exemplo, as proteínas Ecp6 de *Cladosporium fulvum* e Slp1 de *Magnaporthe oryzae* sequestram oligômeros de quitina originários da parede celular do fungo, impedindo a imunidade ativada por MAMPs (de Jonge *et al.*, 2010; Mentlak *et al.*, 2012). Estas proteínas contém domínios LysM (*Lysin Motif* – InterPro ID IPR018392), os quais são reconhecidos módulos de ligação a carboidratos. Outra interessante estratégia mediada por efetores é a proteção da parede celular de fungos contra o ataque de enzimas hidrolíticas da planta. Esta estratégia foi inicialmente identificada no patógeno do tomateiro *Cladosporium fulvum*, o qual produz uma pequena proteína, denominada AVR4,

capaz de ligar-se à parede celular do fungo, impedindo o acesso de quitinases da planta (van den Burg *et al.*, 2006). Recentemente, uma função análoga também foi descrita para dois efetores contendo domínios LysM no fungo *Mycosphaerella graminicola* (Marshall *et al.*, 2011; Mentlak *et al.*, 2012).

O basidiomiceto *Moniliophthora perniciosa* é o agente causador da vassoura de bruxa do cacaueiro (*Theobroma cacao*), uma das mais severas doenças que atingem esta cultura (Evans, 2007). Este fungo apresenta um ciclo de vida hemibiotrófico, com duas fases de desenvolvimento distintas: a primeira fase, biotrófica e a segunda, necrotrófica (Evans, 1980). A fase biotrófica da doença causa drásticas alterações morfológicas nos tecidos infectados do cacaueiro, dando origem a ramos anormais denominados “vassouras verdes”. Entre 8 e 12 semanas após a infecção, o fungo assume sua fase necrotrófica e passa a se alimentar dos tecidos mortos da planta, agora denominados “vassouras secas”. Esta doença configura-se como um dos principais fatores limitantes da produção de cacau nas Américas, resultando em perdas de até 90% da produção (Purdy & Schmidt, 1996; Meinhardt *et al.*, 2008).

Durante os últimos anos, muitos esforços foram direcionados para o desenvolvimento de soluções para este problema. Em 2000, o Projeto Genoma Vassoura de Bruxa foi lançado e, desde então, tem apoiado vários estudos envolvendo tanto o patógeno quanto a planta. Adicionalmente, uma abrangente análise de expressão gênica foi recentemente iniciada a partir da construção do Atlas Transcriptômico da Vassoura de Bruxa, uma coleção de bibliotecas de RNA-seq que representam variadas condições de crescimento do fungo *in vitro* bem como estágios específicos da doença. A análise destes dados tem fornecido importantes informações sobre a base molecular desta complexa interação planta-patógeno. Em especial, a análise transcriptômica de vassouras verdes permitiu a identificação de possíveis fatores de patogenicidade no fungo *M. perniciosa*, os quais têm sido alvos de análises específicas. Neste contexto, um gene codificante de uma quitinase foi identificado entre os genes mais expressos pelo fungo *M. perniciosa* durante

sua interação biotrófica com o cacaueiro, o que sugeriu um inesperado papel para a proteína codificada na patogenicidade deste fungo.

Quitinases são enzimas que catalisam a hidrólise de ligações β-1,4 entre os monômeros de N-acetilglicosamina da quitina, principal constituinte da parede celular de fungos e do exoesqueleto de artrópodes. Segundo proposto pelo CAZy (*Carbohydrate Active Enzymes Database*; http://www.cazy.org), quitinases são classificadas em duas famílias distintas de glicosil hidrolases (GH), denominadas GH18 e GH19. Estas duas famílias não possuem origem evolutiva em comum, apresentando diferentes sequências de aminoácidos, estrutura tridimensional e mecanismos catalíticos (Fukamizo, 2000). Os papéis biológicos desempenhados pelas quitinases variam consideravelmente entre os organismos. Em bactérias, as quitinases estão principalmente associadas com nutrição (Bhattacharya *et al.*, 2007). Em insetos, quitinases estão associadas ao desenvolvimento pós-embrionário e a degradação de exoesqueleto velho (Merzendorfer & Zimoch, 2003). Em plantas e mamíferos, quitinases constituem um dos mecanismos de defesa contra patógenos (Sahai & Manocha, 1993). Já em fungos, quitinases participam na morfogênese da parede celular, degradação de quitina exógena para obtenção de nutrientes (por exemplo, em fungos entomopatogênicos ou micoparasitas), e defesa contra outros fungos e artrópodes (Hartl *et al.*, 2012). No entanto, uma participação direta de quitinases na virulência de fungos fitopatogênicos nunca foi descrita.

Neste trabalho, apresentamos a caracterização de uma quitinase de *M. perniciosa* com possível papel efetor na patogenicidade deste fungo sobre o cacaueiro. Esta proteína, denominada MpChi, apresenta uma alteração em seu sítio catalítico que elimina sua atividade quitinolítica sem, no entanto, afetar sua capacidade de ligação à quitina. Considerando-se que a proteína MpChi parece ser preferencialmente produzida durante o estágio biotrófico da vassoura de bruxa, um possível papel na proteção do fungo *M. perniciosa* contra o ataque de enzimas hidrolíticas produzidas pela planta é apresentado e discutido neste capítulo.

MATERIAIS E MÉTODOS

Material biológico

Os experimentos foram realizados com o isolado CP02 de *M. perniciosa* e com a variedade "Comum" de *Theobroma cacao*, a qual é suscetível à vassoura de bruxa. A cepa Origami II (Novagen) de *Escherichia coli* foi utilizada para a expressão heteróloga da proteína MpChi.

Caracterização *in silico* do gene *MpChi* e da proteína codificada

O Atlas Transcriptômico da Vassoura de Bruxa foi inspecionado para verificarmos a expressão do gene *MpChi* em 35 diferentes bibliotecas de RNA-seq, as quais representam as mais variadas condições de crescimento e desenvolvimento de *M. perniciosa*, tanto *in vitro* quanto *in planta.* A sequência codante predita do gene *MpChi* foi confirmada através do sequenciamento de cDNA. A predição de domínios na proteína codificada e a verificação do peptídeo sinal para secreção foram realizadas utilizando-se o servidor InterProScan (Zdobnov & Apweiler, 2001) e o programa SignalP 4.0 (Petersen *et al.*, 2011), respectivamente. Sequências de quitinases de outros organismos foram utilizadas na construção de um alinhamento de proteínas com o programa ClustalW (Thompson *et al.*, 2002).

Expressão heteróloga em *E. coli*

O gene *MpChi* foi amplificado a partir do cDNA de vassoura verde utilizando-se os *primers* 5` GAATTCGGATGCAAACCGAAAAATTAC 3` e 5` AAGCTTCTACTTGGACAATCCGGCAC 3`. O fragmento resultante foi clonado no vetor pGEM-T Easy (Promega) e, posteriormente, sequenciado para a verificação de erros na sequência. Em seguida, o gene foi digerido com as enzimas de restrição *EcoR*I e *Hind*III e ligado no vetor pET-SUMO (Invitrogen), previamente digerido com as mesmas enzimas. Esta construção também foi sequenciada para confirmação da clonagem. Subsequentemente, a cepa Origami II de *E. coli* foi transformada com esta construção para expressão da proteína MpChi. A expressão da proteína foi realizada à temperatura de 18^{o}C

durante 16 horas, utilizando-se 0.05 mM de IPTG. As células foram então precipitadas, lisadas por sonicação e a proteína recombinante foi purificada por cromatografia de afinidade utilizando-se a coluna *HiTrap Chelating HP* (GE Healthcare), a qual possui afinidade pela cauda de histidina adicionada na porção N-terminal da proteína recombinante. A cauda de histidina e a proteína SUMO fusionadas foram removidas através de digestão com a protease ULP-1 (*Ubiquitin-like-specific protease*, Invitrogen). A proteína MpChi purificada foi obtida através de uma segunda cromatografia de afinidade com a mesma coluna. A concentração final de proteína foi determinada através do método de Bradford usando BSA como padrão.

Medição de atividade quitinolítica

Os ensaios para verificação de atividade quitinolítica foram realizados com 10 ng da proteína MpChi recombinante, utilizando-se o kit *Chitinase Assay Kit Fluorimetric* (Sigma), segundo instruções do fabricante. O fluorímetro *EnSpire Multimode Reader* (PerkinElmer) foi usado para detecção de fluorescência. Três substratos diferentes foram empregados: *4-Methylumbelliferyl N,N`-diacetyl-β-D-chitobioside*, *4-Methylumbelliferyl N-acetyl-β-D-glucosaminide* e *4-Methylumbelliferyl β-D-N,N`,N``-triacetylchitotriose*. Estes substratos permitem a detecção de diferentes tipos de atividades quitinolíticas (quitobiosidases, N-acetilglicosaminidases e endoquitinases, respectivamente). Quitinases de *Trichoderma* (Sigma) foram utilizadas como controle positivo neste ensaio.

Teste de ligação a polissacarídeos

Os ensaios de ligação a polissacarídeos foram realizados conforme descrito em trabalhos anteriores (van den Burg *et al.*, 2006; de Jonge *et al.*, 2010). Basicamente, 40 µg de MpChi foram independentemente incubados com 10 mg de *chitin beads* (NEB), quitina de casca de camarão (Sigma), quitosano (Sigma), xilano (Sigma) ou celulose (Sigma) em um volume de 800 µL de água. Após duas horas em agitação à temperatura ambiente, a fração insolúvel foi precipitada por

centrifugação (5 min, 13.000*g*) e o sobrenadante foi coletado. A fração insolúvel foi lavada três vezes com água e subsequentemente fervida em 200 µL de SDS 1%. A presença da proteína no sobrenadante e no *pellet* foi examinada por SDS-PAGE, utilizando-se o corante *Coomassie Blue*.

RESULTADOS

O gene *MpChi* é altamente expresso durante o estágio biotrófico da vassoura de bruxa

A inspeção de bibliotecas de RNA-seq construídas a partir de plantas infectadas no estágio de vassoura verde revelou que o gene *MpChi* se encontra entre os genes mais expressos pelo fungo durante sua interação biotrófica com o cacaueiro (Tabela 1). Notavelmente, outros genes altamente expressos constituem candidatos a efetores (CSEP – *candidate secreted effector protein*), os quais são fundamentais para a virulência de microrganismos fitopatogênicos (ver Capítulo II).

Tabela 1. Genes mais expressos por *M. perniciosa* durante o estágio de vassoura verde da doença vassoura de bruxa. Os valores de expressão gênica foram obtidos por RNA-seq e são dados em RPKM (*reads per kilobase of exon model per million mapped reads*).

			RPKM - réplicas biológicas					
	GeneID	**Descrição**	**I**	**II**	**III**	**IV**	**V**	**Média**
1	MP13831	*No hits* (CSEP)	46929	73269	92347	81569	99726	**78768**
2	MP14755	*No hits* (CSEP)	81359	50559	66895	80813	63706	**68666**
3	MP14757	*No hits* (CSEP)	22280	19508	25857	26988	36924	**26311**
4	MP15869	*No hits*	35943	10310	17432	24200	19664	**21510**
5	MP13352	MpPR-1g	9087	16110	17565	20693	20955	**16882**
6	MP15868	*Hypothetical protein*	17139	5891	9999	12292	12487	**11562**
7	MP16558	*No hits* (CSEP)	12633	9645	9796	10502	12082	**10932**
8	MP09913	*No hits* (CSEP)	2158	13116	13536	9831	11175	**9963**
9	MP14724	*No hits*	8825	7706	11322	8516	11262	**9526**
10	MP13834	*No hits* (CSEP)	5428	6944	11119	9966	12647	**9221**
11	MP13136	*No hits*	2731	10837	10438	8946	9477	**8486**
12	MP09729	alcohol dehydrogenase domain protein	5827	13795	8202	6696	6565	**8217**
13	MP09537	MpChi	8245	5988	5994	7049	6650	**6785**
14	MP15315	MpCP12	3866	5004	6870	4943	5938	**5324**
15	MP15025	endoglucanase v-like protein	2608	5567	5461	5741	4365	**4749**

A expressão do gene *MpChi* foi então inspecionada em 35 bibliotecas diferentes de RNA-seq do fungo através do Atlas Transcriptômico da Vassoura de Bruxa (Figura 1). Nenhuma expressão significativa foi verificada em condições de desenvolvimento *in vitro* do patógeno, em estruturas reprodutivas (basidiomata) ou em basidiósporos. Além disso, a expressão do gene também se mostrou baixa no estágio de vassoura seca da doença, indicando que o gene *MpChi* desempenhe seu papel especificamente durante o estágio biotrófico da vassoura de bruxa.

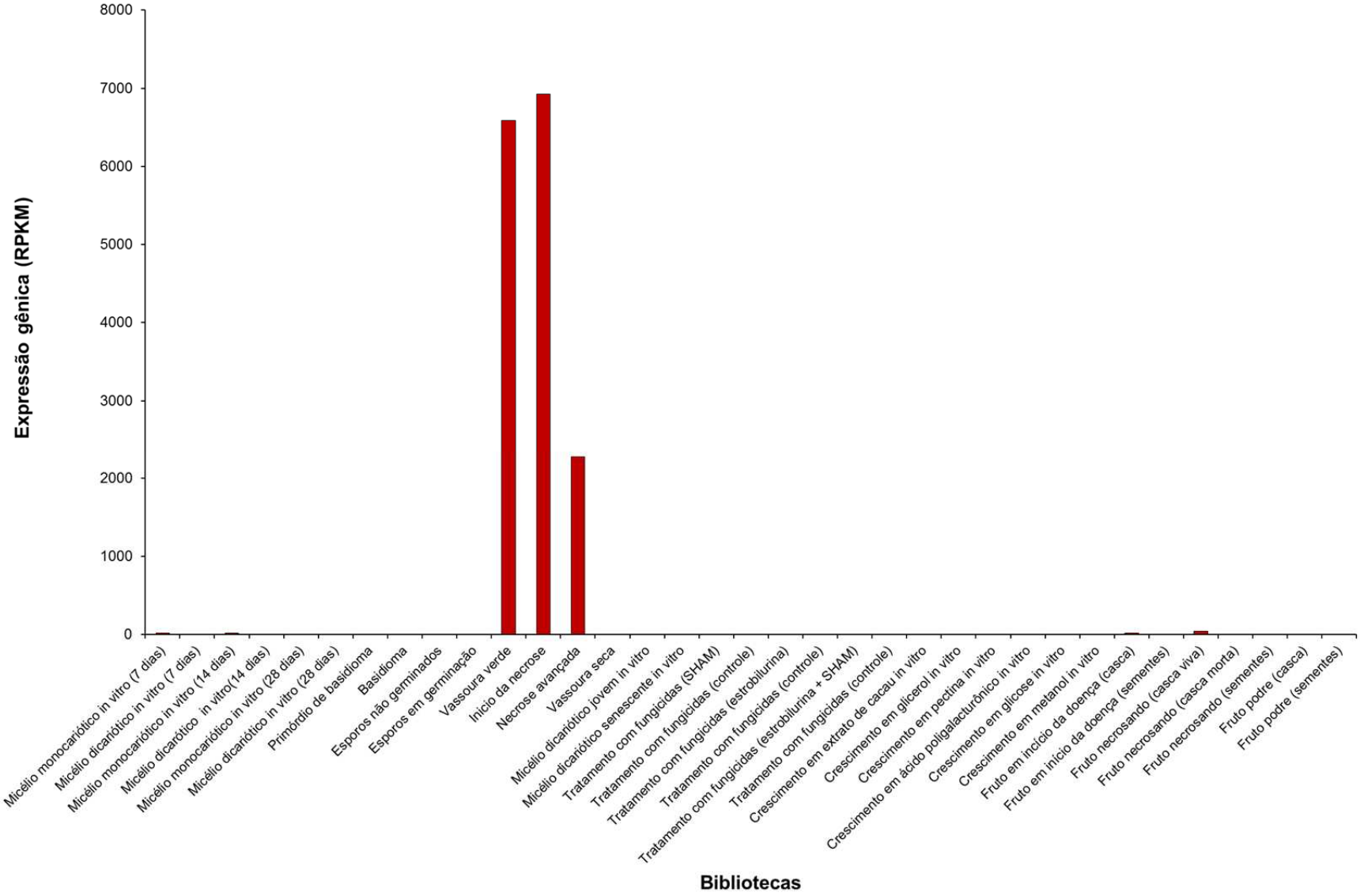

Figura 1. Perfil de expressão do gene *MpChi* em diferentes estágio de desenvolvimento e condições de crescimento do fungo *M. perniciosa*. Verifica-se que este gene é altamente expresso apenas durante a interação com o hospedeiro vivo. Os dados foram obtidos através de inspeção de bibliotecas de RNA-seq que fazem parte do Atlas Transcriptômico da Vassoura de Bruxa. Os valores de expressão gênica são apresentados em RPKM (*reads per kilobase of exon model per million mapped reads*).

A proteína MpChi possui uma mutação em seu sítio ativo

O sítio ativo de quitinases da família GH18 é constituído pela sequência consenso DXXDXDXE, sendo o glutamato (E) o aminoácido responsável pela doação de elétrons durante a hidrólise do substrato (Huang *et al.*, 2012). O gene *MpChi* possui uma alteração natural em sua sequência que resulta na substituição do glutamato (E) por uma glutamina (Q) no sítio ativo da proteína codificada (Figura 2). Curiosamente, esta mutação é conhecida por extinguir a atividade quitinolítica em diferentes quitinases (Watanabe *et al.*, 1993; Papanikolau *et al.*, 2001; van Aalten *et al.*, 2001; Lu *et al.*, 2002; Bortone *et al.*, 2002; Synstad *et al.*, 2004; Ohnuma *et al.*, 2011). Por outro lado, o sítio de ligação à quitina é formado pela sequência SXXGG, a qual se encontra conservada na proteína MpChi (Figura 2), sugerindo que esta proteína retenha sua capacidade de ligação à quitina.

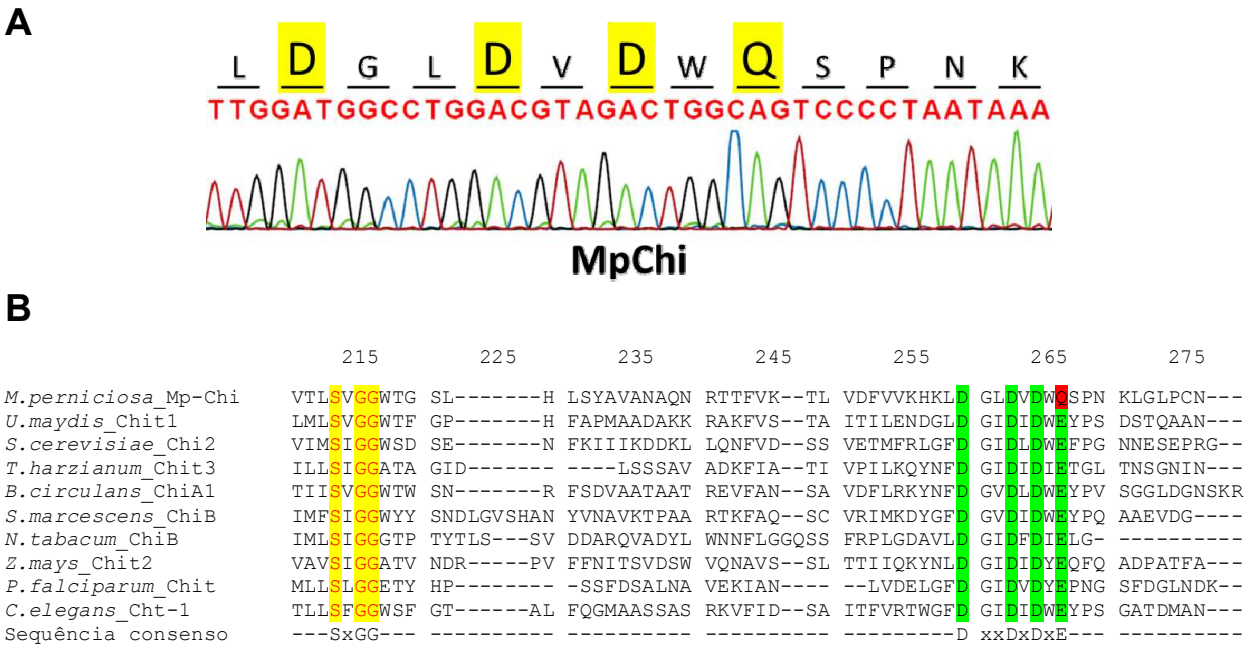

Figura 2. Análise do sítio ativo da quitinase MpChi de *M. perniciosa*. (A) Confirmação da sequência do sítio catalítico da proteína MpChi através de sequenciamento de DNA. (B) Alinhamento da região catalítica da quitinase MpChi de *M. perniciosa* com outras quitinases da família GH18 de diferentes organismos. O sítio de ligação ao substrato, destacado em amarelo, está presente na quitinase MpChi. No entanto, esta proteína exibe uma glutamina, destacada em vermelho, no lugar do glutamato encontrado na região catalítica das demais quitinases da família GH18. A sequência consenso mostrada na figura destaca apenas os aminoácidos conservados do sítio de ligação ao substrato e da região catalítica. Códigos de acesso no Uniprot: *Ustilago maydis* Chit1=Q9HEQ7; *S. cerevisiae* Chi2=Q06350; *T. harzianum*=Q96UW2; *B. circulans*=P20533; *Serratia marcescens* ChiB=Q547S1; *Nicotiana tabacum* ChiB=P29061; *Zea mays* Chit2=B6U7J7; *Plasmodium falciparum* Chit=Q8I4R4; *Caenorhabditis elegans* Cht-1=Q11174.

Produção da proteína MpChi recombinante

Uma vez que o gene *MpChi* é altamente expresso durante o estágio de vassoura verde, utilizamos cDNA produzido a partir de RNA extraído de uma planta infectada para amplificar a região codante deste gene. Para expressão da proteína em *E. coli*, a região que codifica o peptídeo sinal para secreção foi excluída. O gene amplificado foi clonado nos vetores pGEM-T Easy e pET-SUMO. A cepa Origami II de *E. coli* foi então transformada com o gene *MpChi* ligado ao vetor pET-SUMO e utilizada na expressão da proteína recombinante. Diferentes parâmetros (temperatura, tempo de indução e concentração de IPTG) foram inicialmente testados para se determinar a condição ótima para produção de grandes quantidades da proteína de forma solúvel (dados não mostrados). A proteína recombinante foi eficientemente produzida após indução com 0.05mM de IPTG, à temperatura de 18ºC durante 16h. A proteína MpChi foi então produzida em larga escala e purificada através de cromatografia de afinidade. A figura 3 ilustra a produção da proteína MpChi recombinante em *E. coli*.

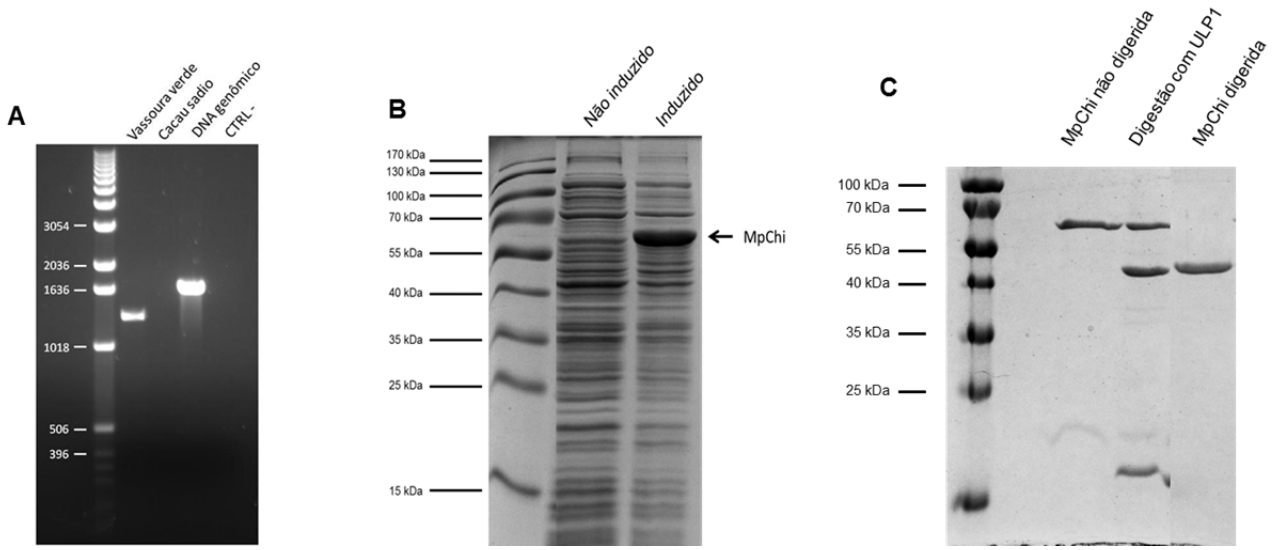

Figura 3. Produção da proteína MpChi em *E. coli*. (A) Isolamento do gene *MpChi* por PCR. Como esperado, o gene é amplificado a partir de cDNA de plantas infectadas (vassoura verde) e no controle positivo da reação (DNA genômico). Não se obteve amplificação ao se utilizar cDNA de cacau sadio ou água (controle negativo: CTRL-) como *template* da reação. (B) Produção da proteína MpChi em *E. coli* após adição de 0.05mM de IPTG. Observa-se uma banda bastante intensa com a massa molecular predita para proteína recombinante (58.5 kDa) apenas na amostra induzida. (C) Purificação da proteína MpChi recombinante. A proteína MpChi não digerida contém a fusão His-Tag e SUMO em sua porção N-terminal. Esta fusão é removida após digestão com a enzima ULP-1.

MpChi não possui atividade quitinolítica mas apresenta capacidade de ligação à quitina

A proteína recombinante foi utilizada para verificação de atividade quitinolítica em ensaios fluorimétricos. Notavelmente, não foi possível detectar nenhum tipo de atividade quitinolítica (quitobiosidase, N-acetilglicosaminidase ou endoquitinase). Em contraste, o controle positivo apresentou clara atividade quitinolítica (Figura 4A). Ainda que com atividade quitinolítica ausente, verificamos que a proteína MpChi é capaz de se ligar especificamente à quitina, principal constituinte da parede celular de fungos (Figura 4B). Esta proteína não se liga à quitina deacetilada (quitosano), nem a polissacarídeos constituintes de parede celular de plantas (celulose e xilano).

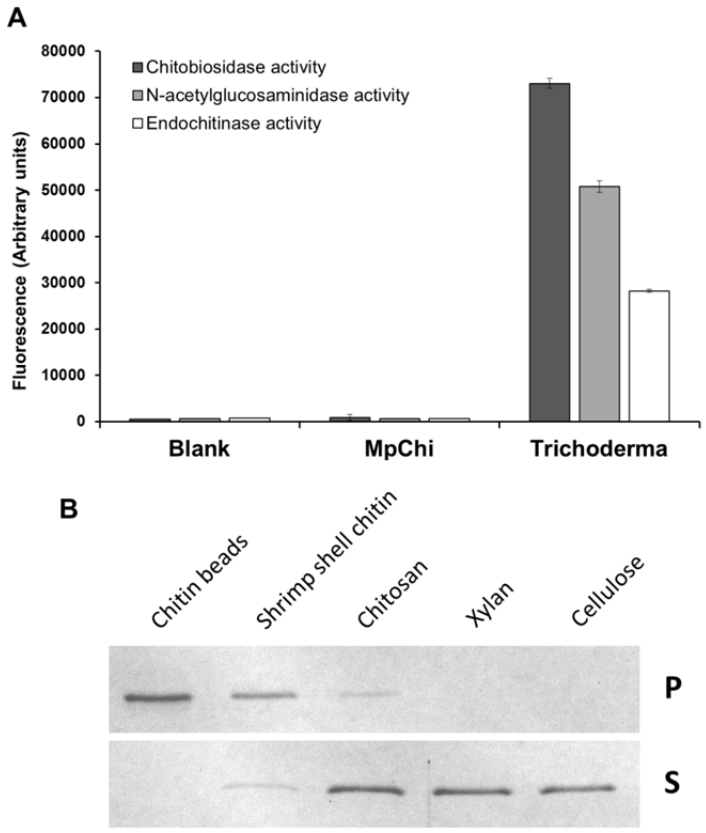

Figura 4. A proteína MpChi de *M. perniciosa* não possui atividade quitinolítica, mas retém a capacidade de ligação à quitina. (A) Ensaio de atividade utilizando substratos específicos para a detecção de três atividades quitinolíticas diferentes: quitobiosidase, N-acetilglicosaminidase e endoquitinase. Uma mistura de quitinases de *Trichoderma* foi utilizada como controle positivo do experimento. As barras de erros representam o desvio padrão de três medições. (B) Ensaio de ligação da proteína MpChi a diferentes substratos. Verifica-se que a proteína é capaz de ligar-se especificamente à quitina. P: fração precipitada (ligada ao substrato); S: Fração solúvel (não ligada ao substrato).

DISCUSSÃO

Neste trabalho, apresentamos a caracterização de um potencial efetor possivelmente envolvido na proteção do patógeno *M. perniciosa* contra quitinases produzidas pelo cacaueiro. A proteção da parede celular mediada por efetores é uma estratégia compartilhada por diferentes fungos fitopatogênicos (van den Burg *et al.*, 2006; Marshall *et al.*, 2011; Mentlak *et al.*, 2012), sugerindo um importante papel na evolução da patogenicidade destes organismos. Curiosamente, esta estratégia parece ter sido desenvolvida de forma independente nos diferentes fungos, uma vez que proteínas não relacionadas estão envolvidas neste mecanismo. Em *Cladosporium fulvum*, o efetor AVR4 protege o fungo da ação de enzimas hidrolíticas ligando-se à parede celular por meio de um domínio de ligação à quitina encontrado em invertebrados (van den Burg *et al.*, 2006). Já em *Mycosphaerella graminicola*, a proteção da parede celular é mediada por proteínas contendo domínios LysM (Marshall *et al.*, 2011). Neste contexto, a utilização de uma quitinase inativa por *M. perniciosa* constitui um modelo inovador e bastante interessante. Definições clássicas propõem que efetores são proteínas que evoluem rapidamente, sendo espécie-específicas ou conservadas apenas em espécies filogeneticamente próximas (Stergiopoulos & De Wit, 2009). No entanto, quitinases são proteínas presentes em diferentes grupos de organismos, desde bactérias até eucariotos superiores. Deste modo, a estratégia adotada por *M. perniciosa* é um interessante exemplo de como os genomas de fungos fitopatogênicos podem ser moldados para originar variadas estratégias de patogenicidade. Neste sentido, este modelo pode exemplificar um mecanismo peculiar de evolução de efetores em fungos.

Os resultados apresentados suportam uma possível participação da proteína MpChi na patogenicidade de *M. perniciosa* sobre seu hospedeiro. Notavelmente, o gene *MpChi* é distintivamente expresso durante a interação biotrófica do fungo com o cacaueiro (Figura 1), estando inclusive entre os genes com os maiores níveis de expressão durante o estágio de vassoura verde da doença (Tabela 1). Outros genes altamente expressos neste estágio incluem efetores putativos, sugerindo que o gene *MpChi* tenha importante função na patogenicidade de *M.*

perniciosa. A ausência de atividade quitinolítica da proteína MpChi e a sua capacidade de ligação à quitina (Figura 3) suportam a ideia de que esta proteína possa se ligar à parede celular do fungo, protegendo-a da ação de enzimas hidrolíticas produzidas pela planta como estratégia de defesa. Em suporte a esta hipótese, quitinases do cacaueiro pertencentes às famílias GH18 e GH19 são bastante induzidas durante a vassoura de bruxa (ver Capítulo 2), o que demandaria mecanismos eficientes de proteção da parede celular do patógeno. Experimentos estão em andamento para verificarmos se, de fato, a proteína MpChi é capaz de proteger *M. perniciosa* contra a ação de quitinases exógenas.

A visualização em microscópio da localização celular da proteína MpChi é uma interessante abordagem para fortalecer a hipótese proposta. Neste sentido, a etapa final deste trabalho também incluirá a produção e purificação da proteína MpChi fusionada à proteína GFP (G*reen Fluorescent Protein*) em *E. coli*, de modo que sua possível ligação à parede celular fúngica possa ser visualizada *in vivo*. Alternativamente, esta fusão também foi realizada durante a construção de um cassete para a transformação de *M. perniciosa* (dados não apresentados). Nesta construção, a fusão MpChi-GFP estará sob controle de um promotor responsivo a metanol (identificado através do Atlas Transcriptômico da Vassoura de Bruxa), de forma que a produção da proteína possa ser iniciada de forma controlada através da adição de metanol ao meio de cultura do fungo. Entretanto, é importante ressaltar que tal abordagem experimental é bastante arriscada em vista das limitações do nosso modelo de estudo. Desta forma, o uso de uma espécie modelo de fungo, como a levedura *Saccharomyces cerevisiae*, poderá ser uma opção viável neste experimento.

Além de um papel na proteção da parede celular do fungo, é possível que a proteína MpChi atue como quelante de fragmentos de quitina liberados pelo patógeno durante a colonização do hospedeiro. Assim, os fragmentos de quitina liberados não seriam detectados pelo cacaueiro, impedindo a elicitação de respostas de defesa. Tal mecanismo já foi demonstrado para as proteínas Ecp6 de *Cladosporium fulvum*, Slp1 de *Magnaporthe oryzae* e MgLysM3 de

Mycosphaerella graminicola, todas contendo o domínio LysM (de Jonge *et al.*, 2010; Marshall *et al.*, 2011; Mentlak *et al.*, 2012). Neste sentido, a conclusão deste trabalho também envolverá a verificação da existência de uma atividade similar na proteína MpChi.

Finalmente, a comprovação definitiva da participação da proteína MpChi na patogenicidade de *M. perniciosa* requer a construção de linhagens mutantes ou silenciadas para o gene *MpChi*. A manipulação genética do patógeno *M. perniciosa* consiste na principal limitação de nosso atual modelo de estudo, de forma que não dispomos de linhagens mutantes até o momento. Uma abordagem alternativa consiste na superexpressão do gene *MpChi* em plantas modelo (por exemplo, *Arabidopsis* ou tomateiro), e verificação da susceptibilidade a patógenos fúngicos em comparação a plantas não transformadas. De modo geral, os resultados obtidos neste trabalho são inovadores e de grande relevância para o entendimento das estratégias infectivas adotadas por *M. perniciosa* durante o estabelecimento da vassoura de bruxa. Experimentos adicionais deverão fortalecer a hipótese proposta, o que posicionará a proteína MpChi como um interessante modelo de efetor em fungos.

REFERÊNCIAS

Bhattacharya D, Nagpure A, Gupta RK (2007) Bacterial chitinases: properties and potential. Crit Rev Biotechnol **27**: 21-28

Boller T, Felix G (2009) A renaissance of elicitors: perception of microbe-associated molecular patterns and danger signals by pattern-recognition receptors. Annu Rev Plant Biol **60**: 379-406

Bortone K, Monzingo AF, Ernst S, Robertus JD (2002) The structure of an allosamidin complex with the *Coccidioides immitis* chitinase defines a role for a second acid residue in substrate-assisted mechanism. J Mol Biol **320**: 293-302

de Jonge R, van Esse HP, Kombrink A, Shinya T, Desaki Y, Bours R, van der Krol S, Shibuya N, Joosten MH, Thomma BP (2010) Conserved fungal LysM effector Ecp6 prevents chitin-triggered immunity in plants. Science **329**: 953-955

Dou D, Zhou JM (2012) Phytopathogen effectors subverting host immunity: different foes, similar battleground. Cell Host Microbe **12**: 484-495

Evans HC (1980) Pleomorphism in *Crinipellis perniciosa*, causal agent of witches' broom disease of cocoa. Transactions of the British Mycological Society **74**: 515-523

Evans HC (2007) Cacao diseases-the trilogy revisited. Phytopathology **97**: 1640-1643

Fukamizo T (2000) Chitinolytic enzymes: catalysis, substrate binding, and their application. Curr Protein Pept Sci **1**: 105-124

Hartl L, Zach S, Seidl-Seiboth V (2012) Fungal chitinases: diversity, mechanistic properties and biotechnological potential. Appl Microbiol Biotechnol **93**: 533-543

Huang QS, Xie XL, Liang G, Gong F, Wang Y, Wei XQ, Wang Q, Ji ZL, Chen QX (2012) The GH18 family of chitinases: their domain architectures, functions and evolutions. Glycobiology **22**: 23-34

Jones JD, Dangl JL (2006) The plant immune system. Nature **444**: 323-329

Lu Y, Zen KC, Muthukrishnan S, Kramer KJ (2002) Site-directed mutagenesis and functional analysis of active site acidic amino acid residues D142, D144 and E146 in *Manduca sexta* (tobacco hornworm) chitinase. Insect Biochem Mol Biol **32**: 1369-1382

Marshall R, Kombrink A, Motteram J, Loza-Reyes E, Lucas J, Hammond-Kosack KE, Thomma BP, Rudd JJ (2011) Analysis of two in planta expressed LysM effector homologs from the fungus *Mycosphaerella graminicola* reveals novel functional properties and varying contributions to virulence on wheat. Plant Physiol **156**: 756-769

Meinhardt LW, Rincones J, Bailey BA, Aime MC, Griffith GW, Zhang D, Pereira GA (2008) *Moniliophthora perniciosa*, the causal agent of witches' broom disease of cacao: what's new from this old foe? Mol Plant Pathol **9**: 577-588

Mentlak TA, Kombrink A, Shinya T, Ryder LS, Otomo I, Saitoh H, Terauchi R, Nishizawa Y, Shibuya N, Thomma BP, *et al.* (2012) Effector-mediated suppression of chitin-triggered immunity by *Magnaporthe oryzae* is necessary for rice blast disease. Plant Cell **24**: 322-335

Merzendorfer H, Zimoch L (2003) Chitin metabolism in insects: structure, function and regulation of chitin synthases and chitinases. J Exp Biol **206**: 4393-4412

Ohnuma T, Numata T, Osawa T, Mizuhara M, Varum KM, Fukamizo T (2011) Crystal structure and mode of action of a class V chitinase from *Nicotiana tabacum*. Plant Mol Biol **75**: 291-304

Papanikolau Y, Prag G, Tavlas G, Vorgias CE, Oppenheim AB, Petratos K (2001) High resolution structural analyses of mutant chitinase A complexes with substrates provide new insight into the mechanism of catalysis. Biochemistry **40**: 11338-11343

Petersen TN, Brunak S, von HG, Nielsen H (2011) SignalP 4.0: discriminating signal peptides from transmembrane regions. Nat Methods **8**: 785-786

Purdy LH, Schmidt RA (1996) Status of cacao witches' broom: biology, epidemiology, and management. Annu Rev Phytopathol **34**: 573-594

Sahai AS, Manocha MS (1993) Chitinases of Fungi and Plants - Their Involvement in Morphogenesis and Host-Parasite Interaction. Fems Microbiology Reviews **11**: 317-338

Stergiopoulos I, De Wit PJ (2009) Fungal effector proteins. Annu Rev Phytopathol **47**: 233-263

Synstad B, Gaseidnes S, van Aalten DM, Vriend G, Nielsen JE, Eijsink VG (2004) Mutational and computational analysis of the role of conserved residues in the active site of a family 18 chitinase. Eur J Biochem **271**: 253-262

Thompson JD, Gibson TJ, Higgins DG (2002) Multiple sequence alignment using ClustalW and ClustalX. Curr Protoc Bioinformatics **Chapter 2**: Unit

van Aalten DM, Komander D, Synstad B, Gaseidnes S, Peter MG, Eijsink VG (2001) Structural insights into the catalytic mechanism of a family 18 exo-chitinase. Proc Natl Acad Sci U S A **98**: 8979-8984

van den Burg HA, Harrison SJ, Joosten MH, Vervoort J, De Wit PJ (2006) *Cladosporium fulvum* Avr4 protects fungal cell walls against hydrolysis by plant chitinases accumulating during infection. Mol Plant Microbe Interact **19**: 1420-1430

Watanabe T, Kobori K, Miyashita K, Fujii T, Sakai H, Uchida M, Tanaka H (1993) Identification of glutamic acid 204 and aspartic acid 200 in chitinase A1 of *Bacillus circulans* WL-12 as essential residues for chitinase activity. J Biol Chem **268**: 18567-18572

Zdobnov EM, Apweiler R (2001) InterProScan--an integration platform for the signature-recognition methods in InterPro. Bioinformatics **17**: 847-848

Capítulo IV

The fungal pathogen *Moniliophthora perniciosa* has genes similar to plant PR-1 that are highly expressed during its interaction with cacao

Paulo José P.L. Teixeira*, Daniela P.T. Thomazella*, Ramon O. Vidal, Paula F.V. do Prado, Osvaldo Reis, Renata M. Baroni, Sulamita F. Franco, Piotr Mieczkowski, Gonçalo A.G. Pereira, Jorge M.C. Mondego

* Autores com igual contribuição

Trabalho publicado na revista *PLoS ONE*, Setembro de 2012, Vol. 9: e45929.

APRESENTAÇÃO

Proteínas da família PR-1 (*Pathogenesis-related* 1) de plantas são marcadores típicos de respostas de defesa contra patógenos, tendo comprovada atividade antifúngica. Curiosamente, uma primeira inspeção do *draft* do genoma do fungo *Moniliophthora perniciosa* revelou a existência de quatro genes que codificam proteínas similares às PR-1 de plantas. Posteriormente, com os novos sequenciamentos do genoma de *M. perniciosa* e a construção do Atlas Transcriptômico da Vassoura de Bruxa, outros sete genes *PR-1* foram identificados, totalizando onze genes neste fitopatógeno. Notavelmente, cinco destes genes são altamente expressos durante a interação biotrófica do fungo com o cacaueiro, o que sugere uma potencial participação das proteínas por eles codificadas na patogenicidade de *M. perniciosa*. Em concordância, análises do Atlas Transcriptômico da Vassoura de Bruxa mostraram que alguns membros da família *MpPR-1* estão entre os genes mais expressos por *M. perniciosa* no estágio de vassoura verde da doença. Ainda, dois destes genes também são altamente expressos durante a germinação dos esporos do fungo, um estágio bastante comprometido com o estabelecimento da infecção. Com base nestas importantes descobertas, iniciou-se um estudo mais detalhado dos genes *MpPR-1* de *M. perniciosa*. Este capítulo apresenta a primeira caracterização desta família gênica em um fungo fitopatogênico durante sua interação com a planta hospedeira. Os resultados e hipóteses apresentados têm servido como base para estudos funcionais específicos que visam à elucidação da participação de tais genes no processo infectivo de *M. perniciosa* e desenvolvimento da doença vassoura de bruxa no cacaueiro.

OPEN ACCESS Freely available online

PLOS ONE

The Fungal Pathogen *Moniliophthora perniciosa* Has Genes Similar to Plant PR-1 That Are Highly Expressed during Its Interaction with Cacao

Paulo J.P.L. Teixeira[1☯], Daniela P.T. Thomazella[1☯], Ramon O. Vidal[1,2], Paula F.V. do Prado[1], Osvaldo Reis[1], Renata M. Baroni[1,3], Sulamita F. Franco[1], Piotr Mieczkowski[4], Gonçalo A.G. Pereira[1]*, Jorge M.C. Mondego[3]

1 Departamento de Genética, Evolução e Bioagentes, Universidade Estadual de Campinas, Campinas, São Paulo, Brazil, **2** Laboratório Nacional de Biociências, Campinas, São Paulo, Brazil, **3** Centro de Pesquisa e Desenvolvimento em Recursos Genéticos Vegetais, Instituto Agronômico de Campinas, Campinas, São Paulo, Brazil, **4** Department of Genetics, School of Medicine, University of North Carolina at Chapel Hill, Chapel Hill, North Carolina, United States of America

Abstract

The widespread SCP/TAPS superfamily (SCP/Tpx-1/Ag5/PR-1/Sc7) has multiple biological functions, including roles in the immune response of plants and animals, development of male reproductive tract in mammals, venom activity in insects and reptiles and host invasion by parasitic worms. Plant Pathogenesis Related 1 (PR-1) proteins belong to this superfamily and have been characterized as markers of induced defense against pathogens. This work presents the characterization of eleven genes homologous to plant *PR-1* genes, designated as *MpPR-1*, which were identified in the genome of *Moniliophthora perniciosa*, a basidiomycete fungus responsible for causing the devastating witches' broom disease in cacao. We describe gene structure, protein alignment and modeling analyses of the MpPR-1 family. Additionally, the expression profiles of *MpPR-1* genes were assessed by qPCR in different stages throughout the fungal life cycle. A specific expression pattern was verified for each member of the *MpPR-1* family in the conditions analyzed. Interestingly, some of them were highly and specifically expressed during the interaction of the fungus with cacao, suggesting a role for the MpPR-1 proteins in the infective process of this pathogen. Hypothetical functions assigned to members of the *MpPR-1* family include neutralization of plant defenses, antimicrobial activity to avoid competitors and fruiting body physiology. This study provides strong evidence on the importance of *PR-1-like* genes for fungal virulence on plants.

Citation: Teixeira PJPL, Thomazella DPT, Vidal RO, Prado PFVdo, Reis O, et al. (2012) The Fungal Pathogen *Moniliophthora perniciosa* Has Genes Similar to Plant PR-1 That Are Highly Expressed during Its Interaction with Cacao. PLoS ONE 7(9): e45929. doi:10.1371/journal.pone.0045929

Editor: Dee A. Carter, University of Sydney, Australia

Received March 21, 2012; **Accepted** August 27, 2012; **Published** September 20, 2012

Funding: This study was supported by funds from Fundação de Amparo à Pesquisa do Estado de São Paulo (FAPESP, 2006/53553-3, 2007/50262-0, 2009/51018-1 and 2009/50119-9). The funders had no role in study design, data collection and analysis, decision to publish, or preparation of the manuscript.

Competing Interests: The authors have declared that no competing interests exist.

* E-mail: goncalo@unicamp.br

☯ These authors contributed equally to this work.

Introduction

The basidiomycete fungus *Moniliophthora perniciosa* is the causative agent of witches' broom disease (WBD) in cacao. This devastating disease is responsible for large losses in cacao plantations in the Americas and is a potential threat to other cacao-growing areas throughout the world [1,2]. *M. perniciosa* displays a hemibiotrophic lifestyle, with sequential biotrophic (infective) and necrotrophic stages in the plant. These two mycelial stages are morphologically distinct: whereas the biotrophic mycelium is monokaryotic, the necrotrophic stage is dikaryotic and presents clamp connections for nuclei transfer.

The disease cycle initiates when fungal basidiospores infect meristematic tissues of cacao – such as shoots, fruits and floral cushions – where they germinate and develop as biotrophic monokaryotic hyphae. *M. perniciosa* does not use any specialized infection structure to enter the plant (i.e. apressorium), as observed for the majority of biotrophic and hemibiotrophic fungi [3]. This fungus enters the host tissues through stomata or wounds and colonizes the plant apoplast as thick monokaryotic hyphae. In this stage of the disease, the parasitic fungus causes drastic morpho-physiological alterations in the host, resulting in the formation of hyperplastic and hypertrophic stems, known as green brooms. During the disease progression, the pathogen switches to its necrotrophic dikaryotic stage, which parallels the death of the infected plant tissue. In this phase of WBD, known as dry broom, *M. perniciosa* colonizes the dead plant and can be found in the intracellular spaces of cacao. After alternating wet and dry periods, the fungus produces basidiomata that release basidiospores, reinitiating the disease cycle [1,2].

During recent years, efforts have been directed to develop a solution to control this disease. In 2000, the WBD genome initiative (www.lge.ibi.unicamp.br/vassoura) was launched and, since then, it has supported several molecular and biochemical studies involving both the pathogen and the plant [4–9]. With the recent technological advances in the area of DNA sequencing, transcriptomes representing a variety of growth and developmental conditions of *M. perniciosa* – including transcriptomes of the fungus developing *in planta* – were sequenced using the RNA-seq technology. As a result, a comprehensive database named WBD

Transcriptome Atlas has been constructed, and has contributed important information on the molecular basis of the *M. perniciosa*-cacao interaction (Teixeira *et al.*, manuscript in preparation).

The establishment of a disease process depends on the ability of the pathogen to overcome or neutralize plant defenses and then initiate a parasitic relationship with its host. However, to halt pathogenic colonization, plants have developed an arsenal of defense responses, which include induction of pathogenesis-related (PR) genes [10], production of secondary metabolites as well as reinforcement of cell walls. Also, usually triggered by the recognition of a pathogen attack, plants produce highly toxic radicals, such as nitric oxide and reactive oxygen species, which can lead to the establishment of a local cell death (the hypersensitive response, HR). Among the induced pathogenesis-related genes, PR-1s have been frequently identified and used as markers of plant defense responses [10]. Notably, they were shown to have microbicide activity against oomycetes and fungi [11–14].

PR-1 proteins are members of a superfamily named SCP/TAPS (Sperm-Coating Protein/Tpx-1/Ag5/PR-1/Sc7) or CAP (Cysteine-rich secretory proteins, Antigen 5, and Pathogenesis-related 1). This superfamily has members throughout the eukaryotic kingdom, suggesting an important role for these proteins in the biology of eukaryotes [15,16]. Thus far, only a single report has shown the existence of enzymatic activity for a SCP/TAPS protein [17]. The protein Tex31 of the predatory marine mollusk *Conus textile* showed serine-proteolytic activity against a specific pro-peptide precursor of a venom toxin [17]. In addition, structural analyses indicated that four highly conserved amino acids (two histidines and two glutamates) form the putative catalytic site of SCP/TAPS proteins [16–22]. Although the existence of biochemical activity has not been shown for any other SCP/TAPS proteins, they are associated with various biological processes, such as male reproductive tract development [23,24], immune responses in plants and animals [25], venom activity of reptiles and insects [26–29] and host invasion by parasites [30–32].

In fungal species, SCP/TAPS proteins have been studied in *Saccharomyces cerevisiae*, in which they are highly expressed under nutrient starvation conditions [33]. In the basidiomycete *Schizophyllum commune*, SCP/TAPS proteins have been associated with fruiting body formation [34]. Interestingly, in the ascomycetes *Candida albicans* and *Fusarium oxysporum*, deletion of a SCP/TAPS gene impaired virulence on animals, indicating a role for this class of genes in fungal pathogenicity [35,36]. Considering that PR-1 proteins are widespread markers of the induced defense response in plants, what would be the function of their homologs in a plant pathogenic fungus, such as *M. perniciosa*?

This article describes the identification of a SCP/TAPS family in the *M. perniciosa* genome, the analysis of structural features of these genes, and their expression profile throughout *M. perniciosa* development. *M. perniciosa* SCP/TAPS proteins were modeled, and some structural differences were revealed among them. Based on these results, we present a hypothetical model in which SCP/TAPS proteins play a role in *M. perniciosa* pathogenicity by interfering with the defense system of cacao plants.

Results

Characterization of the *PR-1* gene family in *M. perniciosa*

Annotation of a genome draft of *M. perniciosa* [7], and inspection of fungal EST libraries [6,8] identified four *PR-1*-like genes in this pathogen (*MpPR-1a* to *MpPR-1d*). Later, improvements in the genome assembly obtained with next generation sequencing data (unpublished data) allowed the identification of seven additional members of the *MpPR-1* family (*MpPR-1e* to *MpPR-1k*), totaling eleven *PR-1*-like genes in *M. perniciosa*. These members are very heterogeneous in size and gene structure, with coding sequences (CDS) ranging from 447 to 1,152 nucleotides and intron composition varying between two to five introns. Three of these genes (*MpPR-1c*, *MpPR-1d* and *MpPR-1j*) are organized *in tandem*. Sequence details of these eleven genes are shown in Table 1, and their respective structures (exon-intron positions) are depicted in figure S1.

Hydrophobic signal peptide sequences predicted with the TargetP program [37] were identified in all eleven *MpPR-1* sequences (NN score >0.80), strongly suggesting that these proteins are secreted. Additionally, all MpPR-1 proteins showed a single SCP/TAPS domain (InterPro ID IPR014044), as predicted by the InterProScan server [38]. These domains were approximately 130 amino acids in length and ranged between 34% and 82% of the total amino acid sequence of an individual MpPR-1 protein (Fig. 1A). In addition to the SCP/TAPS domain, MpPR-1b and MpPR-1g present N-terminal and C-terminal extensions, respectively. No other InterProScan predicted domain was identified in these extensions or in any of the MpPR-1 proteins described. Interestingly, a careful manual inspection revealed that the C-terminal extension of MpPR-1g is rich in residues of lysine (K) and glutamic acid (E) that are mostly organized in alternating positions, resulting in the formation of a "KEKE" motif [39] (Fig. 2). The MpPR-1b N-terminal extension is also a low complexity region, being rich in serine, threonine and proline residues. However, no described motif could be recognized.

Alignment of the amino acid sequences encoded by all *MpPR-1* genes revealed significant similarity only over the SCP/TAPS domains (Fig. 1B). The amino acids proposed to form the putative catalytic site of SCP/TAPS proteins (two histidines and two glutamic acids, shown in red) were identified in six MpPR-1s (MpPR-1b, MpPR-1c, MpPR-1d, MpPR-1e, MpPR-1h and MpPR-1j). In contrast, MpPR-1a presented two, MpPR-1f had only one and MpPR-1g, MpPR-1i and MpPR-1k had none of the four conserved residues (Fig. 1B).

Protein structure modeling

To explore the tertiary structural characteristics within the SCP/TAPS domains of the MpPR-1 family members, we created homology models using the fold prediction metaserver I-TASSER (Fig. 3). The derived models indicated that the MpPR-1 SCP/TAPS domains adopt the α-β-α sandwich conformation, which is common to all superfamily members across the species studied [16,18] (Fig. 3A). Furthermore, all MpPR-1 proteins possess the large cleft proposed to constitute the SCP/TAPS active site. As mentioned above, six MpPR-1 proteins (MpPR-1b, MpPR-1c, MpPR-1d, MpPR-1e, MpPR-1h and MpPR-1j) have the four conserved residues of the putative catalytic site. These residues are localized within this cleft (Fig. 3B) and are found in the same direction of the orthologous amino acids identified in previous SCP/TAPS crystal structures [18,21,22,25]. These residues are lacking (MpPR-1g, MpPR-1i and MpPR-1k) or partially absent (MpPR-1a and MpPR-1f) in other members of the MpPR-1 family (Fig. 3C), indicating some diversification in their mode of action.

Remarkably, MpPR-1b and MpPR-1g contain two modules: the SCP/TAPS domain and either N-terminal (MpPR-1b) or C-terminal (MpPR-1g) extensions. Protein models indicate that such extensions are structurally organized and have α-helix conformations (Fig. 3A). These additional regions possibly confer a different activity or regulation to these proteins.

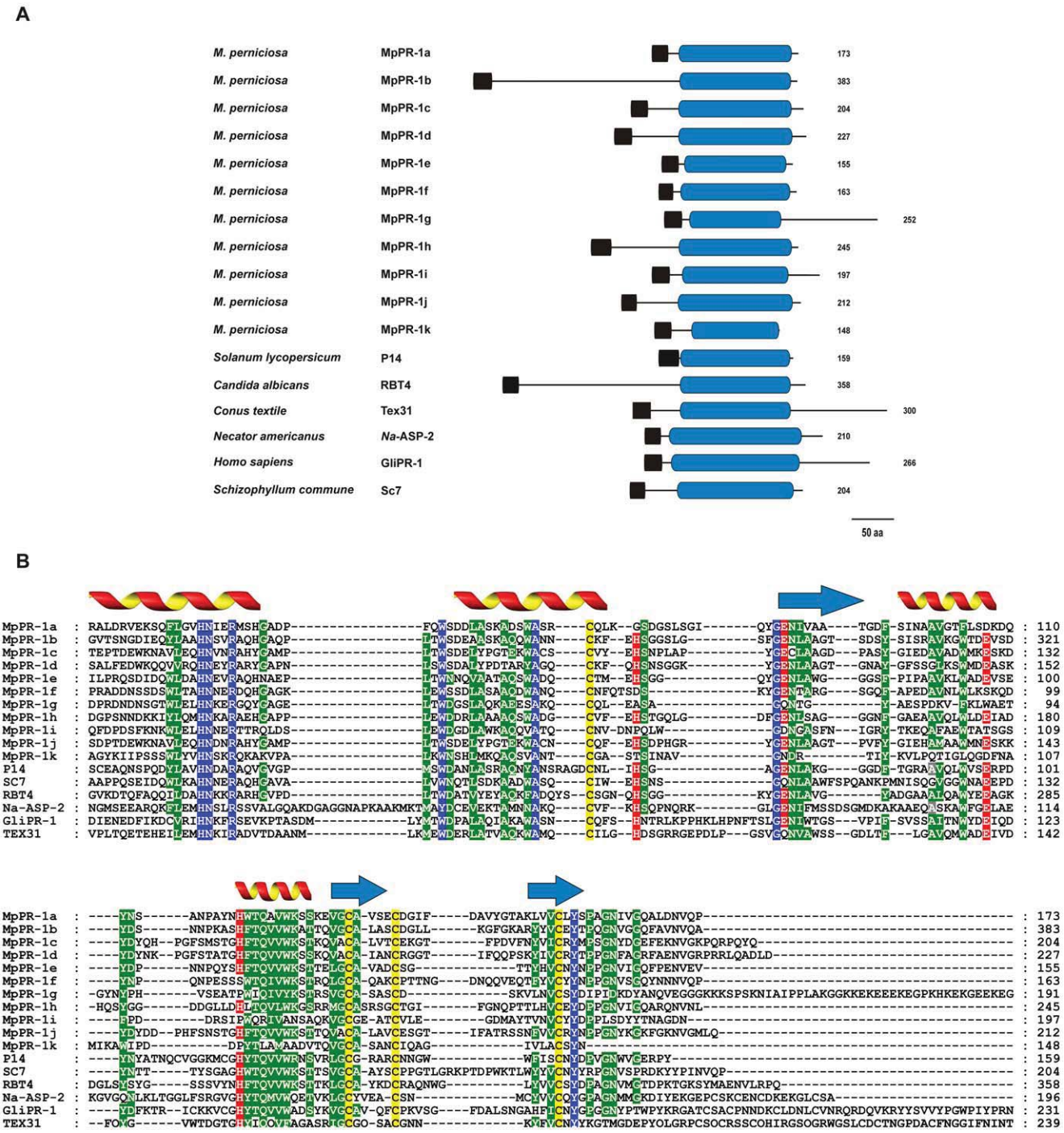

Figure 1. Comparison of MpPR-1 and SCP/TAPS proteins of representative organisms. (A) Domain arrangement of SCP/TAPS proteins. Hydrophobic signal peptides are shown in black and SCP/TAPS domains are represented in blue. The numbers on the right show the size of each protein. Large N-terminal and C-terminal expansions are observed in MpPR-1b and MpPR-1g, respectively. (B) Alignment of the conserved domain of SCP/TAPS proteins. In general, the SCP/TAPS superfamily members show similarities only over the SCP/TAPS domain. Conserved residues (100% of identity) are shown in blue and semi-conserved residues (at least 60% of identity) in green. Putative active site residues are highlighted in red and cysteines in yellow. Secondary structure elements are shown above the alignment (arrow: β-sheets; helix: α-helixes). P14, tomato PR-1 (GenBank P04284); RBT4, repressed by TUP1 from *Candida albicans* (GenBank AAG09789); Tex31, SCP/TAPS from the mollusk *Conus textile* (GenBank CAD36507); Na-ASP-2, *Necator americanus* secreted protein (GenBank AAP41952); GliPR-1, human glioma PR-1 protein (GenBank P48060); SC7, SCP/TAPS from the basidiomycete *Schizophyllum commune* (GenBank P35794).
doi:10.1371/journal.pone.0045929.g001

Table 1. Characteristics of the eleven *MpPR-1* genes identified in the *M. perniciosa* genome.

Gene name	GenBank accession number	CDS size (bp)	Number of introns	Protein size (aa)	Signal peptide	BlastX First Hit (Swissprot)*	BlastP First Hit (NCBI-NR)*
MpPR-1a	JN620340	522	2	173	Yes (NN score = 0.894)	SC14 (1e-19) *Schizophyllum commune*	XP_001876569.1- predicted protein (1e-54) *Laccaria bicolor*
MpPR-1b	JN620341	1152	5	383	Yes (NN score = 0.844)	SC7 (3e-25) *Saccharomyces cerevisiae*	XP_001873270.1- *predicted protein* (2e-63) *Laccaria bicolor*
MpPR-1c	JN620342	615	4	204	Yes (NN score = 0.898)	PRY1 (1e-28) *Saccharomyces cerevisiae*	XP_001889714.1- predicted protein (2e-48) *Laccaria bicolor*
MpPR-1d	JN620343	684	5	227	Yes (NN score = 0.951)	PRY1 (3e-31) *Saccharomyces cerevisiae*	XP_001889714.1- predicted protein (8e-66) *Laccaria bicolor*
MpPR-1e	JN620344	468	3	155	Yes (NN score = 0.919)	PR-1C (6e-35) *Nicotiana tabacum*	XP_003038868.1- hypothetical protein (2e-45) *Schizophyllum commune*
MpPR-1f	JN620345	492	3	163	Yes (NN score = 0.947)	SC7 (4e-25) *Schizophyllum commune*	CCA68148 – related to PRY1 (8e-42) *Piriformospora indica*
MpPR-1g	JN620346	759	4	252	Yes (NN score = 0.905)	SC7 (4e-13) *Schizophyllum commune*	EFY95292.1 – hypothetical protein (4e-15) *Metarhizium anisopliae*
MpPR-1h	JN620347	738	5	245	Yes (NN score = 0.804)	PR-1B (5e-24) *Nicotiana tabacum*	XP_001828886.1- hypothetical protein (3e-41) *Coprinopsis cinerea*
MpPR-1i	JN620348	498	3	165	Yes (NN score = 0.940)	SC7 (4e-05) *Schizophyllum commune*	EGO02028.1- hypothetical protein (3e-10) *Serpula lacrymans*
MpPR-1j	JN620349	639	4	212	Yes (NN score = 0.918)	PRY3 (8e-30) *Saccharomyces cerevisiae*	XP_001889714.1- predicted protein (2e-54) *Laccaria bicolor*
MpPR-1k	JN620350	447	2	148	Yes (NN score = 0.944)	P14 (2e-03) *Solanum lycopersicum*	XP_002578075.1- venom allergen 21 (4e-09) *Schistosoma mansoni*

*e-values are shown in parentheses.

doi:10.1371/journal.pone.0045929.t001

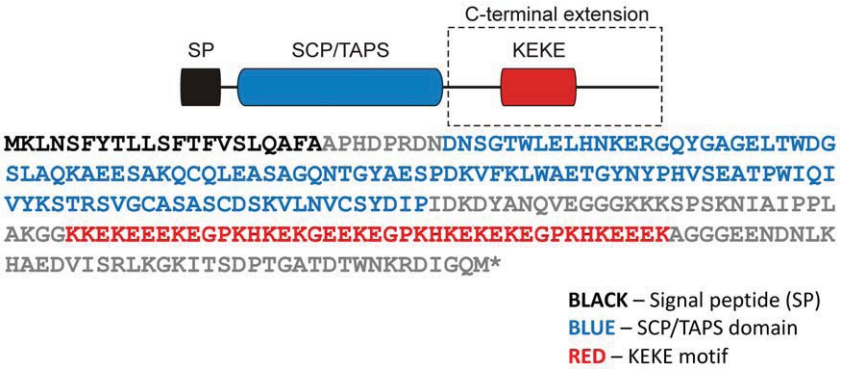

Figure 2. Domains identified in the MpPR-1g protein. In addition to the SCP/TAPS domain, this protein has a KEKE motif in its C-terminal extension. This motif is known to mediate the interaction with other proteins or ions.
doi:10.1371/journal.pone.0045929.g002

Expression profile of *MpPR-1* genes throughout *M. perniciosa* development

The expression pattern of *MpPR-1* family members was assessed by quantitative real time PCR (qPCR) throughout the different developmental stages of *M. perniciosa*. As shown in Figure 4, each *MpPR-1* gene showed a specific expression profile: expression of *MpPR-1a*, *MpPR-1b*, *MpPR-1d* and *MpPR-1i* genes was relatively uniform, with nearly similar expression values for most conditions analyzed. In contrast, *MpPR-1e* was up-regulated in the dikaryotic hyphae, whereas *MpPR-1j* was exclusively expressed in mushrooms (basidiomata). Strikingly, five *MpPR-1* genes (*MpPR-1c*, *MpPR-1f*, *MpPR-1g*, *MpPR-1h*, and *MpPR-1k*) were highly expressed during the biotrophic interaction of the fungus with the cacao plant (green broom stage of WBD). These genes were poorly expressed in the necrotrophic hyphae (dry broom stage of

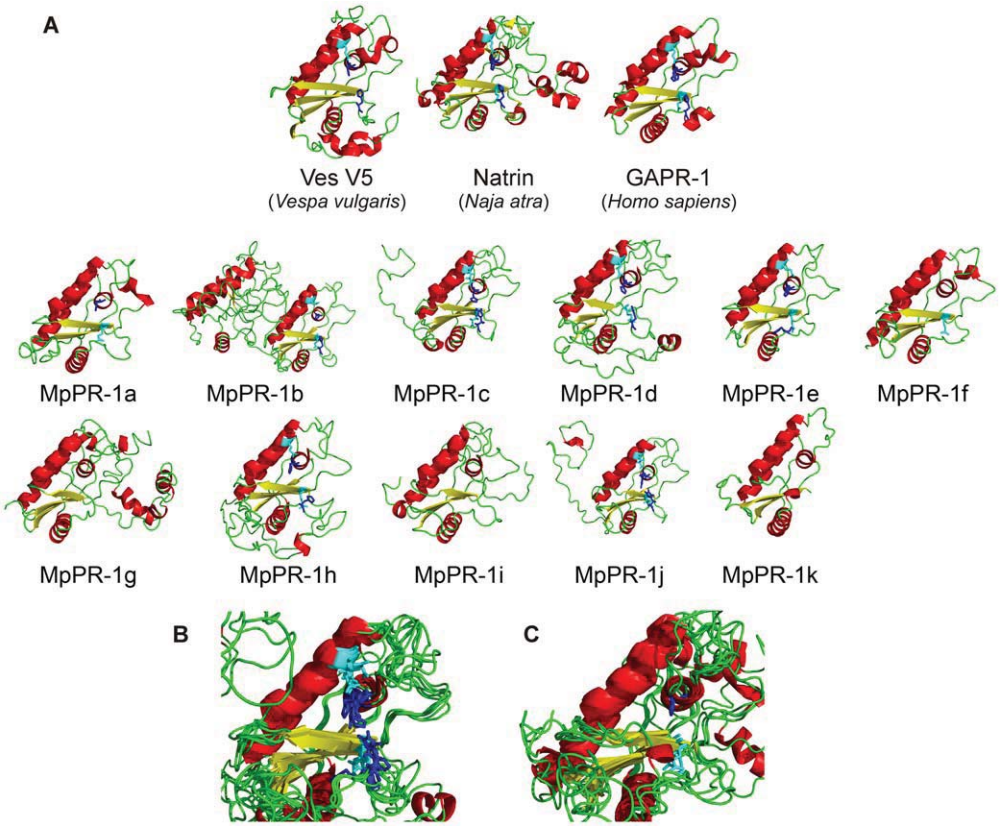

Figure 3. Homology modeling of MpPR-1 proteins. (A) Ribbon stick representation showing the folding of eleven MpPR-1 proteins and three SCP/TAPS proteins used to obtain these models. The putative residues forming the catalytic site are highlighted in dark blue (histidines) and light blue (glutamic acids). Note the presence of an additional protein module in MpPR-1b and MpPR-1g. These modules respectively correspond to the N-terminal and C-terminal extensions observed in these proteins. (B) MpPR-1b, MpPR-1c, MpPR-1d, MpPR-1e, MpPR-1h and MpPR-1j have the four putative active site residues of the SCP/TAPS domain. (C) These residues are partially or completely absent in MpPR-1a, MpPR-1f, MpPR-1g, MpPR-1i and MpPR-1k.
doi:10.1371/journal.pone.0045929.g003

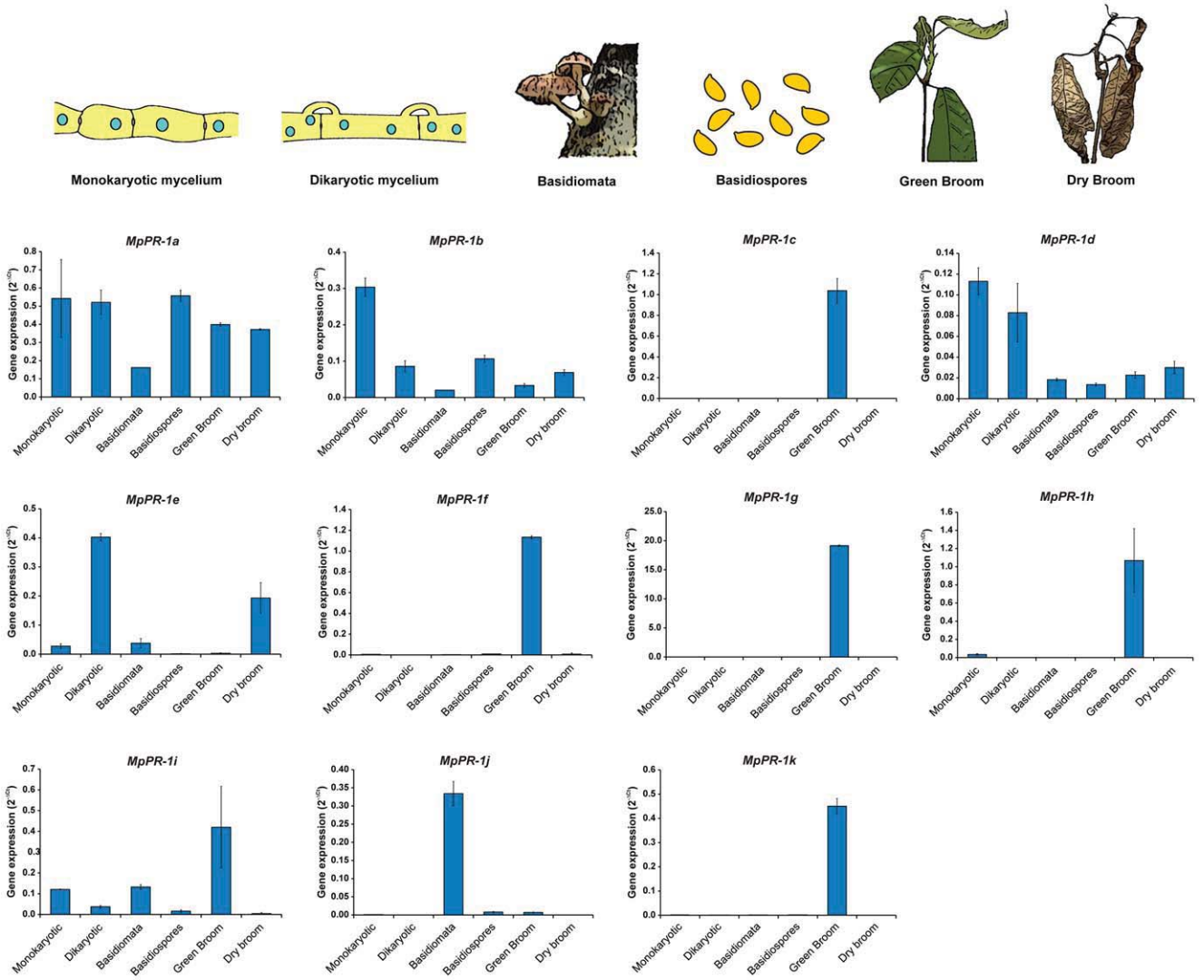

Figure 4. Transcriptional profile of *MpPR-1* family members throughout the *M. perniciosa* life cycle. Each *MpPR-1* gene has a distinct expression profile during fungal development. "Monokaryotic" and "Dikaryotic" hyphae represent the two mycelial stages (biotrophic and necrotrophic) grown under *in vitro* conditions. "Green broom" and "dry broom" correspond to the biotrophic and necrotrophic stages of *M. perniciosa*, respectively, during its interaction with cacao. Analyses were performed by qPCR and the *M. perniciosa β-actin* gene was used as endogenous control to normalize data. Error bars represent standard deviations determined with two biological replicates. Representative drawings of the conditions analyzed are shown on the top.
doi:10.1371/journal.pone.0045929.g004

WBD) and in the *ex planta* conditions, suggesting a specific role for the encoded proteins in fungal pathogenicity.

Characterization of an *MpPR-1* cluster

As mentioned above, genes *MpPR-1c*, *MpPR-1d* and *MpPR-1j* are arranged *in tandem* over a region of approximately 5 kbp in the *M. perniciosa* genome (Fig. 5). This gene cluster points to the occurrence of gene duplication events during the evolution of the *MpPR-1* family. Indeed, the proteins encoded by these three genes are more similar to each other than to other MpPR-1 members (data not shown). In accordance, these three genes have very similar structures, with a minor difference in *MpPR-1d*, which has an additional intron and a mini-exon following exon 2 (Fig. S1). Importantly, genes *MpPR-1c* and *MpPR-1j* are also highly similar at the nucleotide level (84% identity), indicating a recent event of gene duplication. Despite their similarity, these genes have distinct expression profiles: whereas *MpPR-1j* is highly expressed in basidiomata, *MpPR-1c* is mainly expressed during cacao infection (green broom stage of WBD) (Figs. 4 and 5).

Discussion

In this study, we identified a family of genes encoding proteins of the SCP/TAPS superfamily in the plant pathogen *Moniliophthora perniciosa*. SCP/TAPS proteins are found in a vast number of organisms, including plants, insects, mammals, fungi, mollusks and worms. Plant Pathogenesis-related proteins (PR-1) belong to this superfamily and are known to accumulate after pathogen invasion [10]. Despite being broadly spread, evidence for the importance of fungal SCP/TAPSs in plant-pathogen interactions has not yet been described.

M. perniciosa has a larger number (11) of *SCP/TAPS* genes encoding PR-1-like secreted proteins than other fungal species analyzed to date (Table S1). Although these proteins have a single

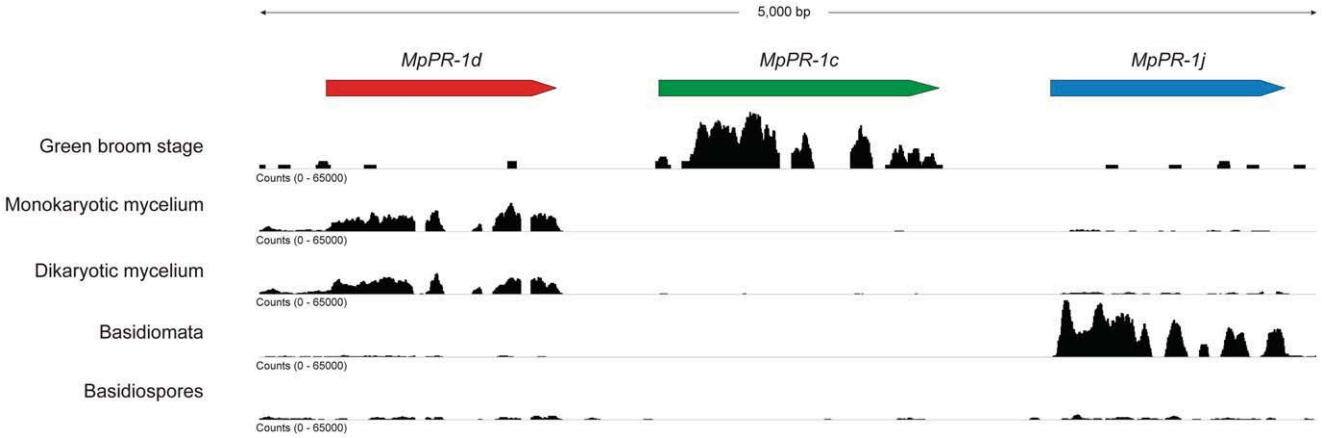

Figure 5. Genomic organization and transcriptional profile of the *MpPR-1* gene cluster found in *M. perniciosa*. The *MpPR-1c*, *MpPR-1d* and *MpPR-1j* genes are arranged *in tandem* over a region of approximately 5 kbp. Analysis of the WBD RNA-seq Atlas shows the expression profile of these *MpPR-1* genes in different conditions (green broom – *in planta* development of the biotrophic monokaryotic hyphae; monokaryotic mycelium; dikaryotic mycelium; basidiomata and basidiospores). Data were visualized using the Integrative Genomics Viewer [62]. The black coverage plot shows cumulative RNA-seq read coverage along the transcripts in all different conditions. Note that these genes were named according to the order they were identified in the fungal genome, and the nomenclature does not necessarily reflect their relative localization in the genome.
doi:10.1371/journal.pone.0045929.g005

SCP/TAPS domain, they are very divergent in sequence (Fig. 1B). Some of them show extensions in their N-terminal (MpPR-1b) or C-terminal (MpPR-1g) regions (Fig. 1A and Fig. 3A). Also, six MpPR1s (MpPR-1b, MpPR-1c, MpPR-1d, MpPR-1e, MpPR-1h and MpPR-1j) have all four conserved amino acids (two histidines and two glutamates) of the active site proposed for SCP/TAPS proteins, whereas the other five proteins (MpPR-1a, MpPR-1f, MpPR-1g, MpPR-1i and MpPR-1k) lack the catalytic tetrad (Fig. 1B and Fig. 3). However, the basic signatures of SCP/TAPS domains remain conserved.

The high number of genes and the variation in protein sequence of MpPR-1 members may reflect a process of diversification of this gene family in *M. perniciosa*. In accordance, the cluster including three *MpPR-1* members (Fig. 5) indicates the occurrence of recent events of gene duplication, which are central for the generation of genetic variability. In this regard, functional diversity may occur within this family, and different MpPR-1s likely play a particular role in *M. perniciosa* biology.

Although widely distributed among several species, the functions of SCP/TAPS proteins are still uncertain. Their broad distribution indicates that they play a role in a plethora of biological processes. In the mushroom-forming basidiomycete *Schizophyllum commune*, SCP/TAPS proteins were identified in the basidiomata, being involved in the formation of pseudo-parenchymous tissue of this reproductive structure [34]. In a similar way, *MpPR-1j* is exclusively expressed in the basidiomata of *M. perniciosa*, suggesting a role for this isoform in the physiology/metabolism of fruiting bodies. In contrast, we also identified *SCP/TAPS* genes in the genomes of some basidiomycetes that do not produce mushrooms (e.g., *Ustilago maydis*, *Puccinia graminis*, *Melampsora spp* and *Cryptococcus spp*) (data not shown). Therefore, it is likely that SCP/TAPS proteins have functions in basidiomycetes other than fruiting body development/physiology.

In response to pathogen invasion, plants typically produce PR-1 proteins, which have antimicrobial activity and, consequently, are able to inhibit the development of fungi and oomycetes [11–13]. Considering that, we hypothesize that some MpPR-1s could play a role in limiting the growth of other microbial competitors (e.g., oomycetes from the genus *Phytophthora*, responsible for causing black pod rot in cacao), thus favoring *M. perniciosa* colonization during WBD progression. Functional experiments are needed to confirm the existence of antimicrobial activity in any of the MpPR-1 proteins identified.

Gene expression analyses revealed that five *MpPR-1* genes (*MpPR-1c*, *MpPR-1f*, *MpPR-1g*, *MpPR-1h* and *MpPR-1k*) are strikingly up-regulated in the green broom stage of WBD, when the fungus grows biotrophically within the plant tissues (Fig. 4). Remarkably, inspection of the WBD RNA-seq Transcriptome Atlas (Teixeira *et al.*, manuscript in preparation) revealed that *MpPR-1g* and *MpPR-1h* are among the most highly expressed genes of *M. perniciosa* during its biotrophic interaction with cacao. Moreover, in addition to the green broom stage, *MpPR-1f* and *MpPR-1h* are notably expressed in germinating basidiospores (Fig. S2), a critical stage for the establishment of infection. None of these genes were significantly expressed in non-germinating spores or in the dry broom stage of WBD (Fig. 4 and Fig. S2), strongly indicating a major role for the encoded proteins in the infective (biotrophic) stage of *M. perniciosa*. Similarly, *SCP/TAPS* genes identified in some animal parasitic worms (*Schistosoma mansoni*, *Brugia malayi*, *Necator americanus* and *Ancylostoma caninum*) are highly expressed in the infective stage and are considered important pathogenicity factors [30,31,40–42]. In these parasites, SCP/TAPSs are supposed to contribute to their virulence by modulating the host immune response [15,16].

Recently, a SCP/TAPS protein in the plant-parasitic nematode *Globodera rostochiensis* (Gr-VAP1) was shown to function as an effector by interacting with the tomato cysteine protease Rcr3, which is also a target of the Avr2 effector from the fungus *Cladosporium fulvum* [43]. In addition, SCP/TAPS proteins have been identified in other plant infecting nematodes (e.g. *Heterodera glycines*, *Meloidogyne incognita* and *Bursaphelenchus xylophilus*), and these are thought to be required for the establishment of parasitism [44–48]. Considering the expression pattern of some *SCP/TAPS* genes in *M. perniciosa* and the functions ascribed for the encoded proteins in other pathogenic organisms, it is plausible that some MpPR-1s play a role in the *M. perniciosa*-cacao interaction and may be candidate effectors of this fungal pathogen. Accordingly, a recent study that aimed at the identification of putative effectors in *Melampsora larici-populina* and *Puccinia graminis* reported the enrichment of SCP/TAPSs in the predicted secretome of these rust fungi

[49]. A fungal *SCP/TAPS* gene was also identified in EST libraries produced from rye infected with the ascomycete pathogen *Claviceps purpurea* [50], suggesting that these genes might also be important in other plant-fungus interactions.

In recent years, a role for SCP/TAPSs as virulence factors has emerged in many organisms. It is likely that these proteins converged as pathogenicity mechanisms in distinct pathogens/parasites from either plants or animals. Whereas the function of fungal SCP/TAPSs as virulence factors in plant pathogens remains to be confirmed, previous studies demonstrated that these proteins are required for fungal virulence on animals (e.g. *C. albicans* and *F. oxysporum*) [35,36]. The ascomycete *F. oxysporum* is a multi-host pathogen that is able to infect both plants and animals. Previous work by Prados-Rosales *et al.* verified that *fpr1*, one of the six *SCP/TAPS* genes from this pathogen, is required for fungal virulence on animals but not on plants [36]. Given that the *F. oxysporum* genome contains five other *SCP/TAPS* genes, the absence of a phenotype on plants can be explained by the occurrence of functional redundancy in this gene family. Notably, there is evidence that *fpr1* is part of a gene family that has expanded in *F. oxysporum* and in other plant pathogenic Sordariomycetes [36].

Although the precise activity of SCP/TAPSs is currently unknown, Prados-Rosales *et al.* presented the first genetic evidence for a biological function of the proposed active site of SCP/TAPS proteins [36]. The authors demonstrated that the integrity of the active site is required for *F. oxysporum* virulence on animals. In *M. perniciosa*, six MpPR-1s (MpPR-1b, MpPR-1c, MpPR-1d, MpPR-1e, MpPR-1h and MpPR-1j) contain all four amino acids of the proposed active site. In contrast, the other five proteins do not have the complete catalytic tetrad (Fig. 1B). In this regard, it is possible that *M. perniciosa* PR-1s have distinct mode of actions. For instance, whereas those proteins with the complete catalytic tetrad can function as enzymes, the other PR-1s may act as inhibitors.

Concomitantly to the up-regulation of some *MpPR-1* genes *in planta*, we identified a cacao *PR-1* gene over-expressed in the green broom stage of WBD (Fig. S3). Based on these findings, we suggest that some MpPR-1s could act as competitive inhibitors of the plant PR-1, modulating the cacao immune response. It has already been shown that the SCP/TAPS protein *Na*-ASP-2 of the hookworm *Necator americanus* has a high structural similarity to chemokines, and this protein is proposed to be an antagonistic ligand of receptors that activate the immune system of the vertebrate host [51]. Furthermore, NIF (Neutrophil inhibitory factor), a SCP/TAPS protein from *Ancylostoma caninum*, interferes with the host immune system by interacting with neutrophil receptors [32]. Confirmation of this interesting mechanism in the *M. perniciosa*-cacao interaction may be of primary relevance to the understanding of many other plant diseases and will shed light on our understanding of PR-1 functions.

Among the *MpPR-1* genes that are highly expressed *in planta*, *MpPR-1g* is the only one with a C-terminal extension in addition to the SCP/TAPS domain (Fig. 1A and Fig. 3A). This additional region is rich in lysine (K) and glutamic acid (E) residues, which are mostly organized in alternating positions, resulting in the formation of a "KEKE" motif [39] (Fig. 2). This motif is known to mediate protein-protein associations [39,52] and is also able to bind divalent ions, such as calcium and zinc [53]. Calcium is an important regulator of many cellular processes, including plant defense responses [54]. In this regard, this additional module may be important in determining the mode of action of MpPR-1g. Whether this protein interacts with other proteins, particularly cacao proteins, and/or interferes with the plant calcium signaling during infection should be the object of future studies.

Overall, this study presents important evidence on the role of fungal SCP/TAPSs in the context of a plant-pathogen interaction. Although the precise function of each MpPR-1 family member is currently unknown, the information provided in our study suggests they have potential roles in some important biological processes, such as fruiting body metabolism, spore penetration and modulation of the host defense response. As a consequence, our results may inform the study of the role of PR-1-encoding genes in other organisms, particularly phytopathogens. Further studies concerning the *M. perniciosa PR-1* gene family will focus on the characterization of this interesting family in terms of fungal development and roles in the *M. perniciosa* interaction with cacao.

Materials and Methods

Biological material

Isolate CP02 of *Moniliophthora perniciosa* (Stahel) Aime & Phillips-Mora [55], was used to perform the experiments. Under *in vitro* conditions, the fungus can only be maintained as a dikaryotic mycelium, and all other developmental stages (basidiomata, basidiospores and monokaryotic mycelium) are obtained from the dikaryotic stage. The reproductive structures (basidiomata) were produced in laboratory according to the protocol described by Pires *et al.* [8]. Fresh basidiomata were used to collect basidiospores according to Frias *et al.* [56].

Basidiospores suspensions were utilized for the *in vitro* production of the monokaryotic mycelia. For this purpose, approximately 3.75×10^5 basidiospores were inoculated in 125 ml Erlenmeyer flasks containing 50 ml liquid medium (LMCpL+), as described by Meinhardt *et al.* [57]. Liquid cultures were maintained at 28°C and incubated under agitation at 120 rpm. Dikaryotic mycelium was inoculated in the same medium and maintained under the same conditions. Both mycelia were collected 7 days post inoculation to perform the experiments.

Theobroma cacao L. cv. "Comum" was used to perform the infection experiments. Three-months-old plantlets were inoculated with 30 µL of a basidiospore suspension (1×10^5 spores mL^{-1}) according to the procedure described by Frias *et al.* [56]. Plantlets were kept in a greenhouse under controlled conditions of temperature (26°C) and humidity (>80%). Green brooms (biotrophic stage) and dry brooms (necrotrophic stage) were collected 30 and 105 days post inoculation, respectively.

Sequence analysis

Inspection of the *M. perniciosa* genome led to the identification of eleven genes encoding proteins similar to plant pathogenesis-related proteins 1 (PR-1). These genes were named *MpPR-1a* to *MpPR-1k* according to the order they were discovered. The complete open reading frames (ORFs) of these genes were predicted using the program Augustus [58] and confirmed by cDNA sequencing. These sequences have been submitted to GenBank with the accession numbers JN620340 to JN620350. Blast searches were performed using the NCBI-NR and Swissprot databases. Domain prediction of the encoded proteins was performed using the InterProScan server [38] and the presence of a signal peptide for secretion was predicted using the software TargetP 1.1 [37].

Total RNA extraction and cDNA synthesis

With the exception of basidiospores, samples were ground to a fine powder in liquid nitrogen using a pestle and mortar. Basidiospores walls were broken by vortexing the sample in RNA extraction buffer (Buffer RLT, RNeasy Plant Mini Kit) and 200 mg glass beads (0.4–0.6 µm, Sigma-Aldrich, St. Louis, MO,

EUA). RNA isolation was performed using the RNeasy Plant Mini Kit (Qiagen, Valencia, CA, USA) according to the manufacturer's instructions. RNA was treated with DNAse I AmpGrade (Invitrogen, Carlsbad, CA, USA) and its concentration was accessed using the ND-1000 spectrophotometer (NanoDrop, Wilmington, DE, USA). cDNA was synthesized from 1 µg total RNA using the SuperScript II Reverse Transcriptase (Invitrogen), according to the manufacturer's instructions.

Gene expression assays

Quantitative real time PCR (qPCR) was performed on a StepOne Plus Real Time PCR System (Applied Biosystems, Foster City, CA, USA) using Sybr Green I dye for the detection of PCR products. Each reaction contained 8 µl SYBR Green PCR Master Mix (Applied Biosystems), 250 nM each primer and 50 ng cDNA template in a final volume of 16 µl. No-template reactions were included as negative controls for each set of primers used. The thermal cycling conditions were 94°C for 10 min, followed by 40 cycles of 94°C for 15 s, 53°C for 30 s and 60°C for 1 min, with fluorescence detection at the end of each cycle. In addition, a melting curve analysis was performed to verify the amplification of a single product per reaction. All reactions were conducted in technical triplicates using two independent biological replicates of each sample. The *M. perniciosa β-actin* gene was used to normalize data and expression levels are presented as $2^{-\Delta Ct}$. Primers used in this assay are shown in Table S2.

Protein structure modeling

The fold recognition-based method was implemented using the I-TASSER server [59], which constructed structure models for each MpPR-1 protein using folds of the most similar proteins deposited in the PDB (Protein Data Bank) database (http://www.rcsb.org/pdb). The main templates were based on the structure of three proteins: i) Natrin (PDB – 1xta), a component of the venom of the snake *Naja atras*; ii) GAPR-1 (PDB – 1smb), a SCP/TAPS protein associated with the membrane of the human Golgi system; and iii) Ves V5 (PDB – 1qnx), present in the venom of the wasp *Vespula vulgaris*. The modeled structures were validated by analyzing the Ramachandran plots generated by PROCHECK [60], and the models were displayed using the software PyMOL [61].

Supporting Information

Figure S1 Structure of the *MpPR-1* genes. Exons are represented by boxes, while introns are shown as lines. Exons are colored to highlight the regions encoding important protein features: predicted signal peptides (black), SCP/TAPS domain (blue) and the remaining ORF (gray).
(TIF)

Figure S2 Expression levels of *MpPR-1* genes in germinating and non-germinating basidiospores. *MpPR-1f* and *MpPR-1h* are highly expressed in germinating basidiospores, supporting a role for the encoded proteins in the establishment of witches' broom disease. Data are part of the WBD Transcriptome Atlas and were obtained by RNA-seq sequencing. Gene expression values are given in Reads Per Kilobase of exon model per Million mapped reads (RPKM).
(TIF)

Figure S3 Gene expression levels of a cacao *PR-1* (ID CGD0027635) in infected and healthy plants. Similar to some *MpPR-1* genes, a cacao *PR-1* (*TcPR-1*) is up-regulated in the green broom stage of WBD. The analysis was performed by qPCR and the *T. cacao α-tubulin* gene (ID CGD0029727) was used as endogenous control to normalize data. Gene IDs refer to the Cacao Genome Database (http://www.cacaogenomedb.org). The qPCR assay was conducted as described in the Material and Methods section and primers used in the experiment were: TcPR-1_F: 5′ ACCTTATGGCGAGAACCTTG 3′, TcPR-1_R: 5′ GGAGTAATCATAGTCGGCCTTC 3′, TcTub_F: 5′ ACCAATCTTAACCGCCTTGTCT 3′ and TcTub_R: 5′ GTTAGTCTGGAACTCAGTCACAT 3′.
(TIF)

Table S1 Number of *SCP/TAPS* genes in fungal species with different lifestyles. Numbers correspond to the genes coding proteins with the InterPro ID IPR014044.
(DOC)

Table S2 Primers used for quantitative real time PCR analyses of *M. perniciosa* PR-1 genes.
(DOC)

Acknowledgments

We thank Dr. Halley Caixeta de Oliveira (State University of Campinas) for critical reading of the manuscript.

Author Contributions

Conceived and designed the experiments: PJPLT JMCM. Performed the experiments: PJPLT DPTT ROV PFVP OR RMB SFF JMCM . Analyzed the data: PJPLT DPTT ROV JMCM. Contributed reagents/materials/analysis tools: PM. Wrote the paper: PJPLT DPTT JMCM GAGP.

References

1. Meinhardt LW, Rincones J, Bailey BA, Aime MC, Griffith GW, et al. (2008) *Moniliophthora perniciosa*, the causal agent of witches' broom disease of cacao: what's new from this old foe? Mol Plant Pathol 9: 577–588.
2. Purdy LH, Schmidt RA (1996) STATUS OF CACAO WITCHES' BROOM: biology, epidemiology, and management. Annu Rev Phytopathol 34: 573–594.
3. Perfect SE, Green JR (2001) Infection structures of biotrophic and hemibiotrophic fungal plant pathogens. Mol Plant Pathol 2: 101–108.
4. Scarpari LM, Meinhardt LW, Mazzafera P, Pomella AW, Schiavinato MA, et al. (2005) Biochemical changes during the development of witches' broom: the most important disease of cocoa in Brazil caused by *Crinipellis perniciosa*. J Exp Bot 56: 865–877.
5. Garcia O, Macedo JA, Tiburcio R, Zaparoli G, Rincones J, et al. (2007) Characterization of necrosis and ethylene-inducing proteins (NEP) in the basidiomycete *Moniliophthora perniciosa*, the causal agent of witches' broom in *Theobroma cacao*. Mycol Res 111: 443–455.
6. Rincones J, Scarpari LM, Carazzolle MF, Mondego JM, Formighieri EF, et al. (2008) Differential gene expression between the biotrophic-like and saprotrophic mycelia of the witches' broom pathogen *Moniliophthora perniciosa*. Mol Plant Microbe Interact 21: 891–908.
7. Mondego JM, Carazzolle MF, Costa GG, Formighieri EF, Parizzi LP, et al. (2008) A genome survey of *Moniliophthora perniciosa* gives new insights into Witches' Broom Disease of cacao. BMC Genomics 9: 548.
8. Pires AB, Gramacho KP, Silva DC, Goes-Neto A, Silva MM, et al. (2009) Early development of *Moniliophthora perniciosa* basidiomata and developmentally regulated genes. BMC Microbiol 9: 158.
9. Thomazella DP, Teixeira PJ, Oliveira HC, Saviani EE, Rincones J, et al. (2012) The hemibiotrophic cacao pathogen *Moniliophthora perniciosa* depends on a mitochondrial alternative oxidase for biotrophic development. New Phytol 194: 1025–1034.
10. Van Loon LC, Rep M, Pieterse CM (2006) Significance of inducible defense-related proteins in infected plants. Annu Rev Phytopathol 44: 135–162.
11. Rauscher M, Adam AL, Wirtz S, Guggenheim R, Mendgen K, et al. (1999) PR-1 protein inhibits the differentiation of rust infection hyphae in leaves of acquired resistant broad bean. Plant J 19: 625–633.
12. Niderman T, Genetet I, Bruyere T, Gees R, Stintzi A, et al. (1995) Pathogenesis-related PR-1 proteins are antifungal. Isolation and characterization of three 14-kilodalton proteins of tomato and of a basic PR-1 of tobacco with inhibitory activity against *Phytophthora infestans*. Plant Physiol 108: 17–27.

13. Kiba A, Nishihara M, Nakatsuka T, Yamamura S (2007) Pathogenesis-related protein 1 homologue is an antifungal protein in *Wasabia japonica* leaves and confers resistance to *Botrytis cinerea* in transgenic tobacco. PLANT BIOTECHNOLOGY 24: 247–254.
14. Zhu F, Xu M, Wang S, Jia S, Zhang P, et al. (2012) Prokaryotic expression of pathogenesis related protein 1 gene from *Nicotiana benthamiana*: antifungal activity and preparation of its polyclonal antibody. Biotechnol Lett .
15. Cantacessi C, Campbell BE, Visser A, Geldhof P, Nolan MJ, et al. (2009) A portrait of the "SCP/TAPS" proteins of eukaryotes–developing a framework for fundamental research and biotechnological outcomes. Biotechnol Adv 27: 376–388.
16. Gibbs GM, Roelants K, O'Bryan MK (2008) The CAP superfamily: cysteine-rich secretory proteins, antigen 5, and pathogenesis-related 1 proteins–roles in reproduction, cancer, and immune defense. Endocr Rev 29: 865–897.
17. Milne TJ, Abbenante G, Tyndall JD, Halliday J, Lewis RJ (2003) Isolation and characterization of a cone snail protease with homology to CRISP proteins of the pathogenesis-related protein superfamily. J Biol Chem 278: 31105–31110.
18. Fernandez C, Szyperski T, Bruyere T, Ramage P, Mosinger E, et al. (1997) NMR solution structure of the pathogenesis-related protein P14a. J Mol Biol 266: 576–593.
19. Henriksen A, King TP, Mirza O, Monsalve RI, Meno K, et al. (2001) Major venom allergen of yellow jackets, Ves v 5: structural characterization of a pathogenesis-related protein superfamily. Proteins 45: 438–448.
20. Serrano RL, Kuhn A, Hendricks A, Helms JB, Sinning I, et al. (2004) Structural analysis of the human Golgi-associated plant pathogenesis related protein GAPR-1 implicates dimerization as a regulatory mechanism. J Mol Biol 339: 173–183.
21. Guo M, Teng M, Niu L, Liu Q, Huang Q, et al. (2005) Crystal structure of the cysteine-rich secretory protein stecrisp reveals that the cysteine-rich domain has a K^+ channel inhibitor-like fold. J Biol Chem 280: 12405–12412.
22. Shikamoto Y, Suto K, Yamazaki Y, Morita T, Mizuno H (2005) Crystal structure of a CRISP family $Ca2^+$ -channel blocker derived from snake venom. J Mol Biol 350: 735–743.
23. Mizuki N, Sarapata DE, Garcia-Sanz JA, Kasahara M (1992) The mouse male germ cell-specific gene Tpx-1: molecular structure, mode of expression in spermatogenesis, and sequence similarity to two non-mammalian genes. Mamm Genome 3: 274–280.
24. Gibbs GM, Orta G, Reddy T, Koppers AJ, Martinez-Lopez P, et al. (2011) Cysteine-rich secretory protein 4 is an inhibitor of transient receptor potential M8 with a role in establishing sperm function. Proc Natl Acad Sci U S A 108: 7034–7039.
25. Szyperski T, Fernandez C, Mumenthaler C, Wuthrich K (1998) Structure comparison of human glioma pathogenesis-related protein GliPR and the plant pathogenesis-related protein P14a indicates a functional link between the human immune system and a plant defense system. Proc Natl Acad Sci U S A 95: 2262–2266.
26. Lu G, Villalba M, Coscia MR, Hoffman DR, King TP (1993) Sequence analysis and antigenic cross-reactivity of a venom allergen, antigen 5, from hornets, wasps, and yellow jackets. J Immunol 150: 2823–2830.
27. King TP, Spangfort MD (2000) Structure and biology of stinging insect venom allergens. Int Arch Allergy Immunol 123: 99–106.
28. Mochca-Morales J, Martin BM, Possani LD (1990) Isolation and characterization of helothermine, a novel toxin from *Heloderma horridum horridum* (Mexican beaded lizard) venom. Toxicon 28: 299–309.
29. Wang J, Shen B, Guo M, Lou X, Duan Y, et al. (2005) Blocking effect and crystal structure of natrin toxin, a cysteine-rich secretory protein from *Naja atra* venom that targets the BKCa channel. Biochemistry 44: 10145–10152.
30. Hawdon JM, Jones BF, Hoffman DR, Hotez PJ (1996) Cloning and characterization of Ancylostoma-secreted protein. A novel protein associated with the transition to parasitism by infective hookworm larvae. J Biol Chem 271: 6672–6678.
31. Chalmers IW, McArdle AJ, Coulson RM, Wagner MA, Schmid R, et al. (2008) Developmentally regulated expression, alternative splicing and distinct sub-groupings in members of the *Schistosoma mansoni* venom allergen-like (SmVAL) gene family. BMC Genomics 9: 89.
32. Moyle M, Foster DL, McGrath DE, Brown SM, Laroche Y, et al. (1994) A hookworm glycoprotein that inhibits neutrophil function is a ligand of the integrin CD11b/CD18. J Biol Chem 269: 10008–10015.
33. Zúñiga S, Boskovic J, Garcia-Cantalejo JM, Jim nA, Ballesta JP, et al. (1999) Deletion of 24 open reading frames from chromosome XI from *Saccharomyces cerevisiae* and phenotypic analysis of the deletants. Gene 233: 141–150.
34. Schuren FH, Asgeirsdottir SA, Kothe EM, Scheer JM, Wessels JG (1993) The Sc7/Sc14 gene family of *Schizophyllum commune* codes for extracellular proteins specifically expressed during fruit-body formation. J Gen Microbiol 139: 2083–2090.
35. Braun BR, Head WS, Wang MX, Johnson AD (2000) Identification and characterization of TUP1-regulated genes in *Candida albicans*. Genetics 156: 31–44.
36. Prados-Rosales RC, Roldan-Rodriguez R, Serena C, Lopez-Berges MS, Guarro J, et al. (2012) A PR-1-like Protein of *Fusarium oxysporum* Functions in Virulence on Mammalian Hosts. J Biol Chem 287: 21970–21979.
37. Emanuelsson O, Brunak S, von HG, Nielsen H (2007) Locating proteins in the cell using TargetP, SignalP and related tools. Nat Protoc 2: 953–971.
38. Zdobnov EM, Apweiler R (2001) InterProScan–an integration platform for the signature-recognition methods in InterPro. Bioinformatics 17: 847–848.
39. Realini C, Rogers SW, Rechsteiner M (1994) KEKE motifs. Proposed roles in protein-protein association and presentation of peptides by MHC class I receptors. FEBS Lett 348: 109–113.
40. Murray J, Gregory WF, Gomez-Escobar N, Atmadja AK, Maizels RM (2001) Expression and immune recognition of *Brugia malayi* VAL-1, a homologue of vespid venom allergens and Ancylostoma secreted proteins. Mol Biochem Parasitol 118: 89–96.
41. Cantacessi C, Hofmann A, Young ND, Broder U, Hall RS, et al. (2012) Insights into SCP/TAPS Proteins of Liver Flukes Based on Large-Scale Bioinformatic Analyses of Sequence Datasets. PLoS One 7: e31164.
42. Del Valle A, Jones BF, Harrison LM, Chadderdon RC, Cappello M (2003) Isolation and molecular cloning of a secreted hookworm platelet inhibitor from adult *Ancylostoma caninum*. Mol Biochem Parasitol 129: 167–177.
43. Lozano-Torres JL, Wilbers RH, Gawronski P, Boshoven JC, Finkers-Tomczak A, et al. (2012) Dual disease resistance mediated by the immune receptor Cf-2 in tomato requires a common virulence target of a fungus and a nematode. Proc Natl Acad Sci U S A 109: 10119–10124.
44. Gao B, Allen R, Maier T, Davis EL, Baum TJ, et al. (2001) Molecular characterisation and expression of two venom allergen-like protein genes in *Heterodera glycines*. Int J Parasitol 31: 1617–1625.
45. Lozano J, Smant G (2011) Survival of Plant-parasitic Nematodes inside the Host. In: Perry RN, Wharton DA, editors. Molecular and Physiological Basis of Nematode Survival. Oxfordshire: CABI. 28–62.
46. Ding X, Shields J, Allen R, Hussey RS (2000) Molecular cloning and characterisation of a venom allergen Ag5-like cDNA from *Meloidogyne incognita*. Int J Parasitol 30: 77–81.
47. Wang X, Li H, Hu Y, Fu P, Xu J (2007) Molecular cloning and analysis of a new venom allergen-like protein gene from the root-knot nematode *Meloidogyne incognita*. Exp Parasitol 117: 133–140.
48. Kang JS, Koh YH, Moon YS, Lee SH (2012) Molecular properties of a venom allergen-like protein suggest a parasitic function in the pinewood nematode *Bursaphelenchus xylophilus*. Int J Parasitol 42: 63–70.
49. Saunders DG, Win J, Cano LM, Szabo LJ, Kamoun S, et al. (2012) Using hierarchical clustering of secreted protein families to classify and rank candidate effectors of rust fungi. PLoS One 7: e29847.
50. Oeser B, Beaussart F, Haarmann T, Lorenz N, Nathues E, et al. (2009) Expressed sequence tags from the flower pathogen *Claviceps purpurea*. Mol Plant Pathol 10: 665–684.
51. Asojo OA, Goud G, Dhar K, Loukas A, Zhan B, et al. (2005) X-ray structure of Na-ASP-2, a pathogenesis-related-1 protein from the nematode parasite, *Necator americanus*, and a vaccine antigen for human hookworm infection. J Mol Biol 346: 801–814.
52. Kobayashi YM, Alseikhan BA, Jones LR (2000) Localization and characterization of the calsequestrin-binding domain of triadin 1. Evidence for a charged beta-strand in mediating the protein-protein interaction. J Biol Chem 275: 17639–17646.
53. Realini C, Rechsteiner M (1995) A proteasome activator subunit binds calcium. J Biol Chem 270: 29664–29667.
54. Reddy AS, Ali GS, Celesnik H, Day IS (2011) Coping with stresses: roles of calcium- and calcium/calmodulin-regulated gene expression. Plant Cell 23: 2010–2032.
55. Aime MC, Phillips-Mora W (2005) The causal agents of witches' broom and frosty pod rot of cacao (chocolate, *Theobroma cacao*) form a new lineage of Marasmiaceae. Mycologia 97: 1012–1022.
56. Frias GA, Purdy LH, Schimidt RA (1995) An inoculation method for evaluating resistance of cacao to *Crinipellis perniciosa*. Plant Disease 79: 787–791.
57. Meinhardt LW, Bellato CM, Rincones J, Azevedo RA, Cascardo JC, et al. (2006) *In vitro* production of biotrophic-like cultures of *Crinipellis perniciosa*, the causal agent of witches' broom disease of *Theobroma cacao*. Curr Microbiol 52: 191–196.
58. Stanke M, Steinkamp R, Waack S, Morgenstern B (2004) AUGUSTUS: a web server for gene finding in eukaryotes. Nucleic Acids Res 32: W309–W312.
59. Roy A, Kucukural A, Zhang Y (2010) I-TASSER: a unified platform for automated protein structure and function prediction. Nat Protoc 5: 725–738.
60. Laskowski RA, MacArthur MW, Moss DS, Thornton JM (1993) Procheck – A Program to Check the Stereochemical Quality of Protein Structures. Journal of Applied Crystallography 26: 283–291.
61. DeLano WL (2002) The PyMOL Molecular Graphics System. http://www.pymol.org.
62. Robinson JT, Thorvaldsdottir H, Winckler W, Guttman M, Lander ES, et al. (2011) Integrative genomics viewer. Nat Biotechnol 29: 24–26.

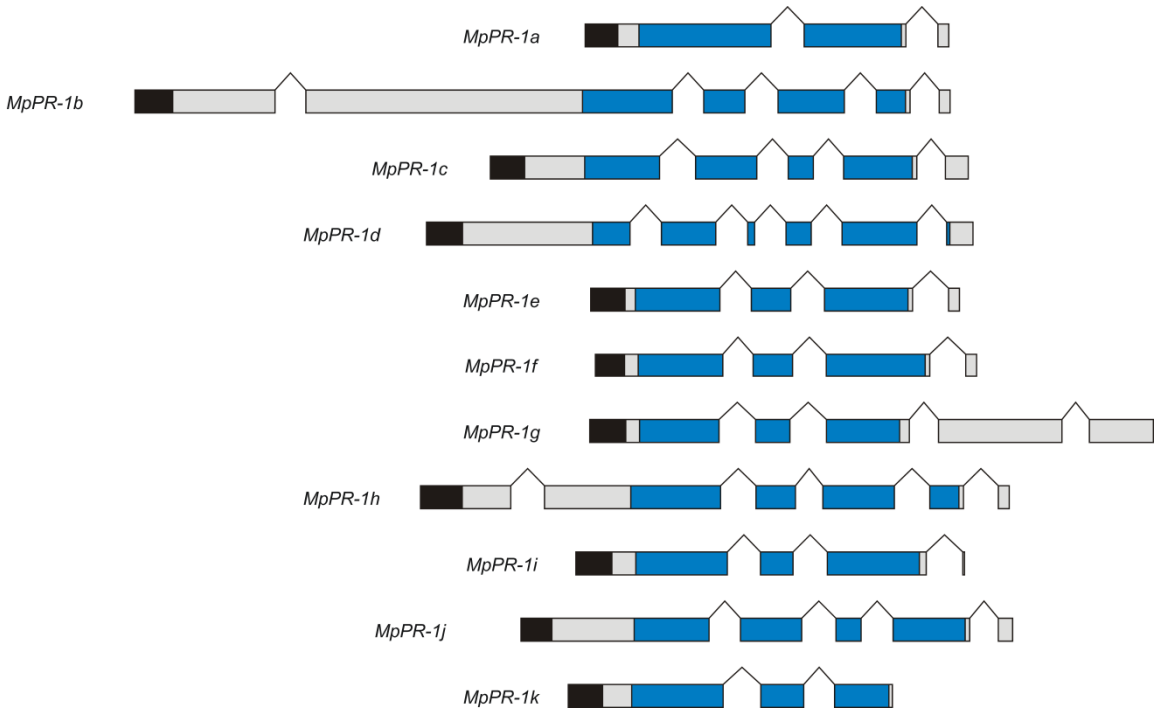

Supplemental Figure 1. Structure of the *MpPR-1* genes. Exons are represented by boxes, while introns are shown as lines. Exons are colored to highlight the regions encoding important protein features: predicted signal peptides (black), SCP/TAPS domain (blue) and the remaining ORF (gray).

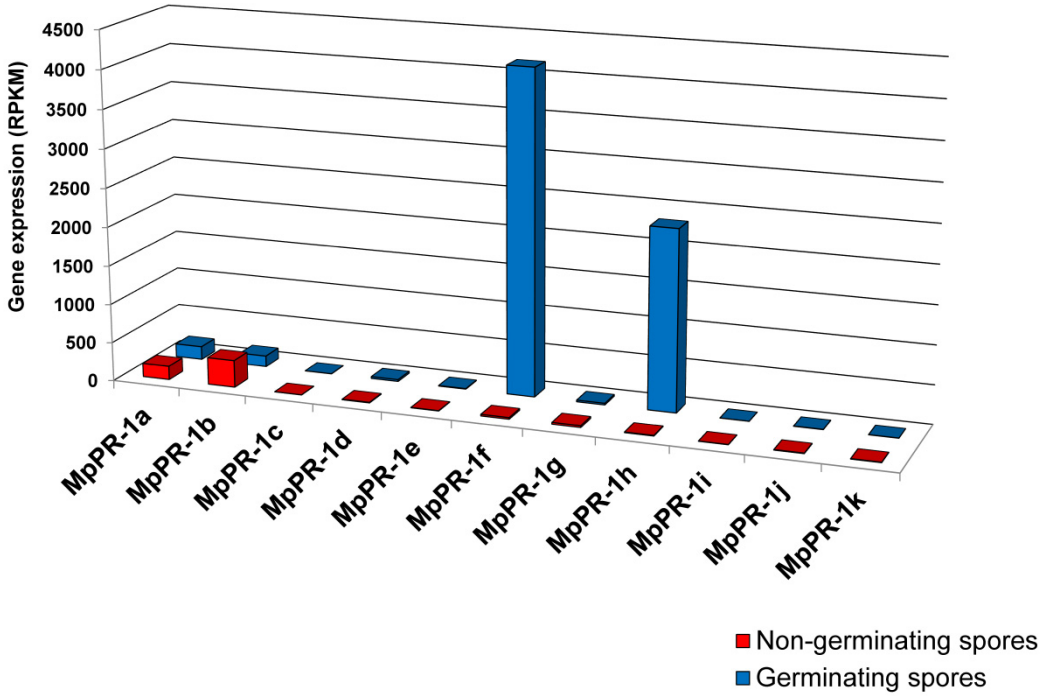

Supplemental Figure 2. Expression levels of *MpPR-1* genes in germinating and non-germinating basidiospores. *MpPR-1f* and *MpPR-1h* are highly expressed in germinating basidiospores, supporting a role for the encoded proteins in the establishment of witches' broom disease. Data are part of the WBD Transcriptome Atlas and were obtained by RNA-seq sequencing. Gene expression values are given in Reads Per Kilobase of exon model per Million mapped reads (RPKM).

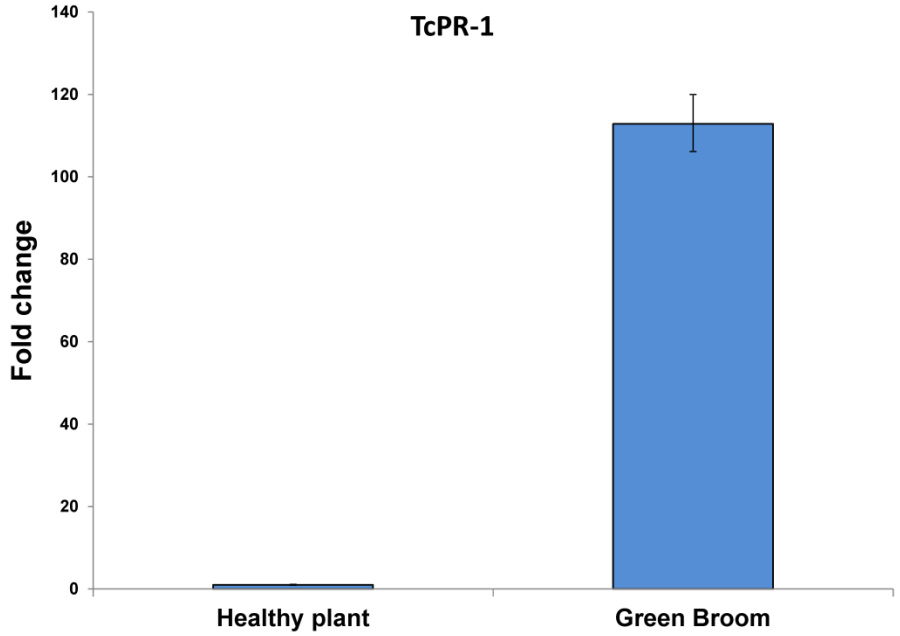

Supplemental Figure 3. Gene expression levels of a cacao *PR-1* (ID CGD0027635) in infected and healthy plants. Similar to some *MpPR-1* genes, a cacao *PR-1* (*TcPR-1*) is up-regulated in the green broom stage of WBD. The analysis was performed by qPCR and the *T. cacao α-tubulin* gene (ID CGD0029727) was used as endogenous control to normalize data. Gene IDs refer to the Cacao Genome Database (http://www.cacaogenomedb.org). The qPCR assay was conducted as described in the Material and Methods section and primers used in the experiment were: TcPR-1_F: 5` ACCTTATGGCGAGAACCTTG 3`, TcPR-1_R: 5` GGAGTAATCATAGTCGGCCTTC 3`, TcTub_F: 5` ACCAATCTTAACCGCCTTGTCT 3` and TcTub_R: 5` GTTAGTCTGGAACTCAGTCACAT 3`.

Supplemental Table 1. Number of *SCP/TAPS* genes in fungal species with different lifestyles. Numbers correspond to the genes coding proteins with the InterPro ID IPR014044.

Fungal species	SCP/TAPS genes	Lifestyle
Botrytis cinerea[1]	5	Necrotrophic pathogen (Ascomycete)
Sclerotinia sclerotiorum[1]	3	Necrotrophic pathogen (Ascomycete)
Fusarium graminearum[1]	5	Hemibiotrophic pathogen (Ascomycete)
Magnaporthe oryzae[1]	7	Hemibiotrophic pathogen (Ascomycete)
Ustilago maydis[1]	2	Biotrophic pathogen (Basidiomycete)
Melampsora larici-populina[2]	10	Biotrophic pathogen (Basidiomycete)
Puccinia graminis[1]	7	Biotrophic pathogen (Basidiomycete)
Phanerochaete chrysosporium[2]	2	Saprotrophic (Basidiomycete)
Postia placenta[2]	1	Saprotrophic (Basidiomycete)
Schizophyllum commune[2]	5	Saprotrophic (Basidiomycete)
Serpula lacrymans[2]	2	Saprotrophic (Basidiomycete)
Coprinopsis cinerea[1]	2	Saprotrophic (Basidiomycete)
Laccaria bicolor[2]	9	Ectomycorrhizal (Basidiomycete)
Moniliophthora perniciosa	11	Hemibiotrophic pathogen (Basidiomycete)

[1] Data from genomes sequenced by the Broad Institute of Harvard and MIT (http://www.broadinstitute.org/)
[2] Data from genomes sequenced by the Department of Energy Joint Genome Institute (http://www.jgi.doe.gov/)

Supplemental Table 2. Primers used for quantitative real time PCR analyses of *M. perniciosa PR-1* genes.

Gene name	Forward primer	Reverse primer
β-actin	5' CCCTTCTATCGTCGGTCGT 3'	5` AGGATACCACGCTTGGATTG 3'
MpPR-1a	5` AGTTGAAAGGCTCAGATGGAT 3`	5` AGTGATTATAGGCGGGATTGG 3`
MpPR-1b	5` TAGCGACAGTTATTCCATTTCC 3`	5` GACTTGAGTTGTGGCTTTCC 3`
MpPR-1c	5` CAAACACACAGAACCGACT 3`	5` GTGGGTTACTGTGTTCATACA 3`
MpPR-1d	5` CACTCAAGTTGTCTGGAAGAG 3`	5` CTGGTAACTTTGCTGGACG 3`
MpPR-1e	5' CCGAGCCTTTGACCTGGA 3'	5' CCCAAGTTCTGTAGTGGATTTCC 3'
MpPR-1f	5' ACCAGTGCAACTTCCAGACTTC 3'	5' CACACGATTTGGGTCCAGC 3'
MpPR-1g	5' CTAAGCAATGTCAACTCGAGGC 3'	5' CCCAACACTTCTGGTTGACTTG 3'
MpPR-1h	5' CCGCGGTTCAGCTATGGC 3'	5' CACGTGGAGCGTAGTGGG 3'
MpPR-1i	5' CGCAGCTTTGGGGCGATA 3'	5' GGTAGCTTCACCACATCCAAC 3'
MpPR-1j	5` GCCAGTTTGAGCACAGTGACC 3`	5` AGTTGGAAAAATGTGGGTCGTCA 3`
MpPR-1k	5` CGATAGGTCTACAGGGTGATTTC 3`	5` AGAACTATCCCCGCTTGAATAC 3`

Capítulo V

Novel Receptor-like kinases in cacao contain PR-1 extracellular domains

Paulo José P.L. Teixeira, Gustavo G.L. Costa, Gabriel L. Fiorin, Gonçalo A.G. Pereira, Jorge M.C. Mondego

Trabalho aceito para publicação na revista *Molecular Plant Pathology.*

APRESENTAÇÃO

Uma primeira linha de defesa em plantas pode ser ativada pelo reconhecimento de moléculas conservadas em microrganismos denominadas MAMPs (*Microbe-Associated Molecular Patterns*). Uma das classes de receptores que participam do reconhecimento de MAMPs é formada por proteínas transmembrana que possuem um domínio quinase citoplasmático e um domínio variável extracelular, sendo denominadas RLKs (*receptor-like kinases*). Enquanto o domínio quinase das RLKs realiza a transdução de sinais dentro da célula, o domínio extracelular é responsável por determinar a natureza da molécula reconhecida pelo receptor. Assim, RLKs são normalmente classificadas em dezenas de grupos com base neste domínio extracelular. Notavelmente, a análise do genoma do cacaueiro revelou a existência de uma nova classe de RLKs contendo proteínas PR-1 na região extracelular. PR-1s são proteínas secretadas por plantas em resposta ao ataque de patógenos, nunca tendo sido caracterizadas como receptores anteriormente. Por este motivo, decidimos realizar uma análise mais detalhada dos dois genes PR-1 quinases (PR-1RKs) identificados no genoma do cacaueiro. A inspeção do Atlas Transcriptômico da Vassoura de Bruxa revelou que um destes genes é induzido em resposta à infecção por *M. perniciosa*, sugerindo um possível papel no sistema imune do hospedeiro. Este *short communication* apresenta hipóteses quanto à origem e função destas proteínas PR-1RK, marcando o início de um projeto que visa à caracterização destes novos receptores do cacaueiro.

Novel Receptor-Like Kinases in Cacao Contain PR-1 Extracellular Domains

Paulo José Pereira Lima Teixeira[1], Gustavo Gilson Lacerda Costa[1], Gabriel Lorencini Fiorin[1], Gonçalo Amarante Guimarães Pereira[1], Jorge Maurício Costa Mondego[2,#]

[1] Laboratório de Genômica e Expressão, Departamento de Genética, Evolução e Bioagentes, Instituto de Biologia, Universidade Estadual de Campinas (Unicamp), CP 6109, Campinas, SP,13083-970, Brazil
[2] Centro de Pesquisa e Desenvolvimento em Recursos Genéticos Vegetais, Instituto Agronômico de Campinas (IAC), Campinas, SP, 13075-630, Brazil

[#] Corresponding author: Jorge Maurício Costa Mondego
Address: Avenida Theodureto de Almeida Camargo, 1500. Fazenda Santa Elisa. Instituto Agronômico de Campinas. Campinas, SP, 13075-630, Brazil
E-mail: jmcmondego@gmail.com, jmcmondego@iac.sp.gov.br; Phone: 55-19-3202-1798

Running Title: PR-1 Receptor-Like Kinases in Cacao
Keywords: receptor-Like kinases, PR-1 proteins, cacao, plant defense, witches' broom disease, *Moniliophthora perniciosa*

SUMMARY

Members of the pathogenesis-related protein 1 (PR-1) family are well-known markers of plant defense responses, forming part of the arsenal of secreted proteins produced upon pathogen recognition. Here, we report the identification of two cacao (*Theobroma cacao* L.) PR-1s that are fused to transmembrane regions and serine/threonine kinase domains, in a manner characteristic of receptor-like kinases (RLKs). These proteins (TcPR-1f and TcPR-1g) were named PR-1 receptor kinases (PR-1RKs). Phylogenetic analysis of RLKs and PR-1 proteins from cacao indicated that PR-1RKs originated from a fusion between sequences encoding PR-1 and the kinase domain of a LecRLK (Lectin Receptor-like Kinase). Retrotransposition marks surround *TcPR-1f*, suggesting that retrotransposition was involved in the origin of PR-1RKs. Genes with a similar domain architecture to cacao PR-1RKs were found in rice (*Oryza sativa*), barrel medic (*Medicago truncatula*) and a non-phototrophic bacterium (*Herpetosiphon aurantiacus).* However, their kinase domains differed from those found in LecRLKs, indicating the occurrence of convergent evolution. *TcPR-1g* expression was up-regulated in the biotrophic stage of witches' broom disease, suggesting a role for PR-1RKs during cacao defense responses. We hypothesize that PR-1RKs transduce a defense signal by interacting with a PR-1 ligand.

Pathogenesis-related (PR) proteins are produced by plants during pathogen infection. Members of the PR-1 family are well-known markers of plant defense responses (Van Loon *et al.*, 2006) and some of these have been found to inhibit the development of fungi and oomycetes *in vitro* (Niderman *et al*., 1995; Rauscher *et al*., 1999). Although these proteins are widely recognized as components of the plant defense system, their function has not been well defined. PR-1 proteins are part of the SCP/TAPS superfamily (Sperm-Coating Protein/Tpx-1-Ag5-PR-1-Sc7), which consists of proteins from a wide phylogenetic spectrum involved in defense responses, pathogenesis and reproduction (Cantacessi *et al*., 2009; Gibbs *et al*., 2008). In addition to a conserved SCP/TAPS domain, many proteins from the SCP/TAPS superfamily contain C-terminal extensions that have functional domains (Gibbs *et al*., 2008). Curiously, the plant PR-1 proteins experimentally characterized to date contain only the SCP/TAPS domain, and lack any C-terminal domain extension.

Cacao (*Theobroma cacao* L.) is one of the most economically important perennial crops in the world, producing the main feedstock for the chocolate industry (Afoakwa *et al*., 2008). However, cacao production is severely hindered by diseases caused by fungi and oomycetes (Evans *et al*., 2007). Hence, the study of proteins associated with plant immunity can provide clues for the development of strategies to control pathogen infection in cacao plantations. Based on evidence that *PR-1* genes are related to defense responses in plants (Van Loon *et al.*, 2006), we searched for these genes in the cacao genome. First, we used the sequence of the tomato PR-1 protein P14 (Fernández *et al*., 1997; GenBank P04284) as bait in a tBLASTn search of the Cacao Genome Database (http://www.cacaogenomedb.org), a consortium from MARS/USDA-ARS that sequenced the Matina 1-6 genotype. Matina 1-6 is representative of the Forastero genetic background most commonly found in cacao producing countries. Thirteen genes with significant sequence similarity (BlastP positives > 55%; E-value < 1e- 25) to P14 were identified in the Matina 1-6 cacao genome (Table 1). We named these genes *TcPR-1a* to *TcPR-1m*. Consistent with Blast analyses, a search for members of the SCP/TAPS family (InterPro IPR001283) using the InterProScan server

(Quevillon *et al.,* 2005; http://www.ebi.ac.uk/Tools/pfa/iprscan) also revealed the existence of thirteen protein models in cacao. The InterPro analysis also revealed that the thirteen PR-1 proteins from *T. cacao* have predicted hydrophobic signal peptides, indicating that these proteins are potentially directed to the secretory pathway. Additionally, all of these proteins contain complete SCP/TAPS domains. Strikingly, two TcPR-1s (TcPR-1f and TcPR-1g) contain extensions in the C-terminal portion that are similar to a serine/threonine kinase domain (S-TKc; InterPro IPR000719; Figure 1A). Both TcPR-1f and TcPR-1g contain a stretch of 23 hydrophobic amino acids that form a membrane-spanning helix between the SCP/TAPS and S-TKc domains, strongly suggesting that these proteins are anchored in a cell membrane (Figure 1A). To determine the cellular localization of these proteins, we performed an *in silico* analysis using the PSORT program (Nakai and Horton, 1999). As expected, these two proteins localized to the plasma membrane. Such protein architecture (i.e., an extracellular region, a hydrophobic stretch, and a kinase domain) is characteristic of receptor-like kinases (RLKs).

Table 1. : Characteristics of the thirteen PR-1 gene models found in *T. cacao*.

TcPR-1	Gene ID*	Chromosome	Putative protein size (aa)	Putative coding sequence size (bp)
TcPR-1a	CGD0027643	7	159	477
TcPR-1b	CGD0027642	7	156	468
TcPR-1c	CGD0027635	7	162	486
TcPR-1d	CGD0027628	7	164	492
TcPR-1e	CGD0027640	7	165	495
TcPR-1f	CGD0008870	2	619	1857
TcPR-1g	CGD0006833	10	582	1746
TcPR-1h	CGD0021343	5	173	519
TcPR-1i	CGD0021746	5	236	708
TcPR-1j	CGD0031974	9	185	555
TcPR-1k	CGD0013072	**	195	585
TcPR-1l	CGD0000407	1	177	531
TcPR-1m	CGD0027644	7	159	477

* Gene IDs according to the Cacao Genome Database (v0.9 - http://www.cacaogenomedb.org)

** This gene model was mapped in a *T. cacao* supercontig (super_217) that was not assembled in any cacao chromosome.

RLKs are a large group of transmembrane receptors that perceive extracellular signals, which are transduced via phosphorylation activation and lead to intracellular responses (Walker, 1994). RLKs are one of the largest gene families in plants. For instance, the Arabidopsis genome encodes approximately 600 RLKs, whereas more than 1100 RLK genes are present in the rice genome (Dardick *et al.,* 2007; Gish and Clark, 2011; Morillo and Tax, 2006; Shiu and Bleecker, 2001; Shiu and Bleecker, 2003; Shiu *et al*., 2004). RLKs have been organized into different structural classes, based on the identity of their extracellular domain and on phylogenetic relationships of their kinase domain (Shiu and Bleecker, 2001). These receptors underwent tremendous expansion and diversification, mostly in their extracellular domains, indicating the necessity of variation in the extracellular binding domains for the recognition of a vast range of ligands (Shiu and Bleecker, 2003; Lehti-Shiu *et al*., 2009), which can be brassinosteroids (Wang *et al*., 2001), polysaccharides such as chitin (Miya *et al*., 2007), or peptides such as CLAVATA 3 (Trotochaud *et al*., 2000), flagellin (Gomez-Gomez and Boller, 2000; Zipfel *et al*., 2004) and the bacterial elongation factor EF-Tu (Zipfel *et al*., 2006).

Many RLKs are involved in developmental processes in plants, such as floral organ abscission (HAESA, Jinn *et al*., 2000) and reproduction (FERONIA; Escobar-Restrepo *et al*., 2007). Other RLKs are part of the defensive arsenal against pathogens (Afzal *et al*., 2008; Greeff *et al*., 2012; Torii *et al.,* 2004). RLKs involved in plant immunity are so-called pattern-recognition receptors (PRRs). They detect microbe or pathogen associated molecular patterns (MAMPs/PAMPs) and, upon binding of their cognate ligands, set off defense responses (Boller and Felix, 2009; Greeff *et al*., 2012; Monaghan and Zipfel, 2012). Some reports show that loss of function of RLKs enhances susceptibility to pathogens (Chen *et al*., 2006; Wan *et al.,* 2008; Zipfel *et al*., 2004), attesting to their role as plant immune receptors. However, ligands have been identified for only a few RLK-PRRs: FLS2 (Zipfel *et al*., 2004), Xa21 (Lee *et al*., 2009), EFR (Zipfel *et al*., 2006), and CERK1 (Miya *et al*., 2009). Molecules such as chitin (Kaku *et al*., 2006) and peptidoglycan (Liu *et al*., 2012; Willmann *et al*., 2011) were shown to interact with Receptor-like

proteins (RLPs), which are transmembrane receptors that lack a kinase domain (Wang *et al*., 2008).

To confirm the protein models of cacao PR-1 RLKs (hereafter referred to as PR-1RK), we designed oligonucleotides based on the sequences of the N- and C-terminals of TcPR-1f and TcPR-1g and used as templates genomic DNA and cDNA isolated from plantlets of cv. Comum, an Amazonic variety of the Forastero group of cacao (Vello and Garcia, 1971) that is very similar to the Matina 1-6 cultivar (Soria, 1966). A comparison of the genomic and cDNA amplifications revealed that *TcPR-1RKs* contain no introns spanning their coding sequences.

We examined the TcPR-1f and TcPR-1g protein sequences for features of serine threonine kinases. The cytoplasmic region of both proteins contains the eleven kinase subdomains typical of serine/threonine kinases described by Walker (1994), including the subdomain I (ATP-binding site; consensus GXGXXG), and subdomains VIb (consensus DxKxxN) and VIII (consensus GTxxYxAPE), which potentially discriminate serine/threonine kinases from tyrosine kinases (Figure 1A). Thus, both proteins are candidate serine/threonine kinases. However, some plant RLKs that were predicted to be Ser/Thr kinases (e.g. BAK1 and BRI1) have been shown to be dual-specificity kinases (Oh *et. al*., 2010; Oh *et. al*., 2011). In this context, functional assays are necessary to confirm the specificity of the cacao PR-1RK kinase domains.

In addition, both PR-1RKs can be classified as RD kinases, because they contain an arginine (R) residue preceding the core catalytic aspartate (D) residue in subdomain VIb (Johnson *et al*., 1996; Figure 1A). Although most kinases involved in microbial detection are non-RD kinases (lacking the arginine residue before the catalytic aspartate), RD kinases such as ERECTA (Godiard *et al*., 2003), WAKL22 (Diener *et al*., 2005), and especially BAK1 (Chinchilla *et al*., 2007; Heese *et al*., 2007; Roux *et al*., 2011), have been found to contribute to pathogen resistance.

To investigate the origin of cacao PR-1RK proteins, we searched for RLKs in the Cacao Genome Database (http://www.cacaogenomedb.org). For this, we used the InterProScan server to identify cacao proteins containing a kinase domain (IPR000719) and one of the InterPro domains

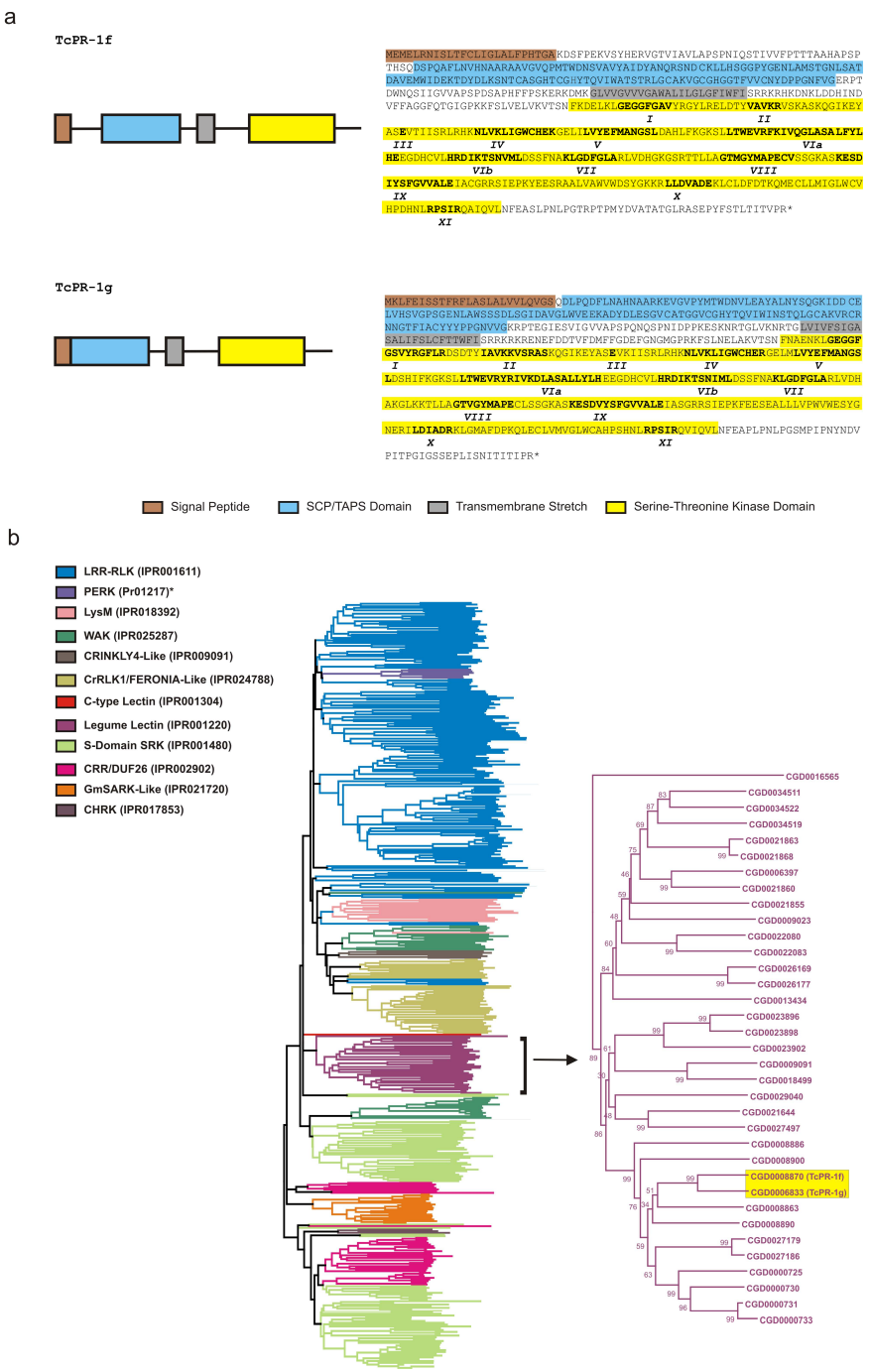

Figure 1. PR-1RK kinase domain signature and cacao RLKs phylogenetic tree. A - Domain organization and protein kinase signatures of TcPR-1RK proteins. The signal peptide (SP) is indicated in brown; the hydrophobic transmembrane region (TM) in gray; and SCP/TAPS (PR-1-like) and serine/threonine kinase domains in blue and yellow, respectively. The eleven (I-XI) typical motifs of protein kinases are indicated below the amino acids depicted in bold. B - Phylogenetic analysis of RLKs from cacao. The branches of the phylogenetic tree are colored according to the identity of the extracellular domains of RLKs as predicted by InterProScan software (left legend). The right panel depicts an expanded view of the legume lectin (LecRLKs) clade. The yellow box depicts PR-1RK proteins clustered together with LecRLKs. The tree was constructed as a consensus of 10000 bootstrap replicates, using Neighbor-Joining and dist-P parameters. Bootstrap values are shown in the tree. *PR01217 is a PRINTs database domain corresponding to the former InterPro domain IPR002965, which was removed from the database.

commonly found in the extracellular region of plant RLKs (Figure 1B). For example, CHRK (Chitinase receptor kinases) receptors contain kinase (IPR000719) and glycoside hydrolase (IPR017853) domains. Based on this analysis, we found that cacao has at least 480 putative RLKs. We then extracted the kinase domain sequences of these proteins and aligned them using Clustal Omega (Sievers *et al*., 2011). The weighing matrix used was BLOSUM62 and the alignments generated were manually adjusted following the subdomain signatures of eukaryotic kinases. Next, we used MEGA5 (Tamura *et al*., 2011) to generate a phylogenetic tree by means of the Neighbor-Joining Method with 10000 bootstrap replicates (Figure 1B). Distance-p and complete deletion parameters were applied. To classify the cacao sequences into RLK subfamilies, each tree leaf node was annotated according to previous studies (Lehti-Shiu *et al*., 2009; Shiu and Bleecker, 2003). Curiously, no cacao protein was similar to the RLK containing a thaumatin extracellular domain. TcPR-1f and TcPR-1g fit into the legume lectin (LecRLK) clade (Figure 1B), suggesting that PR-1RKs arose from these receptor-like kinases.

We also inspected the position of PR-1RK genes in the genome of cacao Matina 1-6. *TcPR-1f* is located on chromosome 2. By examining the genomic location of this gene, we identified four C-Type LecRLKs in its vicinity; three downstream and one upstream of the gene (Figure 2A). Interestingly, the LecRLK genes forming this cluster are phylogenetically close to PR-1RKs (Figure 1B). These LecRLKs share 65-70% sequence identity with both TcPR-1f and TcPR1-g (Figure 2A). The genomic proximity of LecRLKs with a PR-1RK reinforces the notion that PR-1RKs may have originated from these receptor-like kinases. *TcPR-1g* is located on chromosome 10. In contrast to *TcPR-1f*, no RLKs were found close to this gene, which is surrounded by genes encoding an N-acetylglucosaminidase and a LOB domain-containing protein.

We also verified the location of the eleven secreted PR-1 proteins in the cacao genome. Five of these occur in a cluster on chromosome 7 (Table 1; Figure 2A). An alignment of the SCP/TAPS domain of TcPR-1 proteins was used to construct a bootstrap consensus tree inferred from 1000 replicates. This analysis indicated that TcPR-1f and TcPR-1g are part of a clade

containing proteins of the PR-1 cluster on chromosome 7 (Figure 2B). The PR-1 domain of TcPR-1f shares approximately 60-70% sequence identity with PR-1 genes positioned in tandem on chromosome 7. This result suggests that genes similar to those forming the TcPR-1 cluster fused with a kinase domain of a LecRLK, giving rise to PR-1RKs.

The formation of new chimeric proteins has been related to molecular mechanisms such as exon shuffling, gene duplication, retrotransposition, or combinations of these (Jones *et al*., 2005; Long *et al.*, 2003; Nisole *et al.*, 2004; Wang *et al.,* 2006). Therefore, we searched for retrotransposition marks in both LecRLK and PR-1 clusters, using RepeatMasker (Smit *et al*., unpublished data) and REPbase tools (Jurka, 1998). We identified a region of 770 bp that was similar to the LTR Copia-like retrotransposon in the LecRLK cluster (Figure 2A). Additionally, we detected a pair of inverted repeats that flanks the most upstream LecRLK in the cluster and a tandem repeat region of approximately 3800 bp (Figure 2A). Curiously, the *TcPR-1f* PR-1 domain is flanked by direct repeats, which have been associated with transposon insertion sites (Warren *et al*., 1997). We did not find evidence of transposition events in the PR-1 cluster or close to *TcPR-1g*. The presence of retrotransposition marks and repetitive elements around *TcPR-1f* suggests that transposition mechanisms could be involved in the origin of PR-1RKs.

To evaluate whether other plant species contain proteins with domain architecture similar to the cacao PR-1RKs, we conducted a search in the Entrez Protein Database using CDART (Geer *et al*., 2002). Two proteins from the *Oryza sativa* Japonica group (EEE56976; NP_001172960) and one from the Indica group (EAY85816) have a domain structure similar to that of PR-1RKs, but contain two SCP/TAPS domains instead of one. Curiously, one protein from the legume barrel medic (*Medicago truncatula*; XP_003608315) and one from the non-phototrophic predatory bacterium *Herpetosiphon aurantiacus* (YP_001547555) contain an inverse arrangement of PR-1RK domains, having an N-terminal kinase domain followed by a C-terminal SCP/TAPS domain.

To establish if fusions of rice and *M. truncatula* PR-1RKs also occurred between PR-1-like proteins and LecRLKs, we performed Blast analyses using the kinase domains of these proteins.

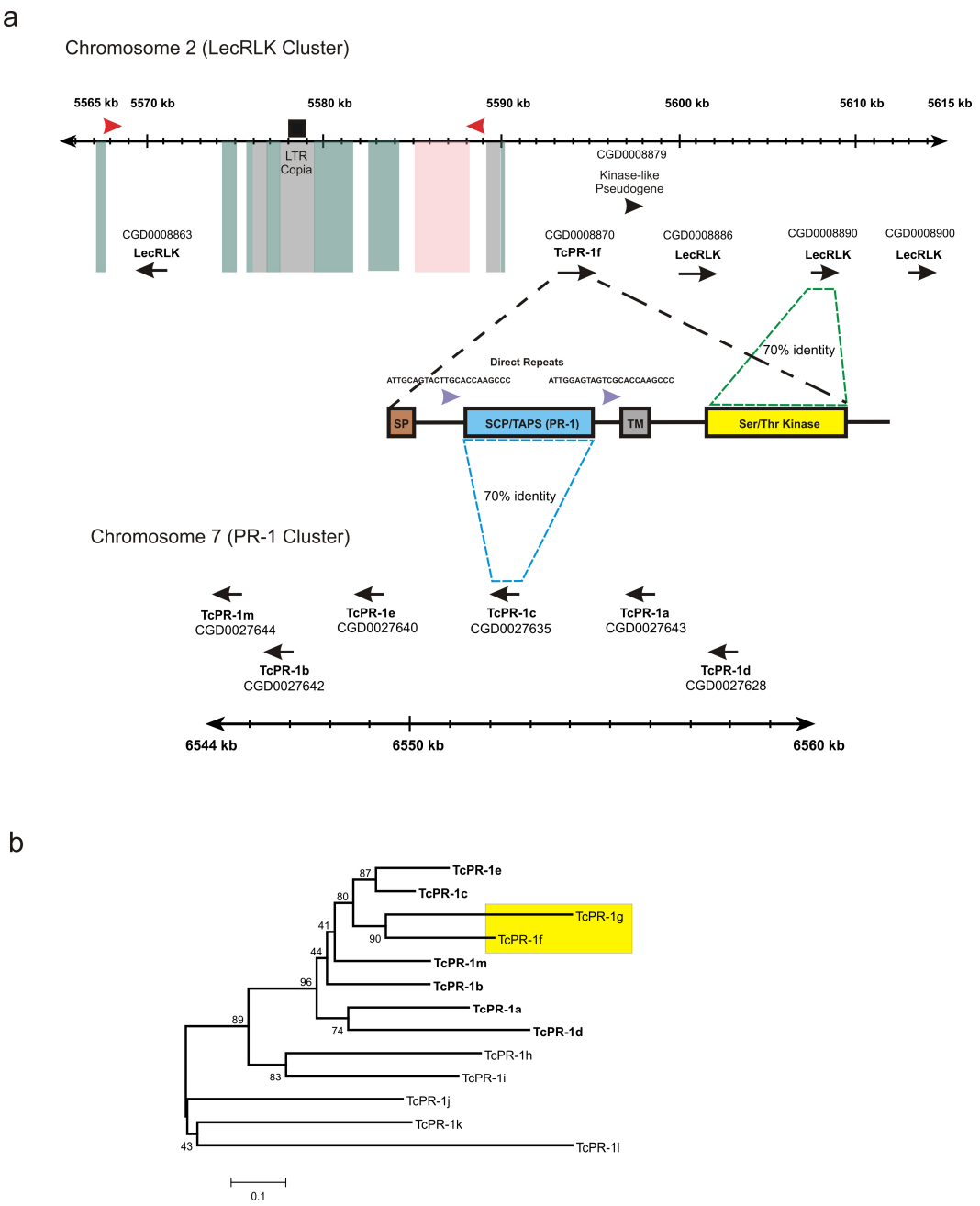

Figure 2. LecRLK and TcPR-1 clusters in the cacao genome and the proposed origin of PR-1RKs.
A - *TcPR-1f* is located in a cluster of LecRLKs on chromosome 2 of cacao. The *TcPR-1f* kinase domain shares a high level of sequence identity with kinase domains of the LecRLKs located in this cluster (i.e., CGD000890; green dashed line). On the other hand, the PR-1 domain of *TcPR-1f* shares a high level of sequence identity with genes present in a PR-1 cluster on *T. cacao* chromosome 7 (i.e., *TcPR-1c*; blue dashed line). The LecRLK cluster has signatures commonly associated with transposition events: black box - long terminal repeat (LTR) of Copia-like retrotransposon; dark gray shading - repetitive regions with at least 300 copies in the cacao genome; dark green shading - sequencing gaps; red arrowheads - inverted repeats; rose shading - tandem repeat region; lilac arrowheads: direct repeats flanking the SCP/TAPS (PR-1) domain of *TcPR-1f*. B - Phylogenetic analysis of cacao PR-1 proteins. Members that form the PR-1 cluster are depicted in bold. Notice the location of PR-1RKs (TcPR-1f and TcPR-1g; yellow box) in the clade of PR-1 cluster genes. The tree was constructed as a consensus of 5000 bootstrap replicates, using Neighbor-Joining and dist-P parameters. Bootstrap values are shown in the tree.

All hits from rice and *M. truncatula* PR-1RKs were similar to the CRR-RLK and LRR-RLK subfamilies, respectively. The presence of PR-1RKs in rice with kinase domains similar to CRR-RLKs was previously reported (Shiu *et al*., 2004). These results indicate that PR-1RKs originated from independent events of fusion between PR-1 and kinase domains in different plant species, representing a rare example of convergent evolution of domain architectures (Gough, 2005).

Based on evidence that both PR-1 proteins and RLKs are involved in plant defense responses, we decided to evaluate the transcription of *TcPR-1RK* genes through RNA-seq data derived from the witches' broom disease (WBD) Transcriptome Atlas (Teixeira *et al*., unpublished data). WBD, a severe phytopathological problem in the Americas, is caused by the hemibiotrophic basidiomycete *Moniliophthora perniciosa* (Stahel) (Aime and Philips-Mora, 2005; Meinhardt *et al*., 2008; Purdy and Schimdt, 1996). The infection experiments were performed using cacao seedlings of the variety 'Comum' grown for approximately three months in a greenhouse under controlled conditions of temperature (26ºC) and humidity (>80%), and a photoperiod of 12 h. Apical meristems of five plantlets were infected with 30 µL of a *M. perniciosa* basidiospore suspension (10^5 spores mL^{-1}), according to Frias *et al.* (1995). Infected tissues were collected 30 days after inoculation, representing the green broom stage of WBD. Green brooms are hyperplastic cacao stems colonized by the biotrophic mycelia of *M. perniciosa* (Meinhardt *et al*., 2008). Five biological replicates were utilized in this experiment and non-infected plants were used as controls. The inspection of the RNA-seq data revealed that *TcPR-1g* is up-regulated in infected plants ($p<0.001$), whereas *TcPR-1f* is only expressed at low levels in the conditions analyzed (Figure 3). The up-regulation of *TcPR-1g* expression during the green broom stage may indicate a role for this novel receptor in defense responses against pathogens. The *TcPR-1g* expression profile fits the 'Receptor Swarm Hypothesis' (Lehti-Shiu *et al*., 2009), which posits that the expression of RLKs increases after pathogen perception in compatible interactions.

It seems reasonable to speculate that the extracellular domain of PR-1RKs binds to the same ligands as secreted PR-1s. However, the precise function and identity of these putative

ligands of plant PR-1 proteins remain elusive. Because PR-1s seem to play fundamental roles in plant immunity, pathogens may have evolved effector proteins to interfere with PR-1 activity. Indeed, it was recently shown that a candidate effector from the powdery mildew fungus *Blumeria graminis* interacts with a PR-1 protein from barley (Zhang *et al*., 2012). In this regard, we hypothesize that RLKs with a PR-1 extracellular domain may interact with putative ligands of secreted PR-1 proteins, which would trigger a defense response. The identification of PR-1RK ligands and the downstream signals transduced upon the activation of PR-1RKs will illuminate their mechanisms of action and provide clues about the roles of PR-1 proteins in plant immunity.

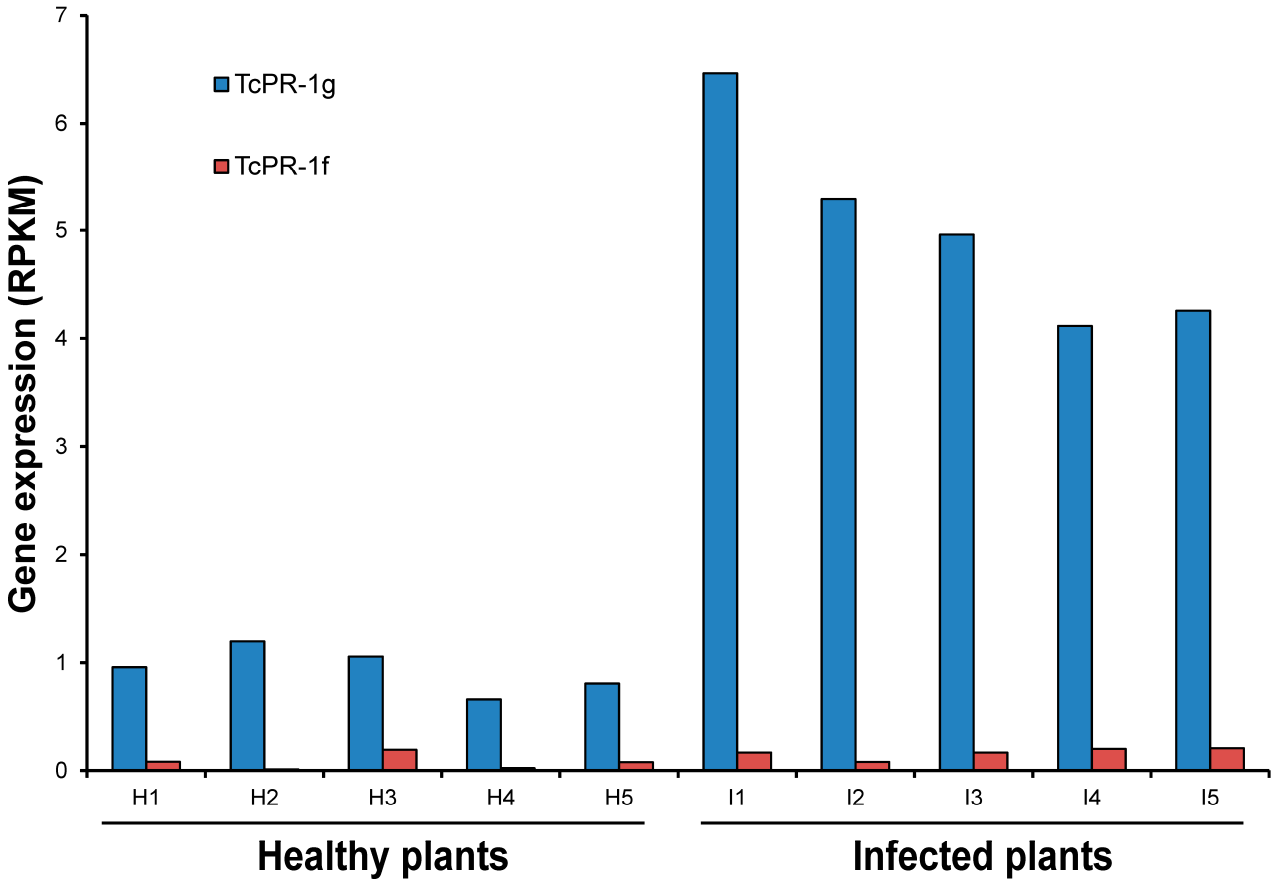

Figure 3. Gene expression analysis of cacao PR-1RK during the biotrophic stage of witches' broom disease. The *TcPR-1g* gene is up-regulated in infected plants, whereas no significant expression was detected for *TcPR-1f*. Data were obtained by RNA-seq sequencing of five replicates for each condition (healthy control and infected plants). Gene expression values are given in reads per kilobase of exon model per million mapped reads (RPKM).

ACKNOWLEDGEMENTS

This work was funded by the *Fundação de Amparo à Pesquisa do Estado de São Paulo* (FAPESP - project numbers 2009/51018-1, 2009/50119-9 and 2012/07657-2).

REFERENCES

Afoakwa, E.O., Paterson, A., Fowler, M. and Ryan, A. (2008) Flavor formation and character in cocoa and chocolate: a critical review. *Crit. Rev. Food. Sci. Nutr.* 48, 840-857.

Afzal, A.J., Wood, A.J. and Lightfoot, D.A. (2008). Plant receptor-like serine threonine kinases: roles in signaling and plant defense. *Mol. Plant Microbe Interact*. 21, 507-517.

Aime, M.C. and Phillips-Mora, W. (2005) The causal agents of witches' broom and frosty pod rot of cacao (chocolate, *Theobroma cacao*) form a new lineage of Marasmiaceae. *Mycologia*, 97, 1012-1022.

Boller, T. and Felix, G. (2009) A renaissance of elicitors: perception of microbe-associated molecular patterns and danger signals by pattern-recognition receptors. *Annu. Rev. Plant Biol.* 60, 379-406.

Cantacessi, C., Campbell, B.E., Visser, A., Geldhof, P., Nolan, M.J., Nisbet, A.J., Matthews, J.B., Loukas, A., Hofmann, A., Otranto, D., Sternberg, P.W. and Gasser, R.B. (2009) A portrait of the "SCP/TAPS" proteins of eukaryotes - developing a framework for fundamental research and biotechnological outcomes. *Biotechnol. Adv*. 27, 376-388.

Chen, X., Shang, J., Chen, D., Lei, C., Zou, Y., Zhai, W., Liu, G., Xu, J., Ling, Z., Cao, G., Ma, B., Wang, Y., Zhao, X., Li, S. and Zhu, L. (2006) A B-lectin receptor kinase gene conferring rice blast resistance. *Plant J*. 46, 794-804.

Chinchilla, D., Zipfel, C., Robatzek, S., Kemmerling, B., Nürnberger, T., Jones, J.D., Felix, G. and Boller, T. (2007) A flagellin-induced complex of the receptor FLS2 and BAK1 initiates plant defence. *Nature*, 448, 497-500.

Dardick, C., Chen, J., Richter, T., Ouyang, S. and Ronald, P. (2007) The rice kinase database. A phylogenomic database for the rice kinome. *Plant Physiol.* 143, 579–586.

Diener, A.C. and Ausubel, F.M. (2005) Resistance to *Fusarium oxysporum* 1, a dominant Arabidopsis disease-resistance gene, is not race specific. *Genetics*, 171, 305–321.

Escobar-Restrepo, J.M., Huck, N., Kessler, S., Gagliardini, V., Gheyselinck, J., Yang, W.C. and Grossniklaus, U. (2007) The FERONIA receptor-like kinase mediates male–female interactions during pollen tube reception. *Science*, 317, 656–660.

Evans, H.C. (2007) Cacao diseases-the trilogy revisited. *Phytopathology*, 97, 1640-1643.

Fernández, C., Szyperski, T., Bruyère, T., Ramage, P., Mösinger, E. and Wüthrich, K. (1997) NMR solution structure of the pathogenesis-related protein P14a. *J. Mol. Biol*. 26, 576-593.

Frias, G. A., Purdy, L. H., and Schmidt, R. A. (1995) An inoculation method for evaluating resistance of cacao to *Crinipellis perniciosa*. *Plant Dis*. 79, 787– 791.

Geer, L.Y., Domrachev, M., Lipman, D.J. and Bryant, S.H. (2002) CDART: protein homology by domain architecture. *Genome Res*. 12, 1619-1623.

Gibbs, G.M., Roelants, K. and O'Bryan, M.K. (2008) The CAP superfamily: cysteine-rich secretory proteins, antigen 5, and pathogenesis-related 1 proteins-roles in reproduction, cancer, and immune defense. *Endocr. Rev*. 29, 865-897.

Gish, L.A. and Clark, S.E. (2011) The RLK/Pelle family of kinases. *Plant J.* 66, 117-127.

Godiard, L., Sauviac, L., Torii, K.U., Grenon, O., Mangin, B., Grimsley, N.H. and Marco, Y. (2003) ERECTA, an LRR receptor-like kinase protein controlling development pleiotropically affects resistance to bacterial wilt. *Plant J*. 36: 353–365.

Gomez-Gomez, L. and Boller, T. (2000) FLS2: an LRR receptor-like kinase involved in the perception of the bacterial elicitor flagellin in Arabidopsis. *Mol. Cell*, 5, 1003–1011.

Gough, J. (2005) Convergent evolution of domain architectures (is rare). *Bioinformatics,* 21,1464-1471.

Greeff, C., Roux, M., Mundy, J. and Petersen, M. (2012) Receptor-like kinase complexes in plant innate immunity. *Front*. *Plant Sci.* 3, 209.

Heese, A., Hann, D.R., Gimenez-Ibanez, S., Jones, A.M., He, K., Li, J., Schroeder, J.I., Peck, S.C. and Rathjen, J.P. (2007). The receptor-like kinase SERK3/BAK1 is a central regulator of innate immunity in plants. *Proc. Natl. Acad. Sci. USA*. 104,12217-1222.

Jinn, T. L., Stone, J. M. and Walker, J. C. (2000) HAESA, an Arabidopsis leucine-rich repeat receptor kinase, controls floral organ abscission. *Genes Dev.* 14, 108-117.

Johnson, L.N., Noble, M.E. and Owen, D.J. (1996) Active and inactive protein kinases: structural basis for regulation. *Cell*, 85, 149–158.

Jones, C.D., Custer, A.W. and Begun, D.J. (2005) Origin and evolution of a chimeric fusion gene in *Drosophila subobscura*, *D. madeirensis* and *D. guanche*. *Genetics,* 170, 207-219.

Jurka, J. (1998) Repeats in genomic DNA: mining and meaning. *Curr*. *Opin*. *Struct*. *Biol*. 8, 333-337.

Kaku, H., Nishizawa, Y., Ishii-Minami, N., Akimoto-Tomiyama, C., Dohmae, N., Takio, K., Minami, E. and Shibuya, N. (2006). Plant cells recognize chitin fragments for defense signaling through a plasma membrane receptor. *Proc. Natl. Acad. Sci. USA* 103, 11086–11091.

Lee, S.W., Han, S.W., Sririyanum, M., Park, C.J., Seo, Y.S. and Ronald, P.C. (2009) A type I-secreted, sulfated peptide triggers XA21-mediated innate immunity. *Science*, 326, 850-853.

Lehti-Shiu, M.D., Zou, C., Hanada, K. and Shiu, S.H. (2009) Evolutionary history and stress regulation of plant receptor-like kinase/pelle genes. *Plant Physiol.* 150, 12-26.

Liu, B., Li, J.F., Ao, Y., Qu, J., Li, Z., Su, J., Zhang, Y., Liu, J., Feng, D., Qi, K., He, Y., Wang, J. and Wang, H.B. (2012) Lysin motif-containing proteins LYP4 and LYP6 play dual roles in peptidoglycan and chitin perception in rice innate immunity. *Plant Cell,* 24, 3406-3419.

Long, M., Betran, E., Thornton, K. and Wang, W. (2003) The origin of new genes: Glimpses from the young and old. *Nat. Rev. Genet.* 4, 865–875.

Meinhardt, L.W., Rincones, J., Bailey, B.A., Aime, M.C., Griffith, G.W., Zhang, D. and Pereira, G.A. (2008) *Moniliophthora perniciosa*, the causal agent of witches' broom disease of cacao: what's new from this old foe? *Mol. Plant Pathol*. 9, 577-588.

Miya, A., Albert, P., Shinya, T., Desaki, Y., Ichimura, K., Shirasu, K., Narusaka, Y., Kawakami, N., Kaku, H. and Shibuya N. (2007) CERK1, a LysM receptor kinase, is essential for chitin elicitor signaling in Arabidopsis. *Proc. Natl. Acad. Sci. USA*, 104, 19613–19618.

Monaghan, J. and Zipfel, C. (2012) Plant pattern recognition receptor complexes at the plasma membrane. *Curr*. *Opin*. *Plant Biol*. 15, 349-357.

Morillo, S.A. and Tax, F.E. (2006) Functional analysis of receptor-like kinases in monocots and dicots. *Curr*. *Opin*. *Plant Biol.* 9, 460- 469.

Nakai, K. and Horton, P. (1999) PSORT: a program for detecting sorting signals in proteins and predicting their subcellular localization. *Trends Biochem. Sci*. 24, 34–36.

Niderman, T., Genetet, I., Bruyère, T., Gees, R., Stintzi, A., Legrand, M., Fritig, B. and Mösinger, E. (1995) Pathogenesis-related PR-1 proteins are antifungal. Isolation and characterization of three

14-kilodalton proteins of tomato and of a basic PR-1 of tobacco with inhibitory activity against *Phytophthora infestans*. *Plant Physiol*. 108, 17-27.

Nisole, S., Lynch, C., Stoye, J.P. and Yap, M.W. (2004) A Trim5-cyclophilin A fusion protein found in owl monkey kidney cells can restrict HIV-1. *Proc. Natl. Acad. Sci. USA*, 101, 13324–13328.

Oh, M.H., Wang, X., Kota, U., Goshe, M.B., Clouse, S.D. and Huber, S.C. (2009) Tyrosine phosphorylation of the BRI1 receptor kinase emerges as a component of brassinosteroid signaling in Arabidopsis. *Proc. Natl. Acad. Sci. USA*, 106, 658–663.

Oh, M.H., Wang, X., Wu, X., Zhao, Y., Clouse, S.D and Huber SC. (2010) Autophosphorylation of Tyr-610 in the receptor kinase BAK1 plays a role in brassinosteroid signaling and basal defense gene expression. *Proc. Natl. Acad. Sci. USA*, 107, 17827-17832.

Purdy, L.H. and Schmidt, R.A. (1996) Status of cacao witches' broom: biology, epidemiology, and management. *Annu. Rev. Phytopathol.* 34, 573-594.

Quevillon, E., Silventoinen, V., Pillai, S., Harte, N., Mulder, N., Apweiler, R. and Lopez, R. (2005) InterProScan: protein domains identifier. *Nucl. Acids Res*. 33 (Web Server Issue): w116-W120.

Rauscher, M., Adám, A.L., Wirtz, S., Guggenheim, R., Mendgen, K. and Deising, H.B. (1999) PR-1 protein inhibits the differentiation of rust infection hyphae in leaves of acquired resistant broad bean. *Plant J.* 19, 625-633.

Roux, M., Schwessinger, B., Albrecht, C., Chinchilla, D., Jones, A., Holton, N., Malinovsky, F.G., Tör, M., de Vries, S. and Zipfel, C. (2011) The Arabidopsis leucine-rich repeat receptor–like kinases BAK1/SERK3 and BKK1/SERK4 are required for innate immunity to hemibiotrophic and biotrophic athogens. *Plant Cell*, 23, 2440–2455.

Schultz, J., Milpetz, F., Bork, P. and Ponting, C.P. (1998) SMART, a simple modular architecture research tool: identification of signaling domains. *Proc. Natl. Acad. Sci. USA*, 95, 5857-5864.

Shiu, S.H. and Bleecker, A.B. (2001) Receptor-like kinases from Arabidopsis form a monophyletic gene family related to animal receptor kinases. *Proc. Natl. Acad. Sci. USA* 98, 10763–10768.

Shiu, S.H. and Bleecker, A.B. (2003) Expansion of the receptor-like kinase/Pelle gene family and receptor-like proteins in Arabidopsis. *Plant Physiol*. 132, 530-543.

Shiu, S.H., Karlowski, W.M., Pan, R., Tzeng, Y.H., Mayer, K.F. and Li W,H. (2004) Comparative analysis of the receptor-like kinase family in Arabidopsis and rice. *Plant Cell*, 16, 1220-1234.

Sievers, F., Wilm, A., Dineen, D., Gibson, T.J,. Karplus, K., Li, W., Lopez, R., McWilliam, H., Remmert, M., Söding, J., Thompson, J.D. and Higgins, D.G. (2011) Fast, scalable generation of high-quality protein multiple sequence alignments using Clustal Omega. *Mol. Syst. Biol*. 7, 539.

Soria, J.V. (1996) Obtención de clones de cacao por el método de índices de selección. *Turrialba*, 16, 119-124.

Tamura, K., Peterson, D., Peterson, N., Stecher, G., Nei, M. and Kumar, S. (2011) MEGA5: molecular evolutionary genetics analysis using maximum likelihood, evolutionary distance, and maximum parsimony methods. *Mol. Biol. Evol.* 28, 2731-2739.

Torii, K.U. (2004) Leucine-rich repeat receptor kinases in plants: structure, function, and signal transduction pathways. *Int*. *Rev*. *Cytol*. 234, 1-46.

Trotochaud, A.E., Jeong, S. and Clark, S.E. (2000) CLAVATA3, a multimeric ligand for the CLAVATA1 receptor-kinase. *Science*, 289, 613–617.

Van Loon, L.C., Rep, M. and Pieterse CM (2006) Significance of inducible defense-related proteins in infected plants. *Annu. Rev. Phytopathol*. 44, 135-162.

Vello, F. and Garcia J.R. (1971) Características das principais variedades de cacau cultivadas na Bahia. *Theobroma*, 1, 3-10.

Walker, J.C. (1994) Structure and function of the receptor-like protein kinases of higher plants. *Plant Mol. Biol*. 26, 1599-1609.

Wan, J., Zhang, X.C., Neece, D., Ramonell, K.M., Clough, S., Kim, S.Y., Stacey, M.G. and Stacey, G. (2008) A LysM receptor-like kinase plays a critical role in chitin signaling and fungal resistance in Arabidopsis. *Plant Cell*, 20, 471–481.

Wang, G., Ellendorff, U., Kemp, B., Mansfield, J.W., Forsyth, A., Mitchell, K., Bastas, K., Liu, C.M., Woods-Tör, A., Zipfel, C., de Wit, P.J., Jones, J.D, Tör, M. and Thomma, B,P. (2008) A genome-wide functional investigation into the roles of receptor-like proteins in Arabidopsis. *Plant Physiol*. 147, 503-517.

Wang, W., Zheng, H., Fan, C., Li, J., Shi, J., Cai, Z., Zhang, G., Liu, D., Zhang, J., Vang, S., Lu, Z., Wong, G.K., Long, M. and Wang, J. (2006) High rate of chimeric gene origination by retroposition in plant genomes. *Plant Cell*, 18, 1791-1802.

Wang, Z.-Y., Seto, H., Fujioka, S., Yoshida, S. and Chory, J. (2001) BRI1 is a critical component of a plasma-membrane receptor for plant steroids. *Nature*, 410, 380–383.

Warren, A.M., Hughes, M.A. and Crampton, J.M. (1997) Zebedee: a novel copia-Ty1 family of transposable elements in the genome of the medically important mosquito *Aedes aegypti*. *Mol. Gen. Genet*. 254, 505-513.

Willmann, R., Lajunen, H.M., Erbs, G., Newman, M.A., Kolb, D., Tsuda, K., Katagiri, F., Fliegmann, J., Bono, J.J., Cullimore, J.V., Jehle, A.K., Götz, F., Kulik, A., Molinaro, A., Lipka, V., Gust, A.A. and Nürnberger, T. (2011) Arabidopsis lysin-motif proteins LYM1 LYM3 CERK1 mediate bacterial peptidoglycan sensing and immunity to bacterial infection. *Proc Natl Acad Sci USA*, 108, 19824-19829.

Zhang, W.J., Pedersen, C., Kwaaitaal, M., Gregersen, P.L., Mørch, S.M., Hanisch, S., Kristensen, A., Fuglsang, A.T., Collinge, D.B. and Thordal-Christensen, H. (2012) Interaction of barley powdery mildew effector candidate CSEP0055 with the defence protein PR17c. *Mol. Plant Pathol*. 13, 1110-1119.

Zipfel, C., Robatzek, S., Navarro, L., Oakeley, E.J., Jones, J.D., Felix, G. and Boller, T. (2004) Bacterial disease resistance in Arabidopsis through flagellin perception. *Nature*, 428, 764–67.

Zipfel, C., Kunze, G., Chinchilla, D., Caniard, A., Jones, J.D., Boller, T. and Felix, G. (2006) Perception of the bacterial PAMP EF-Tu by the receptor EFR restricts Agrobacterium-mediated transformation. *Cell*, 125, 749–760.

Capítulo VI

The hemibiotrophic cacao pathogen *Moniliophthora perniciosa* depends on a mitochondrial alternative oxidase for biotrophic development

Daniela P.T. Thomazella*, Paulo José P.L. Teixeira*, Halley C. Oliveira, Elzira E. Saviani, Johana Rincones, Isabella M. Toni, Osvaldo Reis, Odalys Garcia, Lyndel W. Meinhardt, Ione Salgado, Gonçalo A.G. Pereira

* Autores com igual contribuição

Trabalho publicado na revista *New Phytologist*, Junho de 2012, Vol. 194, pp. 1025-1034.

APRESENTAÇÃO

Este trabalho descreve o uso de vias respiratórias distintas nos dois estágios miceliares de *Moniliophthora perniciosa*. Durante seu estágio biotrófico, o patógeno utiliza uma via alternativa de respiração, a qual é mediada pela enzima oxidase alternativa (AOX). Apesar de fornecer menor quantidade de energia, esta via respiratória é resistente a moléculas de defesa produzidas pela planta que atuam na cadeia respiratória principal do fungo. Em seu estágio necrotrófico, o patógeno passa a utilizar majoritariamente a via respiratória principal, obtendo uma maior quantidade de energia, capaz de suportar seu desenvolvimento e colonização dos tecidos mortos do hospedeiro. Fruto principal do doutorado da Dr. Daniela Thomazella (Processo FAPESP 2006/50794-0), o trabalho contribuiu sobremaneira para o entendimento do processo de transição da fase biotrófica para a necrotrófica em *M. perniciosa*, um fenômeno central, mas pouco compreendido no desenvolvimento de fungos hemibiotróficos. Além da importante contribuição científica, este trabalho resultou em uma grande conquista na área tecnológica: uma potencial composição fungicida baseada na combinação de um inibidor da cadeia respiratória principal e da AOX para controle da doença vassoura de bruxa e possivelmente de outras doenças tropicais. Com base em nossos resultados, um pedido de patente foi depositado no INPI (BR1020120246724). Como consequência da sua relevância, o estudo foi divulgado pelos jornais Folha de São Paulo (28/03/2012), O Estado de São Paulo (22/05/2012), O Globo (23/05/2012), Valor Econômico (24/07/2012), pelas revistas Exame (22/05/2012) e Agência FAPESP (22/05/2012) e pelo renomado jornal internacional *Financial Times* (23/05/2012). As descobertas deste trabalho têm servido de base para uma série de novas pesquisas coordenadas por nosso grupo, que incluem a resolução da estrutura tridimensional da AOX, a síntese de moléculas mais estáveis e eficientes para inibição desta enzima e a verificação da efetividade das combinações fungicidas contra outros patógenos de interesse para a agricultura brasileira.

New Phytologist

Research

The hemibiotrophic cacao pathogen *Moniliophthora perniciosa* depends on a mitochondrial alternative oxidase for biotrophic development

Daniela P. T. Thomazella[1]*, Paulo José P. L. Teixeira[1]*, Halley C. Oliveira[2], Elzira E. Saviani[2], Johana Rincones[1], Isabella M. Toni[1], Osvaldo Reis[1], Odalys Garcia[1], Lyndel W. Meinhardt[3], Ione Salgado[2] and Gonçalo A. G. Pereira[1]

[1]Laboratório de Genômica e Expressão, Departamento de Genética, Evolução e Bioagentes, Instituto de Biologia, Universidade Estadual de Campinas (UNICAMP), CP 6109, Campinas, SP 13083-970, Brazil; [2]Departamento de Biologia Vegetal, Instituto de Biologia, Universidade Estadual de Campinas (UNICAMP), CP 6109, Campinas, SP 13083-970, Brazil; [3]Sustainable Perennial Crops Laboratory, USDA–ARS, 10300 Baltimore Ave., Bldg. 001, Beltsville, MD 20705-2350, USA

Author for correspondence:
Gonçalo A. G. Pereira
Tel: +55 19 35216237
Email: goncalo@unicamp.br

Received: *10 November 2011*
Accepted: *11 February 2012*

New Phytologist (2012) **194**: 1025–1034
doi: 10.1111/j.1469-8137.2012.04119.x

Key words: alternative oxidase (AOX), cacao (*Theobroma cacao*), hemibiotrophic, *Moniliophthora perniciosa*, nitric oxide (NO), phase transition, witches' broom disease (WBD).

Summary

- The tropical pathogen *Moniliophthora perniciosa* causes witches' broom disease in cacao. As a hemibiotrophic fungus, it initially colonizes the living host tissues (biotrophic phase), and later grows over the dead plant (necrotrophic phase). Little is known about the mechanisms that promote these distinct fungal phases or mediate the transition between them.
- An alternative oxidase gene *(Mp-aox)* was identified in the *M. perniciosa* genome and its expression was analyzed througout the fungal life cycle. In addition, the effects of inhibitors of the cytochrome-dependent respiratory chain (CRC) and alternative oxidase (AOX) were evaluated on the *in vitro* development of *M. perniciosa*.
- Larger numbers of *Mp-aox* transcripts were observed in the biotrophic hyphae, which accordingly showed elevated sensitivity to AOX inhibitors. More importantly, the inhibition of CRC prevented the transition from the biotrophic to the necrotrophic phase, and the combined use of a CRC and AOX inhibitor completely halted fungal growth.
- On the basis of these results, a novel mechanism is presented in which AOX plays a role in the biotrophic development of *M. perniciosa* and regulates the transition to its necrotrophic stage. Strikingly, this model correlates well with the infection strategy of animal pathogens, particularly *Trypanosoma brucei*, which uses AOX as a strategy for pathogenicity.

Introduction

Fungal plant pathogens have traditionally been classified on the basis of their feeding mechanism into biotrophic, necrotrophic and hemibiotrophic pathogens. Biotrophs are defined by a dependence on the host to complete their life cycle; they derive nutrients from living host cells by forming specialized infection structures, such as haustoria. By contrast, necrotrophs kill the plant and derive nutrients from the dead host cells. In some pathosystems, the pathogen initially keeps cells alive (biotrophic phase), but then kills them at later stages of infection (necrotrophic phase), which characterizes the hemibiotrophic lifestyle (Glazebrook, 2005). Despite being a critical step for the success of most hemibiotrophic infections, the biotrophic phase is, in general, transient and asymptomatic, whereas the necrotrophic phase causes the main disease symptoms in the plant (Munch *et al.*, 2008). The factors responsible for triggering the switch from biotrophy to necrotrophy in hemibiotrophic fungi are still poorly understood, but may depend on key alterations in the pathogen's metabolic status (Dufresne *et al.*, 2000; Pellier *et al.*, 2003).

Some of the world's most devastating phytopathogens display a hemibiotrophic lifestyle. For instance, the hemibiotrophic ascomycete *Magnaporthe oryzae*, which causes the rice blast disease, has emerged as a model for the study of phytopathogenic fungi because of its experimental tractability and economic importance (Dean *et al.*, 2005; Wilson & Talbot, 2009). This pathogen initially colonizes host tissues as a biotroph, without causing detectable symptoms. Approximately 72–96 h after infection, lesions become apparent in the plant, characterizing the necrotrophic growth of *M. oryzae*. No morphological differences appear to exist between these two developmental stages (biotrophic and necrotrophic) in *M. oryzae* (Berruyer *et al.*, 2006). Similarly, the hemibiotrophic lifestyle described for many *Colletotrichum*, *Fusarium* and *Phytophthora* species combines an initial short and asymptomatic period of biotrophic growth that is followed by a destructive necrotrophic phase during which symptoms develop.

*These authors contributed equally to this work.

The basidiomycete *Moniliophthora perniciosa* (formerly *Crinipellis perniciosa*) causes one of the most devastating diseases of cacao (*Theobroma cacao*), namely witches' broom disease (WBD). The *M. perniciosa*–cacao interaction is classified as hemibiotrophic (Purdy & Schmidt, 1996); however, it has certain peculiar features that make its study of prime importance in the field of plant pathology. In contrast with other well-documented hemibiotrophic infections, the biotrophic and necrotrophic phases of *M. perniciosa* are morphologically distinct: the first phase is monokaryotic and the second phase is dikaryotic with clamp connections for nuclear transfer (Meinhardt *et al.*, 2008). Moreover, the biotrophic stage is unusually extended, lasting for 2–3 months in infected tissue. In this stage of WBD, only a few fungal cells are detected; however, drastic biochemical and morphological alterations are observed in the plant, such as the formation of modified stems, termed 'green brooms' (Scarpari *et al.*, 2005). By contrast, necrotrophic growth occurs only during the final stages of infection, when the fungus rapidly colonizes the dead plant tissue, which is called 'dry broom', and produces the fruiting bodies (basidiomata) for reproduction (Purdy & Schmidt, 1996).

In *M. perniciosa*, the factors involved in the switch from biotrophy to necrotrophy seem to be dependent on the availability of soluble nutrients and specific carbon sources (Meinhardt *et al.*, 2006). Attempts to obtain the monokaryotic (biotrophic) mycelium under *ex planta* conditions were initially limited by the rapid transition of this primary fungal stage to the dikaryotic (necrotrophic) phase. The first report of the successful maintenance of the *M. perniciosa* monokaryotic phase under laboratory conditions was in a study of a dual culture of basidiospores with potato callus (Griffith & Hedger, 1994). More recently, the development of a medium with glycerol as the sole carbon source allowed for the extended growth of a biotrophic-like (monokaryotic) mycelium under axenic conditions. However, this mycelial stage is still considerably unstable when grown in culture media (Meinhardt *et al.*, 2006).

In general, laboratory cultivation of the biotrophic stage of fungal species is an uncommon and notable achievement in phytopathology. The vast majority of biotrophic pathogens (*Puccinia* spp., *Melampsora* spp., *Blumeria graminis*) are not cultivable outside of their hosts (Spanu & Kamper, 2010). A counter-example is the maize pathogen *Ustilago maydis*, a well-known cultivable biotroph with a dimorphic lifestyle. In contrast with *M. perniciosa*, the monokaryotic form of *U. maydis* is nonpathogenic and is followed by a dikaryotic parasitic form. Moreover, its monokaryotic phase occurs as yeast-like cells that saprotrophically colonize soil and dead organic matter. In the laboratory, this saprotrophic stage is easily cultivated under axenic conditions and, as in *M. perniciosa*, the *ex planta* culture of the biotrophic hyphae of *U. maydis* is only obtained under specific growth conditions (Day & Anagnostakis, 1971).

Analysis of the *M. perniciosa* genome (Mondego *et al.*, 2008) led to the identification of a gene coding for a mitochondrial alternative oxidase (AOX). This protein is a ubiquinol oxidase that catalyzes the reduction of molecular oxygen to water (Elthon & McIntosh, 1987). It constitutes an alternative respiratory pathway to the 'conventional' and universally conserved cytochrome-dependent respiratory chain (CRC), which involves respiratory complexes III and IV. In contrast with cytochrome *c* oxidase (complex IV), electron transfer through AOX does not involve phosphorylation, and the redox energy is released as heat instead of being used for ATP production (Van Aken *et al.*, 2009). Consequently, the use of the alternative pathway results in only one coupling site for oxidative phosphorylation (complex I), and energy production, based on the amount of ATP, is approximately one-third of that generated by the CRC pathway (Siedow & Umbach, 2000).

AOX occurs in all plants, as well as in certain fungi, protists, bacteria and animals (Elthon & McIntosh, 1987; Joseph-Horne *et al.*, 2001; Stenmark & Nordlund, 2003; Chaudhuri *et al.*, 2006; McDonald *et al.*, 2009). Although broadly conserved, the precise role of this enzyme has only been well characterized in thermogenic plants, such as those of the family Araceae. During the reproductive process of these plants, AOX is a central enzyme and generates heat to volatilize amines and attract pollinators (Wagner *et al.*, 2008). For all other organisms, the function of this alternative respiratory route has been the subject of much debate. The most accepted role assigned to this enzyme is its participation in the stress response associated with CRC restriction, which can be provoked by complex III and IV inhibitors, such as antimycin-A, carbon monoxide, cyanide and nitric oxide (NO). In the presence of these compounds, AOX bypasses complexes III and IV and acts as an overflow valve for electron transport, thus preventing the deleterious oxidative stress associated with the increased generation of mitochondrial reactive oxygen species (ROS) (Maxwell *et al.*, 1999; Ruy *et al.*, 2006; Vanlerberghe *et al.*, 2009).

NO is an important component of the immune response in animals and plants. Apart from its role as a plant signaling molecule, it acts as a potent inhibitor of the pathogen CRC pathway (complex IV), leading to the generation of deleterious oxidative stress (Brown, 1999). Studies with the animal pathogens *Histoplasma capsulatum*, *Trypanosoma brucei*, *Aspergillus fumigatus*, *Paracoccidioides brasiliensis* and *Cryptococcus neoformans* have proposed that AOX mitigates the oxidative and/or nitrosative stress induced by the oxidative burst and NO generation during host infection (Akhter *et al.*, 2003; Nittler *et al.*, 2005; Chaudhuri *et al.*, 2006; Magnani *et al.*, 2008; Hernandez *et al.*, 2011). Based on these studies, AOX has also been proposed to be a resistance mechanism of phytopathogens to evade plant defenses and successfully complete the infection process (Joseph-Horne *et al.*, 2001; Albury *et al.*, 2009). However, this hypothesis has not been confirmed.

In this study, we present strong evidence for a biological role of AOX in the life cycle of a plant pathogen. The *M. perniciosa aox* gene was characterized, and a clear correlation between the hemibiotrophic lifestyle of this fungus and the functionality of the mitochondrial respiratory routes was observed. In addition, this work suggests that AOX may enable respiration to continue during the first stages of WBD, when the pathogen needs to survive in a hostile environment established by the host defense system (e.g. NO burst). Finally, we show that the inhibition of CRC maintained the fungus in its monokaryotic stage, which

may be sustained by AOX-dependent respiration. These data indicate that mitochondrial respiratory pathways and cellular energetic status may play a role in the phase transition and development of phytopathogens.

Materials and Methods

Biological material

The experiments were performed using the *Moniliophthora perniciosa* (Stahel) Aime & Phillips-Mora, (2005) strain FA553 (Mondego *et al.*, 2008). The necrotrophic mycelium was used to produce basidiomata and basidiospores, as described by Griffith & Hedger (1993), with modifications introduced by Niella *et al.* (1999). The monokaryotic (biotrophic-like) mycelium was obtained from basidiospores germinated in a defined medium developed by Meinhardt *et al.* (2006). Transfer of the biotrophic-like mycelium to the nutrient-rich medium MYEA (Malt Yeast Extract Agar) (20 g l^{-1} malt extract, 5 g l^{-1} yeast extract and 20 g l^{-1} agar) induced the transition to the necrotrophic phase. Cultures were maintained at 28°C with agitation of 120 rpm when cultured in liquid media.

Theobroma cacao L. variety 'comum' (Catongo type) was used for infections. Plants were grown for *c.* 3 months in a glasshouse under controlled temperature (26°C) and humidity (> 80%) and a photoperiod of 12 h. Active apical meristems were inoculated with 30 µl of a basidiospore suspension (10^5 spores ml^{-1}), followed by incubation in a humid chamber for 24 h (Frias *et al.*, 1995).

Mitochondrial isolation and measurement of oxygen consumption

AOX activity was evaluated by measuring the oxygen consumption profile of mitochondria isolated from necrotrophic hyphae, the mycelial stage from which a sufficient amount of organelles can be extracted. Mitochondria isolation was conducted according to the protocol described by Gredilla *et al.* (2006). Protein concentration was determined using the Bradford method with BSA as a standard (Bradford, 1976). Oxygen consumption was determined at 27°C using a Clark-type electrode connected to an Oxygraph unit (Hansatech, King's Lynn, Norfolk, UK). Aliquots of purified mitochondria were added to the closed reaction chamber containing 1 ml of the standard respiration buffer (300 mM sucrose, 10 mM KH_2PO_4, 5 mM $MgCl_2$, 1 mM EDTA, 10 mM KCl, 0.1% BSA; pH 7.2). Mitochondria were energized with 10 mM glutamate/malate, followed by the addition of 1 mM ADP. AOX activity was measured in the presence of the CRC inhibitor antimycin-A (10 µM), as the oxygen consumption inhibited by 100 µM *n*-propyl gallate.

Immunodetection of *M. perniciosa* AOX

Purified mitochondria from *M. perniciosa*, rat (negative control) and *Arabidopsis thaliana* (positive control) were resuspended in 1 × Laemmli buffer (5% β-mercaptoethanol, 3.7% glycerol, 1.1% sodium dodecylsulfate (SDS), 23 mM Tris-HCl pH 6.8, 0.01% bromophenol blue) and heated at 95°C for 5 min. Mitochondrial proteins (12.5 µg) were separated by sodium dodecylsulfate-polyacrylamide gel electrophoresis (SDS-PAGE) and transferred to a polyvinylidene difluoride (PVDF) membrane using standard protocols. The membrane was blocked with 5% nonfat milk in TBST (1 × Tris-buffered saline, 0.1% Tween 20) for 1 h and then incubated with a 1 : 100 dilution of the anti-AOX monoclonal antibody (AOA) (Elthon *et al.*, 1989) in TBST for 16 h. Later, the membrane was incubated with a 1 : 10 000 dilution of the secondary anti-mouse IgG antibody in TBST for 1 h. The signal was detected using the ECL Plus Detection System (GE Healthcare, Little Chalfont, Buckinghamshire, UK) on autoradiography film for 5 min. Subunit 3 of the cytochrome *c* oxidase complex (COX3) was used as endogenous control to demonstrate homogeneity in protein loading of the *M. perniciosa* mitochondrial samples. Three micrograms per milliliter of the anti-yeast COX3 antibody (Invitrogen) were used in the immunoblotting, according to the same procedures as described for the AOA.

Gene expression assays

The effects of azoxystrobin (75 µM – Syngenta, Basel, Switzerland) and of the NO donor 1-hydroxy-2-oxo-3-(3-aminopropyl)-3-isopropyl-1-triazene (NOC-5; 400 µM – Sigma) on *Mp-aox* gene expression were evaluated by quantitative PCR (qPCR). To this end, necrotrophic hyphae were grown in liquid cultures (2 g l^{-1} malt extract, 5 g l^{-1} yeast extract and 50 ml l^{-1} glycerol) at 28°C and with agitation of 120 rpm. Seven days later, cultures were independently treated with the different compounds for 4 h and then harvested for RNA extraction. For the analysis of *Mp-aox* gene expression along the *M. perniciosa* life cycle, the different fungal stages were obtained as described in the 'Biological material' section above. To avoid variations in gene expression associated with different growth conditions, biotrophic and necrotrophic hyphae were grown in the biotrophic-maintaining medium. After 7 d of growth, both mycelia were collected to perform the qPCR assays.

Isolation of total RNA from fungal cells was performed using the Plant RNeasy Minikit (Qiagen), and its concentration and quality were assessed with a NanoDrop ND-1000 spectrophotometer (Wilmington, DE, USA). RNA integrity was evaluated on 1% formaldehyde-agarose gel. Synthesis of cDNA was performed with the Superscript II Reverse Transcriptase kit (Invitrogen) using 1 µg of DNAse I-treated total RNA. The housekeeping gene β-*actin* and the *aox* gene were amplified with the gene-specific primer pairs ACTRTF (5′-CCCTTCTATCGTCGGTCGT-3′) and ACTRTR (5′-AGGATACCACGCTTGGATTG-3′), and AOXRTF (5′-GACGTGCCTTTCGGATAGAG-3′) and AOXRTR (5′-CTTGCCAGGAGGAATGGTT-3′), respectively. All qPCRs were performed in a 16-µl mixture containing 1/16 volume of the cDNA preparation, 1/2 volume of SYBR Green Master Mix (Applied Biosystems, Foster City, CA, USA) and 0.2 µM of each primer. Real-time quantifications were executed using the StepOnePlus system (Applied Biosystems)

and the following cycles: 2 min at 50°C, 10 min at 95°C and 40 cycles of 15 s at 95°C, 30 s at 53°C and 60 s at 60°C. Dissociation curves were performed to verify the formation of primer dimers and nonspecific amplifications. Data analysis was completed using the mathematical method proposed by Livak & Schmittgen (2001).

RNA-seq libraries produced as part of the WBD Transcriptome Atlas (P. J. Teixeira, unpublished) were inspected for the expression of the *Mp-aox* gene during the *in planta* development of *M. perniciosa* in green brooms and dry brooms.

Fluorometric measurement of NO in cacao plants

Apical meristems of healthy plantlets and infected cacao seedlings at the green broom stage were collected to evaluate NO generation using the fluorescent indicator 4,5-diaminofluorescein (DAF-2) (Seligman *et al.*, 2008). Approximately 80 mg of each sample were incubated in 0.1 M phosphate buffer (pH 7.2) containing 25 μM DAF-2 for 1 h under dark conditions at room temperature. After removing the tissue and diluting the resulting solution 2.5-fold, fluorescence emission spectra between 500 and 550 nm were recorded with an excitation of 495 nm using a Hitachi F-2500 spectrofluorometer (Hitachi, Chiyoda, Tokyo, Japan). Data were collected from triplicate samples, and fluorescence was expressed in arbitrary fluorescence units.

Inhibition of mycelial growth assay

The effects of CRC and AOX inhibitors on the growth of *M. perniciosa* in the biotrophic and necrotrophic phases were tested *ex planta*. Azoxystrobin (2.5 μM – Syngenta) was used as a CRC inhibitor (Affourtit *et al.*, 2000) and salicylhydroxamic acid (SHAM; 5 mM – Sigma) as an inhibitor of the alternative pathway (Tanton *et al.*, 2003). These drugs were added individually or simultaneously to the MYEA standard growth medium. The importance of each mitochondrial pathway (CRC and alternative) was assessed by evaluating the effects of these respiratory inhibitors on the growth of the biotrophic and necrotrophic mycelia. To obtain the biotrophic-like hyphae, we germinated *M. perniciosa* basidiospores in the biotrophic-maintaining medium described by Meinhardt *et al.* (2006). After *c.* 7 d of growth, we transferred the biotrophic mycelium to MYEA medium containing the different inhibitors. The necrotrophic mycelium is highly stable and easily maintained under standard laboratory conditions. Therefore, this fungal stage was directly inoculated in MYEA medium with inhibitors, without the need to preculture in a specific medium. To further confirm the effects of SHAM on *M. perniciosa* development, a second AOX inhibitor (*n*-propyl gallate) was also tested.

Results

Mp-aox gene expression, protein production and AOX activity are coordinately regulated in *M. perniciosa*

The *aox* gene in *M. perniciosa* (*Mp-aox* – GenBank accession number JF826501) is a single-copy gene of 1616 nucleotides and comprises ten exons and nine introns. *Mp-aox* encodes a protein of 378 amino acids that has the conserved motifs described for other plant and fungal AOXs (Vanlerberghe & McIntosh, 1997; Tanton *et al.*, 2003; Albury *et al.*, 2009; McDonald, 2009). Moreover, no significant differences were found between the primary structure of *M. perniciosa* AOX (Mp-AOX) and those described in other fungi (data not shown).

Gene expression and western blot analyses showed that treatment of the *M. perniciosa* necrotrophic mycelium with the CRC inhibitor azoxystrobin induces *Mp-aox* transcription (Fig. 1a) and increases Mp-AOX protein levels (Fig. 1b), as observed in other plant and fungal species (Minagawa *et al.*, 1992; Sakajo *et al.*, 1993; Vanlerberghe & McIntosh, 1994; Yukioka *et al.*, 1998). In agreement, oxygen consumption by isolated mitochondria of the azoxystrobin-treated mycelium was moderately affected by antimycin-A (CRC inhibitor) and highly sensitive to *n*-propyl gallate (AOX inhibitor) (Fig. 1c). Conversely, the addition of antimycin-A to mitochondrial preparations of nontreated control cells was sufficient to inhibit oxygen consumption (Fig. 1c), showing that the *M. perniciosa* AOX is functional and activated under specific conditions (e.g. CRC inhibition). Moreover, these data suggest that the enzyme is coordinately regulated at gene expression, protein production and activity levels.

Mp-aox expression is up-regulated in *M. perniciosa* during the biotrophic phase

We evaluated the *ex planta* expression profile of the *Mp-aox* gene to identify specific conditions during the development of *M. perniciosa* in which *Mp-aox* is activated. As shown in Fig. 2(a), gene expression was not significantly different among basidiospores, necrotrophic mycelium and mushrooms (basidiomata). However, a larger amount of *aox* transcripts was verified in the monokaryotic biotrophic-like mycelium when compared with other fungal stages (Fig. 2a). In accordance, measurement of the respiratory rates of these different life stages demonstrated that the biotrophic-like mycelium was the sole fungal stage affected by the AOX inhibitor *n*-propyl gallate (Supporting Information Fig. S1, Methods S1). Finally, supporting these results, inspection of the RNA-seq database (P. J. Teixeira, unpublished) demonstrated that the *M. perniciosa aox* gene is over-expressed in green brooms, when compared with dry brooms, showing a direct correlation between the *ex planta* and *in planta* analyses (Fig. 2b).

Evaluation of NO generation during the green broom stage of WBD

At *c.* 15 d after inoculation of basidiospores in cacao seedlings, the first symptoms of WBD were observed in the infected plants. Mature green brooms at 22 d post-inoculation were used to evaluate NO generation using the DAF-2 method. Increased amounts of NO were detected in mature green brooms in comparison with healthy, noninoculated plants of the same age (Fig. 3a).

Given that *Mp-aox* expression is elevated in the biotrophic hyphae, we used the necrotrophic mycelium to determine

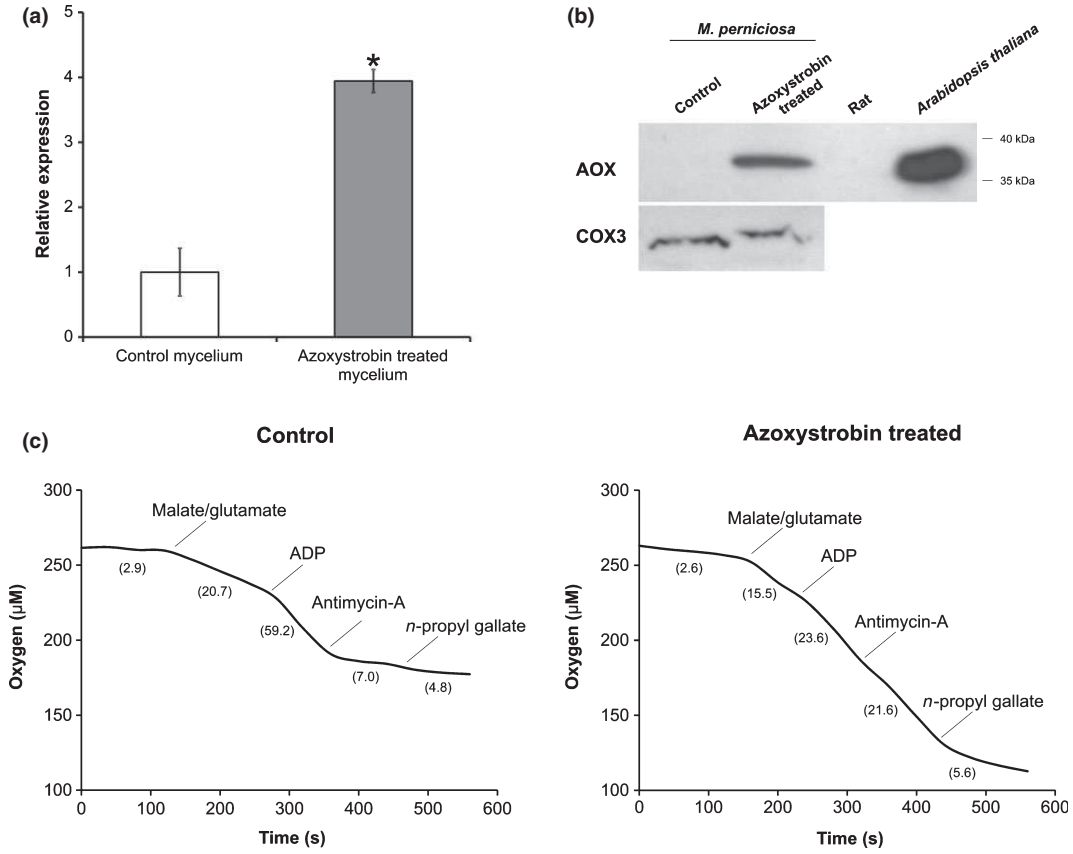

Fig. 1 *Mp-aox* gene expression, protein production and alternative oxidase (AOX) activity are well correlated in *Moniliophthora perniciosa*. (a) Relative expression levels of the *Mp-aox* gene in azoxystrobin-treated vs nontreated cells of the necrotrophic hyphae analyzed by quantitative PCR assays. The β-*actin* gene was used as an endogenous control (Student's *t*-test: *, $P < 0.01$; Error bars represent standard deviation −SD). (b) Immunoblotting assay showing the presence of the Mp-AOX protein in mitochondria isolated from azoxystrobin-treated mycelium of *M. perniciosa*. No signal was detected in mitochondria of nontreated hyphae. The subunit 3 of the cytochrome *c* oxidase complex (COX3) was used as endogenous control. Rat and *Arabidopsis thaliana* mitochondria were used as negative and positive controls, respectively. (c) Oxygen consumption by purified mitochondria from the necrotrophic mycelium of *M. perniciosa.* Mitochondrial suspensions were added to the oxygraph chamber containing the reaction medium and were energized with 10 mM malate/glutamate and 1 mM ADP. AOX activity was assessed in the presence of antimycin-A (10 μM), as the remaining respiration inhibited by *n*-propyl gallate (100 μM). Mitochondrial oxygen consumption of nontreated hyphae showed high sensitivity to antimycin-A, but was unaffected by *n*-propyl gallate. In contrast, mitochondrial oxygen consumption of azoxystrobin-treated cells was poorly affected by antimycin-A, but greatly inhibited by *n*-propyl gallate. The numbers in parentheses represent the oxygen consumption rates in nmol min^{-1} mg^{-1} protein. In all of these assays, azoxystrobin-treated cells were incubated with 75 μM azoxystrobin for 4 h. Control refers to nontreated mycelium.

whether this gene is responsive to the radical NO. Following treatment with the NO donor NOC-5, a fourfold induction of *Mp-aox* expression was observed (Fig. 3b). Similar to azoxystrobin, NO potentially inhibits the CRC pathway (Brown, 1999), and *Mp-aox* induction may be a consequence of this process.

Effects of respiratory inhibitors on the development of the biotrophic-like and necrotrophic mycelia in *M. perniciosa*

Because gene-specific mutants of *M. perniciosa* are unavailable, we employed specific inhibitors of the cytochrome and alternative routes of electron transfer to confirm the role of AOX in the metabolism/development of *M. perniciosa*. Azoxystrobin and SHAM were used to inhibit the CRC and alternative pathways, respectively. These drugs were added individually as well as simultaneously to growth medium, subsequently inoculated with either the biotrophic-like or necrotrophic mycelium (Fig. 4).

As reported previously (Meinhardt *et al.*, 2006), inoculation of the biotrophic-like mycelium in standard growth medium caused biotrophic-like hyphae to switch to the necrotrophic phase (Fig. 4a, top panel, Fig. 4b). Analysis of mycelial morphology showed that the switch started between 24 and 48 h after inoculation and, within 5 d, monokaryotic hyphae were no longer observed. Remarkably, in the presence of azoxystrobin (Fig. 4a, top panel, Fig. 4b), the fungus was able to grow for an extended time as a monokaryotic mycelium (*c.* 30 d), suggesting that CRC inhibition, which results in a low energetic status and possibly high AOX respiration, may favor biotrophic development. Furthermore, in the presence of SHAM (Fig. 4a, top panel), biotrophic growth was completely halted, reinforcing the idea that the alternative respiratory route is the primary mitochondrial pathway during this mycelial stage. In addition, we used another AOX inhibitor (*n*-propyl gallate) to further confirm the effects of AOX inhibition on fungal development. As expected, the biotrophic mycelium showed a higher

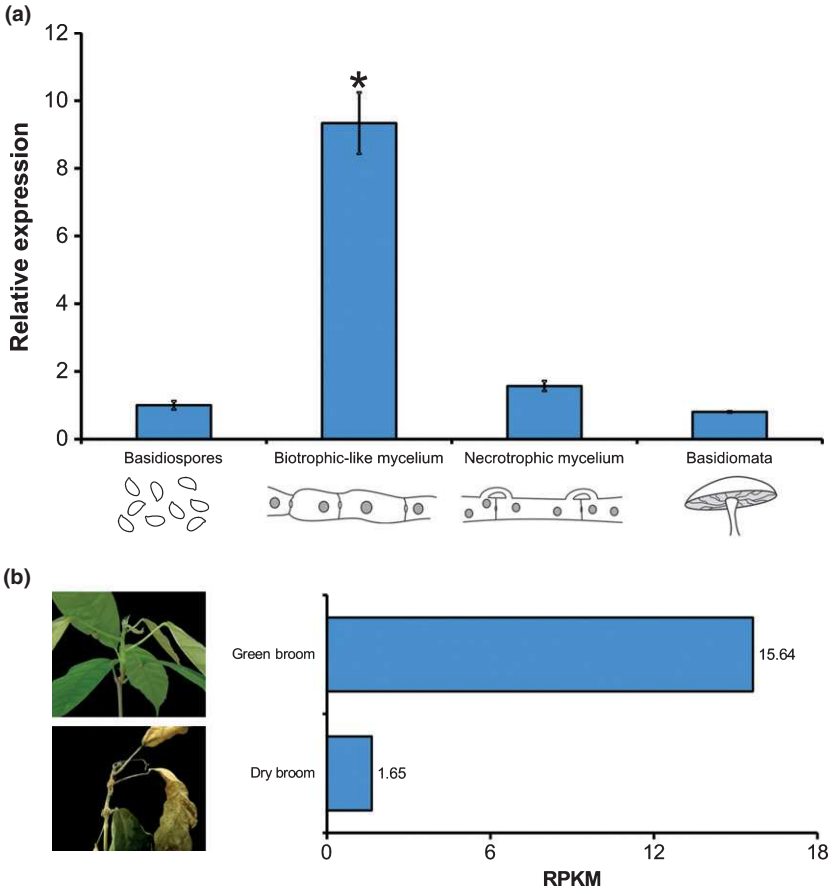

Fig. 2 Expression analysis of *Mp-aox* in the *ex planta* and *in planta* development of *Moniliophthora perniciosa*. (a) Relative expression of *Mp-aox* in each developmental stage of *M. perniciosa* – basidiospores, biotrophic-like (monokaryotic) mycelium, necrotrophic (dikaryotic) mycelium and basidiomata – as analyzed by quantitative PCR. β-*actin* gene expression was used as an endogenous control (Student's *t*-test: *, $P < 0.01$). Representative drawings of each of the life cycle stages are shown. (b) *In planta* expression of *Mp-aox* was assessed after inspection of the witches' broom disease (WBD) RNA-seq Transcriptome Atlas (P. J. Teixeira, unpublished). Gene expression values are expressed in RPKM (reads per kilobase of exon per million mapped reads).

sensitivity to this inhibitor in comparison with the necrotrophic mycelium (Fig. S2).

The necrotrophic mycelium developed in the presence of both respiratory inhibitors – azoxystrobin and SHAM – at the concentrations tested (Fig. 4a, bottom panel). Only when azoxystrobin was combined with the AOX inhibitor SHAM did necrotrophic mycelium development stop completely (Fig. 4a, bottom panel). Therefore, these data indicate that an interplay between the two respiratory pathways (CRC and alternative routes) may exist during this second fungal stage, as confirmed by the results presented in Fig. 1.

Discussion

Moniliophthora perniciosa displays a hemibiotrophic lifestyle with a peculiar mode of nutrition: after initial penetration, it grows for *c.* 60–90 d as a biotroph in the intercellular spaces of the plant – a period of drastic morphological and physiological alterations of the infected tissues (Scarpari *et al.*, 2005). The necrotrophic mycelium appears only during the final stages of the disease, colonizing the dead plant tissues (Meinhardt *et al.*, 2008). The switch between these two growth phases is associated with remarkable morphological, genetic and physiological changes in the hyphae (Meinhardt *et al.*, 2006; Rincones *et al.*, 2008). This study demonstrated that these two life strategies (biotrophic and necrotrophic) use different electron transfer pathways for cell respiration. Although the necrotrophic phase mainly depends on the CRC pathway with an inducible alternative respiration, the biotrophic stage primarily relies on the activity of an alternative respiratory pathway.

Activation of the mitochondrial alternative pathway is associated with a considerable reduction in cell energy production (Elthon & McIntosh, 1987). For this reason, the up-regulation of *Mp-aox* gene expression (Fig. 2a) may explain the slow growth observed during biotrophic development (Meinhardt *et al.*, 2006). Previous work by Affourtit *et al.* (1999) demonstrated that functional expression of the plant *aox* gene in the yeast *Schizosaccharomyces pombe*, which naturally lacks the alternative pathway, significantly reduces total biomass and growth rate, a phenotype that resembles the biotrophic phase in *M. perniciosa* (Meinhardt *et al.*, 2006, 2008). Moreover, in agreement with the dependence of the biotrophic hyphae on AOX respiration, we verified that SHAM and *n*-propyl gallate completely halted biotrophic development, suggesting that AOX inhibition may represent an effective strategy for stalling the progression of WBD during its early stages (Figs 4, S2). A similar strategy has been successfully employed to control sleeping sickness caused by the protozoan *T. brucei*. The infective phase (bloodstream form) of *T. brucei* greatly depends on the activity of the alternative route, and treatment with AOX inhibitors (SHAM/ascofuranone) results in trypanocidal effects (Chaudhuri *et al.*, 2006).

The increased expression of the *Mp-aox* gene (Fig. 2a) and the greater activity of *M. perniciosa* AOX (Fig. S1, Methods S1) in the biotrophic-like mycelium suggest that the enzyme may play a

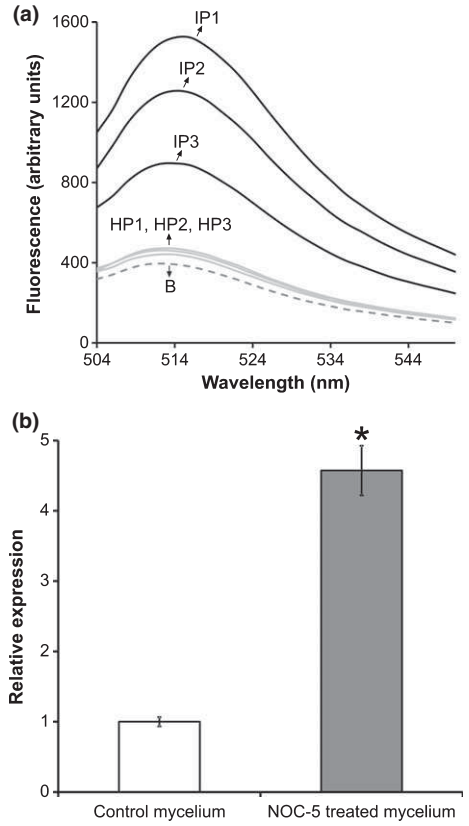

Fig. 3 Participation of nitric oxide (NO) in the *Moniliophthora perniciosa*–cacao interaction. (a) Measurement of NO generation by healthy (control) and infected cacao seedlings using the 4,5-diaminofluorescein (DAF-2) fluorimetric method. NO fluorescence of the meristems from each individual plant is shown. The emission at 515 nm corresponds to the maximum fluorescence emitted by DAF-2T, a fluorescent product directly related to the amount of NO in the medium. IP, infected plants; HP, healthy plants; B, blank, which corresponds to the DAF-2 fluorophore diluted in phosphate buffer (0.1 M, pH 7.2) in the absence of tissues. (b) Quantitative PCR assays were performed to evaluate the relative expression of *Mp-aox* in response to the treatment of the necrotrophic hyphae with the NO donor 1-hydroxy-2-oxo-3-(3-aminopropyl)-3-isopropyl-1-triazene (NOC-5) (400 μM) for 4 h (Student's *t*-test: *, $P < 0.01$).

role during this specific fungal stage. Accordingly, inspection of the WBD Transcriptome Atlas (P. J. Teixeira, unpublished) showed that this gene is up-regulated during the green broom stage of WBD (wherein the fungus grows biotrophically) when compared with the dry broom stage (which is colonized by the necrotrophic hyphae) (Fig. 2b). Despite having a negative effect on the fungal growth rate, AOX may be associated with the detoxification of mitochondrial ROS generated during the initial stages of infection (Scarpari *et al.*, 2005; Ceita *et al.*, 2007; Rincones *et al.*, 2008).

In general, plants produce large amounts of NO in response to biotrophic and hemibiotrophic pathogen infection (Delledonne *et al.*, 1998). In addition to activating defense signaling pathways of the plant, NO can inhibit fungal cells directly by disrupting the mitochondrial complex IV, which increases ROS production, causing oxidative and nitrosative stresses (Brown & Borutaite, 2002; Romero-Puertas *et al.*, 2004). Moreover, the NO superoxide derivative peroxynitrite causes damage to a variety of mitochondrial components through oxidizing reactions, leading to the irreversible inhibition of mitochondrial respiration (Brown, 1999; Brown & Borutaite, 2002). In this study, we observed elevated amounts of NO in infected seedlings compared with the levels found in healthy cacao plants (Fig. 3a). Therefore, we speculate that the ability of the biotrophic mycelium to survive in cacao tissues may strongly depend on mechanisms that circumvent NO-induced CRC impairment. In this regard, AOX may provide *M. perniciosa* with protection against the harmful effects of NO and its derivatives on the mitochondrial respiratory chain. In support of this hypothesis, we verified that *Mp-aox* gene expression is up-regulated by the NO donor NOC-5 *ex planta* (Fig. 3b). Thus, our data indicate that increased NO production occurs during host infection, and fungal AOX may play a protective role in overcoming the harmful effects of this compound on the mitochondrial respiratory chain. If so, during biotrophic development, *M. perniciosa* may slow its growth rate in order to focus on detoxification.

In addition to the protective role of AOX against plant defenses, we also suggest that the enzyme may participate in the regulation of the hemibiotrophic development of *M. perniciosa*. We demonstrate that the switch from the biotrophic-like to the necrotrophic phase is prevented by azoxystrobin, and the fungus continues to grow as a biotrophic mycelium for an extended time in the presence of this inhibitor (Fig. 4). Modulation of the switch between biotrophy and necrotrophy in hemibiotrophic fungi has not been well characterized; however, a few studies have demonstrated that this transition depends on key alterations in the pathogen's metabolism (Dufresne *et al.*, 2000; Pellier *et al.*, 2003). Therefore, we propose that the low-energy metabolic status caused by the inhibition of the CRC pathway, together with high AOX respiration, may be important requirements for the maintenance of biotrophic growth, as well as for the control of the phase transition process in *M. perniciosa*.

Previous work by Evans (1980) has suggested that an unstable molecule produced by the plant is responsible for the maintenance of the biotrophic phase in *M. perniciosa*. In the absence of this molecule, the fungus would rapidly switch to the necrotrophic phase. According to our results, *ex planta* maintenance of the biotrophic mycelium is directly related to inhibition of the CRC route. Thus, we propose that plant NO generation during infection may be the factor responsible for the control of biotrophic development *in planta*. We then speculated that, on the death of the plant tissues, NO-dependent inhibition of the respiratory chain would cease and an increase in the cytochrome/AOX ratio would supply the necessary energy (ATP) for intense pathogen growth during the necrotrophic phase. In this regard, AOX may be a switch regulating the development of these two life strategies in *M. perniciosa* (biotrophic and necrotrophic phases). Our study is the first report of the participation of AOX in the development of a plant pathogen, which sheds light on the physiological functions of this enzyme as well as on the mechanisms that control the phase transition process in phytopathogens, a central step during infection.

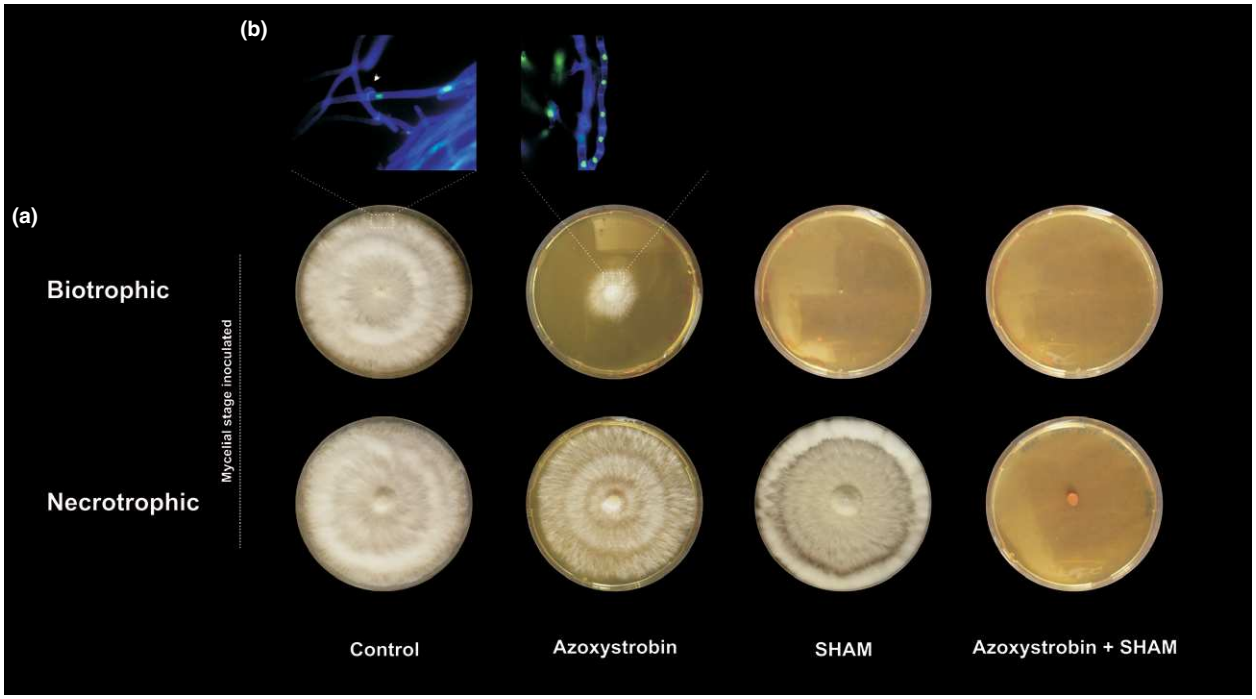

Fig. 4 Growth of *Moniliophthora perniciosa* in the presence of the respiratory inhibitors azoxystrobin and salicylhydroxamic acid (SHAM). (a) Monokaryotic biotrophic-like phase (top panel) and dikaryotic necrotrophic phase (bottom panel) were inoculated in culture medium containing the cytochrome-dependent respiratory chain (CRC) inhibitor azoxystrobin (2.5 μM), the alternative oxidase (AOX) inhibitor SHAM (5 mM) or both drugs. Control, no treatment. (b) Microscopy images show that, as expected, in the control, the biotrophic inoculum switched to the necrotrophic phase (the white arrow shows the presence of clamp connections, which are an exclusive feature of the necrotrophic hyphae). By contrast, in the presence of azoxystrobin, the transition was prevented, and the fungus maintained the biotrophic morphology, as indicated by the presence of a single nucleus per cell. All photographs were taken at 21 d post-inoculation.

Finally, we verified that AOX conferred resistance to the fungicide azoxystrobin during both mycelial stages in *M. perniciosa* (Figs 1, 4). This is because the biotrophic-like and necrotrophic hyphae were able to grow in the presence of this CRC inhibitor, but the combination of the two respiratory inhibitors (azoxystrobin and SHAM) was lethal and completely inhibited the development of these mycelia. Indeed, for the majority of other phytopathogens, such as *Mycosphaerella graminicola*, *Botrytis cinerea* and *M. oryzae*, AOX has been shown to function as an effective mechanism to rescue the fungus from oxidative stress conditions induced by azoxystrobin fungicides (Avila-Adame & Koller, 2002; Miguez *et al.*, 2004; Ishii *et al.*, 2009).

Despite the well-documented function of AOX in fungicide resistance, the nature of the environmental stress conditions in which this enzyme plays a role during the development of phytopathogens is still unknown. A primary approach to understand AOX function during the development of a plant pathogen was performed using the hemibiotrophic fungal model *M. oryzae*. However, deletion of the *aox* gene in this fungus had no effect on fungal pathogenicity or life cycle, thus refuting the hypothesis that AOX contributes to the virulence or development of this phytopathogen (Avila-Adame & Koller, 2002).

Although *M. oryzae* is a good and well-characterized model for understanding many hemibiotrophic infections, a remarkable difference exists between the life strategies of *M. oryzae* and *M. perniciosa*. Although the biotrophic phase in *M. oryzae* lasts only a few days (Ribot *et al.*, 2008), *M. perniciosa* exhibits an unusually extended biotrophic stage (60–90 d) during which the fungus is in continuous contact with the living plant tissues (Evans, 1980; Meinhardt *et al.*, 2008; Mondego *et al.*, 2008). During this extended biotrophic phase, the alternative pathway may play a central role in the survival of *M. perniciosa*, which has to deal with a hostile environment established during infection. In this regard, the *M. perniciosa*–cacao pathosystem has more in common with the long-term interactions established between animal pathogens and their hosts (e.g. sleeping sickness caused by *T. brucei*, cryptococcal disease caused by *C. neoformans*, aspergillosis caused by *A. fumigatus*, paracoccidioidomycosis caused by *P. brasiliensis*, etc.) than those described for other hemibiotrophic phytopathogenic fungi (Akhter *et al.*, 2003; Chaudhuri *et al.*, 2006; Magnani *et al.*, 2008; Hernandez *et al.*, 2011). Indeed, a parallel can be drawn between the life strategies of *M. perniciosa* and *T. brucei*. As in *M. perniciosa*, the protozoan *T. brucei* uses an AOX-dependent respiratory pathway during its infective stage inside the mammalian host. However, during its reproductive cycle inside the insect vector, the protozoan's respiration is primarily dependent on the activity of the cytochrome pathway (Chaudhuri *et al.*, 2006). This strategy seems to help *T. brucei* overcome host defense mechanisms that are mainly based on the induction of oxidative stress (Fang & Beattie, 2003).

In conclusion, this work presents a novel mechanism describing the development of phytopathogens that has a remarkable

parallel to the mechanisms evolved in animal parasites. In addition, we believe that our work contributes to the understanding of the alternative respiratory pathway, which appears to be involved in the hemibiotrophic life cycle of a phytopathogenic fungus. Finally, based on the importance of AOX in the *M. perniciosa* life cycle, we believe that this enzyme is a promising target for the development of new chemicals to disrupt *M. perniciosa* development and to effectively control WBD. Whether the enzyme also plays a role in the development of other phytopathogens, particularly in other hemibiotrophic fungi, should be the subject of future studies.

Acknowledgements

We thank Dr Gisele Monteiro and Dr Jorge Mondego for critical reading of the manuscript, Eduardo Fomighieri and Marcelo Carazzolle for assistance with bioinformatics, Dr Sérgio Uyemura for kindly providing the anti-AOX monoclonal antibody and Paula Prado for assistance with western blotting assays. This study was supported by the Fundação de Amparo à Pesquisa do Estado de São Paulo (FAPESP, 2006/50794-0 and 2009/50119-9) and Conselho Nacional de Desenvolvimento Científico e Tecnológico (CNPq, 472710/2008-7).

References

Avila-Adame C, Koller W. 2002. Disruption of the alternative oxidase gene in *Magnaporthe grisea* and its impact on host infection. *Molecular Plant–Microbe Interactions* **15**: 493–500.

Affourtit C, Albury MS, Krab K, Moore AL. 1999. Functional expression of the plant alternative oxidase affects growth of the yeast *Schizosaccharomyces pombe*. *Journal of Biological Chemistry* **274**: 6212–6218.

Affourtit C, Heaney SP, Moore AL. 2000. Mitochondrial electron transfer in the wheat pathogenic fungus *Septoria tritici*: on the role of alternative respiratory enzymes in fungicide resistance. *Biochimica et Biophysica Acta* **1459**: 291–298.

Aime MC, Phillips-Mora W. 2005. The causal agents of witches' broom and frosty pod rot of cacao (chocolate, *Theobroma cacao*) form a new lineage of Marasmiaceae. *Mycologia* **97**: 1012–1022.

Akhter S, McDade HC, Gorlach JM, Heinrich G, Cox GM, Perfect JR. 2003. Role of alternative oxidase gene in pathogenesis of *Cryptococcus neoformans*. *Infection and Immunology* **71**: 5794–5802.

Albury MS, Elliott C, Moore AL. 2009. Towards a structural elucidation of the alternative oxidase in plants. *Physiologia Plantarum* **137**: 316–327.

Berruyer R, Poussier S, Kankanala P, Mosquera G, Valent B. 2006. Quantitative and qualitative influence of inoculation methods on *in planta* growth of rice blast fungus. *Phytopathology* **96**: 346–355.

Bradford MM. 1976. A rapid and sensitive method for the quantitation of microgram quantities of protein utilizing the principle of protein–dye binding. *Analytical Biochemistry* **72**: 248–254.

Brown GC. 1999. Nitric oxide and mitochondrial respiration. *Biochimica et Biophysica Acta* **1411**: 351–369.

Brown GC, Borutaite V. 2002. Nitric oxide inhibition of mitochondrial respiration and its role in cell death. *Free Radical Biology and Medicine* **33**: 1440–1450.

Ceita GO, Macêdo JNA, Santos TB, Alemanno L, Da Silva Gesteira A, Micheli F, Mariano AC, Gramacho KP, Da Costa Silva D, Meinhardt LW *et al.* 2007. Involvement of calcium oxalate degradation during programmed cell death in *Theobroma cacao* tissues triggered by the hemibiotrophic fungus *Moniliophthora perniciosa*. *Plant Science* **173**: 106–117.

Chaudhuri M, Ott RD, Hill GC. 2006. Trypanosome alternative oxidase: from molecule to function. *Trends in Parasitology* **22**: 484–491.

Day PR, Anagnostakis SL. 1971. Corn smut dikaryon in culture. *Nature: New Biology* **231**: 19–20.

Dean RA, Talbot NJ, Ebbole DJ, Farman ML, Mitchell TK, Orbach MJ, Thon M, Kulkarni R, Xu JR, Pan H *et al.* 2005. The genome sequence of the rice blast fungus *Magnaporthe grisea*. *Nature* **434**: 980–986.

Delledonne M, Xia Y, Dixon RA, Lamb C. 1998. Nitric oxide functions as a signal in plant disease resistance. *Nature* **394**: 585–588.

Dufresne M, Perfect S, Pellier AL, Bailey JA, Langin T. 2000. A GAL4-like protein is involved in the switch between biotrophic and necrotrophic phases of the infection process of *Colletotrichum lindemuthianum* on common bean. *Plant Cell* **12**: 1579–1590.

Elthon TE, McIntosh L. 1987. Identification of the alternative terminal oxidase of higher plant mitochondria. *Proceedings of the National Academy of Sciences, USA* **84**: 8399–8403.

Elthon TE, Nickels RL, McIntosh L. 1989. Monoclonal antibodies to the alternative oxidase of higher plant mitochondria. *Plant Physiology* **89**: 1311–1317.

Evans HC. 1980. Pleomorphism in *Crinipellis perniciosa*, causal agent of Witches' broom disease of cocoa. *Transactions of the British Mycological Society* **74**: 515–526.

Fang J, Beattie DS. 2003. Alternative oxidase present in procyclic *Trypanosoma brucei* may act to lower the mitochondrial production of superoxide. *Archives of Biochemistry and Biophysics* **414**: 294–302.

Frias G, Purdy LH, Schmidt RA. 1995. An inoculation method for evaluating resistance of cacao to *Crinipellis perniciosa*. *Plant Disease* **79**: 787–791.

Glazebrook J. 2005. Contrasting mechanisms of defense against biotrophic and necrotrophic pathogens. *Annual Review of Phytopathology* **43**: 205–227.

Gredilla R, Grief J, Osiewacz HD. 2006. Mitochondrial free radical generation and lifespan control in the fungal aging model *Podospora anserina*. *Experimental Gerontology* **41**: 439–447.

Griffith GW, Hedger JN. 1993. A novel method for producing basidiocarps of the cocoa pathogen *Crinipellis perniciosa* using a bran–vermiculite medium. *European Journal of Plant Pathology* **99**: 227–230.

Griffith GW, Hedger JN. 1994. Dual culture of *Crinipellis perniciosa* and potato callus. *European Journal of Plant Pathology* **100**: 371–379.

Hernandez RO, Gonzalez A, Almeida AJ, Tamayo D, Garcia AM, Restrepo A, McEwen JG. 2011. Alternative oxidase mediates pathogen resistance in *Paracoccidioides brasiliensis* infection. *PLoS Neglected Tropical Diseases* **5**: e1353.

Ishii H, Fountaine J, Chung WH, Kansako M, Nishimura K, Takahashi K, Oshima M. 2009. Characterization of QoI-resistant field isolates of *Botrytis cinerea* from citrus and strawberry. *Pest Management Science* **65**: 916–922.

Joseph-Horne T, Hollomon DW, Wood PM. 2001. Fungal respiration: a fusion of standard and alternative components. *Biochimica et Biophysica Acta* **1504**: 179–195.

Livak KJ, Schmittgen TD. 2001. Analysis of relative gene expression data using real-time quantitative PCR and the $2^{-\Delta\Delta}C_T$ method. *Methods* **25**: 402–408.

Magnani T, Soriani FM, Martins VdP, Policarpo AC, Sorgi CA, Faccioli LH, Curti C, Uyemura SA. 2008. Silencing of mitochondrial alternative oxidase gene of *Aspergillus fumigatus* enhances reactive oxygen species production and killing of the fungus by macrophages. *Journal of Bioenergetics and Biomembranes* **40**: 631–636.

Maxwell DP, Wang Y, McIntosh L. 1999. The alternative oxidase lowers mitochondrial reactive oxygen production in plant cells. *Proceedings of the National Academy of Sciences, USA* **96**: 8271–8276.

McDonald AE. 2009. Alternative oxidase: what information can protein sequence comparisons give us? *Physiologia Plantarum* **137**: 328–341.

McDonald AE, Vanlerberghe GC, Taples JF. 2009. Alternative oxidase in animals: unique characteristics and taxonomic distribution. *Journal of Experimental Biology* **212**: 2627–2634.

Meinhardt LW, Bellato CM, Rincones J, Azevedo RA, Cascardo JC, Pereira GAG. 2006. *In vitro* production of biotrophic-like cultures of *Crinipellis perniciosa*, the causal agent of witches' broom disease of *Theobroma cacao*. *Current Microbiology* **52**: 191–196.

Meinhardt LW, Rincones J, Bailey BA, Aime MC, Griffith GW, Zhang D, Pereira GAG. 2008. *Moniliophthora perniciosa*, the causal agent of witches' broom disease of cacao: what's new from this old foe? *Molecular Plant Pathology* **9**: 577–588.

Miguez M, Reeve C, Wood PM, Hollomon DW. 2004. Alternative oxidase reduces the sensitivity of *Mycosphaerella graminicola* to QOI fungicides. *Pest Management Science* **60**: 3–7.

Minagawa N, Koga S, Nakano M, Sakajo S, Yoshimoto A. 1992. Possible involvement of superoxide anion in the induction of cyanide-resistant respiration in *Hansenula anomala*. *FEBS Letters* **302**: 217–219.

Mondego JM, Carazzolle MF, Costa GG, Formighieri EF, Parizzi LP, Rincones J, Cotomacci C, Carraro DM, Cunha AF, Carrer H *et al.* 2008. A genome survey of *Moniliophthora perniciosa* gives new insights into witches' broom disease of cacao. *BMC Genomics* **9**: 548.

Munch S, Lingner U, Floss DS, Ludwig N, Sauer N, Deising HB. 2008. The hemibiotrophic lifestyle of *Colletotrichum species*. *Journal of Plant Physiology* **165**: 41–51.

Niella G, Resende ML, Castro HA, de Carvalho GA, Silva LHCP. 1999. Improving the methodology of artificial production of basidiomata of *Crinipellis perniciosa*/Aperfeiçoamento da metodologia de produção artificial de basidiocarpos de *Crinipellis perniciosa*. *Fitopatologia Brasileira* **24**: 523–527.

Nittler MP, Hocking-Murray D, Foo CK, Sil A. 2005. Identification of *Histoplasma capsulatum* transcripts induced in response to reactive nitrogen species. *Molecular Biology of the Cell* **16**: 4792–4813.

Pellier AL, Lauge R, Veneault-Fourrey C, Langin T. 2003. CLNR1, the AREA/NIT2-like global nitrogen regulator of the plant fungal pathogen *Colletotrichum lindemuthianum* is required for the infection cycle. *Molecular Microbiology* **48**: 639–655.

Purdy LH, Schmidt RA. 1996. Status of cacao witches' broom: biology, epidemiology, and management. *Annual Review of Phytopathology* **34**: 573–594.

Ribot C, Hirsch J, Balzergue S, Tharreau D, Notteghem JL, Lebrun MH, Morel JB. 2008. Susceptibility of rice to the blast fungus, *Magnaporthe grisea*. *Journal of Plant Physiology* **165**: 114–124.

Rincones J, Scarpari LM, Carazzolle MF, Mondego JM, Formighieri EF, Barau JG, Costa GG, Carraro DM, Brentani HP, Vilas-Boas LA *et al.* 2008. Differential gene expression between the biotrophic-like and saprotrophic mycelia of the witches' broom pathogen *Moniliophthora perniciosa*. *Molecular Plant–Microbe Interactions* **21**: 891–908.

Romero-Puertas MC, Perazzolli M, Zago ED, Delledonne M. 2004. Nitric oxide signalling functions in plant–pathogen interactions. *Cellular Microbiology* **6**: 795–803.

Ruy F, Vercesi AE, Kowaltowski AJ. 2006. Inhibition of specific electron transport pathways leads to oxidative stress and decreased *Candida albicans* proliferation. *Journal of Bioenergetics and Biomembranes* **38**: 129–135.

Sakajo S, Minagawa N, Yoshimoto A. 1993. Characterization of the alternative oxidase protein in the yeast *Hansenula anomala*. *FEBS Letters* **318**: 310–312.

Scarpari LM, Meinhardt LW, Mazzafera P, Pomella AW, Schiavinato MA, Cascardo JC, Pereira GAG. 2005. Biochemical changes during the development of witches' broom: the most important disease of cocoa in Brazil caused by *Crinipellis perniciosa*. *Journal of Experimental Botany* **56**: 865–877.

Seligman K, Saviani EE, Oliveira HC, Pinto-Maglio CA, Salgado I. 2008. Floral transition and nitric oxide emission during flower development in *Arabidopsis thaliana* is affected in nitrate reductase-deficient plants. *Plant and Cell Physiology* **49**: 1112–1121.

Siedow JN, Umbach AL. 2000. The mitochondrial cyanide-resistant oxidase: structural conservation amid regulatory diversity. *Biochimica et Biophysica Acta* **1459**: 432–439.

Spanu P, Kamper J. 2010. Genomics of biotrophy in fungi and oomycetes – emerging patterns. *Current Opinion in Plant Biology* **13**: 409–414.

Stenmark P, Nordlund P. 2003. A prokaryotic alternative oxidase present in the bacterium *Novosphingobium aromaticivorans*. *FEBS Letters* **552**: 189–192.

Tanton LL, Nargang CE, Kessler KE, Li QH, Nargang FE. 2003. Alternative oxidase expression in *Neurospora crassa*. *Fungal Genetics and Biology* **39**: 176–190.

Van Aken O, Giraud E, Clifton R, Whelan J. 2009. Alternative oxidase: a target and regulator of stress responses. *Physiologia Plantarum* **137**: 354–361.

Vanlerberghe GC, Cvetkovska M, Wang J. 2009. Is the maintenance of homeostatic mitochondrial signaling during stress a physiological role for alternative oxidase? *Physiologia Plantarum* **137**: 392–406.

Vanlerberghe GC, McIntosh L. 1994. Mitochondrial electron transport regulation of nuclear gene expression. Studies with the alternative oxidase gene of tobacco. *Plant Physiology* **105**: 867–874.

Vanlerberghe GC, McIntosh L. 1997. Alternative oxidase: from gene to function. *Annual Review of Plant Physiology and Plant Molecular Biology* **48**: 703–734.

Wagner AM, Krab K, Wagner MJ, Moore AL. 2008. Regulation of thermogenesis in flowering Araceae: the role of the alternative oxidase. *Biochimica et Biophysica Acta* **1777**: 993–1000.

Wilson RA, Talbot NJ. 2009. Under pressure: investigating the biology of plant infection by *Magnaporthe oryzae*. *Nature Reviews: Microbiology* **7**: 185–195.

Yukioka H, Inagaki S, Tanaka R, Katoh K, Miki N, Mizutani A, Masuko M. 1998. Transcriptional activation of the alternative oxidase gene of the fungus *Magnaporthe grisea* by a respiratory-inhibiting fungicide and hydrogen peroxide. *Biochimica et Biophysica Acta* **1442**: 161–169.

Supporting Information

Additional supporting information may be found in the online version of this article.

Fig. S1 Measurement of whole cell respiratory rates of the main life stages of *Moniliophthora perniciosa*.

Fig. S2 Effects of *n*-propyl gallate on the *ex planta* development of *Moniliophthora perniciosa*.

Methods S1 Measurement of oxygen consumption by the main life stages of *Moniliophthora perniciosa*.

Please note: Wiley-Blackwell are not responsible for the content or functionality of any supporting information supplied by the authors. Any queries (other than missing material) should be directed to the *New Phytologist* Central Office.

SUPPLEMENTARY METHODS

Measurement of oxygen consumption by the main life stages of *M. perniciosa*

We evaluated the oxygen consumption profile by whole cells of the different developmental stages of *M. perniciosa* (basidiospores, basidiomata, biotrophic and necrotrophic mycelia). Oxygen consumption was determined at 27^{o}C using a Clark-type electrode connected to an Oxygraph unit (Hansatech). The experiments were performed using 2.5x10^{6} spores, the whole mushroom structure (weighing about 55 mg), and approximately 60 mg of each fungal mycelium (biotrophic and necrotrophic mycelia). These fungal structures were individually added to the closed reaction chamber containing 1 mL of culture medium (2 g/L malt extract, 5 g/L yeast extract, and 50ml/L glycerol). AOX activity was measured in the presence of the CRC inhibitor potassium cyanide (1 mM) as the oxygen consumption inhibited by 200 μM *n*-propyl gallate.

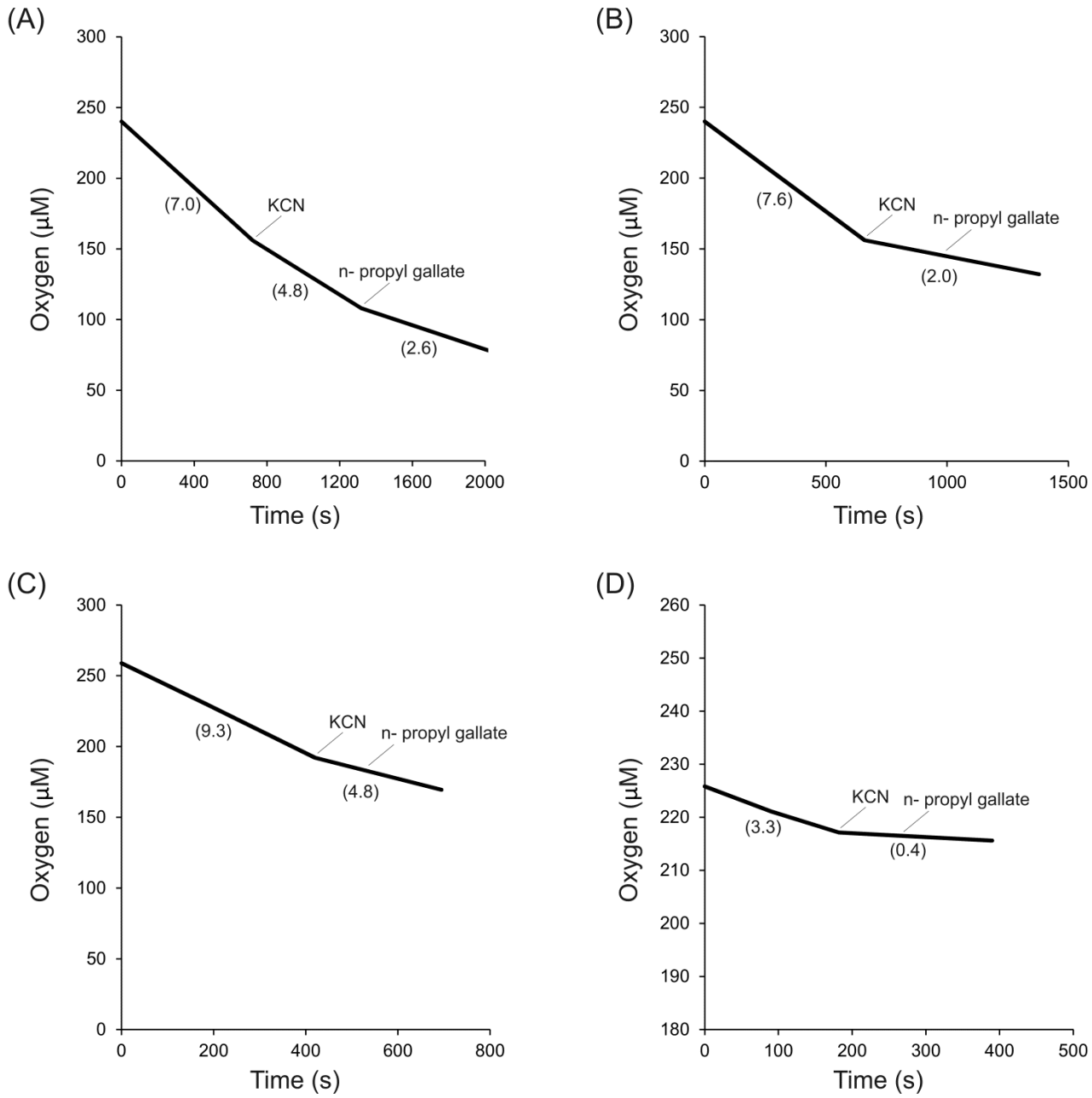

Supplemental Figure 1. Measurement of whole cell respiratory rates of the main life stages of *M. perniciosa*. (A) Biotrophic-like mycelium, (B) necrotrophic mycelium, (C) basidiomata and (D) basidiospores. Oxygen consumption was evaluated in response to 1 mM potassium cyanide (KCN, a CRC inhibitor), followed by addition of 200 µM *n*-propyl gallate (AOX inhibitor). Oxygen consumption by the biotrophic-like mycelium was the sole condition affected by *n*-propyl gallate, thus confirming that the alternative respiratory chain is active during this developmental stage of *M. perniciosa*.

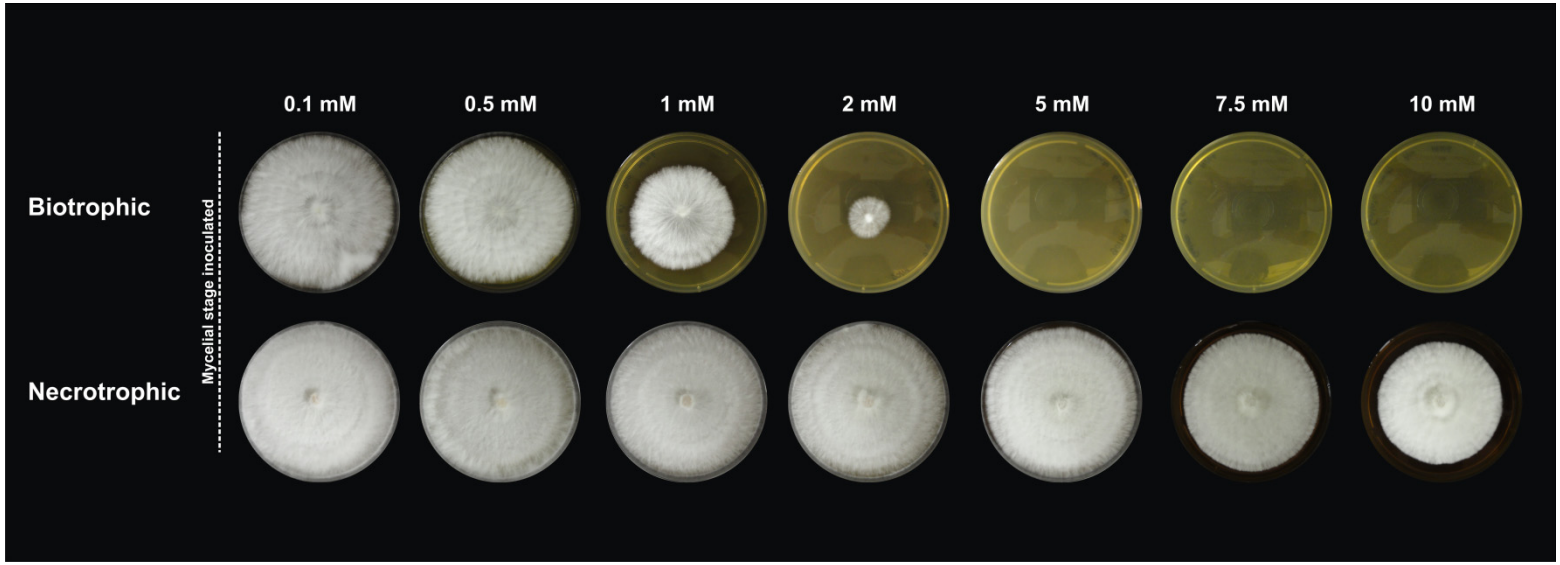

Supplemental Figure 2. Effects of *n*-propyl gallate on the *ex planta* development of *M. perniciosa*. Monokaryotic biotrophic-like phase (upper panel) and dikaryotic necrotrophic phase (lower panel) were inoculated in culture media containing the AOX inhibitor *n*-propyl gallate in a range of different concentrations (from 0.1 to 10 mM). The biotrophic-like mycelium shows a higher sensitivity to *n*-propyl gallate in relation to the necrotrophic mycelium, further confirming the role of AOX on the development of the monokaryotic hyphae of *M. perniciosa*.

CONSIDERAÇÕES FINAIS

O Projeto Genoma Vassoura de Bruxa foi iniciado em 2000 com o principal objetivo de expandir nosso conhecimento a respeito dessa importante doença do cacaueiro e, eventualmente, propor soluções para o problema. Os primeiros trabalhos elucidaram aspectos básicos da biologia do fungo *M. perniciosa* e do cacaueiro, sendo responsáveis pelo estabelecimento de bases para as pesquisas atuais. Com o grande avanço da genômica e o amadurecimento da linha de pesquisa, iniciamos em 2009 a construção de um abrangente banco de dados de transcriptomas visando à realização de análises de expressão gênica em larga escala.

Esta iniciativa, posteriormente denominada “Atlas Transcriptômico da Vassoura de Bruxa”, pode ser considerada um importante avanço para o estudo dessa doença. Com base nos dados obtidos com o Atlas Transcriptômico, diferentes projetos estão sendo iniciados por pesquisadores que integram nosso grupo de pesquisa. Como exemplo, podemos citar a resolução da estrutura de possíveis proteínas efetoras de *M. perniciosa*, as quais devem ter um papel central na virulência deste patógeno. Além disso, genes que participam de uma potencial via metabólica para a síntese do hormônio auxina estão sendo avaliados em *M. perniciosa* com base nos dados de expressão gênica. Novas pesquisas também incluem a identificação e caracterização funcional de mecanismos de resistência a fungicidas, como também de outros genes de virulência de *M. perniciosa*. Ainda, o Atlas Transcriptômico tem servido de base para um grande projeto em genômica comparativa desenvolvido em nosso laboratório. Com base na análise de transcriptomas de ramos e frutos infectados, este projeto buscará identificar estratégias de virulência adotadas por *M. perniciosa* durante a infecção de tecidos específicos do cacaueiro. Ainda, este trabalho realizará análises de genomas e transcriptomas para identificar possíveis mecanismos envolvidos na adaptação deste patógeno a hospedeiros específicos (cacaueiro e tomateiro). Os dados de genômica e trancriptômica de *M. perniciosa* serão ainda comparados com dados obtidos para a espécie proximamente próxima *M. roreri* visando à elucidação de diferenças e semelhanças entre estes dois patógenos do cacaueiro.

Os resultados apresentados nesta tese expandem significativamente nosso atual conhecimento quanto à base molecular da vassoura de bruxa. Em particular, a identificação da ocorrência de um processo de senescência em ramos infectados é extremamente importante e abre novas perspectivas quanto ao entendimento dos mecanismos que regulam o desenvolvimento da vassoura de bruxa e das estratégias de patogenicidade adotadas por fungos hemibiotróficos. Novos trabalhos deverão ser realizados visando-se correlacionar o processo de senescência no hospedeiro com a transição para a fase necrotrófica em *M. perniciosa*. É interessante destacar que nossos resultados indicam que a estratégia de infecção adotada por *M. perniciosa* diferencia-se consideravelmente em relação à de outros fitopatógenos bem estudados. A ocorrência de um processo de senescência prematura no hospedeiro não é uma característica reportada em outras doenças e parece ser um evento importante na infecção do fungo *M. perniciosa* e resultante de sua longa fase biotrófica. Neste sentido, a utilização da enzima AOX durante a interação com o tecido vivo do cacaueiro também é bastante interessante e se relaciona diretamente com a necessidade do patógeno se proteger de moléculas tóxicas produzidas pela planta durante um longo período de interação biotrófica.

De forma geral, os resultados apresentados exemplificam o grande amadurecimento que o Projeto Genoma Vassoura de Bruxa vem alcançando nos últimos anos. Em especial, uma possível estratégia para o controle da doença foi desenvolvida com base no estudo da proteína AOX de *M. perniciosa.* Novas análises ainda devem ser realizadas para a comprovação da eficácia desta estratégia em campo, porém o estudo é um importante avanço nesse sentido. Ainda, os dados obtidos com o Atlas Transcriptômico da Vassoura de Bruxa apontam uma série de outras proteínas com possível papel no estabelecimento da doença, incluindo a quitinase MpChi e proteínas MpPR-1, por exemplo. A caracterização funcional destas proteínas está sendo executada em nosso laboratório de forma que as hipóteses elaboradas possam ser comprovadas. O desenvolvimento de técnicas que permitam a manipulação genética de *M. perniciosa* é de grande importância para a caracterização funcional de genes de interesse e, ao fazer uso das informações fornecidas pelo

Atlas Transcriptômico da Vassoura de Bruxa, poderá ser uma ferramenta de grande utilidade para as pesquisas relacionadas à interação entre o cacaueiro e o fungo *M. perniciosa*.

Anexo I

The Crystal Structure of Necrosis- and Ethylene-Inducing Protein 2 from the Causal Agent of Cacao's Witches' Broom Disease Reveals Key Elements for Its Activity

Gustavo Zaparoli, Mario R.O. Barsottini, Juliana F.de Oliveira, Fabio Dyszy, Paulo José P.L. Teixeira, Joan G. Barau, Odalys Garcia, Antonio José Costa-Filho, Andre L.B. Ambrosio, Gonçalo A.G. Pereira, Sandra M.G. Dias

Trabalho publicado na revista *Biochemistry*, Outubro de 2011, Vol. 50, pp. 9901-9910.

APRESENTAÇÃO

Três genes codificantes de proteínas da família NEP (*Necrosis- and Ethylene-Inducing Protein*) foram identificados no genoma do fungo *Moniliophthora perniciosa* logo no início do Projeto Genoma Vassoura de Bruxa. Ensaios com proteínas recombinantes demostraram que ao menos duas NEPs são capazes de induzir necrose nos tecidos do cacaueiro. Desde então, estas proteínas passaram a ser intensamente estudadas por estarem diretamente relacionadas aos sintomas observados na doença. Sequenciamentos posteriores do genoma de *M. perniciosa* e a construção do Atlas Transcriptômico da Vassoura de Bruxa revelaram a existência de cinco genes *NEP* neste patógeno. Neste trabalho, verificamos que apenas um destes genes (*NEP2*) é distintivamente expresso durante o estágio de necrose do tecido infectado do cacaueiro. Com base nesse resultado, a estrutura tridimensional da proteína NEP2 foi resolvida e, juntamente com ensaios de atividade específicos, revelaram resíduos essenciais para a atividade desta proteína.

BIOCHEMISTRY
including biophysical chemistry & molecular biology

Article

pubs.acs.org/biochemistry

The Crystal Structure of Necrosis- and Ethylene-Inducing Protein 2 from the Causal Agent of Cacao's Witches' Broom Disease Reveals Key Elements for Its Activity

Gustavo Zaparoli,[†,‡] Mario Ramos de Oliveira Barsottini,[†,‡] Juliana Ferreira de Oliveira,[‡] Fabio Dyszy,[§] Paulo José Pereira Lima Teixeira,[†] Joan Grande Barau,[†] Odalys Garcia,[†] Antonio José Costa-Filho,[§] Andre Luis Berteli Ambrosio,[‡] Gonçalo Amarante Guimarães Pereira,[†,‡] and Sandra Martha Gomes Dias*[,‡]

[†]Departamento de Genética e Evolução, IB/UNICAMP, C.P. 6109, 13083-970 Campinas, SP, Brazil

[‡]Laboratório Nacional de Biociências-LNBio, Associação Brasileira de Tecnologia de Luz Síncrotron, 13083-970 Campinas, SP, Brazil

[§]Grupo de Biofísica Molecular Sérgio Mascarenhas, Instituto de Física de São Carlos, Universidade de São Paulo, C.P. 369, 13560-970 São Carlos, SP, Brazil

Supporting Information

ABSTRACT: The necrosis- and ethylene-inducing peptide 1 (NEP1)-like proteins (NLPs) are proteins secreted from bacteria, fungi and oomycetes, triggering immune responses and cell death in dicotyledonous plants. Genomic-scale studies of *Moniliophthora perniciosa*, the fungus that causes the Witches' Broom disease in cacao, which is a serious economic concern for South and Central American crops, have identified five members of this family (termed MpNEP1−5). Here, we show by RNA-seq that MpNEP2 is virtually the only NLP expressed during the fungus infection. The quantitative real-time polymerase chain reaction results revealed that MpNEP2 has an expression pattern that positively correlates with the necrotic symptoms, with MpNEP2 reaching its highest level of expression at the advanced necrotic stage. To improve our understanding of MpNEP2's molecular mechanism of action, we determined the crystallographic structure of MpNEP2 at 1.8 Å resolution, unveiling some key structural features. The implications of a cation coordination found in the crystal structure were explored, and we show that MpNEP2, in contrast to another previously described member of the NLP family, NLP_{Pya} from *Pythium aphanidermatum*, does not depend on an ion to accomplish its necrosis- and electrolyte leakage-promoting activities. Results of site-directed mutagenesis experiments confirmed the importance of a negatively charged cavity and an unforeseen hydrophobic β-hairpin loop for MpNEP2 activity, thus offering a platform for compound design with implications for disease control. Electron paramagnetic resonance and fluorescence assays with MpNEP2 performed in the presence of lipid vesicles of different compositions showed no sign of interaction between the protein and the lipids, implying that MpNEP2 likely requires other anchoring elements from the membrane to promote cytolysis or send death signals.

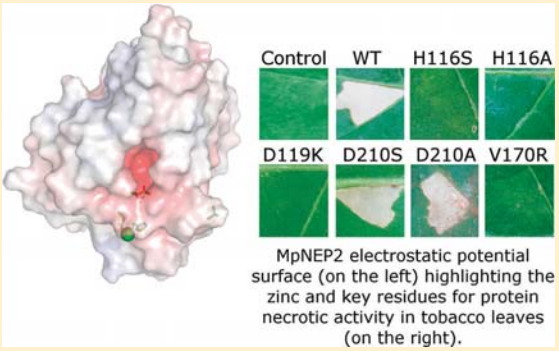

MpNEP2 electrostatic potential surface (on the left) highlighting the zinc and key residues for protein necrotic activity in tobacco leaves (on the right).

Witches' Broom disease of cacao (*Theobroma cacao*), the raw material for chocolate production, is well-regarded as one of the most important phytopathological problems to afflict the southern hemisphere in recent decades, with devastating consequences to the agro-economy of the affected countries.[1] In Brazil, this disease started as an endemic disease within the Amazon region, but after an outbreak in 1989, it was introduced into the largest area of cacao production, the state of Bahia.[2] A severe decrease in the production of cacao then followed, and in less than a decade, Brazil shifted from being the second largest cacao exporter to being a cacao importer. World chocolate production could fall dramatically if this disease, which has devastated South and Central American crops over the past 20 years, were to spread to some of the world's other cacao-producing regions.[3]

Moniliophthora perniciosa, the causal agent of Witches' Broom disease, is a basidiomycete with a hemibiotrophic life cycle.[4,5] Initially, mononucleated basidiospores, dispersed by the wind and rain at night, germinate on rapidly growing tissues, such as meristems and young pods, initiating the biotrophic phase of the disease. When emerging branches are infected, the disease is characterized by an impressive growth of new shoots (green broom), which probably acts as a nutritional sink.[5,6] Eight to twelve weeks after the initial infection, the tissues begin to senesce and are colonized inter- and

Received: August 9, 2011
Revised: October 13, 2011
Published: October 14, 2011

dx.doi.org/10.1021/bi201253b | *Biochemistry* 2011, 50, 9901−9910

intracellularly by the saprotrophic mycelia of *M. perniciosa*. The transition from biotrophic to necrotrophic involves changes not only in the plant but also in the biology of the vegetative mycelia.[7−9] The senescing brooms turn brown, forming the typical necrotic dry broom structures of this disease, which remain attached to the plant. After a dry period of 3−9 months, the brooms produce basidiocarps that release spores into the air and reinitiate the disease cycle.[5] Infected plants produce fewer and lower-quality fruits, compromising the amount of cocoa beans produced.[1]

In recent years, efforts have been made toward understanding the infection process at a molecular level and its correlation with the fungus life cycle.[3] Genomic-scale studies have identified key components resulting from the *M. perniciosa*−cacao interaction. Among them, five DNA sequences encoding putative copies of proteins in the fungus that are similar to the necrosis- and ethylene-inducing peptide 1 (NEP1)-like proteins (NLPs) were identified and have been termed MpNEP1−5.[10,11] NLPs are proposed to perform dual functions in the plant−pathogen interactions, acting both as triggers of immune responses and as toxin-like virulence factors known to promote leaf necrosis.[12] The family contains members from the genomes of more than 50 organisms, including fungi, oomycetes, and bacteria, with either saprotrophic or hemibiotrophic lifestyles.[13] Members of the NLP family share a high degree of sequence similarity, containing a secretory signal sequence, a conserved seven-amino acid motif (GHRHDWE), and two or four conserved cysteine residues. The proteins from this family induce a hypersensitive-like death response in a variety of dicotyledonous plants but not in any known monocotyledonous plants.[14]

Here, we provide evidence that MpNEP2 is strongly expressed during the necrotic stage of the fungus infection. To understand the molecular mechanism of action of MpNEP2, we determined its crystallographic structure at 1.8 Å resolution. The crystal structure data combined with the results of site-directed mutagenesis experiments and functional assays highlighted the importance of the conserved seven-amino acid motif (GHRHDWE) and an unforeseen hydrophobic loop in the necrotic process, offering the basis for the design of compounds with the potential to inhibit the protein. Moreover, to test MpNEP2's potential role as a lipid-binding protein, we performed electron paramagnetic resonance (EPR) studies of four different headgroup and acyl chain spin probe phospholipid vesicles added to MpNEP2, as well as tryptophan fluorescence measurements of MpNEP2 added to equivalent nonlabeled vesicles. The results indicated no change in the EPR spectra of the tested lipids and no significant shift in the tryptophan intensity or wavelength emission peak when the protein was added to the vesicles described above, raising the possibility that, if the protein interacts with the cell membrane to perform its necrotic activity, it likely requires some other anchoring element.

EXPERIMENTAL PROCEDURES

RNA-seq and Quantitative Polymerase Chain Reaction (PCR). *T. cacao* var. Comum was cultivated in a greenhouse under controlled temperature and humidity conditions (from 22 to 28 °C and >50%, respectively). Two-month-old seedlings were then infected with *M. perniciosa* spores as described previously.[15] RNA-seq libraries that were produced as part of the WBD Transcriptome Atlas were inspected for the expression of NLP genes during the *in planta* development of *M. perniciosa*, from the green broom to the dry broom stage (where the plant is virtually consumed by the fungus). The RNA-seq methodology will be described elsewhere (P. L. Teixeira, manuscript in preparation). For the qPCR assays, plant material was collected at five different stages of the disease progression, as follows: no symptoms (10 DAI), first symptoms (swelling, 20 DAI), mature green broom (green broom, 30 DAI), first necrosis symptoms (initial necrosis, 60 DAI), and advanced necrosis (100 DAI). RNA extraction was performed as described by Azevedo and colleagues with minor modifications;[16] the cDNA was synthesized using a SuperScript VILO cDNA Synthesis Kit (Invitrogen), and real-time PCR was conducted according to the Delta-Delta-CT method[17] using primers F-AAGGCAAGACTGCTCTGGTCTA and R-CTTCCTTTCCATCGTCCTTCTCGT and the tubulin gene for endogenous housekeeping.

Heterologous MpNEP2 Production. We constructed a truncated form of MpNEP2 (GenBank accession number EF114673.1) that had its secretion signaling peptide deleted (residues Met1−Ala17). This construct (hereafter termed MpNEP2) was cloned into a modified version of the pETSUMO plasmid (Invitrogen), which contains a histidine tag at its N-terminus, and was used to transform *Escherichia coli* Origami 2 cells (Merck). The cells were lysed, and the clarified soluble fraction was purified by a two-step procedure starting with immobilized metal ion affinity chromatography (IMAC) using a Co^{2+}-charged TALON resin (BD Biosciences) pre-equilibrated with 30 mM Tris-HCl (pH 8.0), 150 mM NaCl, 5 mM imidazole, 0.3 mM TCEP [tris(2-carboxyethyl)phosphine hydrochloride], and 1 mM PMSF (phenylmethanesulfonyl fluoride). The resin was washed extensively with this solution and then incubated overnight at room temperature with an appropriate amount of protease ULP-1 for His-SUMO tag removal. The cleaved protein was eluted from the resin and loaded onto a HiLoad Superdex 75 16/60 gel filtration column (GE Healthcare) pre-equilibrated in 30 mM Tris-HCl (pH 8.0) and 50 mM NaCl. The eluted protein was concentrated to 19 mg/mL as judged by its UV_{280} absorption and calculated coefficient extinction[18] and used for crystallization screens and functional assays. Mutants were obtained with the QuikChange Site-Directed Mutagenesis Kit (Stratagene) by following the manufacturer's instructions and purified according to the protocol developed for the wild-type protein.

X-ray Crystallography. The crystallization experiments were performed at 18 °C using the conventional sitting drop vapor diffusion technique. The drops were made by mixing equal parts of protein and well solution, the latter containing 100 mM sodium acetate (pH 5.0), 20% PEG 6000, and 200 mM $ZnCl_2$. Before data collection at cryogenic temperatures, the harvested crystals were cryoprotected with 5% ethylene glycol added to the mother liquor. A substantially complete X-ray diffraction data set for MpNEP2 was obtained with beamline D03B-MX1 at the Brazilian National Synchrotron Laboratory at a wavelength of 1.608 Å.

Phasing and Refinement. The X-ray diffraction data were processed using Mosflm[19] and merged and scaled with SCALA.[20] The first set of phases was obtained by the molecular replacement technique as implemented in Phaser,[21] using the *Pythium aphanidermatum* NEP_{Pya} monomer (deposited as Protein Data Bank entry 3gnz[22]) as the search model. Following molecular replacement, a density modification was performed using Parrot, which is part of the CCP4 suite,[23,24] and the improved map was then subjected to an automated

dx.doi.org/10.1021/bi201253b | *Biochemistry* 2011, 50, 9901−9910

interpretation with the ARPwARP routine.[25] The positional and *B* factor refinement cycles were performed with Refmac.[26] The manual building of the extra portions and real space refinement, including a Fourier electron density map inspection, were performed with Coot.[27] The solvent water molecules, which were treated as oxygen atoms, were added using the appropriate Coot routine. FFT, part of the CCP4 suite,[24,28] was used to calculate the Fourier anomalous electron density map. The overall stereochemical quality of the final model and the agreement between the model and the experimental data were assessed with Molprobit[29] and the appropriate Coot routines.

Circular Dichroism. MpNEP2 (6 μM, wild type and mutants) was dialyzed against 4 mM sodium phosphate buffer (pH 7.2), and when required, EDTA (62.5 μM) or both EDTA (62.5 μM) and $CaCl_2$ with $ZnCl_2$ (120 μM) were added. The samples were analyzed by far-UV CD spectroscopy (190−260 nm) with a resolution of 1 nm using a JASCO J810 spectropolarimeter. Each data point was generated by averaging 10 accumulations. The secondary structure was estimated on a DICHROWEB interface[30] using the CDSSTR method[30] and Reference Protein Set 4. The mean residue molar ellipticity at 218 nm (MRE $[\theta]_{218}$) was also collected at temperatures ranging from 20 to 60 °C at intervals of 1 °C. The apparent melting temperature (T_{Mapp}), which is the temperature at which the molar ellipticity is between the folded and unfolded states, was used to estimate the stability of the wild-type and mutant protein. The data were analyzed using Origin (OriginLab Corp.) for a sigmoidal fit and an inflection point calculation (T_{Mapp}).

Dynamic Light Scattering. A DynaPro MSTC014 (Protein Solutions Inc., Lakewood, NJ) dynamic light scattering instrument was used to monitor the oligomeric state of MpNEP2 at concentrations between 220 and 260 μM in 4 mM sodium phosphate buffer (pH 7.2) in the absence or presence of either EDTA, $CaCl_2$, or $ZnCl_2$ (1 mM). The assays were performed at 20 °C with an acquisition time of 5−8 s using a 70 μL cuvette and 50−100% laser power. Three hundred acquisitions were obtained in a single measurement, and a PBS solution was used for the calculation of the hydrodynamic radii (R_H) by DYNAMICS version 6.1 (Protein Solutions Inc.). The theoretical R_H value for the monomeric protein was calculated by HYDROPRO[31] using the crystallographic model.

Infiltration of Purified MpNEP2 into Tobacco Leaves. The control solutions, wild-type MpNEP2 and mutants diluted to 500 nM in 10 mM sodium phosphate buffer (pH 7.2), were injected into leaves of *Nicotiana tabacum* var. Petite Havana (4−6 weeks old) as described previously.[11] The infiltration of MpNEP2 in BAPTA-containing buffer (10 mM), a specific calcium ion chelator, was preceded by the infiltration of the same leaves with 10 mM sodium phosphate buffer (pH 7.2) and 10 mM BAPTA. The formation of lesions was documented 5 days after the infiltration of MpNEP2.

Electrolyte Leakage Assay. The electrolyte leakage assay was conducted according to the method of Ottmann and colleagues[22] with modifications. The control solutions, containing purified wild-type or mutant MpNEP2, were injected into tobacco leaves as described above. The infiltrated area was immediately removed, cut into pieces of approximately 0.25 cm^2, and washed with distilled water. After 30 min, the pieces were transferred to fresh Milli-Q water (20 per replica in triplicate), and the intracellular content leakage was measured with a conductivity meter (WTW LF 330, Wissenschaftlich-Technische Werkstätten GmbH) at different time points.

Electron Paramagnetic Resonance (EPR) Spectroscopy. The phospholipids 1,2-dioleoyl-*sn*-glycero-3-phosphocholine (DOPC), 1-palmitoyl-2-oleoyl-*sn*-glycero-3-phospho(1′-*rac*-glycerol) (POPG), 1-palmitoyl-2-oleoyl-*sn*-glycero-3-phospho-L-serine (POPS), 1,2-dioleoyl-*sn*-glycero-3-phosphoethanolamine (DOPE), L-α-phosphatidylcholine from egg yolk (egg PC), and the EPR probes 1-palmitoyl-2-stearoyl(16-doxyl)-*sn*-glycero-3-phosphocholine (16-PC) and 1,2-dipalmitoyl-*sn*-glycero-3-phospho(tempo)choline (DPPTC) were purchased from Avanti Polar Lipids (Alabaster, AL). These lipids were chosen because of their high natural abundance in cell membranes.[32,33] The multilamellar liposomes were prepared by drying appropriate amounts of chloroform stock solutions of DOPC, DOPC and POPG (2:1 molar ratio), DOPC and POPS (2:1 molar ratio) and egg PC and DOPE (2:1 molar ratio) under a stream of N_2. The EPR spin probes were mixed with the DOPC, DOPC/POPG, DOPC/POPS, and egg PC/DOPE chloroformic solutions to give a final concentration of 0.5 mol %. The samples remained under vacuum for 2 h for the removal of the residual solvent, and the dried lipid film was resuspended at a total lipid concentration of 23.8 mM in 4 mM sodium phosphate (pH 7.2). The large unilamellar vesicles (LUVs) were prepared by extruding the multilamellar liposomes with a two-syringe extruder (Avanti Polar Lipids) equipped with two stacked polycarbonate filters with pores with an average diameter of 100 nm (Nucleopore). The continuous wave (CW) EPR spectroscopy experiments were conducted at room temperature (22 ± 1 °C) on a Varian E109 spectrometer operating at X-band. A measured amount of the buffered MpNEP2 solution was added to the suspension of LUVs and incubated for 10 min at room temperature. A final volume of 40 μL of the samples containing MpNEP2/DOPC/spin-label (DPPTC or 16-PC), MpNEP2/DOPC/POPG/spin-label (DPPTC or 16-PC), MpNEP2/DOPC/POPS/spin-label (DPPTC or 16-PC), or MpNEP2/egg PC/DOPE/spin-label (DPPTC or 16-PC) mixtures was drawn into a capillary tube, which was placed in the EPR resonant cavity. Control samples consisted of an LUV suspension without MpNEP2. The final enzyme concentration was 119 μM, and the protein:lipid molar ratio was 1:100. The acquisition conditions were as follows: modulation amplitude, 1.0 G; modulation frequency, 100 kHz; microwave power, 10 mW; field range, 160 G.

Intrinsic Fluorescence Measurements. The fluorescence measurements were recorded on a plate reader spectrofluorimeter (EnVision, Perkin-Elmer) using a 96-well all-black-walled Eppendorf plate and the default configurations of the equipment at 25.5 °C. The intrinsic fluorescence emission spectra of 2 μM MpNEP2 in 4 mM sodium phosphate (pH 7.2) were recorded from 310 to 500 nm after excitation at 295 nm to obtain the fluorescence spectra derived only from the tryptophan residues. The background intensities were always subtracted. Changes in the intrinsic fluorescence of MpNEP2 were also measured upon the addition of 200 μM of the following extruded LUVs: DOPC, DOPC/POPG (2:1 molar ratio), DOPC/POPS (2:1 molar ratio), and DOPC/DOPE (2:1 molar ratio).

RESULTS

The Level of MpNEP2 Expression Reaches Its Highest Point at the Necrotic Stage of the Disease. *M. perniciosa* has five copies of NLP genes in its genome.[10,11] An inspection

dx.doi.org/10.1021/bi201253b | *Biochemistry* 2011, 50, 9901−9910

of RNA-seq libraries that were produced as part of the WBD Transcriptome Atlas (P. L. Teixeira, manuscript in preparation) revealed that only MpNEP2 was significantly expressed during an *in planta* experiment, in which cacao plants were infected with *M. perniciosa*, and samples were collected at different stages of the disease (Figure 1A). Moreover, results of a quantitative real-time PCR assay confirmed that the level of MpNEP2 expression increased along with the extent of the necrosis symptoms, reaching its peak at the advanced necrotic stage when the dry broom symptoms were noticeable (Figure 1B, bottom panel). These results are consistent with the previously described activity of NLP proteins[14] and suggest that MpNEP2 may be the major isoform involved in the necrosis of cacao during the Witches' Broom disease. On the basis of these findings, this protein was selected for additional structural analyses.

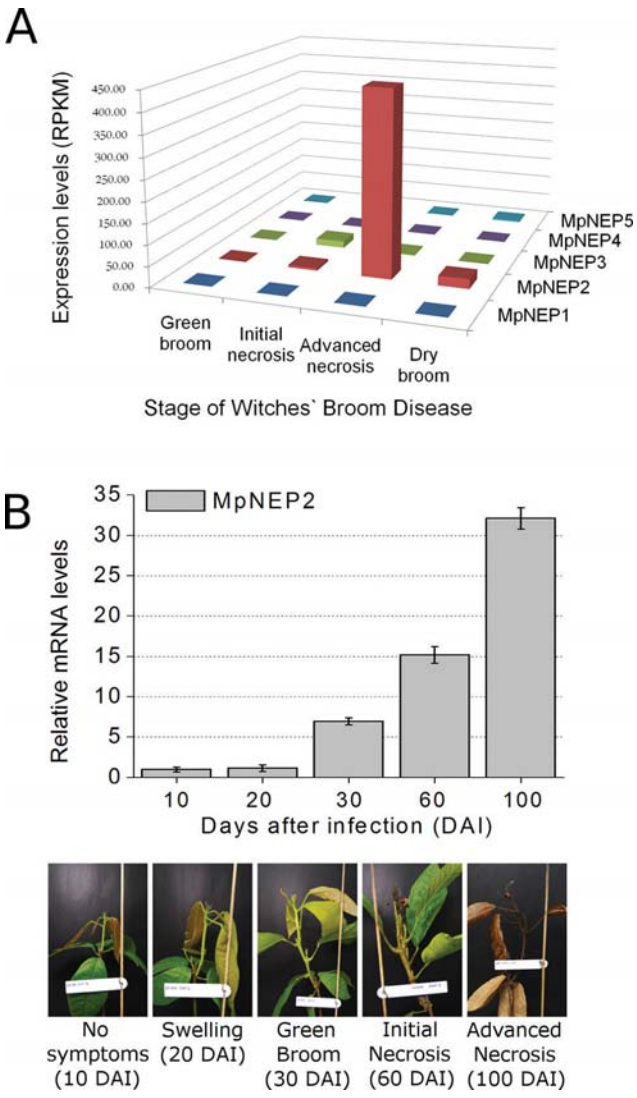

Figure 1. RNA-seq and real-time PCR analysis of MpNEP2 expression during Witches' Broom disease. (A) The RNA samples extracted from the green broom to the dry broom stages of WBD were sequenced and revealed that MpNEP2 is the major NLP found during the development of the disease (NCBI reference numbers EF109894 for MpNEP1, EF114673.1 for MpNEP2, EF164925 for MpNEP3, JN545833 for MpNEP4, and JN545834 for MpNEP5). (B) Real-time PCR confirmed a positive correlation between increasing levels of MpNEP2 and the appearance of necrotic symptoms. The disease stages, illustrated in the bottom panel, were classified as follows: no symptoms (10 DAI), beginning of swelling branches (20 DAI), mature green broom (30 DAI), beginning of necrosis in leaves (60 DAI), and advanced necrosis in branches (100 DAI). The dry broom stage is not shown. RPKM means reads per kilobase of exon model per 1 million mapped reads.

MpNEP2 Crystal Structure. Because we were interested in obtaining an improved understanding on the structural determinants of MpNEP2's mode of action, we determined the crystal structure of MpNEP2 at 1.8 Å resolution. The statistics of the final model are listed in Table 1. According to the Conserved Domain Database,[34] the structure belongs to the NPP1-like necrosis-inducing protein family. The overall architecture of the monomer in the asymmetric unit reveals a single-domain molecule with a fold consisting of a central β-sandwich, with three parallel strands in the first sheet and a five-stranded antiparallel sheet. Three α-helices (α1−α3) surround the second sheet, giving rise to a flat surface. Two large loops (loops 1 and 2) compose the other half of the polypeptide. The formation of an intramolecular disulfide bridge between two conserved cysteine residues within loop 2 (Figure S1 of the Supporting Information), reported to be essential for NLP

Table 1. Parameters and Statistics of Diffraction Data and Refinement[a]

Data Collection	
beamline	D03B-MX1 at LNLS
wavelength (Å)	1.608
space group	C121
unit cell dimensions	a = 89.48 Å, b = 44.21 Å, c = 60.17 Å, β = 110.04°
no. of monomers per asymmetric unit	1
resolution range (Å)	14.52−1.8 (1.9−1.8)
no. of unique reflections	19327 (2522)
average multiplicity	5.1 (3.7)
completeness (%)	93.9 (84.2)
R_{sym} (%)	0.049 (0.170)
$\langle(I)/\sigma(I)\rangle$	24.7 (7.9)
solvent content (%)	50.69
Refinement Statistics and Model Quality	
resolution range (Å)	20−1.8
total no. of reflections used	18298
no. of reflections for R_{free} calculation	1006 (5.2%)
R_f (%)/R_{free} (%)	14.22/19.57
no. of non-H atoms	1945
no. of residues	212
no. of waters	358
average B factor/rmsd (Å)	
main chain	12.6/0.8
side chain	13.56/1.78
solvent	26.16
rmsd from ideal bond length (Å)	0.021
rmsd from ideal angle (deg)	1.924
Ramachandran plot	
most favored region (%)	96.65
additional allowed region (%)	1.91
generously allowed region (%)	1.44

[a]The numbers in parentheses refer to the highest-resolution shell.

dx.doi.org/10.1021/bi201253b | *Biochemistry* 2011, 50, 9901−9910

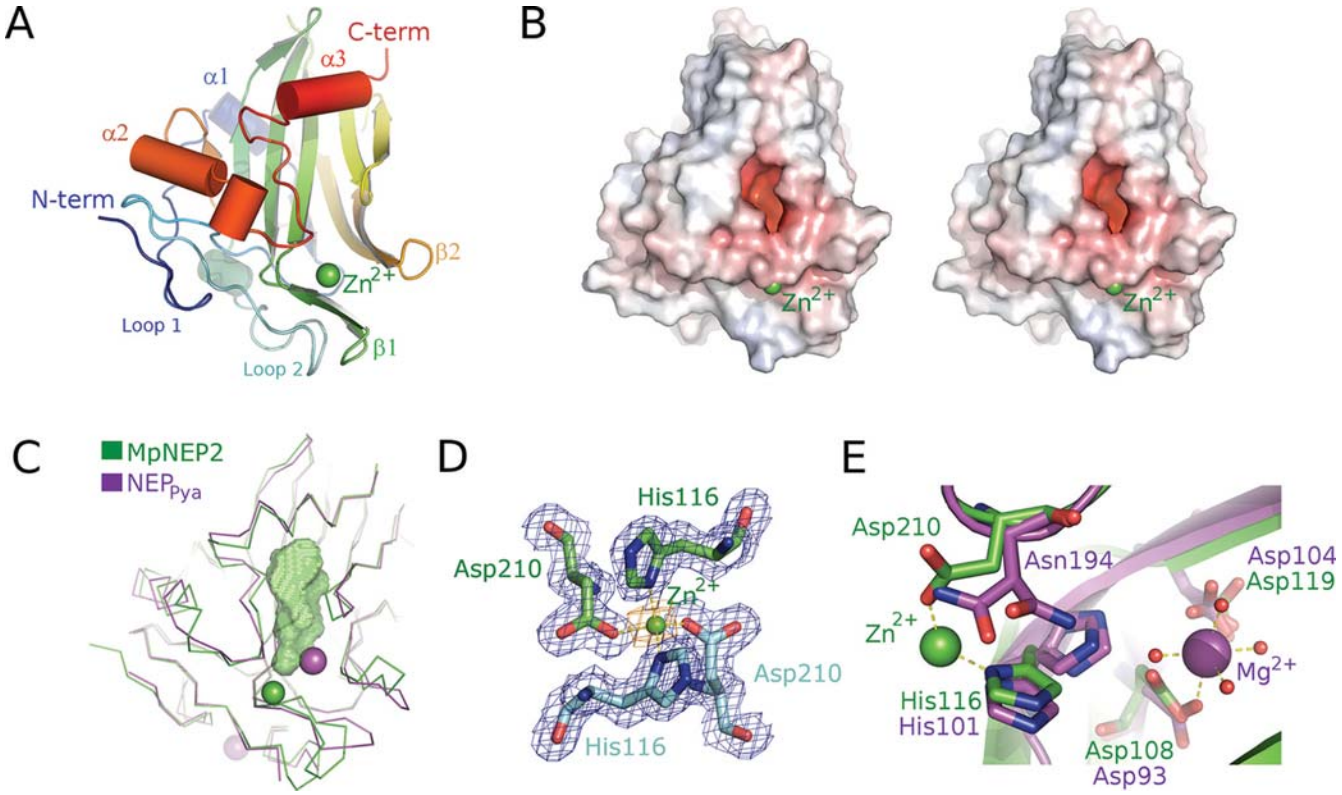

Figure 2. Crystal structure of MpNEP2. (A) Cartoon representation of MpNEP2 with a rainbow coloring scheme from blue (N-terminus) to red (C-terminus) and a text indication of its structural features, including the presence of a zinc ion (green sphere). (B) Stereoview of the electrostatic potential surface mapping calculated by APBS.[32] The color scale that varies from blue to red represents a variation from positive to negative potential, respectively ($\pm 12 k_b T_C e^{-1}$). This panel shows the presence of a very negatively charged cavity and its relative position to the zinc ion. (C) Ribbon representation of the structural superposition of MpNEP2 and NLP_{Pya} (green and purple ribbons, respectively), indicating both the high level of structural identity and distinct positions of the cations in the two models (zinc represented as a green sphere and magnesium represented as a purple sphere). The anionic cavity of MpNEP2 is represented as a green surface. (D) Fourier electron density map, $2F_o - F_c$ (blue mesh), for the residues coordinating to the zinc ion (green sphere), from both symmetry mates, represented as green and cyan sticks. The Fourier anomalous map (orange mesh), at 3σ level, contours the ion. (E) Specifics of the cation coordination in the crystallographic models. Whereas magnesium (purple sphere) is found inside the anionic cavity and is coordinated by Asp93 and Asp104, in the crystal structure of NLP_{Pya}[22] (represented as purple sticks), zinc (green sphere) is coordinated by His116 and Asp210 at the external surface of MpNEP2 (represented as green sticks).

activity,[14] appears to be crucial in stabilizing this loop closer to the β-sheet core of the protein. We can also identify the presence of two small 3_{10}-helices and two adjacent β-hairpins (β1 and β2). The structural features are illustrated in Figure 2A.

Electrostatic surface mapping, using APBS,[35] shows the presence of a strong negatively charged cavity (Figure 2B,C) formed among the five-stranded β-sheet, the loop between helices α2 and α3, and hairpin β1. A strand composed of the conserved sequence "GHRHDWE" defines the bottom of the cavity, which has a volume of 350 Å^3 (Figure 2C), as determined by the 3V server.[36] The negative potential is a contribution of the acidic side chains of Asp108, Asp119, and Glu121 and the main chain carboxyl groups of His118 and Trp120.

We observe a very strong peak, surrounding this cavity, in the Fourier $2F_o - F_c$ electron density map (>10σ in height), which, with respect to its contribution to the dispersive component of the scattering factor, was interpreted as a zinc ion (Figure S1 of the Supporting Information). This ion sits in a 2-fold center of symmetry in the crystal and is coordinated by the side chains of His116 and Asp210 from both the asymmetric unit monomer and its symmetry-related mate (Figure 2D). According to the PISA server,[37] there is an increase in free energy of −24.3 kcal/mol upon ion coordination; however, the resulting protein−protein interface is energetically less favored (0.9 kcal/mol, with a buried interface area of 580 Å^2). A second ion was also modeled on the opposite side of the protein surface, and using the same criteria for the determination of the zinc ion, it was interpreted to be sodium (Figure S1 of the Supporting Information). This cation is coordinated by the side chains of Asp157 and His53, the latter belonging to a symmetry-related monomer. Both zinc and sodium ions are present in the protein solution used for the crystallization at concentrations of 200 mM ($ZnCl_2$) and 50 mM (NaCl), respectively.

MpNEP2 Activity Is Not Ion-Dependent. Ottmann and co-workers[22] showed that the coordination of a divalent cation was crucial to NLP_{Pya} cytolytic activity. In this case, a magnesium ion was found inside the boundaries of a negatively charged cavity in the NLP_{Pya} structure, being coordinated directly by Asp93 and Asp104 (numbering according to NLP_{Pya}'s reference sequence) and four water molecules (Figure 2E). The overall MpNEP2 structure has a fold that is very similar to that of NLP_{Pya} (core rmsd of 1.08 Å), according to Lsqkab,[38] with the major difference between the two structures being the location of their divalent cation, as shown in Figure 2C. Nevertheless, Ottmann and co-workers presented evidence that Mg^{2+} was likely not a physiological ligand, and Ca^{2+} might actually be relevant for protein activity because BAPTA, a Ca^{2+}-

dx.doi.org/10.1021/bi201253b | Biochemistry 2011, 50, 9901−9910

specific scavenger, abolished the plasma membrane disintegrating activity of the NLPs.[22]

Having found a divalent cation in our crystal structure, although it has a different coordination pattern (Figure 2E), we set out to investigate what effect, if any, ions like zinc and calcium would have on the thermal stability and oligomeric state of MpMEP2 and if MpMEP2's necrotic activity is also dependent on calcium.

We first investigated the protein fold stability by determining its melting point using circular dichroism. Neither the presence of zinc nor the presence of calcium significantly altered the apparent melting temperature of MpNEP2 (T_{Mapp} for MpNEP2-$ZnCl_2$ = 41.2 °C, and T_{Mapp} for MpNEP2-$CaCl_2$ = 41.6 °C) relative to the thermal melting point measured in the absence of added divalent cations (T_{Mapp} for MpNEP2 = 39.9 °C) (Figure 3A). The thermal melting point was also obtained for MpNEP2 in the presence of EDTA to chelate any vestigial ions from the protein purification solutions (T_{Mapp} for MpNEP2-EDTA = 39.7 °C). The very similar apparent midpoints of the curves suggested that the presence of the tested cations did not affect the protein's conformational stability.

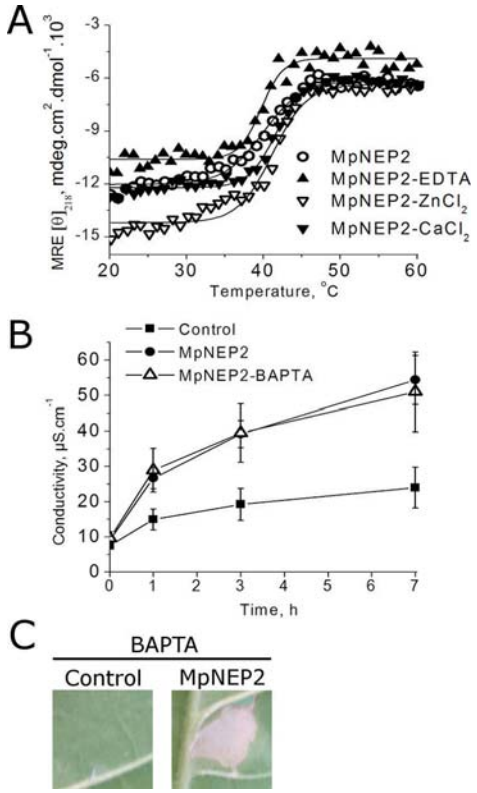

Figure 3. Structural stability, leakage, and necrosis promoting activity of ion-depleted MpNEP2 or MpNEP2 incubated with $CaCl_2$ or $ZnCl_2$. (A) Circular dichroism (CD) of MpNEP2, ion-depleted MpNEP2 (MpNEP2-EDTA), or MpNEP2 incubated with $CaCl_2$ or $ZnCl_2$ at λ = 218 nm measured over a range of temperatures. CD data (millidegrees) were converted to mean residue ellipticity units (MRE, millidegrees square centimeters per decimole) and plotted vs temperature. A sigmoidal curve was fitted, and the inflection point was calculated (T_{Mapp}), showing that ion binding does not influence protein stability and implying no structural role for the binding of the ion. (B) A vehicle solution with BAPTA, a specific Ca^{2+} chelator (Control), and vehicle solution with MpNEP2 (MpNEP2) or MpNEP2 and BAPTA (MpNEP2-BAPTA) was injected into tobacco leaves, and the electrolyte leakage was measured via solution conductivity. (C) A vehicle solution with BAPTA (Control) or a vehicle solution with MpNEP2 and BAPTA (MpNEP2) was injected into tobacco leaves, and the results were documented after 5 days. The data in panel B are the average values from three experiments ± SD, whereas the images in panel C are representative of three experiments.

Next, on the basis of the observations that zinc sits in a 2-fold symmetry center in our crystal structure and, consequently, that an MpNEP2 dimer can be generated by the crystal symmetry operations, we investigated what effects the ions mentioned above would have on the oligomeric state of the protein. Again, little to no change was observed in the hydrodynamic radii (R_H) measured for the protein either in the absence (2.2 nm, peak polydispersion of 4.4%) or in the presence of the cations ($CaCl_2$, 2.3 nm, peak polydispersion of 11%; $ZnCl_2$, 2.4 nm, peak polydispersion of 8.4%) and the chelating agent EDTA (2.3 nm, peak polydispersion of 10%). The calculated R_H value of the monomer, as determined by HYDROPRO using the monomer present in the asymmetric unit of our crystal, was 2.4 nm, leading us to conclude that, under the tested conditions, MpNEP2 is a monomer. The zinc-coordinated symmetric dimer in the crystal is therefore a packing artifact.

Finally, to check if the necrotic wound and electrolyte leakage promoting activities of MpNEP2 were dependent on calcium, the protein was injected into tobacco leaves both in the presence and in the absence of the calcium scavenger BAPTA. An electrolyte leakage assay was performed with leaves that were freshly treated with 10 mM BAPTA added to MpNEP2, and the results, when compared to the results of the same assay performed with MpNEP2 alone, indicated that this infiltration had no effect on the conductivity detected, as shown graphically in Figure 3B. These observations are supported by the images in Figure 3C, which show the detection of necrosis in leaves treated with MpNEP2 and 10 mM BAPTA but not when BAPTA was injected alone (control), clearly indicating that the addition of BAPTA to the vehicle solution did not perturb MpNEP2 activity.

Point Mutations Reveal Important Residues for MpNEP2 Activity. A comparison of the NLP primary sequences found in public databases revealed a strong conservation of a central heptapeptide motif, GHRHDWE,[14] which in MpNEP2 spans residues 115−121. Structurally, this peptide region comprises the bottom of the negatively charged cavity described in the previous section. The importance of this sequence for protein function has already been explored for NLP_{Pya}, for which the authors showed that substitution of either His101 or Asp104 (numbered according to its reference sequence) with alanine substantially abrogates its biological activity.[22] These His and Asp residues are two of the three residues that coordinate the divalent cation in Protein Data Bank entry 3gnz (Figure 2E), being His101 coordination via a water molecule. In the context of MpNEP2, only His116 (equivalent to His101 in NLP_{Pya}) coordinates the zinc ion.

We replaced His116 with either alanine (H116A) or serine (H116S) and Asp119 with a lysine (D119K), where both of these residues are from the conserved seven-residue sequence. The results revealed that all mutations of His116 and Asp119 in MpNEP2 disrupted the protein's ability to promote electrolyte leakage (Figure 4A) and necrotic wounds on tobacco leaves (Figure 4B). The mutation of the Asp119 residue to a lysine likely disturbed the negative potential of the cavity described above (Figure 2B), whereas changing the His116 to either a short nonpolar residue (alanine) or a negative polar residue

dx.doi.org/10.1021/bi201253b | Biochemistry 2011, 50, 9901−9910

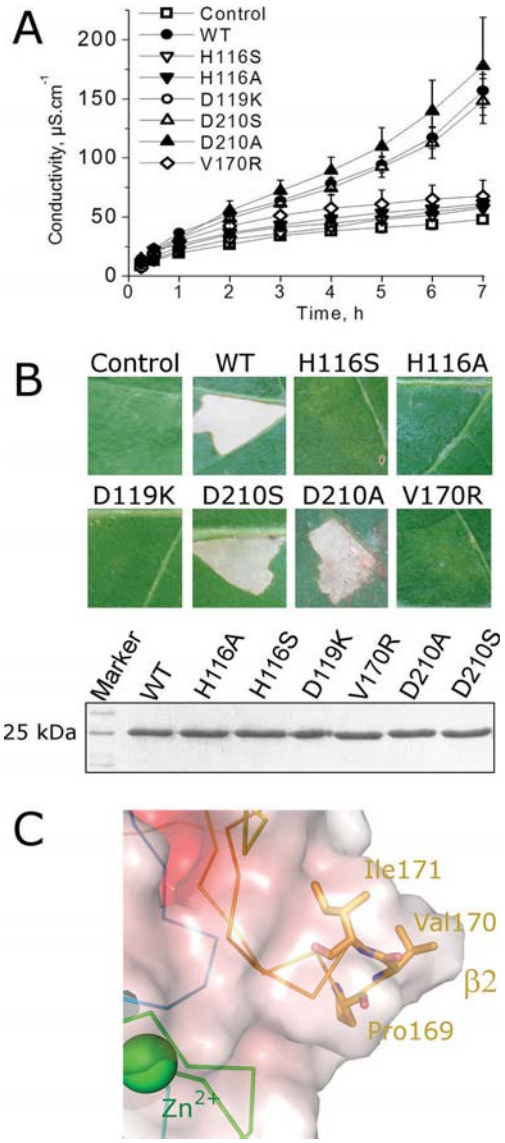

Figure 4. Mutation of residues from the acidic cavity and a hydrophobic loop disrupts MpNEP2 activity. (A) The vehicle solution (Control) or the vehicle solution containing wild-type (WT) MpNEP2 or mutant H116S, H116A, D119K, D210S, D210A, or V170R was injected into tobacco leaves, and the electrolyte leakage was measured by the solution conductivity for 7 h. (B) Additionally, the necrosis promoting activities on tobacco leaves were observed after 5 days. The bottom panel shows a Coomassie-stained SDS−PAGE gel that contained 50 μg of WT and mutant MpNEP2. The data in panel A are average values from three experiments ± SD, and the images in panel B are representative of three experiments. (C) Electrostatic potential surface representation of MpNEP2 β-hairpin β2 ($\pm 12 k_b T_C e^{-1}$), highlighting the hydrophobic β-turn composed of Pro169, Val170, and Ile171. The replacement of Val170 with an arginine residue disrupted protein activity.

(serine) has the potential to interfere with in vivo metal coordination, as found in our structure. To further test the importance of this coordination for protein activity, we replaced the other metal-coordinating residue, namely Asp210, with either alanine or serine. None of these mutations resulted in impaired protein activity (Figure 4A,B), implying that a cation is indeed dispensable for MpNEP2 activity, and H116 might exert its influence via a different mechanism. A circular dichroism analysis of melting temperatures of all mutant proteins assayed here revealed no notably altered tertiary structures within the mutant proteins, suggesting that the observed differences in the biological activities result from changes in the nearby vicinity of the altered residues (Figure S2 of the Supporting Information).

Finally, Kufner and co-workers hypothesized that the membrane attachment of NLP_{Pya} could be driven by a hydrophobic keel-like structure consisting of Trp155, Pro156, and Leu157 (according to their reference sequence), which would penetrate into the lipid core of the membrane like the hydrophobic regions of actinoporins and perfringolysin.[12] The equivalent residues in MpNEP2 are Pro169, Val170, and Ile171, respectively, which are structurally located at the turn of hairpin β2 (Figure 4C). To test this hypothesis, we replaced the apical residue in the turn, Val170, with an arginine. As shown in panels A and B of Figure 4, V170R MpNEP2 is impaired in its electrolyte leakage and necrosis promoting activities. To test MpNEP2's lipid binding capability, we performed EPR experiments with spin-labeled lipid vesicles and protein intrinsic fluorescence assays. The EPR spectra of the headgroup spin probe (DPPTC) or the acyl chain-labeled form (16-PC) incorporated into DOPC, DOPC/POPG (2:1 molar ratio), DOPC/POPS (2:1 molar ratio), or egg PC/DOPE (2:1 molar ratio) LUVs in the presence or absence of MpNEP2 showed no changes in their profile at a 1:100 protein:LUV molar ratio (Figure S3A of the Supporting Information). Similarly, the intrinsic fluorescence measurements of MpNEP2 indicated no significant perturbance in the tryptophan emission spectra after addition of a 100-fold molar excess of DOPC, DOPC/POPG, DOPC/POPS, or DOPC/DOPE unlabeled LUVs (Figure S3B of the Supporting Information).

■ DISCUSSION

Following the genome[10] and RNA sequencing analyses (Figure 1A) of *M. perniciosa*, five copies of NLPs were described, but only MpNEP2 was expressed during the cacao's Witches' Broom disease. A similar situation was described for *Phytophthora sojae* and *Phytophthora ramorum*, in which only a few of the more than 50 described genes are actually expressed during the diseases these organisms cause (stem and root rot of soybean and Sudden Oak Death, respectively).[14,39] The level of expression of MpNEP2 increases along with the necrotic symptoms, reaching its highest level during full necrosis just before the dry broom stage (Figure 1B). The transcripts encoding the necrosis-inducing protein of *P. sojae* (PsojNIP) reached their highest level after the transition of the fungus from the biotrophic to the necrotrophic stage in soybean plants,[40] whereas in *Mycosphaerella graminicola*, an NLP is expressed moments before necrosis symptoms occur.[41] The presence of more than one NEP-encoding gene in the studied genomes agrees with several evolutionary theories that have recently been grouped into a novel model, the "adaptive radiation model".[42] The other copies of the NEP-encoding gene are likely to be the result of recent duplications, having acquired different roles or become pseudogenes.

The founding member of the now-called NLP (NEP1-like protein) family was NEP1 (necrosis- and ethylene-inducing protein 1), which belongs to the organism *Fusarium oxysporum*.[43] The exact mode of action of NLPs during infection and virulence is not yet completely understood. The crystal structure of a NLP family member from the oomycete *Phytium aphanidermatum* (NLP_{Pya}) has recently been described,[22] and it

dx.doi.org/10.1021/bi201253b | *Biochemistry* 2011, 50, 9901−9910

was shown to resemble actinoporins, which are pore-forming toxins from marine invertebrates. The authors of this previous study concluded that NLPs are conserved virulence factors that cause plasma membrane permeabilization and cytolysis in plant cells with a mechanism that is dependent on the coordination of an ion, presumably calcium. As suggested, Ca^{2+} may mediate the docking of NLPs to target membranes, or it might, alternatively, be required for the membrane permeabilizing activity. Because plants seem to be capable of sensing the cellular changes induced by membrane damage, such as the release of host-derived endogenous elicitors or changes in ion homeostasis, NLPs probably trigger plant immunity-associated defenses through their interference with plant tissue integrity.[22] This idea would explain why so many authors had detected a defense response activity in hosts after they were challenged with NLPs.[13,14] The majority of genes that responded to NLPs are associated with general stress responses, which are calcium-dependent, and are actively expressed by plant host cells.[13,14]

Here, we described the crystal structure and mutational and functional studies of another member of the NLP family, MpNEP2, which is found in the causal agent of cacao's Witches' Broom disease, the fungus *M. perniciosa*. This disease is a serious concern to the South and Central American cacao crops, and an effective combat strategy has yet to be described. Like NLP_{Pya} and all the members of the NLP family, MpNEP2 has a conserved heptapeptide motif, GHRHDWE, which is shown to be part of a highly acidic groove (Figure 2B). In NLP_{Pya}, the residues from this motif coordinate an ion, likely Ca^{2+}, which was shown to be essential for protein activity. Although the crystal structure of MpNEP2 also included a cation in the vicinity of the acidic cavity, here we show that this protein does not depend on a cation for the promotion of its necrotic activity. The protein incubated with EDTA was as stable as the protein after the addition of either $ZnCl_2$ or $CaCl_2$ (Figure 3A), as measured by circular dichroism over a range of temperatures, indicating no structure-stabilizing function for these ions in MpNEP2. The wild-type calcium-depleted protein, as well as the Asp210A mutant in which one of the two ion-coordinating residues is replaced, behaved equally well in promoting tissue necrosis and electrolyte leakage when injected into tobacco leaves (Figures 3B,C and 4A,B). On the other hand, the mutation of the other ion-coordinating residue, His116, to either a serine or alanine did disrupt MpNEP2 activity, implying that His116 might be important for MpNEP2 necrotic activity via an alternative mechanism. The mutation of the Asp119 residue within the conserved heptapeptide to a nonpolar or oppositely charged residue disrupted protein activity (Figure 4A,B), reinforcing the importance of the negatively charged cavity for protein function.

The MpNEP2 structure is highly similar to the NLP_{Pya} structure (rsmd of 1.08 Å for Cα atoms). The latter[22] presented a fold highly conserved among the cytolytic actinoporins, especially the actinoporins produced by the sea anemones *Actinia equina* (equinatoxin II) and *Stichodactyla helianthus* (sticholysin II). Sticholysin II is a single-domain protein composed of a tightly folded core of β-sheet strands and two short α-helices, A and B, one on each side of the β-sandwich[44] (Figure S4A of the Supporting Information). The two-dimensional sticholysin II–lipid crystal data led to the proposal that the first 30 residues at the N-terminus, which encompass the amphiphilic α-helix A, are displaced from the body of the molecule upon binding of the lipid to be able to interact with the C-terminus of a neighboring molecule and form a tetramer.[44] The structural and functional data showed that the first contact of the molecule with the lipid membrane is promoted by the region around an exposed aromatic patch of the molecule, which contains tryptophan and tyrosine residues. The side chains of Trp110 and Trp114, which point downward and upward, respectively, with respect to the aromatic cluster, are exposed and very likely involved in the association of this protein region with lipid membranes[44] (Figure S4A of the Supporting Information) because the equivalent residues on equinatoxin II contribute to the fluorescence shifts observed upon lipid binding.[44,45] The crystal structure of sticholysin II complexed with phosphocholine revealed that the phospholipid headgroup binding site is placed exactly at this tryptophan and tyrosine rich segment[44] (Figure S4A of the Supporting Information).

In this work, we provide evidence that, remarkably, mutation of Val170 to an arginine residue abrogated protein necrosis and electrolyte activity, revealing that the triad consisting of Pro169, Val170, and Ile171 might, indeed, be a hydrophobic β-hairpin loop involved in membrane disruption. The aromatic patch described above for sticholysin II does not correlate structurally with the β-hairpin loop in MpNEP2 described here, which has a valine [Val170 (see Figure 4C)] that is important for protein activity (Figure 4A,B) (rmsd of 2.38 Å for Cα atoms upon superimposition of only the β-sheet core). Alternatively, this aromatic region fits within a region on MpNEP2 that has two tryptophan residues exposed to the solvent [Trp228 and Trp230 (Figure S4B of the Supporting Information)]. A possible scenario is that this segment of the protein, along with the hydrophobic β-hairpin loop [both are on the same side of the protein (see Figure S4B of the Supporting Information)], might be involved in the protein–lipid interaction. Moreover, to have a truly porin-like activity, in addition to being able to bind lipids, MpNEP2 must overcome its water-soluble conformation and transform into a lipophilic molecule. This transformation, induced by a lipid surface, would involve tertiary conformational changes. A deeper analysis of the MpNEP2 structural packing revealed that loop 2, as well as α-helix 2 and adjacent loops (Figure S4B of the Supporting Information), packs against the β-sheet core via aromatic stacking between several residues (Figure S4B of the Supporting Information, top right inset). A potential lipid-induced conformational change could displace this part of the protein to expose a lipophilic surface that was previously hidden.

However, EPR or intrinsic protein fluorescence studies conducted in the presence of LUVs containing phospholipids representative of the most common lipids found in plant cell membranes [32] showed no change in the spectra of the labeled lipids upon addition or MpNEP2 or protein tryptophan fluorescence after the incubation with the LUVs, respectively. Although we did not perform an exhaustive search of all types of lipids and their different combinations, these findings suggest that, if MpNEP2 anchors to the membrane to perform its necrotic activity, it likely requires an interaction with another membrane element, which could be either a specific membrane receptor or glycolipoprotein microdomains.[46,47] This finding could offer an explanation of how MpNEP2, as well as others NLPs, differentiates between dicotyledonous and monocotyledonous plants.[14]

During the progression of Witches' Broom disease, the fungal population inside the host becomes larger, and the concentration of molecules involved in quorum sensing signals also

dx.doi.org/10.1021/bi201253b | *Biochemistry* 2011, 50, 9901–9910

increases. A phase change synchronization happens at this point of the disease, and MpNEP2 expression could be a benefit to *M. perniciosa* by releasing nutrients from lysed plant cells and by promoting an increase in the space that would allow the fungi's saprotrophic hyphae to quickly proliferate. The highly acidic cavity described for MpNEP2 and the hydrophobic Pro-Val-Ile loop are promising regions for compound screening and design because both of these regions have been shown to be essential for MpNEP2 necrosis promoting activity.

■ ASSOCIATED CONTENT

Supporting Information

Anomalous X-ray scattering data used to define the nature of the metals found in the structure (Figure S1), apparent melting temperatures measured by circular dichroism, as well as the CD profile at different wavelengths, of all of the mutants described in this paper (Figure S2), EPR and intrinsic fluorescence data in the presence and absence of LUVs (Figure S3), and structural comparisons between the actinoporin sticholysin II and MpNEP2 (Figure S4). This material is available free of charge via the Internet at http://pubs.acs.org.

Accession Codes

The atomic coordinates and diffraction data have been deposited in the Protein Data Bank as entry 3st1.

■ AUTHOR INFORMATION

Corresponding Author

*E-mail: sandra.dias@lnbio.org.br. Telephone: +55 19 3512 3503. Fax: +55 19 3512 1004.

Funding

This work was supported by FAPESP Grants 2010/51884-8 and 2009/50119-9 and Fellowships 2008/50995-0 and 2010/51891-4.

■ ACKNOWLEDGMENTS

We acknowledge the Spectroscopy and Calorimetry and the Robolab facilities at LNBio for technical assistance, as well as the staff of the D03B-MX1 beamline at the Brazilian National Synchrotron Laboratory. We give special thanks to Dr. Alessandra Girasole for the laboratory technical support.

■ ABBREVIATIONS

rmsd, root-mean-square deviation; NLPs, NEP1-like proteins; DAI, days after inoculation of *T. cacao* with *M. perniciosa* spores; SD, standard deviation; WBD, Witches' Broom disease.

■ REFERENCES

(1) Griffith, G. W., Nicholson, J., Nenninger, A., Birch, R. N., and Hedger, J. N. (2003) Witches' brooms and frosty pods: Two major pathogens of cacao. *N. Z. J. Bot. 41* (3), 423−435.

(2) Pereira, J. L., Ram, A., Figuereido, J. M., and de Almeida, L. C. (1989) La primera aparición de la "escoba de bruja" en la principal área productora de cacao del Brasil. *Turrialba 39* (7), 459−461.

(3) Meinhardt, L. W., Rincones, J., Bailey, B. A., Aime, M. C., Griffith, G. W., Zhang, D., and Pereira, G. A. G. (2008) *Moniliophthora perniciosa*, the causal agent of witches' broom disease of cacao: What's new from this old foe? *Mol. Plant Pathol. 9* (5), 577−588.

(4) Aime, M. C., and Phillips-Mora, W. (2005) The causal agents of witches' broom and frosty pod rot of cacao (chocolate, *Theobroma cacao*) form a new lineage of Marasmiaceae. *Mycologia 97* (5), 1012−1022.

(5) Purdy, L. H., and Schmidt, R. A. (1996) Status of cacao witches' broom: Biology, epidemiology, and management. *Annu. Rev. Phytopathol. 34*, 573−594.

(6) Scarpari, L. M., Meinhardt, L. W., Mazzafera, P., Pomella, A. W., Schiavinato, M. A., Cascardo, J. C., and Pereira, G. A. (2005) Biochemical changes during the development of witches' broom: The most important disease of cocoa in Brazil caused by *Crinipellis perniciosa*. *J. Exp. Bot. 56* (413), 865−877.

(7) Delgado, J. C., and Cook, A. A. (1976) Nuclear condition of basidia, basidiospores, and mycelium of *Marasmius perniciosus*. *Can. J. Bot. 54* (1−2), 66−72.

(8) Evans, H. C. (1980) Pleomorphism in *Crinipellis perniciosa*, Causal Agent of Witches Broom Disease of Cocoa. *Trans. Br. Mycol. Soc. 74* (6), 515−523.

(9) Griffith, G. W., and Hedger, J. N. (1994) Dual culture of *Crinipellis perniciosa* and potato callus. *Eur. J. Plant Pathol. 100* (6), 371−379.

(10) Mondego, J. M., Carazzolle, M. F., Costa, G. G., Formighieri, E. F., Parizzi, L. P., Rincones, J., Cotomacci, C., Carraro, D. M., Cunha, A. F., Carrer, H., Vidal, R. O., Estrela, R. C., Garcia, O., Thomazella, D. P., de Oliveira, B. V., Pires, A. B., Rio, M. C., Araujo, M. R., de Moraes, M. H., Castro, L. A., Gramacho, K. P., Gonçalves, M. S., Neto, J. P., Neto, A. G., Barbosa, L. V., Guiltinan, M. J., Bailey, B. A., Meinhardt, L. W., Cascardo, J. C., and Pereira, G. A. (2008) A genome survey of *Moniliophthora perniciosa* gives new insights into witches' broom disease of cacao. *BMC Genomics 9*, 548.

(11) Garcia, O., Macedo, J. A., Tiburcio, R., Zaparoli, G., Rincones, J., Bittencourt, L. M., Ceita, G. O., Micheli, F., Gesteira, A., Mariano, A. C., Schiavinato, M. A., Medrano, F. J., Meinhardt, L. W., Pereira, G. A., and Cascardo, J. C. (2007) Characterization of necrosis and ethylene-inducing proteins (NEP) in the basidiomycete *Moniliophthora perniciosa*, the causal agent of witches' broom in *Theobroma cacao*. *Mycol. Res. 111* (4), 443−455.

(12) Kufner, I., Ottmann, C., Oecking, C., and Nurnberger, T. (2009) Cytolytic toxins as triggers of plant immune response. *Plant Signaling Behav. 4* (10), 977−979.

(13) Pemberton, C. L., and Salmond, G. P. (2004) The Nep1-like proteins: A growing family of microbial elicitors of plant necrosis. *Mol. Plant Pathol. 5*, 353−359.

(14) Gijzen, M., and Nurnberger, T. (2006) Nep1-like proteins from plant pathogens: Recruitment and diversification of the NPP1 domain across taxa. *Phytochemistry 67*, 1800−1807.

(15) Frias, G. A., Purdy, L. H., and Schmidt, R. A. (1995) An inoculation method for evaluating resistance of cacao to *Crinipellis perniciosa*. *Plant Dis. 79* (8), 787−791.

(16) Azevedo, H., Lino-Neto, T., and Tavares, R. M. (2003) An improved method for high-quality RNA isolation from needles of adult maritime pine trees. *Plant Mol. Biol. Rep. 21*, 333−338.

(17) Livac, K. J., and Schmittgen, T. D. (2001) Analysis of relative gene expression data using real-time quantitative PCR and the 2^{2DDCT} method. *Methods 25*, 402−408.

(18) Gasteiger, E., Hoogland, C., Gattiker, A., Duvaud, S., Wilkins, M. R., Appel, R. D., and Bairoch, A. (2005) Protein Identification and Analysis Tools on the ExPASy Server. In *The Proteomics Protocols Handbook* (Walker, J. M., Ed.) pp 571−607, Humana Press, Totowa, NJ.

(19) Leslie, A. G. W. (1992) Recent changes to the MOSFLM package for processing film and image plate data, *Joint CCP4 + ESF-EAMCB Newsletter on Protein Crystallography*, Vol. *26*.

(20) Evans, P. R. (2005) Scaling and assessment of data quality. *Acta Crystallogr. D62*, 72−82.

(21) McCoy, A. J., Grosse-Kunstleve, R. W., Adams, P. D., Winn, M. D., Storoni, L. C., and Read, R. J. (2007) Phaser crystallographic software. *J. Appl. Crystallogr. 40*, 658−674.

(22) Ottmann, C., Luberacki, B., Kufner, I., Koch, W., Brunner, F., and Weyand, M. (2009) A common toxin fold mediates microbial attack and plant defense. *Proc. Natl. Acad. Sci. U.S.A. 106*, 10359−10364.

dx.doi.org/10.1021/bi201253b | *Biochemistry* 2011, 50, 9901−9910

(23) Zhang, K. Y. J., Cowtan, K., and Main, P. (1997) Combining constraints for electron-density modification. *Methods Enzymol. 277*, 53−64.
(24) Collaborative Computational Project, Number 4 (1994) The CCP4 Suite: Programs for Protein Crystallography. *Acta Crystallogr. D50*, 760−763.
(25) Perrakis, A., Morris, R. M., and Lamzin, V. S. (1999) Automated protein model building combined with iterative structure refinement. *Nat. Struct. Biol. 6*, 458−463.
(26) Vagin, A. A., Steiner, R. S., Lebedev, A. A., Potterton, L., McNicholas, S., Long, F., and Murshudov, G. N. (2004) REFMAC5 dictionary: Organisation of prior chemical knowledge and guidelines for its use. *Acta Crystallogr. D60*, 2284−2295.
(27) Emsley, P., Lohkamp, B., Scott, W. G., and Cowtan, K. (2010) Features and development of Coot. *Acta Crystallogr. D66*, 486−501.
(28) Read, R. J., and Schierbeek, A. J. (1988) *J. Appl. Crystallogr. 21*, 490−495.
(29) Chen, V. B., Arendall, W. B. III, Headd, J. J., Keedy, D. A., Immormino, R. M., Kapral, G. J., Murray, L. W., Richardson, J. S., and Richardson, D. C. (2010) MolProbity: All-atom structure validation for macromolecular crystallography. *Acta Crystallogr. D66*, 12−21.
(30) Whitmore, L., and Wallace, B. A. (2008) Protein Secondary Structure Analyses from Circular Dichroism Spectroscopy: Methods and Reference Databases. *Biopolymers 89*, 392−400.
(31) Ortega, A., Amoros, D., and Garc1a de la Torre, J. (2011) Prediction of hydrodynamic and other solution properties of rigid proteins from atomic- and residue-level models. *Biophys. J. 101*, 892−898.
(32) Welti, R., Li, W., Li, M., Sang, Y., Biesiada, H., Zhou, H. E., Rajashekar, C. B., Williams, T. D., and Wang, X. (2002) Profiling membrane lipids in plant stress responses. Role of phospholipase Dα in freezing-induced lipid changes in *Arabidopsis*. *J. Biol. Chem. 277* (35), 31994.
(33) Simon, E. W. (1974) Phospholipids and plant membrane permeability. *New Phytol. 73*, 377.
(34) Marchler-Bauer, A., Lu, S., Anderson, J. B., Chitsaz, F., Derbyshire, M. K., Deweese-Scott, C., Fong, J. H., Geer, L. Y., Geer, R. C., Gonzales, N. R., Gwadz, M., Hurwitz, D. I., Jackson, J. D., Ke, Z., Lanczycki, C. J., Lu, F., Marchler, G. H., Mullokandov, M., Omelchenko, M. V., Robertson, C. L., Song, J. S., Thanki, N., Yamashita, R. A., Zhang, D., Zhang, N., Zheng, C., and Bryant, S. H. (2011) CDD: A Conserved Domain Database for the functional annotation of proteins. *Nucleic Acids Res. 39*, D225−D229.
(35) Baker, N. A., Sept, D., Joseph, S., Holst, M. J., and McCammon, J. A. (2001) Electrostatics of nanosystems: Application to microtubules and the ribosome. *Proc. Natl. Acad. Sci. U.S.A. 98*, 10037−10041.
(36) Voss, N. R., and Gerstein, M. (2010) 3V: Cavity, channel and cleft volume calculator and extractor. *Nucleic Acids Res. 38*, W555−W562.
(37) Krissinel, E., and Henrick, K. (2007) Inference of macromolecular assemblies from crystalline state. *J. Mol. Biol. 372*, 774−797.
(38) Kabsch, W. (1976) A solution for the best rotation to relate two sets of vectors. *Acta Crystallogr. A32*, 922−923.
(39) Bae, H., Bowers, J. H., Tooley, P. W., and Bailey, B. A. (2005) NEP1 orthologs encoding necrosis and ethylene inducing proteins exist as a multigene family in *Phytophthora megakarya*, causal agent of black pod disease on cacao. *Mycol. Res. 109*, 1373−1385.
(40) Qutob, D., Kamoun, S., and Gijzen, M. (2002) Expression of a *Phytophthora sojae* necrosis-inducing protein occurs during transition from biotrophy to necrotrophy. *Plant J. 32*, 361−373.
(41) Motteram, J., Kufner, I., Deller, S., Brunner, F., Hammond-Kosack, K. E., and Nürnberger, T. (2009) Molecular characterization and functional analysis of MgNLP, the sole NPP1 domain-containing protein, from the fungal wheat leaf pathogen *Mycosphaerella graminicola*. *Mol. Plant-Microbe Interact. 22*, 790−799.
(42) Francino, M. P. (2005) An adaptive radiation model for the origin of new gene functions. *Nat. Genet. 37*, 573−578.
(43) Bailey, B. (1995) Purification of a protein from culture filtrates of *Fusarium oxysporum* that induces ethylene and necrosis in leaves of *Erythroxylum coca*. *Phytopathology 85*, 1250−1255.
(44) Mancheño, J. M., Martín-Benito, J., Martínez-Ripoll, M., Gavilanes, J. G., and Hermoso, J. A. (2003) Crystal and Electron Microscopy Structures of Sticholysin II Actinoporin Reveal Insights into the Mechanism of Membrane Pore Formation. *Structure 11*, 1319−1328.
(45) Malovrh, P., Barlic, A., Podlesek, Z., Macek, P., Menestrina, G., and Anderluh, G. (2000) Structure−function studies of tryptophan mutants of equinatoxin II, a sea anemone pore-forming protein. *Biochem. J. 346*, 223−232.
(46) Mongrand, S., Morel, J., Laroche, J., Claverol, S., Carde, J. P., Hartmann, M. A., Bonneu, M., Simon-Plas, F., Lessire, R., and Bessoule, J. J. (2004) Lipid rafts in higher plant cells: Purification and characterization of Triton X-100-insoluble microdomains from tobacco plasma membrane. *J. Biol. Chem. 279* (35), 36277.
(47) Bhat, R. A., and Panstruga, R. (2005) Lipid rafts in plants. *Planta 223*, 5.

dx.doi.org/10.1021/bi201253b | *Biochemistry* 2011, 50, 9901−9910

Anexo II

A potential role for an extracellular methanol oxidase secreted by *Moniliophthora perniciosa* in Witches' broom disease in cacao

Bruno V. de Oliveira, Gleidson S. Teixeira, Osvaldo Reis, Joan G. Barau, Paulo José P.L. Teixeira, Maria Carolina S. do Rio, Romênia R. Domingues, Lyndel W. Meinhardt, Adriana F.P. Leme, Johana Rincones, Gonçalo A.G. Pereira

Trabalho publicado na revista *Fungal Genetics and Biology*, Novembro 2012, Vol. 49, pp. 922-932.

APRESENTAÇÃO

Este trabalho mostra que o fungo *Moniliophthora perniciosa* é capaz de utilizar metanol como única fonte de carbono. A principal fonte deste álcool em plantas é a pectina presente na parede celular. Assim, o trabalho apresenta uma caracterização do metabolismo pectinolítico em *M. perniciosa*, destacando o fato de este fungo possuir uma enzima metanol oxidase extracelular. Dados de RNA-seq foram utilizados na construção de um modelo deste metabolismo em *M. perniciosa,* propondo que a degradação da pectina vegetal pelo fungo libera metanol no meio extracelular, o qual é então imediatamente metabolizado.

Fungal Genetics and Biology 49 (2012) 922–932

Contents lists available at SciVerse ScienceDirect

Fungal Genetics and Biology

journal homepage: www.elsevier.com/locate/yfgbi

A potential role for an extracellular methanol oxidase secreted by *Moniliophthora perniciosa* in Witches' broom disease in cacao

Bruno V. de Oliveira [a], Gleidson S. Teixeira [a], Osvaldo Reis [a], Joan G. Barau [a], Paulo José P.L. Teixeira [a], Maria Carolina S. do Rio [a,c], Romênia R. Domingues [c], Lyndel W. Meinhardt [b], Adriana F. Paes Leme [c], Johana Rincones [a], Gonçalo A.G. Pereira [a,*]

[a] *Laboratório de Genômica e Expressão, Departamento de Genética, Evolução e Bioagentes, Instituto de Biologia, Universidade Estadual de Campinas (UNICAMP), CP 6109, 13083-970 Campinas, SP, Brazil*
[b] *Sustainable Perennial Crops Laboratory, USDA–ARS, 10300 Baltimore Ave., Bldg. 001, Beltsville, MD 20705-2350, USA*
[c] *Laboratório Nacional de Biociências (LNBio), Centro Nacional de Pesquisa em Energia e Materiais (CNPEM), CP 6192, 13083-970 Campinas, Brazil*

ARTICLE INFO

Article history:
Received 28 May 2012
Accepted 2 September 2012
Available online 26 September 2012

Keywords:
Moniliophthora perniciosa
Cacao
Witches' broom disease
Methanol oxidase
Extracellular
Pectin methylesterase

ABSTRACT

The hemibiotrophic basidiomycete fungus *Moniliophthora perniciosa*, the causal agent of Witches' broom disease (WBD) in cacao, is able to grow on methanol as the sole carbon source. In plants, one of the main sources of methanol is the pectin present in the structure of cell walls. Pectin is composed of highly methylesterified chains of galacturonic acid. The hydrolysis between the methyl radicals and galacturonic acid in esterified pectin, mediated by a pectin methylesterase (PME), releases methanol, which may be decomposed by a methanol oxidase (MOX). The analysis of the *M. pernciosa* genome revealed putative *mox* and *pme* genes. Real-time quantitative RT-PCR performed with RNA from mycelia grown in the presence of methanol or pectin as the sole carbon source and with RNA from infected cacao seedlings in different stages of the progression of WBD indicate that the two genes are coregulated, suggesting that the fungus may be metabolizing the methanol released from pectin. Moreover, immunolocalization of homogalacturonan, the main pectic domain that constitutes the primary cell wall matrix, shows a reduction in the level of pectin methyl esterification in infected cacao seedlings. Although MOX has been classically classified as a peroxisomal enzyme, *M. perniciosa* presents an extracellular methanol oxidase. Its activity was detected in the fungus culture supernatants, and mass spectrometry analysis indicated the presence of this enzyme in the fungus secretome. Because *M. pernciosa* possesses all genes classically related to methanol metabolism, we propose a peroxisome-independent model for the utilization of methanol by this fungus, which begins with the extracellular oxidation of methanol derived from the demethylation of pectin and finishes in the cytosol.

1. Introduction

The basidiomycete fungus *Moniliophthora perniciosa* (Aime and Phillips-Mora, 2005) is the causal agent of Witches' broom disease (WBD) in cacao (*Theobroma cacao*), one of the most devastating diseases of cacao in the Americas (Griffith et al., 2003).

M. perniciosa is classified as a hemibiotrophic pathogen and presents two morphologically distinct life phases, biotrophic and necrotrophic, that are correlated with different symptoms during the progression of WBD (Evans, 1980). The biotrophic mycelium is monokaryotic, with no clamp connections, and infects flower cushions, developing fruit, and meristematic tissues. These hyphae inhabit the intercellular space, where they grow slowly at a low density, causing hypertrophy and hyperplasia of the infected branches, which are the main symptoms of the green broom stage (Evans, 1978; Penman et al., 2000; Silva, 1999). These symptoms are caused by a drastic biochemical change during the development of the green brooms (Scarpari et al., 2005). Very little is known about the characteristics of this monokaryotic mycelium *ex planta* because its cultivation is difficult due to its instability; a glycerol-based culture media for the cultivation of a monokaryotic and biotrophic-like mycelia was developed only recently (Meinhardt et al., 2006).

Five to eight weeks after the start of the infection, a dikaryotization process occurs, and the mycelia become necrotrophic, presenting two nuclei per cell that are connected by typical basidiomycete clamp connections. The necrotrophic mycelia rapidly invade the host plant cells, completely destroying the infected tissues and causing the extensive degradation symptoms of the dry

* Corresponding author. Address: Genetics, Evolution and Bioagents Department, Genomics and Expression Laboratory, Institute of Biology, UNICAMP, P.O. Box 6109, 13083-970 Campinas, SP, Brazil. Fax: +55 19 37886235.
E-mail address: goncalo@unicamp.br (G.A.G. Pereira).

1087-1845/$ - see front matter © 2012 Elsevier Inc. All rights reserved.
http://dx.doi.org/10.1016/j.fgb.2012.09.001

broom phase (Delgado and Cook, 1976; Evans and Bastos, 1980; Frias et al., 1991; Griffith and Hedger, 1994). Although the mechanisms that trigger the dikaryotization process in *M. perniciosa* are not yet completely elucidated, recently a study published by our group reported that an alternative oxidase plays a role in the biotrophic development of *M. perniciosa* and regulates the transition to its necrotrophic stage (Thomazella et al., 2012).

The introduction of WBD in Bahia, the main Brazilian cacao-producing state, occurred in 1989 (Pereira et al., 1989). Since then, cacao production has decreased drastically and Brazil has become a net importer of cacao in order to supply the national chocolate industry. Due to the extreme losses in cacao production, in the early 2000s, the Witches' broom Genome Project was initiated to decode the *M. perniciosa* genome and, based on the data acquired, select genes that could be relevant during the progression of WBD for characterization. In 2008, a draft genome analysis and an EST and microarray-based transcriptome study were published (Mondego et al., 2008; Rincones et al., 2008). These studies revealed the presence of sequences similar to methanol oxidase (*mox*), an enzyme that could be related to the previously reported ability of *M. perniciosa* to grow on methanol as the sole carbon source (Mondego et al., 2008), as shown in Fig. 1.

MOX is the key enzyme in methanol metabolism in methylotrophic yeasts and other methanol-degrading organisms. It consists of an octameric flavoprotein that oxidizes methanol to formaldehyde and hydrogen peroxide (Ozimek et al., 2005). The peroxide generated is decomposed by a catalase, and the formaldehyde is subjected either to the action of a dihydroxyacetone synthase (DHAS) or to direct oxidation by the enzymes formaldehyde dehydrogenase (FMDH) and formate dehydrogenase (FDH) (Kaszycki and Koloczek, 2000).

In almost all methanol-degrading organisms, such as the methylotrophic yeasts *Pichia angusta* and *Pichia pastoris* and the ascomycete phytopathogen *Cladosporium fulvum*, MOX is a peroxisomal enzyme (Ozimek et al., 2005; Segers et al., 2001). It is synthesized in the cytosol and imported into the peroxisomes, triggered by a peroxisomal targeting signal (PTS1) that is located in the C-terminal part of the enzyme (Ozimek et al., 2006). To date, the only known exception concerns the MOX produced by the basidiomycete *Gloeophyllum trabeum*, which is secreted into the extracellular space, despite the absence of a clear secretion signal in its sequence (Daniel et al., 2007).

In plants, one of the main sources of methanol is the pectin present in the plant cell walls (Nemecek-Marshall et al., 1995). Pectins are one of the major components of the middle lamellae and primary plant cell walls in dicotyledonous species, where they compose 30–35% of the cell wall dry weight (Pelloux et al., 2007). Pectins are highly complex polysaccharides that are rich in calcium ions, and are formed by a range of different domains, two of which may be distinguished: homogalacturonan and xylogalacturonan. Homogalacturonans are linear chains of α-(1-4)-linked D-galacturonic acid, which can be either methylesterified or acetylesterified. Xylogalacturonan is a homogalacturonan with (1,3)-β-D-xylopyranoside side chains, which like homogalacturonan, can be methylesterified (Willats et al., 2001).

The degradation of the pectin present in plant cell walls is a strategy used by many phytopathogenic fungi to invade the host tissues and establish infection. The fungi *Sclerotinia sclerotiorum* (Guimaraes and Stotz, 2004), *Botrytis cinerea* (Han et al., 2007), and *M. perniciosa* (Rio et al., 2008) produce oxalate, which removes calcium ions bound to pectin to produce calcium oxalate crystals, thus exposing the host cell walls to plant cell wall-degrading enzymes (PCWD) of fungal origin. One of the main PCWDs is pectin methylesterase (PME), an enzyme that removes the methyl ester radicals present in the galacturonic acid backbone in esterified pectin, releasing methanol (Sakai et al., 1993). PMEs are enzymes produced by plants that are related to growth, development, and defense against pathogens (Pelloux et al., 2007), though many

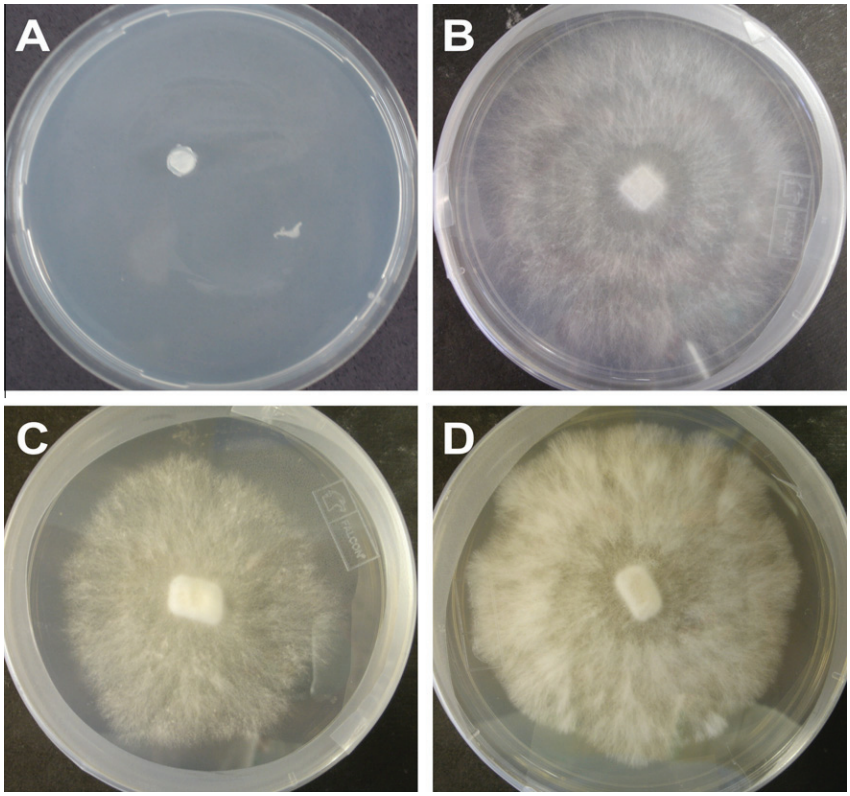

Fig. 1. *M. perniciosa* is able to grow on methanol as the sole carbon source. Minimal medium without any carbon source, which cannot support *M. perniciosa* growth (A, control) and the same media supplemented with glucose (B), methanol (C) and cacao extract (D), at final concentrations of 1% (v/v).

phytopathogenic fungal species secret PMEs as pathogenicity factors. For example, the disruption of the *B. cinerea* pectin methylesterase gene Bcpme1 reduces virulence in several host plants, including apple fruits, grapevines, and *Arabidopsis thaliana* leaves (Valette-Collet et al., 2003). The analysis of *M. perniciosás* genomic and expressed sequences revealed the presence of a sequence similar to a pectin methylesterase.

Although it has been demonstrated that methylotrophic yeasts, such as *Pichia methanolica* (Nakagawa et al., 2005) and *Candida boidinii* (Yurimoto et al., 2000), are able to utilize the methanol released from pectin, very little is known about the correlation between pectin and methanol metabolism among the phytopathogenic fungal species.

In this study, we show that *M. perniciosa* produces a methanol oxidase that is secreted into the extracellular space. Its relative expression *in vitro* and *in planta* is associated with PME expression levels and with the reduction in the level of methyl esterification observed in infected cacao seedlings, suggesting that this fungus metabolizes the methanol generated by pectin degradation. Moreover, we show that *M. perniciosa* possesses all genes related to methanol utilization, and their expression indicates that methanol can be a relevant energy source for this fungus.

2. Material and methods

2.1. Biological material and growth conditions

The isolate FA553 of *M. perniciosa* was used for all experiments in this work (Mondego et al., 2008). In our laboratory, necrotrophic mycelia of this isolate were maintained on plates of Malt Yeast Extract Agar (Difco) at 28 °C. The spores were obtained from necrotrophic mycelia according to the protocol developed by Teixeira et al. (in preparation). Biotrophic-like mycelia were obtained from spore germination in biotrophic maintenance media (Meinhardt et al., 2006).

For all *in vitro* gene expression experiments, both biotrophic-like and necrotrophic mycelia were grown for 7 days at 28 °C, under constant agitation at 120 rpm, in biotrophic liquid media, which contains glycerol as the sole carbon source (Meinhardt et al., 2006); the same media was used for the biotrophic-like and necrotrophic mycelia growth to avoid gene expression variations associated with different growth conditions. After the 7-day growth period, the mycelia were separated from the media by filtration, washed twice in sterile distilled water and inoculated in new aliquots of the same media supplemented with the following sole carbon sources at final concentrations of 1% (w/v): glycerol, glucose, methanol, non-esterified pectin from citrus (Sigma, polygalacturonate) and esterified pectin from citrus (Sigma, degree of esterification, DE $\geqslant$ 85%). After a 24-h period of incubation, the mycelia were separated from the media by filtration, washed twice in sterile distilled water, frozen in liquid nitrogen, and stored at −80 °C for further RNA isolation.

T. cacao L. variety (Catongo) was used for the *M perniciosa* gene expression assays *in planta*. Plants were grown for approximately 3 months in a greenhouse under controlled temperature (26 °C) and humidity (>80%) at a photoperiod of 12 h. After this period of growth, the apical meristems of the plants were removed 2 weeks before the infection with the fungal spores to stimulate growth of the lateral meristems. One day before the infection, the plants were transferred to a high-humidity chamber to induce stomatal opening. We used 30 μl of a solution containing approximately 10^5 spores/ml to infect each plant. Symptoms of WDB were observed, and the plants were harvested based on the progression of symptoms of the disease: asymptomatic, green broom 1, green broom 2 and necrosis; the plants were collected in triplicate for each stage analyzed. As the experimental control, non-infected plants of the same age were collected. All collected plants were frozen in liquid nitrogen and stored at −80 °C freezer for further RNA isolation. For the immunolocalization assays, seedlings from asymptomatic and necrosis stages and their respective non-infected controls of the same age were harvested and fixed in Karnovsky solution overnight at room temperature and under vacuum (Karnovsky, 1965).

2.2. RNA isolation

Mycelia of *M. perniciosa* grown *in vitro* were processed for RNA extraction using the RNeasy Plant Mini Kit (Qiagen) according to the manufacturer's instructions. RNA from infected and non-infected plant material was isolated according to a protocol developed in our laboratory (Vidal et al., 2010). All isolated RNA was qualitatively analyzed in 1% denaturing formaldehyde/agarose gel electrophoresis and quantified using a Nanodrop™ 1000 Spectrophotometer (Thermo Scientific).

2.3. Real-time PCR

One microgram of total RNA from *in vitro* cultures and plant material was treated with RQ1 RNAse–free DNAse (Promega) and used for cDNA synthesis with SuperscriptII® Reverse Transcriptase (Invitrogen) according to the manufacturer's protocol. The online program Primer3 (Rozen and Skaletsky, 2000) was used to design all PCR primers based on the sequences obtained from the Witches' broom Genome Project database (Table 1). The optimal primer annealing temperature was set to 55 °C, and the amplicon size varied from 100 to 110 bp. Quantitative PCR was performed using the SYBRGreen MasterMix (Applied Biosystems), and the fluorescence was detected with the Step One Plus platform (Applied Biosystems). A 16 μl reaction was set with 8 μl of the SYBRGreen MasterMix, 40 ng of cDNA and 100 nM of each primer. The thermal cycling conditions were 94 °C for 10 min, followed by 40 cycles of 94 °C for 15 s, 55 °C for 20 s and 60 °C for 1 min. After amplification, a melt-curve step consisting of one cycle of 94 °C for 15 s and a ramp varying from 60 °C to 94 °C in intervals of 0.3 °C was added to inspect the reactions for the formation of primer dimers and unspecific amplicons. The melting temperatures of the fragments were determined according to the manufacturer's protocol (Table 1). No-template reactions (water) were included as negative controls in every plate for all of the primers used; for plant material analyses, non-infected plants were also assayed to ensure that the fungal primers were not amplifying cacao genetic material.

The data analysis was performed using a mathematical method described previously (Pfaffl, 2001), using the C_t (cycle threshold) mean of biological triplicates. Standard curves for each primer pair were generated by serial cDNA dilutions. The housekeeping genes β-actin and α-tubulin (Table 1) were used to normalize the qPCR reactions for *in vitro* and infected plant material, respectively.

2.4. Methanol oxidase assay

Supernatants of liquid *M. perniciosa* cultures were separated from the mycelia by filtration through several layers of filter paper

Table 1
Primers and melting temperatures (MT) for quantitative SYBRGreen real-time PCR.

	Forward	Reverse	MT (°C)
PME	TTTTGTACTCAAACTTGCATCACC	CTGAAGGAAGATTAGACAGACACG	75.6
MOX	CTGTCGGCGTAGCCTATGTT	TCCACTGCTCAGAACGACAC	82.3
ACT	CCCTTCTATCGTCGGTCGT	AGGATACCACGCTTGGATTG	80.7
TUB	GACCAACAGCTTGTCTTTGC	GACATTGCAAACATCGAGGA	81.0

(Whatman No. 1). The secretome samples were then concentrated 100-fold using an Amicon Ultra-15 Centrifugal Filter Unit with an Ultracel-10 membrane (Millipore) and quantified by the Bradford assay using bovine serum albumin as the standard.

The concentrated supernatants of liquid *M. perniciosa* cultures were used to detect methanol oxidase activity. MOX activity was assayed spectrophotometrically at 405 nm through the oxidation of 2,2-azino-bis(3-ethylbenzo-6-thiazoline sulfonic acid) (ABTS) (Sahm and Wagner, 1973). The reactions were set to a final volume of 2 ml, containing 100 mM of the substrate (methanol, ethanol and 2-propanol), 2 μmol of ABTS, 40 μg of horseradish peroxidase (Sigma), and approximately 10 μg of total protein from the culture supernatants. The reaction was performed at 25 °C in an air-saturated 100 mM potassium phosphate buffer at pH 7.5. The oxidation of ABTS was detected by observing the appearance of a green coloration. The 405 nm absorbance was measured at 1 min intervals. The K_m for methanol and ethanol was calculated as described previously (Segers et al., 2001; Van der Klei et al., 1990).

2.5. Enzymatic in-gel digestion and mass spectrometry analysis

Concentrated supernatants of liquid *M. perniciosa* cultures, obtained as described in Section 2.4, were used in mass spectrometry analysis. SDS–PAGE electrophoresis (12.5%) was used to separate 20 μg of the concentrated protein mixture. The bands corresponding to the molecular mass range from 70 to 75 kDa, as predicted for MOX, were excised from the gel and subjected to in-gel trypsin digestion, which was performed as described previously (Hanna et al., 2000), with modifications. As a negative control, we performed the same preparation with a cell-free culture media.

The resulting peptide solution was dried in a SpeedVac concentrator, resuspended in 20 μl of 0.1% formic acid and an aliquot of 4.5 μl was analyzed in a LTQ Orbitrap Velos mass spectrometer (Thermo Scientific) connected to a nanoflow liquid chromatography (LC–MS/MS) by an EASY-nLC system (Proxeon Biosystem) through a Proxeon nanoelectrospray ion source. Peptides were separated on a 2–90% acetonitrile gradient in 0.1% formic acid using a pre-column EASY-Column (2 cm × id 100 μm, 5 μm particle size) and an analytical column EASY-Column (10 cm × id 75 μm, 3 μm particle size) at a flow rate of 300 nl/min over 45 min. The nanoelectrospray voltage was set to 1.7 kV, and the source temperature was 275 °C. All instrument methods for the Orbitrap Velos were set up in the data-dependent acquisition mode. The full scan MS spectra (m/z 300–2000) were acquired in the Orbitrap analyzer after accumulation to a target value of $1e^6$. The resolution was set to $r = 60{,}000$ and the 20 most intense peptide ions with charge states $\geqslant 2$ were sequentially isolated to a target value of 5000 and fragmented in the linear ion trap by low-energy CID (normalized collision energy of 35%). The signal threshold for triggering an MS/MS event was set to 1000 counts. Dynamic exclusion was enabled with an exclusion size list of 500, exclusion duration of 60 s, and repeat count of 1. An activation $q = 0.25$ and activation time of 10 ms were used (de Souza et al., 2012).

Peak lists (msf) were generated from the raw data files using the software Proteome Discoverer 1.3 (Thermo Fisher Scientific) with Sequest search engine and they were searched against *M. perniciosás* predicted protein database (17,012 sequences) with carbamidomethylation (+57.021 Da) as a fixed modification, oxidation of methionine (+15.995 Da) as a variable modification, one trypsin missed cleavage and a tolerance of 10 ppm for the precursor and of 1 Da for fragment ions, filtered using xcorr cutoffs (+1 > 1.8, +2 > 2.2, +3 > 2.5 and +4 > 3.25) and false discovery rate of 0.01, performed using a reverse *M. perniciosás* predicted protein database.

2.6. Immunofluorescence detection of the level of methyl esterification in infected and non-infected cacao seedlings

The immunolocalization of the methylesterified and non-methylesterified domains of homogalacturonan present in infected and non-infected cacao seedlings was performed as described elsewhere (Buckeridge and Reid, 1994; Orfila and Knox, 2000). The primary antibodies JIM5 and JIM7, which recognize homogalacturonan epitopes with low (0–40%) and high (15–80%) levels of methyl esterification (0–40%), respectively, were used (Willats et al., 2000).

The fixed samples (Section 2.1) were dehydrated, cleared in xylene and infiltrated in Paraplast® Plus (McCormick™). Twelve-micrometer transverse sections of stems from asymptomatic and necrotic infected cacao plants and non-infected controls of the same age were dewaxed with butyl acetate, hydrated and incubated in blocking solution (3% whole milk diluted in 0.01 M saline phosphate buffer pH 7.1) for 30 min. Subsequently, the samples were separately incubated with primary antibodies (1:5 dilution) for 3 h, washed three times with PBS buffer and incubated with Goat Anti-Mouse IgG, (H + L) FITC-conjugated secondary antibody for 1 h at room temperature in the dark. Control samples were incubated only with the secondary antibody for 1 h at room temperature in the dark. The samples were immediately analyzed with an Olympus BX51 epifluorescence microscope. At least 10 different sections of each plant were analyzed.

2.7. Transcriptomic analysis using RNA-seq

The RNA isolated from *M. perniciosa* necrotrophic mycelia induced in glycerol or methanol (Section 2.1) was processed for global transcriptome analysis by large scale mRNA sequencing (RNA-seq). Libraries were prepared according the manufacturer's instructions (Illumina). The mRNA was purified from 10 μg of total RNA using Sera-Mag Magnetic Oligo(dT) Beads (Thermo Scientific), and fragmented in the presence of divalent cations under high temperatures. The fragmented mRNA was used to synthesize the cDNA. The first strand was synthesized using Superscript II Reverse Transcriptase and random hexamers. Double-stranded cDNA was then produced using the enzymes DNA polymerase I and RNAse H. Subsequently, abrupt extremities were obtained by treatment with the enzymes T4 DNA polymerase and Klenow DNA polymerase; a 3′-adenine was added by the enzyme Klenow exo-Adapters with an overhang thymine were added, and non-ligated adapters were purified in gel. Finally, the libraries were enriched through 15 cycles of amplification using primers that anneal to the adaptors. The libraries were quantitative and qualitatively assayed with the Qubit fluorometer (Invitrogen) and the Experion capillary electrophoresis system (Bio-RAD). Each library was subjected to a 36-cycle single end sequencing in the Genome Analyzer II_x platform (Illumina).

To identify expressed genes, the reads obtained from large scale sequencing were mapped against the *M. perniciosa* genomic database using the mapping tool Bowtie (Langmead, 2010), allowing one mismatch. Ambiguous reads that mapped with similar scores to several sites were discarded. The measure of gene expression was calculated in terms of RPKM (reads per kilobase per million mapped reads) (Mortazavi et al., 2008).

3. Results

3.1. Sequence analysis of M. perniciosa methanol oxidase

The *M. perniciosa* predicted protein database (17,012 sequences) was analyzed, and three sequences with the potential to encode

methanol oxidase were initially identified. These sequences were compared to MOX sequences from other organisms by the Blast algorithm against the NR database and subjected to a search of conserved domains and classical MOX motifs, using the CDD and Pfam databases. Fig. 2A shows a scheme of the three predicted MOX sequences. All described MOX from fungal species contain two GMC-oxidoreductase (GMC, glucose–methanol–choline) domains and a conserved ADP-binding β–α–β motif on the N-terminal portion of the protein (Ozimek et al., 2005). As shown in Fig. 2A, the sequences 2 and 3 lack the N-terminal β–α–β motif and sequence 3 presents an incomplete N-terminal GMC-oxidoreductase domain; moreover, these sequences are shorter than sequence 1 and MOX sequences from other organisms, in which protein size varies from 650 to 670 amino acids. Because sequence 1 is the only sequence that contains both complete GMC-oxidoreductase domains and the classical β–α–β motif and because it was the only sequence previously identified in cacao-extract-induced EST libraries (Rincones et al., 2008), we focused our work on this gene. This sequence will be referred to as *Mp_mox*.

The *Mp_mox* genomic (GenBank ID: JX024739) sequence and complete CDS present 3490 and 1953 nucleotides, respectively, containing 29 exons and 28 introns. The predicted protein contains 650 amino acids and has a molecular weight of approximately 72 kDa. Fig. 2B shows an alignment of the C-terminal part of the *M. perniciosa* MOX with sequences from the methylotrophic yeasts *P. pastoris* and *P. methanolica*, the ascomycete fungus *C. fulvum* and the basidiomycete species *Coprinopsis cinerea* and *G. trabeum*, and the predicted sequences 2 and 3. *Mp-mox* shares 89% identity with *C. cinerea* and *G. trabeum* sequences compared with its 52% identity with the other species mentioned above. Sequence analysis with the program InterPro Scan Sequence Search (http://www.ebi.ac.uk/Tools/pfa/iprscan) showed the existence of two conserved GMC-oxidoreductase domains: an N-terminal domain corresponding to the amino acids 7–313 and a C-terminal domain that spans from amino acid 427 to 614. Residues 13–18 contain a putative flavin adenine dinucleotide (FAD) binding site (GGGPAG) within the predicted ADP-binding β–α–β motif, which is present in most FAD-binding proteins (Ozimek et al., 2005; Wierenga et al., 1986). An N-glycosylation site at the residue 323 was predicted with a score of 0.5229 by the software NetNGlyc 1.0 (http://www.cbs.dtu.dk/services/NetNGlyc).

One of the main characteristics of MOX from most organisms is the presence of a peroxisomal targeting signal, PTS1, at the C-terminal region of the protein. The (S/A/C)-(K/R/H)-(L/A) tripeptide interacts with the Pex5p receptor protein, leading to the importation of the protein by the peroxisomes (de Hoop and Ab, 1992). As shown in Fig. 2B, the *M. perniciosa* MOX sequence lacks PTS1. Otherwise, the last 26 amino acids (marked in gray) show a high similarity with the terminal residues of the *G. trabeum* and *C. cinerea* sequences; this sequence appears to be a particular characteristic of MOX from basidiomycete species as it differs substantially from the C-terminal sequences of other fungal species.

3.2. M. perniciosa MOX is a secreted protein

One hundred-fold concentrated culture supernatants (secretome) from *M. perniciosa* were assayed for MOX activity. As described in Section 2.4, MOX activity was assayed by following the oxidation of ABTS at 405 nm with a spectrophotometer. Table 2 shows MOX relative activity and K_m values in different substrates. As shown in Table 2, the preferred substrate for MOX is methanol, but it also shows a high activity when the substrate is ethanol.

LC–MS/MS analysis on an LTQ Orbitrap-Velos mass spectrometer was used to confirm the presence of methanol oxidase in the extracellular extracts of *M. perniciosa* cultures. The concentrated fungal secretome was electrophoretically separated in a 12.5% one dimensional SDS–PAGE gel. As MOX is predicted to have a molecular mass of approximately 72 kDa, the bands corresponding to the molecular mass range of 70–75 kDa were excised from the gel (Fig. 3A) and analyzed in the LTQ-Orbitrap-Velos mass spectrometer. A total of 2722 spectral counts were assigned to 205 proteins of the *M. perniciosa* predicted protein database. As shown in Fig. 3B, three unique MOX peptides were identified, totaling 7% of protein coverage. This finding confirms that *M. pernciosa* secretes this enzyme into the extracellular space, despite the absence of a predicted secretory signal peptide in its

Table 2
Relative activity and K_m values for MOX in different substrates.

Substrate	Relative activity (%)[a]	K_m (mM)
Methanol	100	17.3
Ethanol	88	21.2
2-Propanol	7	–

[a] Activities are given relative to methanol.

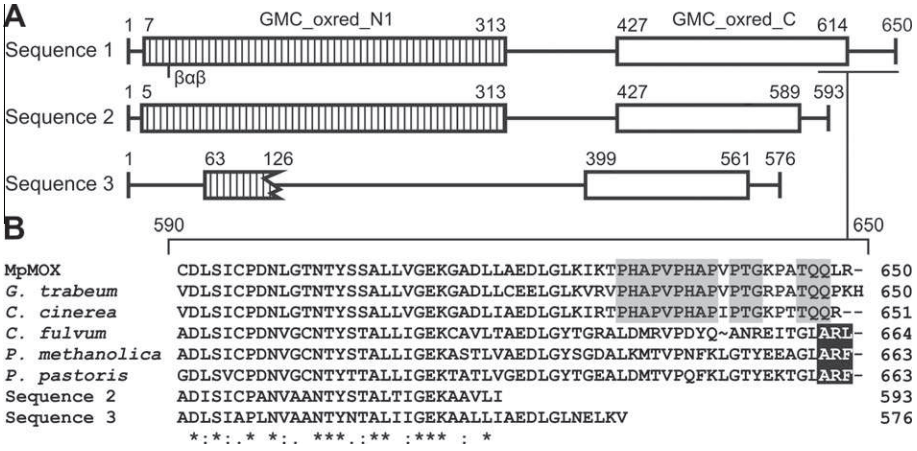

Fig. 2. (A) Schematic alignment of the three sequences identified with the potential to encode methanol oxidase in the *M. perniciosa* genome, showing their amino acid length and the presence of conserved domains. (B) Alignment of the C-terminal sequence of Mp-mox from *M. perniciosa* (GenBank ID: JX024739) with MOX from *Gloeophyllum trabeum* (ABI14440.1), *Coprinopsis cinerea* (XP_001838223.2), *Cladosporium fulvum* (AAF82788.1), *Pichia methanolica* (AAF02494.1) and *Pichia pastoris* (AAB57850.1) and the other two predicted sequences from *M. perniciosa*. The identical amino acid residues are indicated with asterisks. The specific C-terminal sequence present in MOX from the basidiomycete species is labeled in gray, and the C-terminal peroxisomal targeting signal (PTS1) present in MOX from the ascomycetes and methylotrophic yeasts is labeled in black.

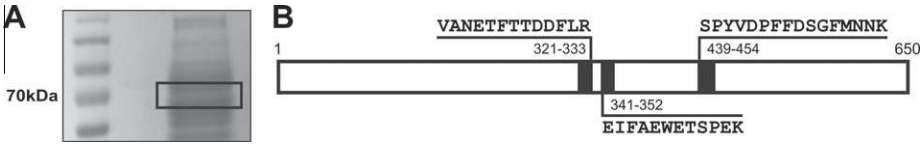

Fig. 3. MOX from *M. perniciosa* is an extracellular enzyme. (A) SDS–PAGE from *M. perniciosa* secretome indicating a 70–75 kDa band that was excised from the gel and subjected to mass spectrometry analysis. (B) Mass spectrometry analysis identified three unique MOX peptides.

Table 3
Peptide sequences identified by mass spectrometry analysis.

Peptide sequence	Spectral counts	Charge	*m*/*z*	MH + [Da]
VANETFTTDDFLR	1	+2	764.8710	1528.7348
SPSPYVDPFFDSGFMNNK	1	+2	1032.9590	2064.9107
EIFAEWETSPEK	1	+2	733.3496	1465.6919

M – oxidation of methionine.

sequence. The peptide sequences, the number of spectral counts, and their *m*/*z* are detailed in Table 3.

3.3. Mp-mox is upregulated in the presence of methanol and esterified pectin

The relative expression of *Mp-mox* and *Mp-pme* transcripts was measured by Real-time PCR in both biotrophic-like and necrotrophic mycelia grown *in vitro* in the presence of glycerol, glucose, methanol, polygalacturonate or pectin with 90% esterification. As shown in Fig. 4, there was a 12- and 9-fold increase in the expression of *Mp-mox* in the biotrophic-like and necrotrophic mycelia, respectively, in the presence of methanol when compared with glycerol as the carbon source. This is consistent with the fact that methanol is a substrate for MOX and a known inducer of its expression in other organisms (Ozimek et al., 2005). In the presence of esterified pectin, both *Mp-mox* and *Mp-pme* genes were upregulated. The expression of *Mp-mox* and *Mp-pme* was increased approximately 10 and 9 times, respectively, in both types of mycelium. This result suggests that the methanol released during the demethylation of pectin by the enzyme PME is a substrate for MOX, which shows an increased level of expression. Interestingly, in the presence of non-esterified pectin, neither gene was upregulated, thus reinforcing the hypothesis that the demethylation of pectin is a key process for *Mp-mox* and *Mp-pme* upregulation. The lack of variation in gene expression between the biotrophic-like and necrotrophic mycelia show that, although these mycelia produce distinct symptoms in the progression of WBD, they may exhibit similar characteristics when grown under the same conditions *in vitro*. The expression of these genes in the presence of glucose did not show any difference when compared to growth in glycerol.

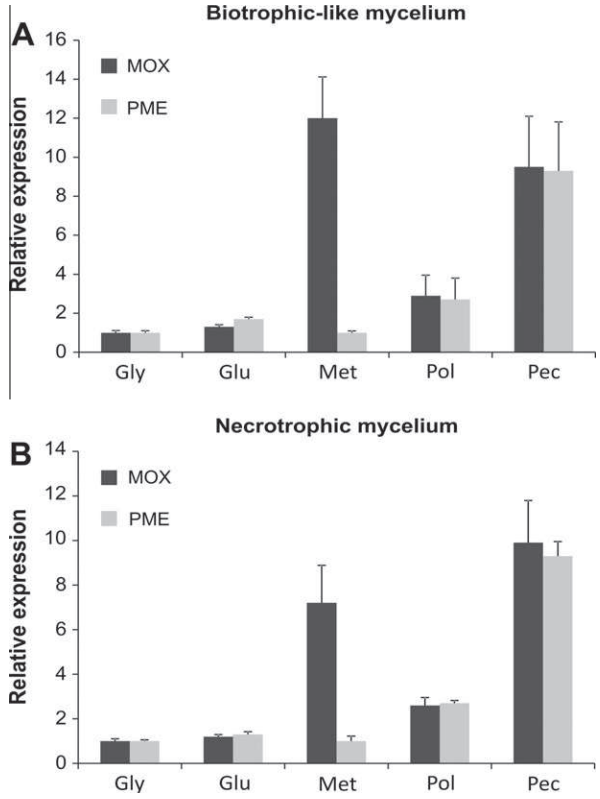

Fig. 4. *Mp-mox* and *Mp-pme* relative expression in the biotrophic-like and necrotrophic mycelium from *M. perniciosa* grown *in vitro* and supplemented with different sole carbon sources. Gly: glycerol; Glu, glucose; Met: methanol; Pol: polygalacturonate (pectin DE 0%); Pec: pectin, DE > 85%. The values are means of biological triplicates and the bars indicate the standard error of the mean. The data were normalized to the β-actin gene and the condition Gly was considered as the control of the experiment and was used to normalize the other conditions expression values.

3.4. The reduction of the level of methyl esterification in infected cacao seedlings is correlated with the higher levels of M. perniciosa Mp-pme relative gene expression in planta

Mp-mox and *Mp-pme* relative expression in infected cacao plants was measured by Real-time quantitative PCR. As described in Section 2.1, 3-month-old cacao seedlings were infected with *M. perniciosa* spores. The symptoms of WBD were observed and the plants were harvested according to the progression of the disease: asymptomatic, green broom 1, green broom 2 and necrosis. As shown in Fig. 5A, *Mp-mox* and *Mp-pme* are coregulated during the progression of WBD in the stages analyzed. The relative expression of both genes is reduced in the green broom phase compared with the asymptomatic stage and increases during the necrosis stage, when the expression of both genes reaches their highest level.

Spores of *M. perniciosa* infect cacao plants as biotrophic mycelia, which grow slowly and at low densities in the infected plants. As the disease progresses, the amount of fungal material *in planta* increases, reaching a maximum at the late stages of the dry broom phase when the necrotrophic mycelia completely colonizes the infected tissues (Evans, 1978; Frias et al., 1991; Griffith and Hedger, 1994). Fig. 5B shows the amplification plots and Ct, with a threshold of 0.1, for the housekeeping gene α-tubulin in the four stages of WBD analyzed. The C_t difference for the α-tubulin gene between the asymptomatic ($C_t = 30$) and the necrosis phase ($C_t = 23$) indicates that there is approximately 100 times more fungal material in the infected plants during the necrosis phase than in the previous stages. The relatively higher *Mp-mox* and *Mp-pme* expression levels in the necrosis phase, in conjunction with the higher number of mycelia infecting the plants during this phase, led us to hypothesize that the final quantity of the transcripts of these genes and,

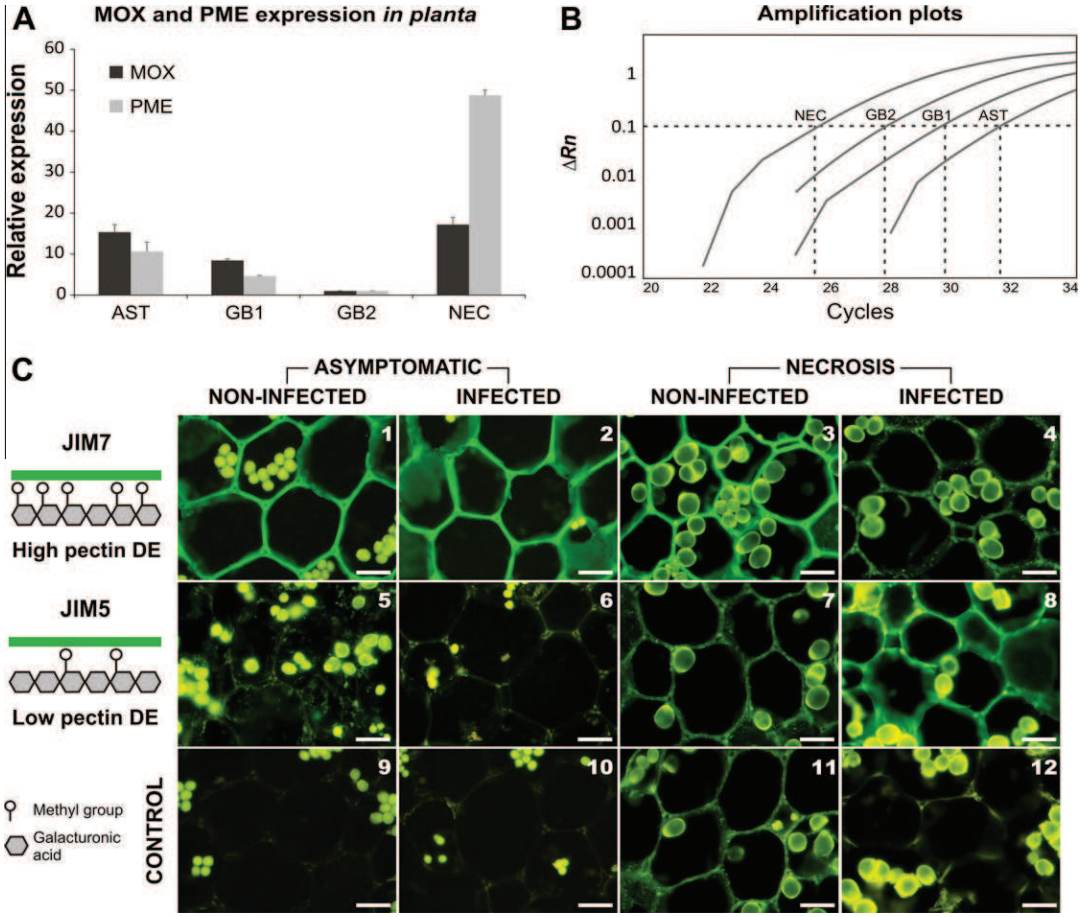

Fig. 5. (A) *Mp-mox* and *Mp-pme* relative expression *in planta* in different stages of the progression of WBD: AST, asymptomatic; GB1: green broom 1; GB2, green broom 2 and NEC: necrosis. The values are means of biological triplicates and the bars indicate the standard error of the mean. The data were normalized to the α-tubulin gene and the condition GB2 was used to normalize the other conditions expression values. (B) Amplification plots of the α-tubulin gene in the four stages of the progression of WBD analyzed, with a threshold of 0.1, showing an increase of the amount of fungal material infecting cacao in the late stages of the disease; (C) Immunofluorescence detection of the pectic homogalacturonan domain in infected and non-infected cacao seedlings (stem tissues in transverse section). Infected asymptomatic plants (2, 6 and 10) and same age non-infected plants (1, 5 and 9); infected necrotic plants (4, 8, and 12) and same age non-infected plants (3, 7 and 11). Bar = 25 μm.

possibly, their protein products, would be even higher in the infected plants.

Because PMEs remove the methyl esters from the pectin backbone, we decided to test this hypothesis by analyzing the level of methyl esterification present in the cell walls of infected cacao seedlings during the asymptomatic and necrotic stages and their respective non-infected same age controls. If there is a higher level of PME enzyme due to the combined effect of the upregulation of *Mp-pme* during the necrotrophic stage and the greater amount of fungal material present in this stage, there should be an inverse correlation with the degree of pectin methyl esterification in the cell wall of infected plants at this stage.

As mentioned in Section 2.6, the monoclonal antibodies JIM5 and JIM7 were used in this work to characterize the level of methyl esterification in the pectic domain homogalacturonan. JIM5 recognizes pectin with low DE (0–40%) and JIM7 labels pectin with high esterification content (15–80%) (Willats et al., 2000).

As shown in Fig. 5C, strong JIM7 labeling was observed in the infected and non-infected asymptomatic samples analyzed (Fig. 4C: 1 and 2); however, comparing the negative control samples (Fig. 5C: 9 and 10), which were labeled only with the secondary antibody, with the samples treated with JIM5 (Fig. 5C: 5 and 6), no JIM5 labeling is observed in the treated samples. JIM5 and JIM7 are able to unspecifically label pectic domains with 15–40% DE. Therefore, the fact that the samples were labeled only by JIM7 indicates that both infected asymptomatic and its same age non-infected control present a high degree of methyl esterification (>40%).

On the other hand, infected plants showing necrosis and their non-infected same age controls show an inverse pattern of methyl esterification: the comparison between the negative control (Fig. 5C: 11) and the samples treated with the primary antibodies leads to the conclusion that non-infected plants were strongly labeled by JIM7 and were not labeled by JIM5 (Fig. 5C: 3 and 7). These data indicate a high level of methyl esterification, while infected plants were strongly marked by JIM5 and weakly by JIM7 (Fig. 5C: 4 and 8), in comparison to their negative control (Fig. 5: 12), thus indicating a low level of methyl esterification. The apparent labeling of some samples from the negative control is related with their auto fluorescence.

These results, in conjunction with the *M. perniciosa Mp-pme* expression *in planta* (Fig. 5A) and the higher amount of fungal material present in the infected tissues (Fig. 5B), strongly suggest a participation of the fungal PME enzyme in the demethylation process of cacao pectin during the necrotrophic stage of WBD.

4. Discussion

Methanol oxidase has been primarily studied in the methylotrophic yeasts *Pichia, Candida, Hansenula,* and *Torulopsis* (Veenhuis et al., 1983). The capability of these organisms to grow on

methanol as the sole carbon source is due to the production of large amounts of MOX; in the presence of methanol, MOX can reach 30% of the total soluble protein produced by these organisms (Giuseppin et al., 1988). However, very little is known about this enzyme among the basidiomycete and/or phytopathogenic fungal species.

In this study, we describe an extracellular methanol oxidase from the phytopathogenic basidiomycete species *M. perniciosa*. The deduced 650 amino acid sequence shows 51–53% identity and 65–67% similarity to MOX from methylotrophic yeasts and ascomycete species and 85–89% identity and 93–95% similarity to other basidiomycete species, indicating that this enzyme is highly conserved among the basidiomycetes.

MOX is a classical peroxisomal enzyme. In methylotrophic yeasts and ascomycetes, the enzyme is produced in the cytosol as 70–75 kDa monomers and post-transcriptionally imported into the peroxisomes, where they are assembled into active octamers (Gunkel et al., 2004). The importation of the protein into the peroxisomes is generally triggered by the recognition of peroxisome targeting signals (PTS) present in the sequence of imported proteins by peroxin (PEX) receptors. PTS1, a C-terminal tripeptide motif, that generally complies with the consensus sequence (S/A/C)(K/R/H)(L/M), is recognized by the protein Pex5p (Gould et al., 1987; Waterham et al., 1997). PTS2, recognized by the peroxin Pex7p, is a N-terminal sequence formed by a very general sequence, (R/K)(L/V/I)X5(H/Q)(L/A), that is present in just a few peroxisomal enzymes (Lazarow, 2006). *M. perniciosa* methanol oxidase, as shown in Fig. 2, lacks both PTS1 and PTS2 sites, which is in agreement with the enzyme activity assays and mass spectrometry analysis showing that this enzyme is secreted to the extracellular space.

To date, the only described extracellular MOX belongs to the lignin-degrading basidiomycete *G. trabeum* (Daniel et al., 2007). However, the protein sequence lacks any clear secretion signal. The authors suggested that the differences in MOX targeting compared with the known yeast peroxisomal localization were traced to a unique C-terminal sequence of the *G. trabeum* enzyme, which is apparently responsible for the protein's extracellular translocation. *M. perniciosa* MOX contains an identical C-terminal sequence when compared to *G. trabeum* and predicted MOX from other basidiomycetes that are completely different from the known peroxisomal MOX. Because *M. perniciosa* MOX also lacks a predicted secretion signal, we suggest that its unique C-terminal sequence is the signal component that leads to the translocation of this enzyme to a secretory pathway, given that this is the only significant sequence difference between *M. perniciosa* and other basidiomycete MOX compared with the yeast and ascomycete peroxisomal *mox* genes.

In methylotrophic yeasts, methanol oxidase is regulated at the transcriptional level by a repression and/or derepression mechanism (Ozimek et al., 2005). In *P. angusta*, the expression of *mox* is subject to a strong carbon catabolite repression, as the *mox* gene is completely repressed by growth on glucose; this substrate inhibits peroxisome proliferation, even in the presence of methanol. On the other hand, *mox* transcripts are detected when cells are grown on methanol or glycerol as the sole carbon sources (Roggenkamp et al., 1984; Veenhuis et al., 1983). In *M. perniciosa*, the *Mp-mox* gene is detected when the mycelia is grown *in vitro* in glycerol and strongly induced in the presence of methanol, in both biotrophic-like and necrotrophic mycelia (Fig. 4). However, gene repression is not observed because the mycelia grown in glucose express *Mp-mox* at a similar magnitude as when grown in glycerol.

The analysis of the *M. perniciosa* genome revealed that the fungus possesses all the genes classically related to the methanol degradation pathway (GenBank ID: JX024739–JX024749). RNA-seq-based transcriptome analysis showed that all of these genes are upregulated in the necrotrophic mycelia supplemented with methanol when compared to those supplemented with glycerol.

Table 4
Prediction of the subcellular localization of the enzymes involved in the methanol metabolism pathway in *M. perniciosa*. Catalase and pectin methylesterase are predicted as secreted; the other enzymes are predicted as cytoplasmatic, except for OAH, predicted as mitochondrial. However, MOX is as secreted protein, as show in Section 3.2, despite the absence of a predicted signal peptide. *Abbreviations*: cyto, cytoplasmatic; nucl, nuclear; pero, peroxisomal; extr, extracellular, mito, mitochondrial.

Gene	SignalP	Psort prediction	PeroxiP
MOX	N	cyto: 19.0, cyto_nucl: 11.5, pero: 4.0, nucl: 2.0	N
CAT	Y	extr: 23.0, mito: 3.0	N
FMDH	N	cyto: 26.0	N
FDH	N	cyto: 15.5, cyto_nucl: 8.5, E.R.: 4.0, mito: 3.0, extr: 3.0	N
DHAS	N	cyto: 16.0, cyto_nucl: 9.5, pero: 5.0, extr: 3.0	N
DHAK	N	cyto: 21.5, cyto_nucl: 11.5, extr: 5.0	N
FBPA	N	cyto: 24.5, cyto_nucl: 13.5	N
FBPT	N	cyto: 17.0, cyto_nucl: 15.3, cyto_mito: 10.5, extr: 2.0	N
OAH	N	mito: 11.0, cyto: 5.0, plas: 3.0, extr: 3.0, pero: 3.0	N
PME	Y	extr: 26.0	N

Based on the values of gene expression and the prediction of the subcellular location of the methanol pathway enzymes, performed by the software SignalP, PsortII and PeroxiP (Table 4), we propose a peroxisome-independent model for methanol degradation in *M. perniciosa* (Fig. 6). According to our model, the methanol released by pectin demethylation is oxidized by an extracellular methanol oxidase, generating formaldehyde and hydrogen peroxide. The peroxide generated may be degraded by an extracellular catalase (CAT) or by a secreted DyP peroxidase (PER), that uses iron ions as co factors. The resulting formaldehyde may be subjected to oxidation by the enzymes formaldehyde dehydrogenase (FMDH) and a NAD-dependent formate dehydrogenase (FDH), generating carbon dioxide. It may also be incorporated in the dihydroxyacetone (DHA) pathway, comprising the enzymes dihydroxyacetone synthase (DHAS), dihydroxyacetone kinase (DHAK), fructose-bisphosphate aldolase (FBPA) and fructose-bisphosphatase (FBPT), whose products are incorporated into the pentose phosphate pathway. One of the subproducts of the DHA pathway is glyceraldehyde 3-phosphate, which can be a precursor for the synthesis of oxaloacetate. Oxaloacetate, an intermediate of the tricarboxylic acid cycle, is also a substrate for the enzyme oxaloacetate acetyl hydrolase (OAH), which generates oxalate. Oxalate is known for its capability to remove calcium ions from the structure of pectin, forming calcium oxalate crystals and allowing further enzymatic pectin degradation by PCWD (Guimaraes and Stotz, 2004). The production of calcium oxalate crystals by *M. perniciosa* necrotrophic mycelia has been previously reported (Rio et al., 2008).

As higher levels of gene expression may correlate to higher amounts of protein produced, we suggest that in *M. perniciosa*, the formaldehyde generated from methanol metabolism is preferentially metabolized by the enzymes FMDH and FDH due to the higher values of RPKM and the fold change when compared with the values of the DHA pathway. Formaldehyde metabolized by the DHA pathway is used in the production of cell constituents used for cell growth and proliferation; on the other hand, its use by FDH and FMDH generates NADH, used as an electron donor for the generation of energy. However, at least a part of the formaldehyde generated is metabolized by the DHA pathway, allowing *M. perniciosa* to grow in methanol as sole carbon source; if all the formaldehyde was metabolized by the FDH and FMDH pathway, no growth on methanol as the sole carbon source would be observed.

In methylotrophic yeasts, the peroxide generated in the peroxisomes by methanol oxidation is decomposed by a catalase (Yurimoto et al., 2011). Because *M. pernciosa* methanol metabolism occurs in the extracellular space, we investigated the presence of an

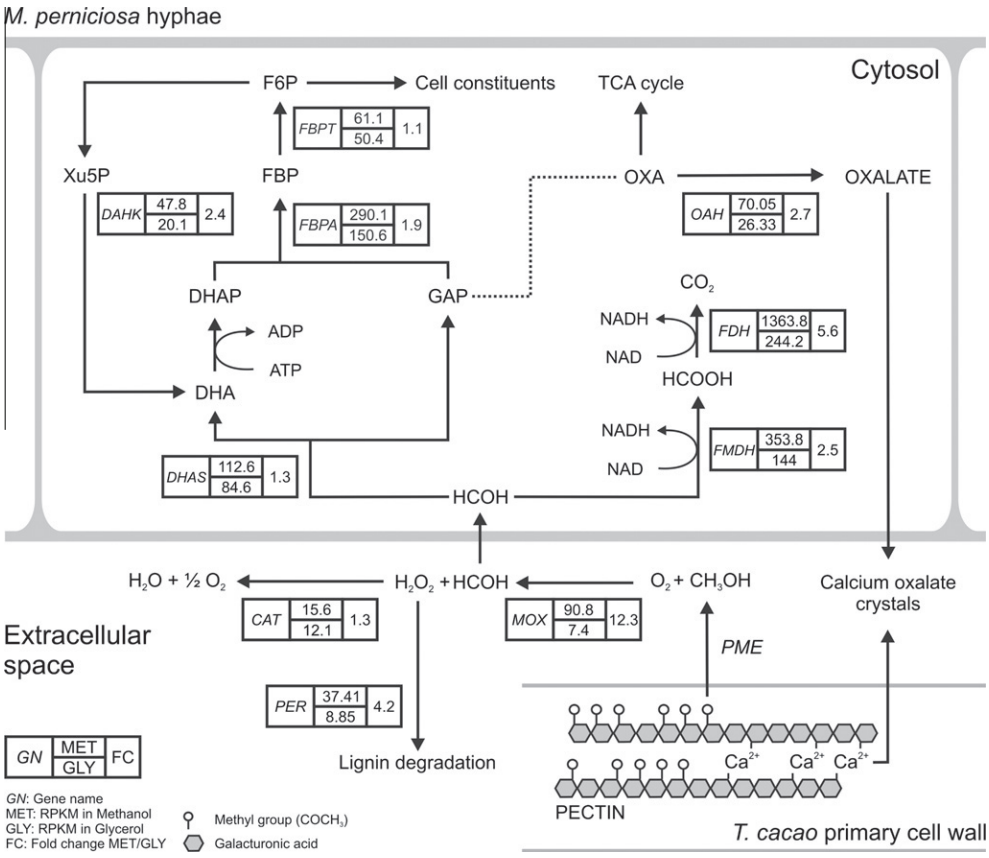

Fig. 6. A peroxisome-independent model for the methanol metabolism pathway in *M. perniciosa*, which is induced at a transcriptional level in cultures supplemented with methanol when compared with cultures supplemented with glycerol. Enzyme abbreviations: MOX, methanol oxidase; CAT, catalase; PER, peroxidase; FMDH, formaldehyde dehydrogenase; FDH, NAD-dependent formate dehydrogenase; DHAS, dihydroxyacetone synthase; DHAK, dihydroxyacetone kinase; FBPA, fructose-bisphosphate aldolase; FBPT, fructose-bisphosphatase; OAH, oxaloacetate acetyl hydrolase, PME: pectin methyl esterase. GenBank ID: JX024739–JX024749. Substrate abbreviations: DHA, dihydroxyacetone; DHAP: dihydroxyacetone phosphate; GAP: glyceraldehyde 3-phosphate; FBP: fructose-1,6-bisphosphate; F6P: fructose 6-phosphate; Xu5P: xylulose 5-phosphate; OXA, oxaloacetate.

extracellular catalase. As shown in Fig. 6, a catalase showing a clear predicted secretory signal (Table 4) is slightly induced in the presence of methanol and its activity is detected in the fungal culture supernatants (data not shown), indicating a possible role in the degradation of the peroxide generated. Moreover, *M. perniciosa* possesses several peroxidases that are predicted to be secreted, which may also participate in peroxide degradation. One of these peroxidases is induced in the methanol RNA-seq libraries, as shown in Fig. 6. A Dyp peroxidase, which uses iron ions as cofactors, shows a 4-fold increase in its expression when *M. perniciosa* is supplemented with methanol compared with supplemented with glycerol. In known plant–pathogen models involving wood-degrading fungal species, such as *Postia placenta, Phanerochaete chrysosporium* and *G. trabeum*, secreted peroxidases are related to lignin degradation (Daniel et al., 2007; Wymelenberg et al., 2010). Moreover, extracellular sources of hydrogen peroxide, such as that generated by methanol oxidation are related to lignin degradation via the Fenton reaction: $H_2O_2 + Fe^{2+} + H^{1+} = OH + Fe^{3+} + H_2O$. The hydroxyl radicals generated by this reaction (·OH) are able to penetrate the plant cells of infected hosts and act as depolymerizing agents, thus causing extensive cell damage (Schlosser et al., 2000). The necrosis observed in the dry broom phase of WBD as a consequence of plant cell death may be caused by, among other factors, lignin degradation via peroxidases and/or the Fenton reaction. Although *M. perniciosa* is not a classical wood-degrading phytopathogen, studies have revealed that this species is probably derived from a saprotrophic ancestral (Aime and Phillips-Mora, 2005; Tiburcio et al., 2010); thus, *M. perniciosa* may have retained its ability to degrade wood.

As shown in Fig. 4, in addition to methanol, MOX expression is also induced in the presence of esterified pectin. Our results show a correlation between the expression of *Mp-mox* and *Mp-pme* in *M. perniciosa* mycelia grown in esterified pectin, suggesting methanol utilization provided by pectin degradation. Interestingly, both genes also exhibit a transcriptional correlation in infected cacao seedlings at the different stages of the progression of WBD that were analyzed. In plants, one of the main sources of methanol is pectin, which is the main constituent of primary cell walls and the middle lamellae of higher plant cells (Nakagawa et al., 2000; Pelloux et al., 2007). The differential expression of *Mp-mox* and *Mp-pme* during the progression of WBD suggests an important role for these genes in the development of the disease, especially during the beginning of necrosis when the mycelia turn necrotrophic and invade the plant cells. The higher relative expression of MOX and PME, in conjunction with the lower level of methyl esterification in the beginning of necrosis, as shown in Fig. 5 by a weak JIM7 labeling and strong JIM5 labeling (Fig. 5C: 3 and 7), may be key steps in the beginning of cell invasion by the mycelia, given that the activity of PME allows further action of other PCWD, such as polygalacturonases and cellulases.

Although PMEs are constantly reported to be pathogenicity factors, because disruption of the *pme* gene in fungi like *B. cinerea* reduces virulence in their respective plant hosts (Valette-Collet et al., 2003), very little is known about the importance of MOX for pathogenicity. The only well-described case refers to the ascomycete fungus *C. fulvum*, in which the deletion of the methanol oxidase gene reduced its virulence in tomato leaves; however, the mechanism of MOX in the pathogenicity of this fungus remained

uncertain (Segers et al., 2001). In phytopathogenicity, MOX has been related to lignin degradation instead of the pectin degradation as proposed in this work. In the wood-degrading basidiomycetes, such as *P. placenta* and *G. trabeum*, MOX is suggested to generate the hydrogen peroxide used for Fentoń s reaction (Daniel et al., 2007; Martinez et al., 2009). Although we cannot discard the possibility that MOX participates in Fentoń s reaction, providing the extracellular hydrogen peroxide used for Fentoń s reaction, our data strongly suggest that *M. perniciosa* methanol oxidase is related to the pectin degradation. Moreover, as *M. perniciosa* is able to grow on methanol as the sole carbon source and possesses the complete pathway for methanol degradation, we also suggest that this fungus utilizes methanol as an energy source, similar to the methylotrophic yeast species. This is in contrast to wood-degrading fungal species, in which methanol degradation is only described as an provider of extracellular generator of hydrogen peroxide (Daniel et al., 2007). Lastly, MOX also uses ethanol as a substrate; in plants, ethanol is derived from fermentative growth on sugars and used as a carbon source via acetaldehyde and the TCA cycle; however, we carefully inspected over 80 RNA-seq libraries and have found no metabolism compatible with ethanol production by the plant (data not shown); on the other hand, our results show evidences for the presence of methanol and for that reason we consider that this is the substrate utilized by the proposed pathway. The disruption of the *Mp-mox* and *Mp-pme* genes from *M. pernciosa* would be a key next step in confirming the role of these two enzymes in the establishment of WBD and will be performed as soon as gene disruption techniques are developed for *M. perniciosa*.

5. Conclusions

In this work, we demonstrate that *M. perniciosa* produces a methanol oxidase that is secreted into the extracellular space. The relative expression of this methanol oxidase *in vitro* and *in planta* is correlated with the *Mp-pme* expression levels and with the reduction in the level of methyl esterification observed in infected cacao plants, suggesting that this fungus metabolizes the methanol generated by pectin degradation. Moreover, we propose a peroxisomal-independent methanol metabolism pathway for *M. perniciosa*, which begins in the extracellular space and ends in the cytosol.

Acknowledgments

We acknowledge the Mass Spectrometry Laboratory at Brazilian Biosciences National Laboratory, CNPEM-ABTLuS, Campinas, Brazil for their support with the mass spectrometry analysis. We also thank Dr. Odalys Garcia Cabrera and Dr. Jorge Maurício Costa Mondego for suggestions and critiques during the development of the experiments, Marcelo Carazolle for bioinformatics support, and Professor Marcos Buckeridge and Dr. Patrícia Pinho Tonini for the support with the immunolocalization experiments. This work was financially supported by CNPq (Process Number: 472710/2008-7) and FAPESP (Process Numbers: 2006/59843-3, 2007/51030-6, and 2009/50119-9).

References

Aime, M.C., Phillips-Mora, W., 2005. The causal agents of Witches' broom and frosty pod rot of cacao (chocolate, *Theobroma cacao*) form a new lineage of Marasmiaceae. Mycologia 97, 1012–1022.

Buckeridge, M.S., Reid, J.S., 1994. Purification and properties of a novel beta-galactosidase or exo-(1→4)-beta-D-galactanase from the cotyledons of germinated *Lupinus angustifolius* L. seeds. Planta 192, 502–511.

Daniel, G., Volc, J., Filonova, L., Plihal, O., Kubatova, E., Halada, P., 2007. Characteristics of *Gloeophyllum trabeum* alcohol oxidase, an extracellular source of H_2O_2 in brown rot decay of wood. Appl. Environ. Microbiol. 73, 6241–6253.

de Hoop, M.J., Ab, G., 1992. Import of proteins into peroxisomes and other microbodies. Biochem. J. 286 (Pt 3), 657–669.

de Souza, T.A., Soprano, A.S., de Lira, N.P., Quaresma, A.J., Pauletti, B.A., Paes Leme, A.F., Benedetti, C.E., 2012. The TAL effector PthA4 interacts with nuclear factors involved in RNA-dependent processes including a HMG protein that selectively binds poly(U) RNA. PLoS One 7, e32305.

Delgado, J.C., Cook, A.A., 1976. Nuclear condition of basidia, basidiospores, and mycelium of Marasmius-Perniciosus. Can. J. Bot. – Rev. Can. Bot. 54, 66–72.

Evans, H.C., 1978. Witches broom disease of cocoa (Crinipellis-Perniciosa) in Ecuador 1. Fungus. Ann. Appl. Biol. 89, 185–192.

Evans, H.C., 1980. Pleomorphism in Crinipellis-Perniciosa, causal agent of Witches broom disease of cocoa. Trans. Brit. Mycol. Soc. 74, 515–523.

Evans, H.C., Bastos, C.N., 1980. Basidiospore germination as a means of assessing resistance to Crinipellis-Perniciosa (Witches broom disease) in cocoa cultivars. Trans. Brit. Mycol. Soc. 74, 525–536.

Frias, G.A., Purdy, L.H., Schmidt, R.A., 1991. Infection biology of Crinipellis-Perniciosa on vegetative flushes of cacao. Plant Dis. 75, 552–556.

Giuseppin, M.L., Van Eijk, H.M., Bes, B.C., 1988. Molecular regulation of methanol oxidase activity in continuous cultures of *Hansenula polymorpha*. Biotechnol. Bioeng. 32, 577–583.

Gould, S.G., Keller, G.A., Subramani, S., 1987. Identification of a peroxisomal targeting signal at the carboxy terminus of firefly luciferase. J. Cell Biol. 105, 2923–2931.

Griffith, G.W., Hedger, J.N., 1994. The breeding biology of biotypes of the Witches-broom pathogen of cocoa Crinipellis-Perniciosa. Heredity. 72, 278–289.

Griffith, G.W., Nicholson, J., Nenninger, A., Birch, R.N., Hedger, J.N., 2003. Witches' brooms and frosty pods: two major pathogens of cacao. NZ J. Bot. 41, 423–435.

Guimaraes, R.L., Stotz, H.U., 2004. Oxalate production by *Sclerotinia sclerotiorum* deregulates guard cells during infection. Plant Physiol. 136, 3703–3711.

Gunkel, K., van Dijk, R., Veenhuis, M., van der Klei, I.J., 2004. Routing of *Hansenula polymorpha* alcohol oxidase: an alternative peroxisomal protein-sorting machinery. Mol. Biol. Cell 15, 1347–1355.

Han, Y., Joosten, H.J., Niu, W., Zhao, Z., Mariano, P.S., McCalman, M., van Kan, J., Schaap, P.J., Dunaway-Mariano, D., 2007. Oxaloacetate hydrolase, the C-C bond lyase of oxalate secreting fungi. J. Biol. Chem. 282, 9581–9590.

Hanna, S.L., Sherman, N.E., Kinter, M.T., Goldberg, J.B., 2000. Comparison of proteins expressed by *Pseudomonas aeruginosa* strains representing initial and chronic isolates from a cystic fibrosis patient: an analysis by 2-D gel electrophoresis and capillary column liquid chromatography–tandem mass spectrometry. Microbiology 146 (Pt 10), 2495–2508.

Karnovsky, M.J., 1965. A formaldehyde–glutaraldehyde fixative of high osmolarity for use in electron microscopy. J. Cell Biol. 27, 137.

Kaszycki, P., Koloczek, H., 2000. Formaldehyde and methanol biodegradation with the methylotrophic yeast *Hansenula polymorpha* in a model wastewater system. Microbiol. Res. 154, 289–296.

Langmead, B., 2010. Aligning short sequencing reads with Bowtie. Curr. Protoc. Bioinfor. Unit 11 7 (Chapter 11).

Lazarow, P.B., 2006. The import receptor Pex7p and the PTS2 targeting sequence. Biochim. Biophys. Acta 1763, 1599–1604.

Martinez, D., Challacombe, J., Morgenstern, I., Hibbett, D., Schmoll, M., Kubicek, C.P., Ferreira, P., Ruiz-Duenas, F.J., Martinez, A.T., Kersten, P., Hammel, K.E., Wymelenberg, A.V., Gaskell, J., Lindquist, E., Sabat, G., BonDurant, S.S., Larrondo, L.F., Canessa, P., Vicuna, R., Yadav, J., Doddapaneni, H., Subramanian, V., Pisabarro, A.G., Lavin, J.L., Oguiza, J.A., Master, E., Henrissat, B., Coutinho, P.M., Harris, P., Magnuson, J.K., Baker, S.E., Bruno, K., Kenealy, W., Hoegger, P.J., Kues, U., Ramaiya, P., Lucash, S., Salamov, A., Shapiro, H., Tu, H., Chee, C.L., Misra, M., Xie, G., Teter, S., Yaver, D., James, T., Mokrejs, M., Pospisek, M., Grigoriev, I.V., Brettin, T., Rokhsar, D., Berka, R., Cullen, D., 2009. Genome, transcriptome, and secretome analysis of wood decay fungus *Postia placenta* supports unique mechanisms of lignocellulose conversion. Proc. Natl. Acad. Sci. USA 106, 1954–1959.

Meinhardt, L.W., Bellato Cde, M., Rincones, J., Azevedo, R.A., Cascardo, J.C., Pereira, G.A., 2006. In vitro production of biotrophic-like cultures of *Crinipellis perniciosa*, the causal agent of Witches' broom disease of *Theobroma cacao*. Curr. Microbiol. 52, 191–196.

Mondego, J.M., Carazzolle, M.F., Costa, G.G., Formighieri, E.F., Parizzi, L.P., Rincones, J., Cotomacci, C., Carraro, D.M., Cunha, A.F., Carrer, H., Vidal, R.O., Estrela, R.C., Garcia, O., Thomazella, D.P., de Oliveira, B.V., Pires, A.B., Rio, M.C., Araujo, M.R., de Moraes, M.H., Castro, L.A., Gramacho, K.P., Goncalves, M.S., Neto, J.P., Neto, A.G., Barbosa, L.V., Guiltinan, M.J., Bailey, B.A., Meinhardt, L.W., Cascardo, J.C., Pereira, G.A., 2008. A genome survey of *Moniliophthora perniciosa* gives new insights into Witches' broom disease of cacao. BMC Genom. 9, 548.

Mortazavi, A., Williams, B.A., McCue, K., Schaeffer, L., Wold, B., 2008. Mapping and quantifying mammalian transcriptomes by RNA-Seq. Nat. Methods 5, 621–628.

Nakagawa, T., Miyaji, T., Yurimoto, H., Sakai, Y., Kato, N., Tomizuka, N., 2000. A methylotrophic pathway participates in pectin utilization by *Candida boidinii*. Appl. Environ. Microbiol. 66, 4253–4257.

Nakagawa, T., Yamada, K., Fujimura, S., Ito, T., Miyaji, T., Tomizuka, N., 2005. Pectin utilization by the methylotrophic yeast *Pichia methanolica*. Microbiology 151, 2047–2052.

Nemecek-Marshall, M., MacDonald, R.C., Franzen, J.J., Wojciechowski, C.L., Fall, R., 1995. Methanol emission from leaves (enzymatic detection of gas-phase methanol and relation of methanol fluxes to stomatal conductance and leaf development). Plant Physiol. 108, 1359–1368.

Orfila, C., Knox, J.P., 2000. Spatial regulation of pectic polysaccharides in relation to pit fields in cell walls of tomato fruit pericarp. Plant Physiol. 122, 775–781.

Ozimek, P., Kotter, P., Veenhuis, M., van der Klei, I.J., 2006. *Hansenula polymorpha* and *Saccharomyces cerevisiae* Pex5p's recognize different, independent peroxisomal targeting signals in alcohol oxidase. FEBS Lett. 580, 46–50.

Ozimek, P., Veenhuis, M., van der Klei, I.J., 2005. Alcohol oxidase: a complex peroxisomal, oligomeric flavoprotein. FEMS Yeast Res. 5, 975–983.

Pelloux, J., Rusterucci, C., Mellerowicz, E.J., 2007. New insights into pectin methylesterase structure and function. Trends Plant Sci. 12, 267–277.

Penman, D., Britton, G., Hardwick, K., Collin, H.A., Isaac, S., 2000. Chitin as a measure of biomass of *Crinipellis perniciosa*, causal agent of witches' broom disease of *Theobroma cacao*. Mycol. Res. 104, 671–675.

Pereira, J.L., Ram, A., Figuereido, J.M., de Almeida, L.C., 1989. La primera aparición de la "Escoba de Bruja"en la principal región productora de cacao del Brasil. Turrialba 36, 459–461.

Pfaffl, M.W., 2001. A new mathematical model for relative quantification in real-time RT-PCR. Nucl. Acids Res. 29, e45.

Rincones, J., Scarpari, L.M., Carazzolle, M.F., Mondego, J.M., Formighieri, E.F., Barau, J.G., Costa, G.G., Carraro, D.M., Brentani, H.P., Vilas-Boas, L.A., de Oliveira, B.V., Sabha, M., Dias, R., Cascardo, J.M., Azevedo, R.A., Meinhardt, L.W., Pereira, G.A., 2008. Differential gene expression between the biotrophic-like and saprotrophic mycelia of the Witches' broom pathogen *Moniliophthora perniciosa*. Mol. Plant–Microbe Interact. 21, 891–908.

Rio, M.C., de Oliveira, B.V., de Tomazella, D.P., Silva, J.A., Pereira, G.A., 2008. Production of calcium oxalate crystals by the basidiomycete *Moniliophthora perniciosa*, the causal agent of witches' broom disease of cacao. Curr. Microbiol. 56, 363–370.

Roggenkamp, R., Janowicz, Z., Stanikowski, B., Hollenberg, C.P., 1984. Biosynthesis and regulation of the peroxisomal methanol oxidase from the methylotrophic yeast *Hansenula polymorpha*. Mol. Gen. Genet. 194, 489–493.

Rozen, S., Skaletsky, H., 2000. Primer3 on the WWW for general users and for biologist programmers. Methods Mol. Biol. 132, 365–386.

Sahm, H., Wagner, F., 1973. Microbial assimilation of methanol. The ethanol- and methanol-oxidizing enzymes of the yeast *Candida boidinii*. Eur. J. Biochem. 36, 250–256.

Sakai, T., Sakamoto, T., Hallaert, J., Vandamme, E.J., 1993. Pectin, pectinase and protopectinase: production, properties, and applications. Adv. Appl. Microbiol. 39, 213–294.

Scarpari, L.M., Meinhardt, L.W., Mazzafera, P., Pomella, A.W., Schiavinato, M.A., Cascardo, J.C., Pereira, G.A., 2005. Biochemical changes during the development of Witches' broom: the most important disease of cocoa in Brazil caused by *Crinipellis perniciosa*. J. Exp. Bot. 56, 865–877.

Schlosser, D., Fahr, K., Karl, W., Wetzstein, H.G., 2000. Hydroxylated metabolites of 2,4-dichlorophenol imply a Fenton-type reaction in *Gloeophyllum striatum*. Appl. Environ. Microbiol. 66, 2479–2483.

Segers, G., Bradshaw, N., Archer, D., Blissett, K., Oliver, R.P., 2001. Alcohol oxidase is a novel pathogenicity factor for *Cladosporium fulvum*, but aldehyde dehydrogenase is dispensable. Mol. Plant–Microbe Interact. 14, 367–377.

Silva, S.D.V.M.K.M., 1999. Histologia da Interação Crinipellis perniciosa em Cacaueiros Suscetível e Resistente à Vassoura-de-Bruxa. Fitopatol. Bras. 24, 54–59.

Teixeira, P.J.P.L., Mondego, J.M.C., Pereira, G.A.G., A method for production of Moniliophthora perniciosa basidiospores in vitro. Manuscript in preparation.

Thomazella, D.P., Teixeira, P.J., Oliveira, H.C., Saviani, E.E., Rincones, J., Toni, I.M., Reis, O., Garcia, O., Meinhardt, L.W., Salgado, I., Pereira, G.A., 2012. The hemibiotrophic cacao pathogen *Moniliophthora perniciosa* depends on a mitochondrial alternative oxidase for biotrophic development. New Phytol.

Tiburcio, R.A., Costa, G.G., Carazzolle, M.F., Mondego, J.M., Schuster, S.C., Carlson, J.E., Guiltinan, M.J., Bailey, B.A., Mieczkowski, P., Meinhardt, L.W., Pereira, G.A., 2010. Genes acquired by horizontal transfer are potentially involved in the evolution of phytopathogenicity in *Moniliophthora perniciosa* and *Moniliophthora roreri*, two of the major pathogens of cacao. J. Mol. Evol. 70, 85–97.

Valette-Collet, O., Cimerman, A., Reignault, P., Levis, C., Boccara, M., 2003. Disruption of *Botrytis cinerea* pectin methylesterase gene Bcpme1 reduces virulence on several host plants. Mol. Plant–Microbe Interact. 16, 360–367.

Van der Klei, I.J., Bystrykh, L.V., Harder, W., 1990. Alcohol oxidase from *Hansenula polymorpha* CBS 4732. Methods Enzymol. 188, 420–427.

Veenhuis, M., Van Dijken, J.P., Harder, W., 1983. The significance of peroxisomes in the metabolism of one-carbon compounds in yeasts. Adv. Microb. Physiol. 24, 1–82.

Vidal, R.O., Mondego, J.M., Pot, D., Ambrosio, A.B., Andrade, A.C., Pereira, L.F., Colombo, C.A., Vieira, L.G., Carazzolle, M.F., Pereira, G.A., 2010. A high-throughput data mining of single nucleotide polymorphisms in *Coffea* species expressed sequence tags suggests differential homeologous gene expression in the allotetraploid *Coffea arabica*. Plant Physiol. 154, 1053–1066.

Waterham, H.R., Russell, K.A., Vries, Y., Cregg, J.M., 1997. Peroxisomal targeting, import, and assembly of alcohol oxidase in *Pichia pastoris*. J. Cell Biol. 139, 1419–1431.

Wierenga, R.K., Terpstra, P., Hol, W.G.J., 1986. Prediction of the occurrence of the ADP-binding βαβ-fold in proteins, using an amino acid sequence fingerprint. J. Mol. Biol. 187, 101–107.

Willats, W.G., Limberg, G., Buchholt, H.C., van Alebeek, G.J., Benen, J., Christensen, T.M., Visser, J., Voragen, A., Mikkelsen, J.D., Knox, J.P., 2000. Analysis of pectic epitopes recognised by hybridoma and phage display monoclonal antibodies using defined oligosaccharides, polysaccharides, and enzymatic degradation. Carbohydrate Res. 327, 309–320.

Willats, W.G., McCartney, L., Mackie, W., Knox, J.P., 2001. Pectin: cell biology and prospects for functional analysis. Plant Mol. Biol. 47, 9–27.

Wymelenberg, A.V., Gaskell, J., Mozuch, M., Sabat, G., Ralph, J., Skyba, O., Mansfield, S.D., Blanchette, R.A., Martinez, D., Grigoriev, I., Kersten, P.J., Cullen, D., 2010. Comparative transcriptome and secretome analysis of wood decay fungi *Postia placenta* and *Phanerochaete chrysosporium*. Appl. Environ. Microbiol. 76, 3599–3610.

Yurimoto, H., Komeda, T., Lim, C.R., Nakagawa, T., Kondo, K., Kato, N., Sakai, Y., 2000. Regulation and evaluation of five methanol-inducible promoters in the methylotrophic yeast *Candida boidinii*. Biochim. Biophys. Acta 1493, 56–63.

Yurimoto, H., Oku, M., Sakai, Y., 2011. Yeast methylotrophy: metabolism, gene regulation and peroxisome homeostasis. Int. J. Microbiol. 2011, 101298.

DECLARAÇÃO

Declaro para os devidos fins que o conteúdo de minha dissertação de Mestrado/tese de Doutorado intitulada "Construção de um atlas transcriptômico para o estudo da doença vassoura de bruxa do cacaueiro":

( ) não se enquadra no § 3º do Artigo 1º da Informação CCPG 01/08, referente a bioética e biossegurança.

Tem autorização da(s) seguinte(s) Comissão(ões):

(X) CIBio – Comissão Interna de Biossegurança , projeto No. CIBio/IB 2011/03, Instituição: Instituto de Biologia. Universidade Estadual de Campinas (Unicamp).

( ) CEUA – Comissão de Ética no Uso de Animais , projeto No._____, Instituição: _____.

( ) CEP - Comissão de Ética em Pesquisa, protocolo No. _____, Instituição: _____

** Caso a Comissão seja externa ao IB/UNICAMP, anexar o comprovante de autorização dada ao trabalho. Se a autorização não tiver sido dada diretamente ao trabalho de tese ou dissertação, deverá ser anexado também um comprovante do vínculo do trabalho do aluno com o que constar no documento de autorização apresentado.*

Paulo José P. L. Teixeira

Aluno: Paulo José Pereira Lima Teixeira

Orientador: Gonçalo Amarante Guimarães Pereira

Para uso da Comissão ou Comitê pertinente:
(X) Deferido ( ) Indeferido

Carimbo e assinatura

Prof. Dr. MARCELO LANCELLOTTI
Presidente da Comissão Interna de Biossegurança
Instituto de Biologia - UNICAMP

Para uso da Comissão ou Comitê pertinente:
( ) Deferido ( ) Indeferido

Carimbo e assinatura